Multiaxial Spine Segment Testing: Position vs Load Control and Physiological Relevance

Jaeyoon (Daniel) Kim

MEng (Biomedical)

Masters Thesis

Principal Supervisor: Associate Professor John J. Costi

Associate Supervisor: Mr. Michael Russo

Submitted to the College of Science and Engineering
in total fulfilment of the requirements of the degree of Master of Engineering (Biomedical)
at Flinders University – Adelaide, Australia

I have provided feedback on this document and the student has implemented it fully.

Supervisor's signature: ________________________

November 8, 2021

Declaration

I hereby declare that the thesis is my own and that; to the best of my knowledge and belief, it contains no material previously produced by another party for a degree or diploma in any university, and that to the best of my knowledge and belief it does not contain any material previously published by another person except where reference is made.

Acknowledgements

I would like to acknowledge and sincerely thank my primary supervisor Associate Professor John Costi whose guidance and support have made this project possible. I would also like to acknowledge Mr. Michael Russo for his significant contribution, not only training on MATLAB coding, surgical skills, and the hexapod but also spending countless hours conducting testings in the hexapod.

I also express appreciation for Mr. Tirad Alsharari and Mr. Richard Stanley for their assistance to prepare specimens. I would like to acknowledge the assistance of Associate Professor Boyin Ding for the wealth of knowledge and trouble shootings on the hexapod. I also would like to acknowledge Ms. Atefa Rezwani for her support to obtain specimens.

Executive Summary

The spine moves in a complex way, but it is unknown whether the spine moves in position control or load control. The study investigated the comparison of mechanical properties between load, position, and hybrid control mode. Three pilot tests were conducted to develop the testing protocol and five sheep lumbar spine segments (L4-L5) were tested on the hexapod. The specimens underwent overnight hydration under preload equivalent to a nucleus pressure of 0.1 MPa. Load control was conducted first, ranges of motion were extracted and applied to position and hybrid control. In each control mode, 11 directional loadings were applied in order of shear, axial rotation, bending, flexion/extension, and compression. Two hours of recovery were performed between control modes. The result showed that there were significant overall within-factors interaction effects of control modes and 6DOF loadings in stiffness, phase angle, hysteresis area, hysteresis loss coefficient, and maximum reaction forces/moments. Significant differences between control modes were observed in bending, flexion, extension, and compression movements. In these directional movements, fluid flow of the disc involves causing cumulative creep and this contributed significant differences. Comparison of hybrid control to load and position control was performed to assess physiological relevance. The differences were found in shear, bending, flexion/extension, and compression. However, it is yet insufficient to determine which control mode presents the more-physiological movement of the spine. Further development of the testing protocol is suggested to match the start point of movement in each control mode. The study is continuing with intention of publication in 2022.

Table of Contents

Table of Figures

Table of Tables

CHAPTER 1: INTRODUCTION

1.1 Motivations

Spines move in complex ways during everyday activities. There are studies done on spinal movement under different control modes (Goel et al. 1995; Pascual et al. 2016), however, it is yet undiscovered whether spines move in position control, load control, or a combination of both. Position control aims to reach a target position no matter what forces or moments are applied against it. For example, bending forward to pick up an item would require position control to reach the item with a certain degree of rotation. The centre of rotation in the spinal disc is fixed under pure position control and this generates off-axis coupling forces and moments. On the other hand, to reach a target load is a matter of load control. For example, after reaching the item, the lifting activity would require load control to ensure the spine can generate moments to move the item. Under multiaxial load control, the disc segment can move its natural centre of rotation. Therefore, the centre of rotation is not fixed and floats under load control. The combination of position and load control (hybrid control) aims to reach a target position with the minimisation of off-axis coupling forces and moments.

The different control modes may result in a different load-displacement curve which has implications for the validity of research findings. These testing methods may identify not only different motion paths but also different mechanical properties, such as stiffness and energy absorption during spinal movements. Analysis of pros and cons between position and load control was discussed (Goel et al. 1995), and qualitative comparison on a load-displacement curve between position and load control was performed (Pascual et al. 2016). The importance of this study is to compare position, load, and hybrid control in 6DOF and investigate the load-displacement curves to reveal more realistic stiffness and energy absorption under different control modes.

1.2 Aims

The primary aim of this study was to compare differences in spine segment mechanical properties between control modes. The specific aims were to:

Aim 1: Develop testing protocols for each position, load, and hybrid control mode.
Aim 2: Compare the stiffness and energy absorption between control modes.
Aim 3: Assess physiological relevance between control modes.

The study of a student from the University of Bath, UK suggested that the standardised testing procedure needs to be developed for ensuring comparisons can be easily made across laboratories (Pascual et al. 2016). Therefore, the first aim of the study was to develop testing protocols. From these protocols, the testings on sheep spine specimens were conducted and result data were compared and analysed to assess physiological relevance.

The pilot tests were conducted to achieve the first aim of the study. The specimens were dissected and prepared before the mechanical testings. For mechanical testings, the specimens were tested on hexapod under 6DOF loadings. The 6DOF testing sequence was adopted from a previous study on the effect of the 6DOF loading sequence on compressive properties of the spine segments (Amin et al. 2016). The data from hexapod were transformed by LabView (National Instruments) and analysed with MATLAB (R2020a, The Mathworks Inc.). Mechanical properties of the specimens such as stiffness, hysteresis area, hysteresis coefficient, phase angle, and maximum reaction forces and moments were obtained from MATLAB. The mechanical properties were compared in mean percentage difference from each control mode to accomplish the second aim. The repeated-measures ANOVA was performed on each outcome property, having two within-subjects factors of control mode and 6DOF loading direction. From the results and discussions, the last aim of assessing physiological relevance between control modes was addressed.

The hypotheses were made regarding the results of the study. These hypotheses were investigated by repeated-measures ANOVA with SPSS.

A. There will be significant differences in mechanical properties between control modes.
B. Lateral bending, flexion, extension, and compression will exhibit greater differences due to the biphasic properties of discs.
C. Hybrid control will exhibit more in-vivo like physiological movements of the lumbar spine compared to position and load controls.

1.3 Thesis outlines

To achieve the aims above, the thesis is organised as following chapters:

Chapter 1 introduces the backgrounds of the thesis highlighting motivations and aims

Chapter 2 provides the review of literature on the knowledge of the anatomy of the lumbar spine, comparison of human and sheep spine, and biomechanics of the spines.

Chapter 3 addresses the methodology of the study including specimen preparation, potting, hydration, hexapod testing, and data analysis.

Chapter 4 presents the main findings and results of the study. Mechanical parameters are used to compare different control modes.

Chapter 5 discusses the results identifying the differences between control modes and assessing physiological relevance.

Finally, **Chapter 6** provides the overall conclusion of the thesis and suggests continuing study on the comparison of control modes.

CHAPTER 2: LITERATURE REVIEW

2.1 Anatomy

The human spine is a central support structure of the body allowing movements such as walking, twisting, sitting, and standing as well as protecting the spinal cord. The spine consists of 33 stacked vertebrae which are classified as cervical, thoracic, lumbar, sacrum, and coccyx from superior to inferior. Intervertebral discs are placed between vertebrae that can distribute the load and ligaments and muscles support the movement.

2.1.1 The Lumbar Vertebrae

The lumbar vertebral column consists of five vertebrae which are named numerically as L1, L2, L3, L4, and L5 from superior to inferior (Adams 2013). The lumbar vertebrae are irregular bones consisting of the vertebral body (anterior part), pedicles, and posterior elements (Figure 2.1).

Removed due to copyright restriction

Figure 2.1 The lumbar vertebrae column (L1-L5) and the division of a lumbar vertebra into three functional components (Bogduk 1997)

The flat superior and inferior surface of the vertebral body is designed for supporting compressive loads. The internal structure of the vertebral body also allows withstanding compressive loads by having a combination of vertical and transverse trabeculae (Figure 2.2) (Bogduk 1997).

Removed due to copyright restriction

Figure 2.2 The lumbar vertebral body in a sagittal section describing vertical (VT) and transverse (TT) trabeculae (Bogduk 1997)

The posterior elements of the lumbar vertebrae control the position of the vertebral body (Adams 2013). The posterior elements consist of the laminae, the superior and anterior articular processes, the left and right transverse processes, and the spinous processes. With these various bars of bone projecting in all directions, the posterior elements can receive different directional forces (Bogduk 1997). The pedicles are not only the connection between the vertebral body and the posterior elements but also have a function of transmitting tension and bending. When the vertebral body slides forwards, the inferior articular processes will block the movement of the superior articular process of the below vertebra (Bogduk 1997).

2.1.2 The Intervertebral Disc

The intervertebral disc produces space between consecutive lumbar vertebrae supporting compression loads and allowing bending movement (Adams 2013). The intervertebral discs must be strong enough to withstand the weight of the body and not to be injured during movement. At the same time, without compromising its strength, the disc needs to be deformable to accomplish desired movements. The intervertebral disc consists of nucleus pulposus (central), anulus fibrosus (peripheral), and vertebral end-plates (superior and anterior) (Figure 2.3).

Removed due to copyright restriction

Figure 2.3 The structure of a lumbar intervertebral disc. The disc consists of a nucleus pulposus (NP) surrounded by an anulus fibrosus (AF), covered between tew vertebral end-plates (VEP) (Bogduk 1997)

2.1.2.1 Nucleus Pulposus

The nucleus pulposus is the gelatinous centre of the intervertebral disc and exhibit fluid-like behaviour under the loads. It is primarily composed of water, proteoglycans, and collagen. Water accounts for approximately 70-85 % (Keyes & Compere 1932; McNally & Adams 1992) of the total weight of the intervertebral disc and this varies significantly with age and degeneration (Adams & Hutton 1983; Kraemer, Kolditz & Gowin 1985). Proteoglycans constitute 30-50% of the dry weight (Adams & Muir 1976; Bogduk 1997; Dickson et al. 1967; Gower & Pedrini 1969) and the water of the nucleus is contained within the structure of these proteoglycans (Bogduk 1997). Collagen constitutes 15-20 % of the dry weight and the remainder consists of various proteins known as non-collagenous proteins (Beard & Stevens 1980; Bogduk 1997; Bushell et al. 1977; Melrose & Ghosh 2019; NAYLOR 1976; Taylor & Little 1965). Under pressure, the nucleus pulposus can be deformed due to its fluid nature and distribute load into all directions.

2.1.2.2 Anulus Fibrosus

The anulus fibrosus consists of around 15 layers of collagen fibres in a highly organised pattern. The collagen fibres in each lamella are oriented in parallel and arranged obliquely at an angle of 65-70° from the vertical (Cassidy, Hiltner & Baer 1989; Marchand & Ahmed 1990; Taylor 1990). However, the direction of the lamellae alters layer by layer. Due to the unique structure of the anulus fibrosus, it is capable to resist tension and compression rather than shear or torsion. The principal component of the anulus fibrosus is water (60-70%) followed by collagen (50-60%) and proteoglycans (about 20%) (Beard & Stevens 1980; Dickson et al. 1967; Gower & Pedrini 1969; NAYLOR 1976; Schmorl 1971). The composition of the anulus fibrosus is similar to the nucleus pulposus, however, the anulus fibrosus also contains elastic fibres which constitutes about 10% (Buckwalter, Cooper & Maynard 1976; Hickey & Hukins 1981; Johnson et al. 1985).

2.1.2.3 Vertebral End-plates

The vertebral end-plates are located at both the superior and inferior end of the intervertebral disc. The two end-plates cover the entire nucleus pulposus, on the other hand, the peripheral anulus fibrosus is not covered by the end-plates (Bogduk 1997). The vertebral end-plates have a strong attachment to the anulus fibrosus, in contrast, the attachment to the vertebral bodies is weak. Therefore, the tear can occur between the vertebral body and the end-plates from certain damage (Coventry, Ghormley & Kernohan 1945; Inoue 1981; Wong & Transfeldt 2007). The end-plates consist of proteoglycans, collagen fibres, and cartilage cells. There are more collagens close to the bone, and more proteoglycans and water near the nucleus pulposus (Roberts, Menage & Urban 1989). By having different compositions across the thickness, the end-plates act like a barrier preventing diffusion.

Figure 2.4 Sagittal view of Functional Spinal Unit (FSU with the anterior longitudinal ligament (ALL) and posterior longitudinal ligaments (PLL) (Newell et al. 2017)

2.1.3 Functional Spinal Unit

The functional spinal unit (FSU) is the smallest mechanical unit that can represent the characteristics of the entire spine. FSU consists of two adjacent vertebrae and an intervertebral disc (vertebra-disc-vertebra segment). FSUs include the anterior and posterior longitudinal ligament and the posterior elements (Figure 2.4).

2.1.4 Comparison of Sheep and Human Lumbar Spine

Obtaining human cadaveric spines are expensive as well as difficult since there would be diversity from age, gender, disease, and other genetic factors. Therefore, animal spines are often used as substitutions to investigate human spinal characteristics. The sheep spine is one of the substitutions and shares a similar anatomical structure to the human spine. Human spines have 5 lumbar vertebrae, on the other hand, sheep spines have 6-7 lumbar vertebrae. Sheep lumbar vertebra and discs are smaller in size compared to human spines (Wilke et al. 1997). Although there are differences in the curvature of the spine, geometry of vertebrae, the number of lumbar vertebrae, sheep spine have the most similarity in lumbar and thoracic regions (Wilke et al. 1997). There is also a similarity between sheep and human lumbar spine in terms of biochemical composition. The nucleus pulposus of the sheep spine consists of approximately 80-86% of water and the anulus pulposus contains collagen content at 30% (Leahy & Hukins 2001; Reid et al. 2002). Therefore, the sheep lumbar spine can be an appropriate model for the studies of the human lumbar spine.

2.2 Biomechanical Testing of the Intervertebral Disc

The human spine moves in multi-directional, 6 degrees of freedom (DOF) movements, under dynamic loads during daily activities. Investigation of the response of spines is critical in developing new spinal implants and surgical treatments for disc injuries. Human and animal FSUs were used to conduct mechanical tests and to investigate the viscoelastic properties of the disc. The mechanical testings have been conducted under uniaxial compression (Koeller et al. 1986; O'Connell et al. 2011), however, the spine experiences loading in multiple directions and a combination of those. Therefore, studies have been developed to investigate the spinal behaviour in 6DOF loadings (Ding et al. 2014; Panjabi et al. 2001; Panjabi, Krag & Goel 1981; Patwardhan et al. 1999; Wilke et al. 1994). 6DOF loadings include left and right lateral shear, posterior and anterior shear, left and right lateral bending, left and right axial rotation, flexion, extension, and compression (Figure 2.5).

Removed due to copyright restriction

Figure 2.5 6DOF loadings along with x, y, and z-axes (Chang, Chang & Cheng 2011)

2.2.1 Shear

Shear loadings are translations of the spine in direction of forward, backward, and sideways which indicate anterior, posterior, and left and right lateral respectively. Investigation on the spine response to shear loadings has its importance in studying injuries and engagement of the facet joints (Kim et al. 2012; Marras et al. 2001). The shear forces generated in the human lumbar spine is typically in the range of 400-800 N (Callaghan & McGill 1995; Freudiger, Dubois & Lorrain 1999; Morris et al. 2000; Potvin, Norman & McGill 1991; Skipor et al. 1985), but the musculature plays a significant role in resisting shear approximately 200 N (Lu et al. 2005).

2.2.2 Lateral Bending

Lateral bending is the loading applied moments along with the x-axis as shown in Figure 2.5, positive and negative direction for right lateral bending and left lateral bending respectively.

The movements result in either the left or right lateral anulus compressed and the other side is elongated. The bending moment could be a major factor of the damages on intervertebral discs and ligaments (Adams 2013). During liftings, the peak bending moment hardly exceeds 25 Nm regardless of several variable factors and this indicates 40% of its elastic limit (Adams 2013). The *in-vivo* range of motion for lateral bending is about 5° for L1-L4, 2° for L4-L5, and 1° for L5-S1 (Adams 2013) (Figure 2.6).

Removed due to copyright restriction

Figure 2.6 Range of motion in the lumbar spine. Values for lateral bending and axial rotation are the average of left and right from the neutral position (Adams 2013)

2.2.3 Axial Rotation

Axial rotation is the torsion of the spine including left and right axial rotation. The bending movements are generally involved in axial rotation movements (Pearcy & Tibrewal 1984). The lamellae in the same direction of axial rotation are stretched and alternating lamellae are loosened under axial rotation. The trunk muscles generate torsional moments of 50-80 Nm (McGill 1992) with the contribution of back muscle about 5 Nm (Macintosh, Pearcy & Bogduk 1993). The *in-vivo* range of motion for axial rotation is only about 1° in the entire lumbar level (Adams 2013) (Figure 2.6).

2.2.4 Flexion and Extension

Flexion is the motion of leaning forwards the entire lumbar spine by unfolding lumbar lordosis and extension is the converse of the flexion (Bogduk 1997). During flexion, the anterior anulus is compressed, while the posterior anulus is stretched and vice versa under extension. The range of motion for flexion (8-13°) is much higher compared to extension (1-5°) (Figure 2.6), due to the posterior elements of the lumbar spine. The facet joints play a role as a limitation of movement under extension. The posterior ligaments (posterior longitudinal ligament, superspinous ligament, and interspinous ligament) (Figure 2.6) are stretched during flexion, on the other hand, only the anterior longitudinal ligament is stretched without other ligaments' engagement under extension (Adams 2013).

2.2.5 Compression

Under compression, the hydrostatic pressure occurs in the nucleus, and the anulus bulges radially outwards (Adams 2013). This results in the lamellae collagen fibres stretching in tension. The response to compression loads depends on the shape and size of the disc (Adams 2013). A high ratio of height to the area will generate higher tensile stresses at the outer anulus, and more radial bulging under the same applied compressive force (Lu, Hutton & Gharpuray 1996). Some experiments quantified that under approximately 2 kN of compressive force results in stretching the collagen fibres by less than 2% and bulging radially by 0.4-1.0 mm (Adams 2013; Stokes 1987).

2.3 Previous Studies

A study discussed on pros and cons of load control and position control analysis on the human spine. The study suggested that the pure moment can be applied in load control mode, and this can simulate clinically relevant motion (Goel et al. 1995). However, the discussion was based on several assumptions without experimental qualitative comparisons. This might be because of the absence of testing equipment, hard to obtain accurate measurements. A recent study has provided qualitative comparisons on the shape of the load-displacement curves obtained from both position and load control (Pascual et al. 2016). The study only conducted comparisons between with and without preload under two control modes.

The importance of this thesis is to introduce hybrid control and perform comparisons between three different control modes that have not yet been published. The thesis also aims to compare important mechanical properties and introduce further discussion assessing physiological relevance between the control modes.

CHAPTER 3: METHODOLOGY

The method of study primarily consists of specimen preparation, potting, hydration, and mechanical testing in the hexapod (Figure 3.1). Pilot testings were required to develop the testing protocol. Based on the result of pilot testings, the testing protocol was modified, and further mechanical testings were conducted repeatedly.

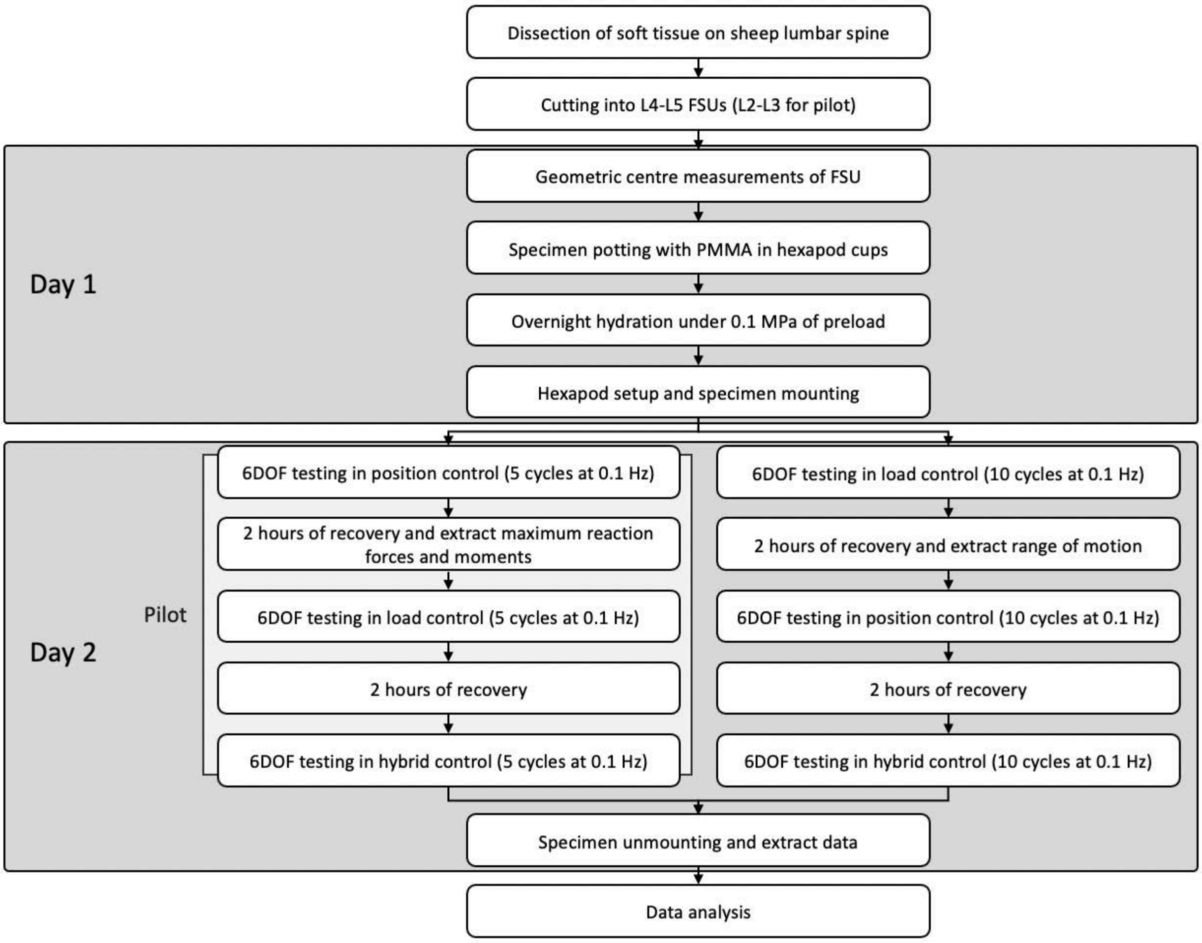

Figure 3.1 Flow chart of main steps of testing protocol

3.1 Specimen Preparation

Two sheep lumbar spines from the same lumbar column were used for the pilot testing. Five sheep lumbar spines were collected from Bamyan Supermarket (5/100 Philip Hwy, Elizabeth South SA 5112) stored in the freezer at -20°C (Table 3.1). The specimens are aged around 2 years and weigh around 20-25 kg of the same breed.

#	Date Collected	Species	Breed	Age	Weight (kg)	Level	Code
1	N/A	Sheep	N/A	N/A	N/A	L4-5	CM01
2	N/A	Sheep	N/A	N/A	N/A	L2-3	CM02
3	19-Aug-21	Sheep	Merino	2yo	20-25	L4-5	CM03
4	19-Aug-21	Sheep	Merino	2yo	20-25	L4-5	CM04
5	19-Aug-21	Sheep	Merino	2yo	20-25	L4-5	CM05
6	19-Aug-21	Sheep	Merino	2yo	20-25	L4-5	CM06
7	19-Aug-21	Sheep	Merino	2yo	20-25	L4-5	CM07

Table 3.1 List of the specimens used for the study. The code name was used for identifying different specimens.

3.1.1 Dissection

Before the dissection of soft tissue, the specimen needs to be put out of the freezer and thawed at room temperature three hours before the dissection. A scalpel and knife were used to remove unwanted muscles and ligaments. During the dissection, the damages on the disc were checked and excluded the specimens which have damages on the desired level of the disc. In this study, however, the damage was found on the specimen for the pilot test. The discs need to be visible while paying attention not to make any damage on the discs (Figure 3.2). Once the dissection is done, the specimen is kept in the freezer again covered by gauze soaked with saline and sealed in plastic bags.

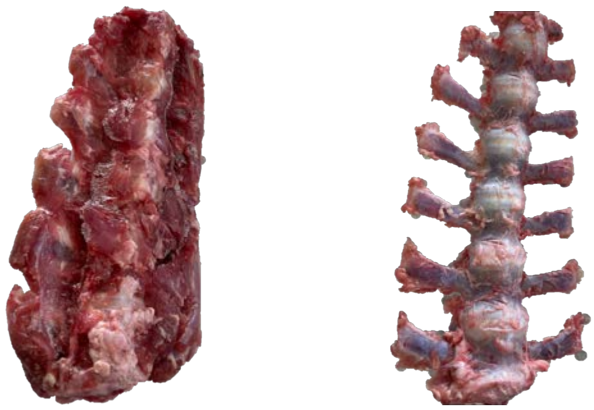

Figure 3.2 The sheep lumbar spine before the dissection (left) and after the dissection (right)

3.1.2 Cutting

Cutting the specimen into FSUs was followed by the dissection. The markings on the specimen were performed before cutting. Visible marks were drawn to indicate where to be cut and where to be kept by marker pens. The specimen was put out of the freezer and thawed at room temperature for three hours. The FSUs were obtained by cutting with a bandsaw machine. The superior and inferior vertebrae were cut parallel to the mid-transverse plane of the intervertebral disc. The height of the FSU must be over 60 mm to avoid failing during hexapod mechanical testings. The transverse processes were removed by cutting (Figure 3.3) and spinal cords were also removed. Each FSU was sealed in plastic bags with proper labels and kept in the freezer.

Figure 3.3 The specimen (FSU, L4-L5) after cutting

3.2 Specimen Potting

Potting is a procedure of fixing the specimen in stainless-steel top and bottom cups of the hexapod performed a day before the mechanical testing. Before potting, the specimen was placed at room temperature for thawing, and measurements of FSU height, superior and inferior vertebra height, the height of the disc, and the dimension of the vertebral end-plates were performed. The measurements of heights of FSU, superior and inferior vertebra, and disc were used to calculate the z-offset of the hexapod. The dimension of vertebral end-plates was calculated by measuring the anterior-posterior diameter and lateral diameter of both superior and inferior end-plates. From the dimension of the superior and inferior top vertebra, the disc area was calculated and used for obtaining preload, follower load, and reference load, equivalent to nucleus pressure of 0.1 MPa, 0.5 MPa, and 0.6 MPa respectively. Specimens were potted in the cup with polymethyl methacrylate (PMMA) which is made of a powder and liquid methyl methacrylate monomer. The ratio of powder to liquid is 2.5 mL to 1mL. The specimen is placed in the bottom cup aligning the centre of the disc and the cup. Once the specimen is positioned properly, the solution of PMMA is poured enough to cover the inferior vertebra, but not the disc. For the potting of the top cup, blocks (8.1 mm or 12.9 mm) were used for increasing the total height of the bottom cup-FSU-top cup to avoid failure of the disc during the hexapod mechanical testing. For the top cup, enough amount of PMMA was poured to cover the gap from blocks and superior vertebra to hold the specimen properly (Figure 3.4) (Appendix A).

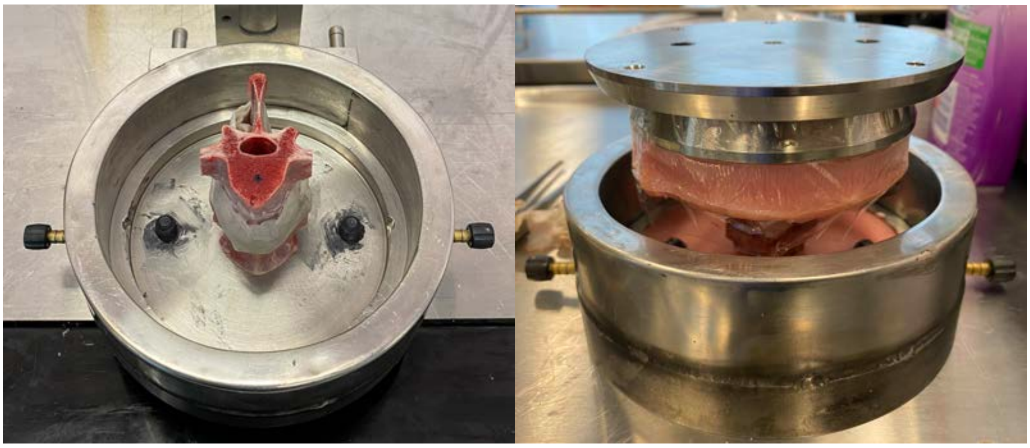

Figure 3.4 Alignment of the centre of the disc and the bottom cup and the disc covered with saline-soaked gauze (left) and completion of potting with the top and bottom cups (right)

3.3 Geometric Centre Measurement

The geometric centre of the specimen was measured after the bottom cup fixation with PMMA. The measurement was performed by measuring the distance between the inner ring of the bottom cup and the centre of the disc. Since the centre of the rotation of the specimen can vary depending on the size of the specimen as well as the position of the specimen in the cup, the hexapod uses offsets to generate movement according to the specimen's centre of rotation. Both x-axis and y-axis distances were measured, and x-offset and y-offset were calculated. The z-offset was obtained from the area of the disc (Section 3.2) (Appendix B).

3.4 Hydration and Preloading

To generate a physiological environment, the specimen was kept hydrated, and preload was applied to the specimen a day prior to the mechanical testing. Due to the viscoelastic properties, the specimens are temperature and hydration-dependent (Costi, Hearn & Fazzalari 2002; Pflaster et al. 1997; Race, Broom & Robertson 2000). Therefore, the specimens were immersed in a 0.15 M phosphate-buffered saline at room temperature throughout the testing (Costi et al. 2008). The specimen was subject to an axial compressive preload overnight (over 12 hours) before the mechanical testing. The preload is equivalent to a nucleus pressure of 0.1 MPa which represents the unloaded condition while sleeping to reach a steady-state of hydration equilibrium (Wilke et al. 1999).

3.5 Hexapod Testing

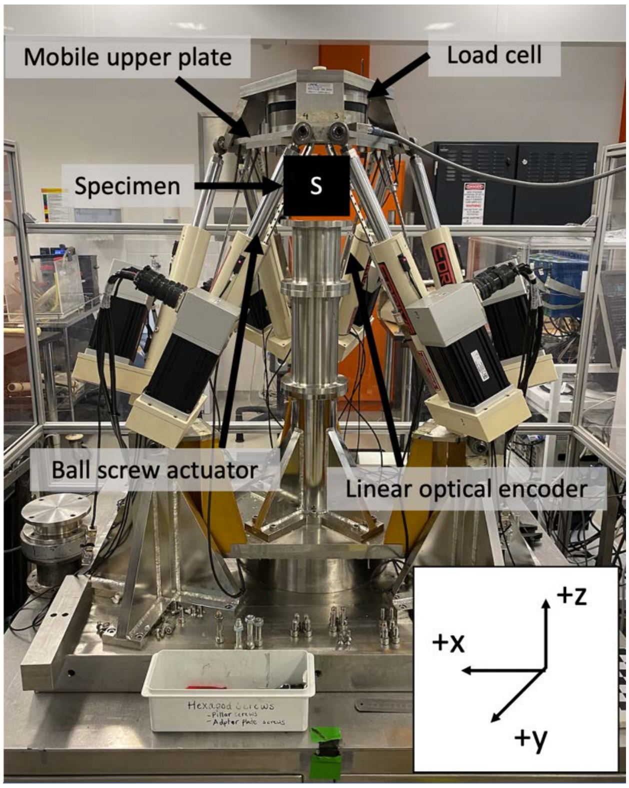

Figure 3.5 The hexapod robot with x, y, and z-axes displaying mobile upper plate, load cell, six ball screw actuators, and six linear optical encoders. Specimen sits on the base pillar as indicated 'S' in the black square.

The hexapod at Flinders University is a mechanical testing robot that can conduct 6DOF loadings based on the Stewart platform (Ding et al. 2014). The hexapod can generate not only single-axis movements but multi-axis displacement and rotations. The hexapod consists of a load cell on the top, a mobile upper plate, and a base pillar where the specimen is inserted in-between. The six ball screw actuators support the load cell which produces the required displacement or rotation. The top cup of the specimen was bolted into the mobile top plate and the bottom cup was bolted to the base pillar. The actuators drive the load cell while the base is fixed, thus the motion can be created to the specimen. Six linear optical encoders are attached to the actuators independently and encoders measure the displacements and rotations of the specimen. The position control was performed by setting the displacement or rotation of the desired axis while the other axes are controlled. The load control allows the specimen to move under pure forces or moments with real-time minimisation of other 5DoF coupling forces or moments. The hybrid control applies the displacement or rotation with minimisation of all off-axis coupling forces and moments.

3.5.1 Pilot Testing

To ensure the testing protocol could meet the aim of the study, pilot testing was conducted in the hexapod. The order of control modes was determined as position control, load control, and hybrid control. 6DOF loadings were applied in each control mode in order of shear, axial rotation, lateral bending, flexion, extension, and compression to minimise the biphasic effect (Costi et al. 2008). A compressive axial follower preload (Patwardhan et al. 1999) was applied to all 6DOF load tests equivalent to a nucleus pressure of 0.5 MPa which represents a relaxed standing load (Wilke et al. 1999). This allows to minimise all off-axis force and moments to zero (Amin et al. 2016).

Under position control, the specimen was subjected to dynamic haversine displacements /rotations in each DOF while in the other 5DOF coupling displacements/rotations were constrained. The displacement amplitudes were applied as: ±0.6 mm for shear tests, ±2° for axial rotation, ±3° for lateral bending, 5° for flexion, 2° for extension, and 0.3mm for compression (Costi et al. 2008) (Figure 3.6). For each DOF, five cycles of dynamic haversine were applied at 0.1Hz, followed by a compressive creep recovery at 0.1MPa equivalent nucleus pressure for two minutes.

From the position control, the maximum reaction forces and moments of the final cycle were extracted and applied to each 6DOF testings in load control mode. The maximum reaction forces and moments were obtained in MATLAB by detecting the maximum value of the final cycle in a load-displacement curve (Figure 3.7). Load control testings were conducted as applied input loads while off-axis forces and moments were minimised via real-time load control (Lawless et al. 2014).

Under hybrid control, the same amplitudes of displacements/rotations were applied to the specimen as in position control while minimising off-axis forces and moments to zero as a combination of position control and load control. Two hours of recovery were conducted between control modes (Figure 3.6).

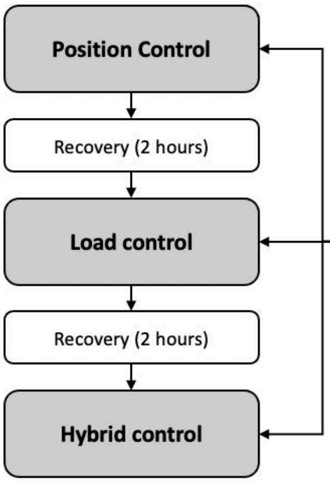

< Sequence of 6DOF loadings >

1	-Tx	-0.6 mm	Left Lateral Shear
2	+Tx	+0.6 mm	Right Lateral Shear
3	-Ty	-0.6 mm	Posterior Shear
4	+Ty	+0.6 mm	Anterior Shear
5	+Rz	+2°	Left Axial Rotation
6	-Rz	-2°	Right Axial Rotation
7	-Ry	-3°	Left Lateral Bending
8	+Ry	+3°	Right Lateral Bending
9	-Rx	-5°	Flexion
10	+Rx	+2°	Extension
11	-Tz	-0.3 mm	Axial Compression

Figure 3.6 Testing protocol and the sequence of 6DOF loadings for each control mode

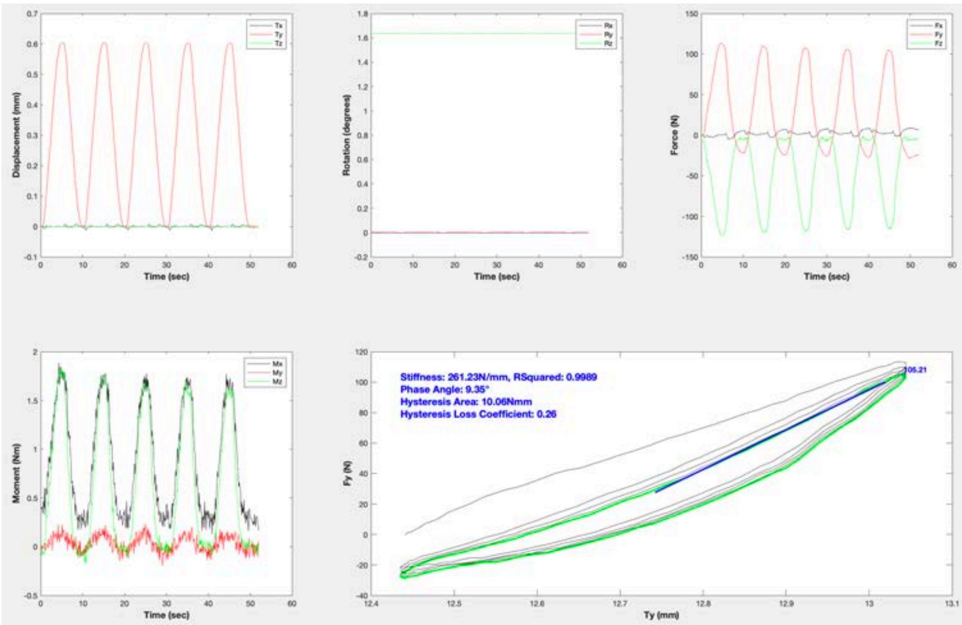

Figure 3.7 Plot of anterior shear test from MATLAB displaying 6DOF plots of displacement, rotation, force, and moment according to time, and a load-displacement curve highlighting final cycle in green with stiffness, phase angle, hysteresis area, and hysteresis coefficient

Specimen CM01 and CM02 (Table 3.1) were subjected to the pilot testings. The data was extracted from the hexapod host computer and converted with LabView. The converted data was processed with MATLAB plotting 6DOF graphs of displacement, rotation, force, and moment according to time, and load-displacement curves with stiffness, phase angle, hysteresis area, hysteresis coefficient, and maximum reaction forces/moments of the final cycle (Figure 3.7) (Appendix C).

3.5.2 Pilot Testing Result

The result from CM01 and CM02 showed that the maximum reaction forces/moment under load control was not able to reach the input load obtained from position control (Figure 3.8) (Appendix D.1, Appendix D.2). Therefore, CM02 was subjected to another testing with 10 cycles at 0.1Hz for each 6DOF load to ensure the hexapod has sufficient time to condition for producing movement as desired loads. The displacement amplitude of flexion was changed to 7° due to the low maximum reaction moments obtained from hybrid control (Appendix D.3). However, with 10 cycles, the result was still not able to reach the same level of input load under load control (Figure 3.8).

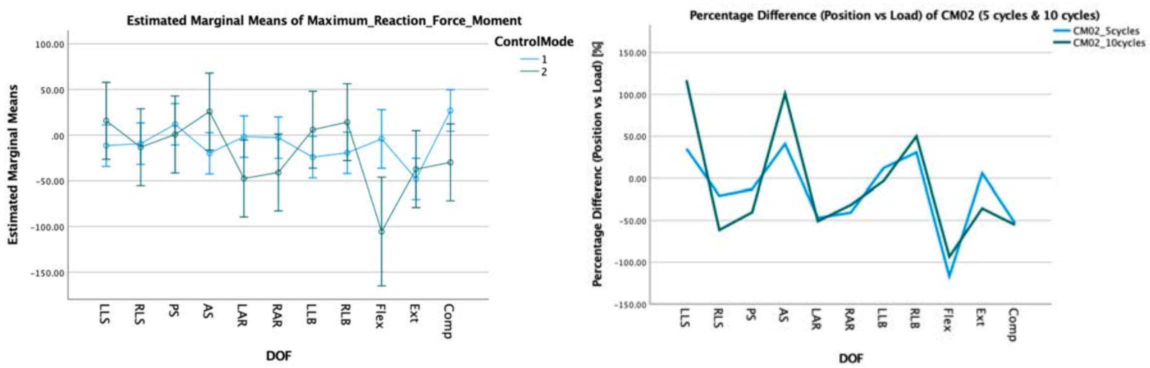

Figure 3.8 Mean (95% CI) percentage difference of maximum reaction forces/moments (ControlMode 1: position control vs load control, ControlMode 2: position control vs hybrid control) from CM01 and CM02 displaying the maximum reaction forces/moments under load control undershoot compared to position control except for PS and Comp (ControlMode1) [Left]. Percentage difference of maximum reaction forces/moments from CM02 with 5 cycles and 10 cycles. The plot indicates load control with 10 cycles undershoot the maximum reaction forces/moments in RLS, PS, LAR, RAR, LLB, Flex, Ext, and Comp compared to position control [Right] Note: LLS=left lateral shear, RLS=right lateral shear, PS=posterior shear, AS=anterior shear, LAR=left axial rotation, RAR=right axial rotation, LLB=left lateral bending, RLB=right lateral bending, Flex=flexion, Ext=extension, and Comp=compression.

3.5.3 Testing

The testing protocol was changed in order of load control, position control, and hybrid control. The sequence of the 6DOF loading remained the same as the pilot test while the amplitude of forces/moments applied as; ±200 N for shear tests, ±5 Nm for axial rotation, lateral bending, flexion, and extension. For compression, an equivalent nucleus pressure of 1.1 MPa was applied (Amin et al. 2016). The ranges of motion under applied forces/moments were extracted and applied to position control and hybrid control. Five sheep lumbar FSUs (L4-L5) were subjected to the tests.

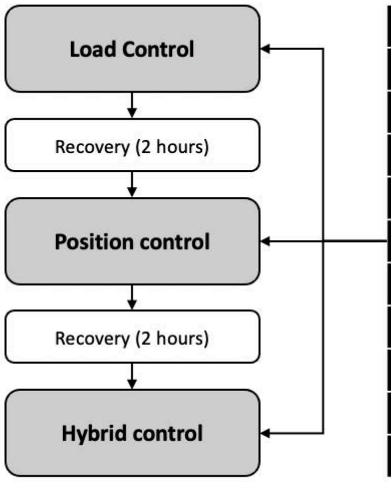

< Sequence of 6DOF loadings >

1	-Tx	-200 N	Left Lateral Shear
2	+Tx	+200 N	Right Lateral Shear
3	-Ty	-200 N	Posterior Shear
4	+Ty	+200 N	Anterior Shear
5	+Rz	+5 Nm	Left Axial Rotation
6	-Rz	-5 Nm	Right Axial Rotation
7	-Ry	+5 Nm	Left Lateral Bending
8	+Ry	-5 Nm	Right Lateral Bending
9	-Rx	+5 Nm	Flexion
10	+Rx	-5 Nm	Extension
11	-Tz	1.1 MPa	Axial Compression

Figure 3.9 Final testing protocol and the sequence of 6DOF loadings for each control mode

3.6 Data and Statistical Analysis

The data from hexapod were converted with LabView and processed with MATLAB plotting 6DOF graphs and load-displacement curves and calculating mechanical properties as described previously (Figure 3.7). The stiffness was calculated as 70-90% of the maximum reaction forces/moments from the last loading cycle (Appendix C).

Two-way repeated-measures ANOVA was performed on each of the outcome measures of stiffness, phase angle, hysteresis area, hysteresis loss coefficient, and maximum reaction forces/ moments, having two within-subjects factors of control modes and 6DOF loadings ($p < 0.05$ significant) (Appendix F.1). Pairwise comparisons using Bonferroni adjustment were performed in each 6DOF loadings between the control modes (Appendix F.2). Finally, the mean percentage differences were compared between load vs position and load vs hybrid as well as between hybrid vs load and hybrid vs position (Appendix G, Appendix H).

CHAPTER 4: RESULTS

No specimens were excluded from the analysis and there was no evidence of tissue putrefaction or slippage of specimens during testing. All the outcome measures of 6DOF loadings from five specimens (n=5) were calculated and included for percentage differences for left lateral bending from CM05 (n=4) (Appendix E.1, Appendix E.2, Appendix E.3, Appendix E.4, Appendix E.5). The hexapod batch file of left lateral bending under position control was overwritten as right lateral bending, thus left lateral bending was not conducted on specimen CM05. Therefore, the statistical analysis contains the outcome measures from CM03, CM04, CM06, and CM07 (n=4) (Appendix F.1, Appendix F.2).

4.1 Stiffness

The overall main effects of control mode ($p < 0.001$), 6DOF loading ($p < 0.001$), and the interaction of control mode*6DOF loading ($p < 0.001$) were significant for stiffness. Significant pairwise differences for stiffness were found between load control and position control in right lateral bending ($p = 0.003$), flexion ($p = 0.028$), and compression ($p = 0.04$), and between load control and hybrid control in right lateral bending ($p = 0.003$), flexion ($p = 0.031$), and compression ($p = 0.038$) (Figure 4.1).

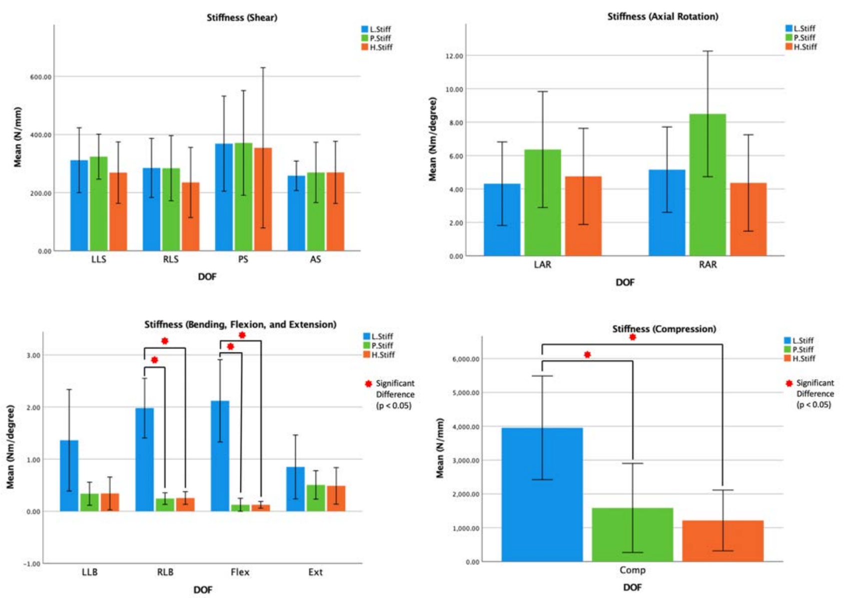

Figure 4.1 Mean (95% CI) comparison of stiffness with L.Stiff for stiffness under load control, P.Stiff for stiffness under position control, and H.Stiff for stiffness under hybrid control

The differences between mean (95% CI) percentage differences of load control to position control and that of load control to hybrid control showed greater in left lateral shear, right lateral shear, left axial rotation, and right axial rotation ($> 10\%$) than other directional loadings (Figure 4.2).

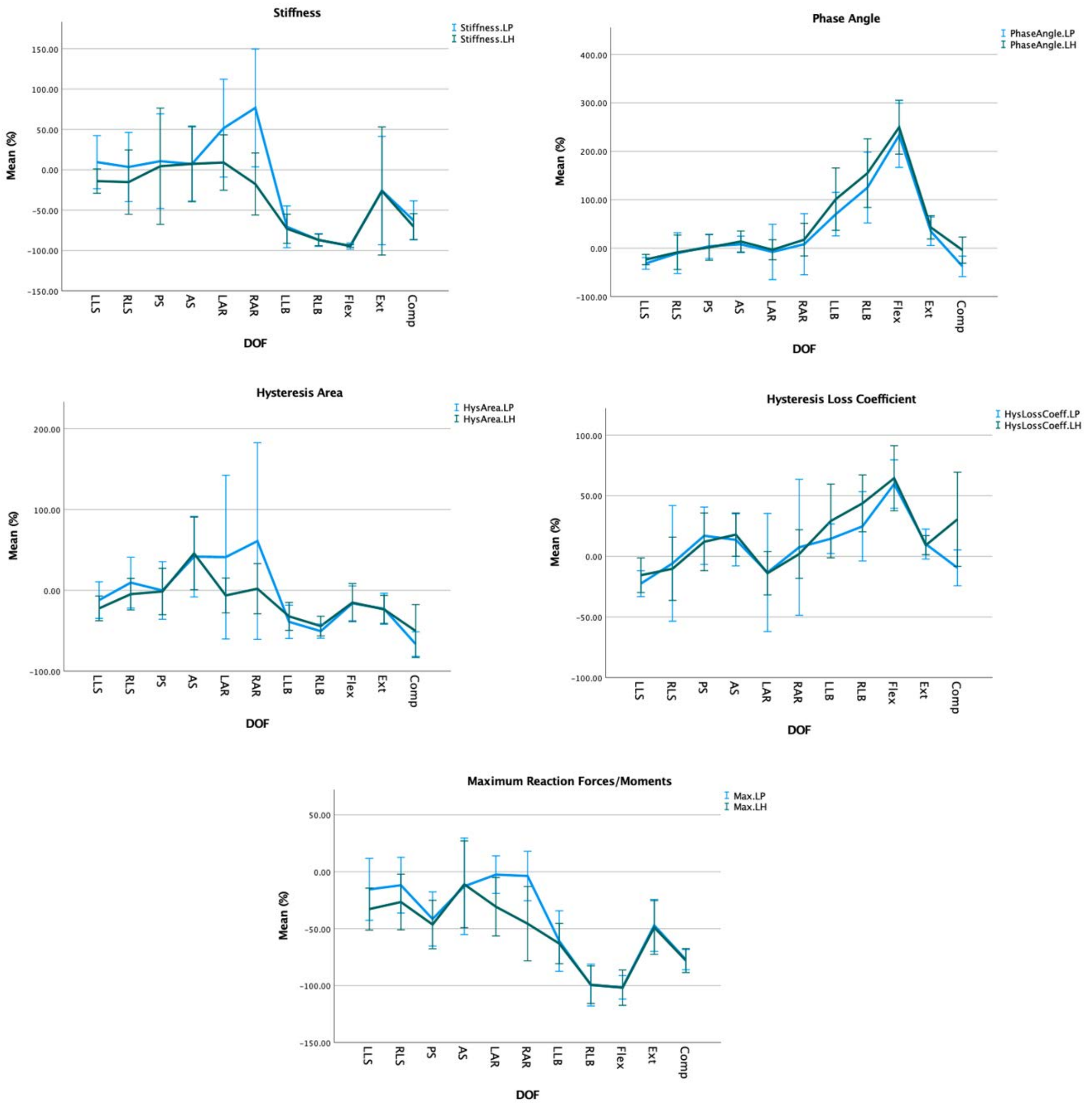

Figure 4.2 Mean (95% CI) percentage differences of load control to position control (LP, blue line) and load control to hybrid control (LH, green line) in stiffness, phase angle, hysteresis area, hysteresis loss coefficient, and maximum reaction forces/moments

4.2 Phase Angle

For phase angle, the overall main effects of control mode ($p < 0.001$), 6DOF loading ($p < 0.001$), and the interaction of control mode*6DOF loading ($p < 0.001$) were significant.

There were significant pairwise differences for phase angle found between load control and position control in left lateral bending ($p = 0.036$) and flexion ($p = 0.008$), and between load control and hybrid control in left lateral bending ($p = 0.039$), right lateral bending ($p = 0.028$), and flexion ($p = 0.003$). The differences between mean (95% CI) percentage differences of load control to position control and that of load control to hybrid control showed greater in left lateral bending, right lateral bending, flexion, and compression ($> 10\%$) than other directional loadings (Figure 4.2).

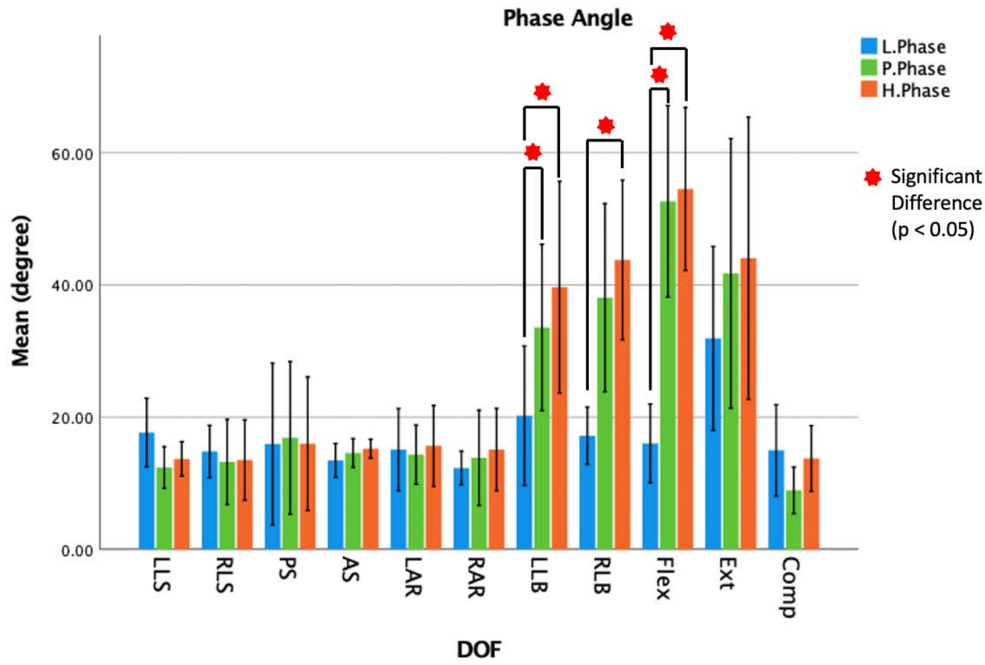

Figure 4.3 Mean (95% CI) comparison of phase angle with L.Phase for phase angle under load control, P.Phase for phase angle under position control, and H.Phase for phase angle under hybrid control

4.3 Hysteresis Area

The overall main effects of 6DOF loading ($p < 0.001$) and the interaction of control mode *6DOF loading ($p = 0.004$) were significant for hysteresis area. The overall main effects of control mode were not significant ($p = 0.805$). There were significant pairwise differences for hysteresis area found between load control and position control in left lateral bending ($p = 0.042$), right lateral bending ($p = 0.003$), and compression ($p = 0.035$), between load control and hybrid control in left lateral bending ($p = 0.04$) and right lateral bending ($p = 0.006$), and between position control and hybrid control in right lateral bending ($p = 0.02$). The greater differences between mean (95% CI) percentage differences of load control to position control and that of load control to hybrid control were found in left lateral shear, right lateral shear, left axial rotation, right axial rotation, and compression ($> 10\%$) than other directional loadings (Figure 4.2).

4.4 Hysteresis Loss Coefficient

For hysteresis loss coefficient, the overall main effects of control mode ($p = 0.004$), 6DOF loading ($p < 0.001$), and the interaction of control mode*6DOF loading ($p < 0.001$) were significant. There were significant pairwise differences for hysteresis loss coefficient found only in flexion between load control and position control ($p = 0.008$) and between load control and hybrid control ($p = 0.018$). The greater differences between mean (95% CI) percentage differences of load control to position control and that of load control to hybrid control were found in left lateral bending, right lateral bending, and compression ($> 10\%$) than other directional loadings (Figure 4.2).

4.5 Maximum Reaction Forces/Moments

The overall main effects of control mode ($p < 0.001$), 6DOF loading ($p < 0.001$), and the interaction of control mode*6DOF loading ($p < 0.001$) were significant for maximum reaction forces/moments. There were significant pairwise differences for maximum reaction forces/moments found between load control and position control in left lateral bending ($p = 0.027$), right lateral bending ($p = 0.005$), flexion ($p < 0.001$), and compression ($p = 0.001$), between load control and hybrid control in left axial rotation ($p = 0.031$), left lateral bending ($p = 0.011$), right lateral bending ($p = 0.003$), flexion ($p < 0.001$), and compression ($p = 0.001$), and between position control and hybrid control in right axial rotation ($p = 0.022$). The differences between mean (95% CI) percentage differences of load control to position control and that of load control to hybrid control showed greater in left lateral shear, right lateral shear, left axial rotation, and right axial rotation ($> 10\%$) than other directional loadings (Figure 4.2).

CHAPTER 5: DISCUSSION

5.1 Comparison of Mechanical Properties

The result identified differences in mechanical properties between control modes. The overall within-subjects effects revealed the first hypothesis of the study that there were significant differences in all mechanical properties between load, position, and hybrid control. The major differences were observed in the bending, flexion, extension, and compression motion of spine segments. In these directional loadings, the stiffness and energy absorption which can be interpreted by hysteresis area were significantly low under load control compared to those under both position and hybrid control as the second hypothesis. This may be induced by the sequence of testing, cumulative creep from the constant application of a follower load during the testing, and/or control system of the hexapod.

The testing sequence was adopted from a previous study to minimise the biphasic effect of the specimen (Costi et al. 2008). Conducting the viscoelastic directions before the poroelastic directions were expected to produce the least cumulative impact from fluid flow (Amin et al. 2016). The shear tests were not expected to generate a fluid transfer, however, the sequence of the 6DOF loading would have impacted the outcome measures as the steep decline was found between axial rotation and bending (Figure 4.1).

Under the motion of bending, flexion, extension, and compression, the fluid flow of the disc was more involved due to the volume change compared to under shear motions. This would result in significant differences under those directions causing cumulative creep. The creep recovery may increase the stiffness by reducing disc height and exerting fluid (Amin et al. 2016). Therefore, the change of disc height may result in exhibiting higher stiffness at later directional tests.

The major factor of the study was to conduct three different control modes as the study desired. To achieve the aims of the study, changes have been made to the functions of the hexapod's control system throughout the study. The adaptive tuning function was applied to the overnight hydration to ensure the specimen undergoes the overnight loading as its natural reactions against it. To allow the specimen to find its neutral position, the function that constrains all the axes except for Tz was applied. Due to the current setting of the control system, the start displacement/rotation points were not able to be changed. The major differences in starting point were found under bending, flexion, extension, and compression. In position and hybrid control, the starting points were different from load control, and this may result in different motion paths although the same amplitudes of range of motion were applied. The adaptive tuning was applied to all control modes, however, load control only used adaptive tuning for the first four cycles and fixed its stiffness after on. This may result in producing undesired outcomes as it would not "pure" load control with fixed control.

Other factors might cause differences in outcome measures such as the potting the specimen and inserting procedure of specimen into the hexapod. The potting was performed and measured offsets by hand, therefore, there should be human errors introduced. The number of bolts was used to assemble base pillars and install the specimen potted in the cup, thus some differences could be made due to the unbalanced forces from bolt screwing. The procedure has changed during the study that the bolts between the mobile top plate and load cell must be screwed with a torque wrench.

5.2 Assessing Physiological Relevance

The study hypothesized that hybrid control would provide a better indication of spinal movement. With a given displacement/rotation in position control, the magnitude of loads would vary along the spine segment because of the off-axis coupling forces/moments and the variation of displacement, zero at the base and desired value at the top (Goel et al. 1995). Another limitation of position control is that it is difficult to obtain desired outcomes with extremely stiff specimens. Load control seems to be a more proper experiment for the spine segment, it also has a limitation that it can produce false results due to the transition of the movement under load control. The response flexion loading can be altered due to the application of compressive force (Panjabi et al. 1977). This may result in miscalculation of the outcomes while compression reduces the stiffness of the specimen (Goel et al. 1995). Therefore, the study investigated comparisons of hybrid control to load control, and hybrid control to position control (Appendix H).

The result showed that there were greater differences between the mean percentage difference of hybrid control to load control and hybrid control to position control; right axial rotation, left lateral bending, right lateral bending, flexion, extension, and compression in stiffness ($> 100\%$), left lateral shear, left lateral bending, right lateral bending, flexion, extension, and compression ($> 20\%$) (Figure 5.1).

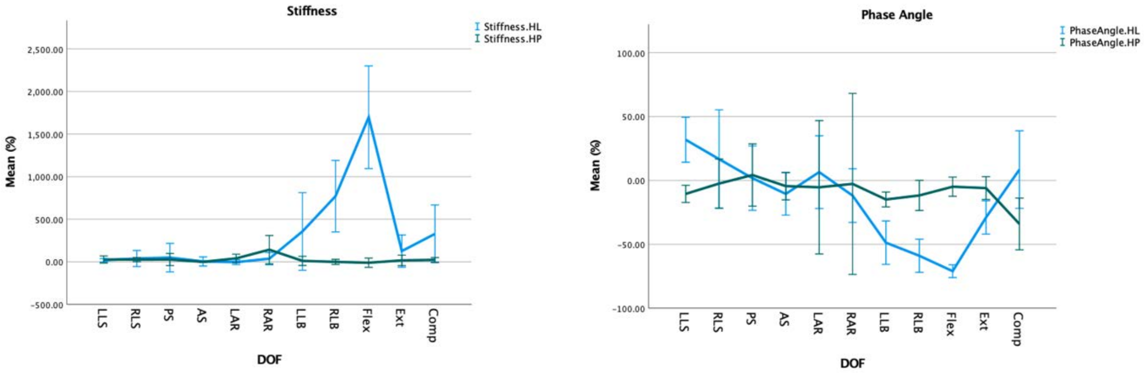

Figure 5.1 Mean (95% CI) percentage differences of hybrid control to load control (HL, blue line) and hybrid control to position control (HP, green line) in stiffness and phase angle

However, the outcome measures of stiffness under hybrid in those directional loadings were too small (> 1 N/mm) to provide an appropriate comparison. Therefore, it is yet difficult to clarify which control mode represents more-physiological spinal movement.

CHAPTER 6: CONCLUSIONS AND FUTURE WORK

6.1 Conclusion

The study developed a testing protocol to compare the outcomes between position control, load control, and hybrid control. The testing protocol was conducted in order of load control, position control, and hybrid control. The ranges of motion were extracted from load control testing and applied to position and hybrid control testings. This provided a better comparison between control modes in shears, but the maximum reaction forces/moments were still not able to reach the input loads in bending, flexion, extension, and compression.

With the test protocol, the study identified differences in mechanical properties between the control modes. Five specimens were subjected to the 11 directional loadings with 5 cycles at 0.1 Hz. Significant differences were found in bending, flexion, extension, and compression supporting a previous study (Amin et al. 2016). This may be attributed to the 6DOF loading sequence, cumulative creep, and the hexapod control system. Due to the different fluid involvement of discs under different directions of loadings, the result exhibited significant differences under the directional motions that cause the change of disc height and fluid excursion. The hexapod control system contributed significantly to the overall testing protocol. There was a different application of adaptive tuning between the control modes, and possible human errors during potting and inserting specimens on the hexapod.

The comparisons of hybrid control to load control and position control displayed differences in lateral shear, bending, flexion, extension, and compression. The study hypothesised that the hybrid control would provide a better demonstration of *in-vivo* like spinal movement, however, there should be more studies and testings followed to assess physiological relevance between the control modes.

There are some limitations from this study that need to be considered. The frequency of each 6DOF loading was fixed at 0.1Hz. The different frequencies would make different outcomes as the specimens have time-dependent viscoelastic properties. The number of specimens also needs to be considered because the sample size of N=5 FSUs would not be reasonable. Due to the limitations of the hexapod control system, it is suggested to develop a function that can control the start point of each directional loadings to obtain an appropriate comparison of motions under different control modes.

6.2 Future Work

Further work is required to develop a testing protocol that can compare mechanical properties more accurately by creating a function of “ramp” the starting point. Due to the different starting points of each control mode, the motion paths showed significantly different stiffness and energy absorption. By ramping up/down the starting point under position and hybrid control to the same level as under load control, it is expected that the outcome provides more similar motion paths between the control modes. This will provide a clue of assessing physiological relevance between position control, load control, and hybrid control.

Different frequency of 6DOF testings needs to be conducted and compared. The study only provided an outcome of 0.1Hz, therefore, testings at lower frequencies would be reasonable to conduct to avoid specimen failure by applying higher loading frequencies.

This study is continuing with intention of publication in 2022. The author is currently being participated in the extension of the thesis study. The “ramp” function is being developed and the testings at 0.01Hz were conducted in flexion. Another directional testing at 0.01Hz will be conducted and data will be compared.

References

Adams, M 2013, *The biomechanics of back pain*, 3rd ed. edn, Edinburgh Scotland : Chucrchill Livingstone/ Elsevier, Edinburgh [Scotland].

Adams, MA & Hutton, WC 1983, 'The mechanical function of the lumbar apophyseal joints', *Spine (Phila Pa 1976)*, vol. 8, no. 3, pp. 327-30.

Adams, P & Muir, H 1976, 'Qualitative changes with age of proteoglycans of human lumbar discs', *Ann Rheum Dis*, vol. 35, no. 4, pp. 289-96.

Amin, DB, Lawless, IM, Sommerfeld, D, Stanley, RM, Ding, B & Costi, JJ 2016, 'The Effect of Six Degree of Freedom Loading Sequence on the In-Vitro Compressive Properties of Human Lumbar Spine Segments', *J Biomech*, vol. 49, no. 14, pp. 3407-14.

Beard, HK & Stevens, R 1980, 'Biochemical changes in the intervertebral disc', *The lumbar spine and back pain. Second ed. London: Pitman Medical*, pp. 407-36.

Bogduk, N 1997, *Clinical anatomy of the lumbar spine and sacrum*, 3rd ed. edn, New York : Churchill Livingstone, New York.

Buckwalter, JA, Cooper, R & Maynard, J 1976, 'Elastic fibers in human intervertebral discs', *The Journal of bone and joint surgery. American volume*, vol. 58, no. 1, pp. 73-6.

Bushell, G, Ghosh, P, Taylor, T & Akeson, W 1977, 'Proteoglycan chemistry of the intervertebral disks', *Clinical Orthopaedics and Related Research (1976-2007)*, vol. 129, pp. 115-23.

Callaghan, JP & McGill, SM 1995, 'Muscle activity and low back loads under external shear and compressive loading', *Spine (Phila Pa 1976)*, vol. 20, no. 9, pp. 992-8.

Cassidy, J, Hiltner, A & Baer, E 1989, 'Hierarchical structure of the intervertebral disc', *Connective tissue research*, vol. 23, no. 1, pp. 75-88.

Chang, T-S, Chang, J-H & Cheng, C-W 2011, 'A pure moment based tester for spinal biomechanics', *Biomechanics in applications*, p. 205.

Costi, JJ, Hearn, TC & Fazzalari, NL 2002, 'The effect of hydration on the stiffness of intervertebral discs in an ovine model', *Clin Biomech (Bristol, Avon)*, vol. 17, no. 6, pp. 446-55.

Costi, JJ, Stokes, IA, Gardner-Morse, MG & Iatridis, JC 2008, 'Frequency-Dependent Behavior of the Intervertebral Disc in Response to Each of Six Degree of Freedom Dynamic Loading : Solid Phase and Fluid Phase Contributions', *Spine (Phila Pa 1976)*, vol. 33, no. 16, pp. 1731-8.

Coventry, MB, Ghormley, RK & Kernohan, JW 1945, 'The intervertebral disc: Its microscopic anatomy and pathology: Part I. Anatomy, development, and physiology', *JBJS*, vol. 27, no. 1, pp. 105-12.

Dickson, I, Happey, F, Pearson, C, Naylor, A & Turner, R 1967, 'Variations in the protein components of human intervertebral disk with age', *Nature*, vol. 215, no. 5096, pp. 52-3.

Ding, B, Cazzolato, BS, Stanley, RM, Grainger, S & Costi, JJ 2014, 'Stiffness analysis and control of a stewart platform-based manipulator with decoupled sensor–actuator locations for ultrahigh accuracy positioning under large external loads', *Journal of Dynamic Systems, Measurement, and Control*, vol. 136, no. 6, p. 061008.

Freudiger, S, Dubois, G & Lorrain, M 1999, 'Dynamic neutralisation of the lumbar spine confirmed on a new lumbar spine simulator in vitro', *Arch Orthop Trauma Surg*, vol. 119, no. 3, pp. 127-32.

Goel, VK, Wilder, DG, Pope, MH & Edwards, WT 1995, 'Controversy Biomechanical Testing of the Spine: Load-Controlled Versus Displacement-Controlled Analysis', *Spine (Philadelphia, Pa. 1976)*, vol. 20, no. 21, pp. 2354-7.

Gower, WE & Pedrini, V 1969, 'Age-related variations in proteinpolysaccharides from human nucleus pulposus, annulus fibrosus, and costal cartilage', *JBJS*, vol. 51, no. 6, pp. 1154-62.

Hickey, D & Hukins, D 1981, 'Collagen fibril diameters and elastic fibres in the annulus fibrosus of human fetal intervertebral disc', *Journal of anatomy*, vol. 133, no. Pt 3, p. 351.

Inoue, H 1981, 'Three-dimensional architecture of lumbar intervertebral discs', *Spine*, vol. 6, no. 2, pp. 139-46.

Johnson, E, Berryman, H, Mitchell, R & Wood, W 1985, 'Elastic fibres in the anulus fibrosus of the adult human lumbar intervertebral disc. A preliminary report', *Journal of anatomy*, vol. 143, p. 57.

Keyes, DC & Compere, EL 1932, 'The normal and pathological physiology of the nucleus pulposus of the intervertebral disc: an anatomical, clinical, and experimental study', *JBJS*, vol. 14, no. 4, pp. 897-938.

Kim, J, Yang, S-J, Kim, H, Kim, Y, Park, JB, DuBose, C & Lim, T-H 2012, 'Effect of Shear Force on Intervertebral Disc (IVD) Degeneration: An In Vivo Rat Study', *Ann Biomed Eng*, vol. 40, no. 9, pp. 1996-2004.

Koeller, W, Muehlhaus, S, Meier, W & Hartmann, F 1986, 'Biomechanical properties of human intervertebral discs subjected to axial dynamic compression—Influence of age and degeneration', *J Biomech*, vol. 19, no. 10, pp. 807-16.

Kraemer, J, Kolditz, D & Gowin, R 1985, 'Water and electrolyte content of human intervertebral discs under variable load', *Spine (Phila Pa 1976)*, vol. 10, no. 1, pp. 69-71.

Lawless, IM, Ding, B, Cazzolato, BS & Costi, JJ 2014, 'Adaptive velocity-based six degree of freedom load control for real-time unconstrained biomechanical testing', *J Biomech*, vol. 47, no. 12, pp. 3241-7.

Leahy, JC & Hukins, DWL 2001, 'Viscoelastic properties of the nucleus pulposus of the intervertebral disk in compression', *J Mater Sci Mater Med*, vol. 12, no. 8, pp. 689-92.

Lu, WW, Luk, KDK, Holmes, AD, Cheung, KMC & Leong, JCY 2005, 'Pure shear properties of lumbar spinal joints and the effect of tissue sectioning on load sharing', *Spine (Phila Pa 1976)*, vol. 30, no. 8, pp. E204-E9.

Lu, YM, Hutton, WC & Gharpuray, VM 1996, 'Can variations in intervertebral disc height affect the mechanical function of the disc?', *Spine (Phila Pa 1976)*, vol. 21, no. 19, pp. 2208-16.

Macintosh, JE, Pearcy, MJ & Bogduk, N 1993, 'THE AXIAL TORQUE OF THE LUMBAR BACK MUSCLES: TORSION STRENGTH OF THE BACK MUSCLES', *Aust N Z J Surg*, vol. 63, no. 3, pp. 205-12.

Marchand, F & Ahmed, AM 1990, 'Investigation of the laminate structure of lumbar disc anulus fibrosus', *Spine*, vol. 15, no. 5, pp. 402-10.

Marras, WS, Davis, KG, Ferguson, SA, Lucas, BR & Gupta, P 2001, 'Spine loading characteristics of patients with low back pain compared with asymptomatic individuals', *Spine (Phila Pa 1976)*, vol. 26, no. 23, pp. 2566-74.

McGill, SM 1992, 'THE INFLUENCE OF LORDOSIS ON AXIAL TRUNK TORQUE AND TRUNK MUSCLE MYOELECTRIC ACTIVITY', *Spine (Phila Pa 1976)*, vol. 17, no. 10, pp. 1187-93.

McNally, D & Adams, MA 1992, 'Internal intervertebral disc mechanics as revealed by stress profilometry', *Spine*, vol. 17, no. 1, pp. 66-73.

Melrose, J & Ghosh, P 2019, 'The noncollagenous proteins of the intervertebral disc', in *The biology of the intervertebral disc*, CRC Press, pp. 189-237.

Morris, FL, Smith, RM, Payne, WR, Galloway, MA & Wark, JD 2000, 'Compressive and shear force generated in the lumbar spine of female rowers', *Int J Sports Med*, vol. 21, no. 7, pp. 518-23.

NAYLOR, A 1976, 'Intervertebral disc prolapse and degeneration: the biochemical and biophysical approach', *Spine*, vol. 1, no. 2, pp. 108-14.

Newell, N, Little, JP, Christou, A, Adams, MA, Adam, C & Masouros, S 2017, 'Biomechanics of the human intervertebral disc: a review of testing techniques and results', *Journal of the mechanical behavior of biomedical materials*, vol. 69, pp. 420-34.

O'Connell, GD, Jacobs, NT, Sen, S, Vresilovic, EJ & Elliott, DM 2011, 'Axial creep loading and unloaded recovery of the human intervertebral disc and the effect of degeneration', *J Mech Behav Biomed Mater*, vol. 4, no. 7, pp. 933-42.

Panjabi, MM, Crisco, JJ, Vasavada, A, Oda, T, Cholewicki, J, Nibu, K & Shin, E 2001, 'Mechanical properties of the human cervical spine as shown by three-dimensional load-displacement curves', *Spine (Phila Pa 1976)*, vol. 26, no. 24, pp. 2692-700.

Panjabi, MM, Krag, MH & Goel, VK 1981, 'A technique for measurement and description of three-dimensional six degree-of-freedom motion of a body joint with an application to the human spine', *J Biomech*, vol. 14, no. 7, pp. 447,51-9,60.

Panjabi, MM, Krag, MH, White III, AA & Southwick, WO 1977, 'Effects of preload on load displacement curves of the lumbar spine', *Orthopedic Clinics of North America*, vol. 8, no. 1, pp. 181-92.

Pascual, SR, Keogh, P, Miles, A & Gheduzzi, S 2016, 'A Comparison of Testing Protocols for the Evaluation of Spinal Biomechanics', in *TransMed Student Conference 2016*.

Patwardhan, AG, Havey, RM, Meade, KP, Lee, B & Dunlap, B 1999, 'A follower load increases the load-carrying capacity of the lumbar spine in compression', *Spine (Phila Pa 1976)*, vol. 24, no. 10, pp. 1003-9.

Pearcy, MJ & Tibrewal, SB 1984, 'Axial rotation and lateral bending in the normal lumbar spine measured by three-dimensional radiography', *Spine (Phila Pa 1976)*, vol. 9, no. 6, pp. 582-7.

Pflaster, DS, Krag, MH, Johnson, CC, Haugh, LD & Pope, MH 1997, 'Effect of test environment on intervertebral disc hydration', *Spine (Phila Pa 1976)*, vol. 22, no. 2, pp. 133-9.

Potvin, JR, Norman, RW & McGill, SM 1991, 'Reduction in anterior shear forces on the [formula omitted] disc by the lumbar musculature', *Clinical biomechanics (Bristol)*, vol. 6, no. 2, pp. 88-96.

Race, A, Broom, ND & Robertson, P 2000, 'Effect of loading rate and hydration on the mechanical properties of the disc', *Spine (Phila Pa 1976)*, vol. 25, no. 6, pp. 662-9.

Reid, JE, Meakin, JR, Robins, SP, Skakle, JMS & Hukins, DWL 2002, 'Sheep lumbar intervertebral discs as models for human discs', *Clin Biomech (Bristol, Avon)*, vol. 17, no. 4, pp. 312-4.

Roberts, S, Menage, J & Urban, J 1989, 'Biochemical and structural properties of the cartilage end-plate and its relation to the intervertebral disc', *Spine*, vol. 14, no. 2, pp. 166-74.

Schmorl, G 1971, 'The human spine in health and disease', in *The human spine in health and disease*, pp. xi, 504-xi, .

Skipor, AF, Miller, JAA, Spencer, DA & Schultz, AB 1985, 'Stiffness properties and geometry of lumbar spine posterior elements', *J Biomech*, vol. 18, no. 11, pp. 821-30.

Stokes, IAF 1987, 'Surface strain on human intervertebral discs', *J. Orthop. Res*, vol. 5, no. 3, pp. 348-55.

Taylor, J 1990, 'The development and adult structure of lumbar intervertebral discs', *J Man Med*, vol. 5, pp. 43-7.

Taylor, T & Little, K 1965, 'Intercellular matrix of the intervertebral disk in ageing and in prolapse', *Nature*, vol. 208, no. 5008, pp. 384-6.

Wilke, HJ, Claes, L, Schmitt, H & Wolf, S 1994, 'A universal spine tester for in vitro experiments with muscle force simulation', *Eur Spine J*, vol. 3, no. 2, pp. 91-7.

Wilke, HJ, Kettler, A, Wenger, KH & Claes, LE 1997, 'Anatomy of the sheep spine and its comparison to the human spine', *The Anatomical Record: An Official Publication of the American Association of Anatomists*, vol. 247, no. 4, pp. 542-55.

Wilke, HJ, Neef, P, Caimi, M, Hoogland, T & Claes, LE 1999, 'New in vivo measurements of pressures in the intervertebral disc in daily life', *Spine (Phila Pa 1976)*, vol. 24, no. 8, pp. 755-62.

Wong, DA & Transfeldt, E 2007, *Macnab's backache*, vol. 304, Lippincott Williams & Wilkins Philadelphia:.

Appendices

Appendix A: Potting Protocol

Short & quick steps (further details found below):

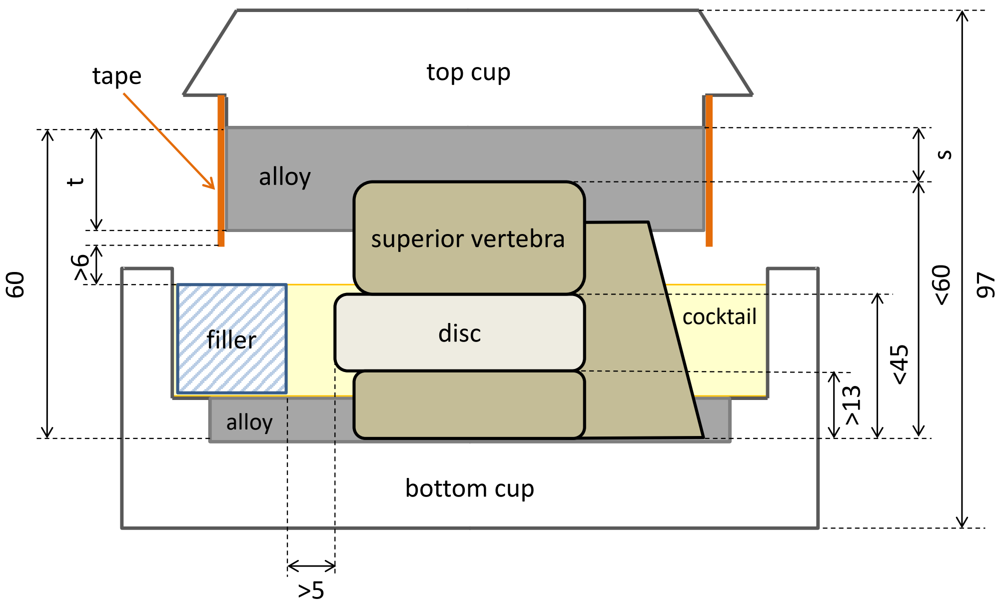

1. Measure height between superior endplate to base of inferior vertebra – this height (x) should be 13mm + disc < x < 45mm

2. Measure total FSU height. If less than 60 mm, use jacking screw to set interior cup separation to 60 mm when potting top cup. [Figure 4]

3. Calculating top cup total alloy height (t) :
4. Calculate Alloy spacing height (s) = **60mm -** FSU height (?)
5. Calculate total top cup alloy height (t) = alloy spacing height (s) ? + **~10mm potting height**
6. Stick tape width (w) = t + 3mm (tape comes in 25 and 50mm width). If a necessary change or trim tape: use Kapton Tape (heat resistant, 280C). Clean attaching surface properly with alcohol. Attach tape tight and evenly without folding. Allow a minimum of 3mm of tape above alloy.
7. Dry Specimen: Assure there is no moisture on bone. Make sure all soft tissue is off of the bone using a scalpel. Bare minimum: Make sure there is about 10 mm of exposed bone on superior and inferior bones (including on posterior elements). Take AP, lateral, and oblique pictures of specimen with label. [Figure 1]

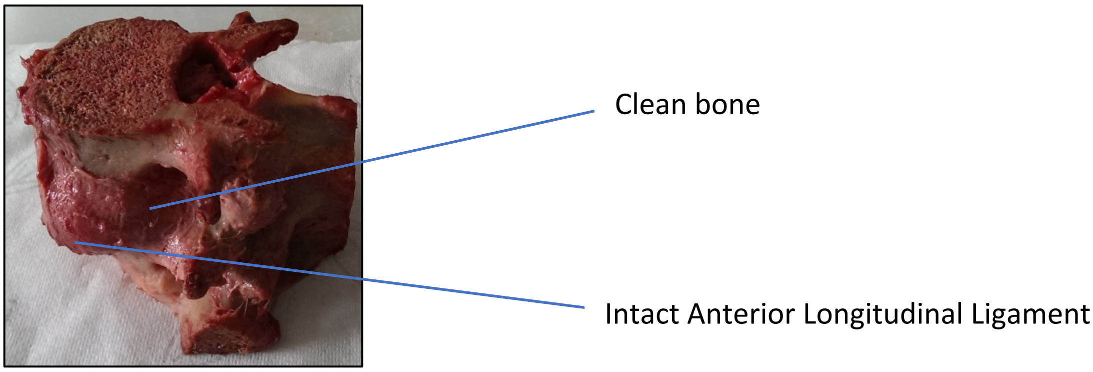

Figure 1

8. Make sure bottom and top cup have been thoroughly cleaned with alcohol.

9. **IMPORTANT**: Make sure grub screws are screwed into thru holes. Do not force the grub screws into threaded holes because it can destroy them. The grub screws can be screwed in with your hand.

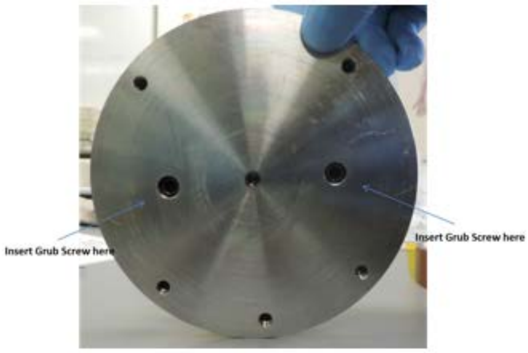

Figure 4: Top cup

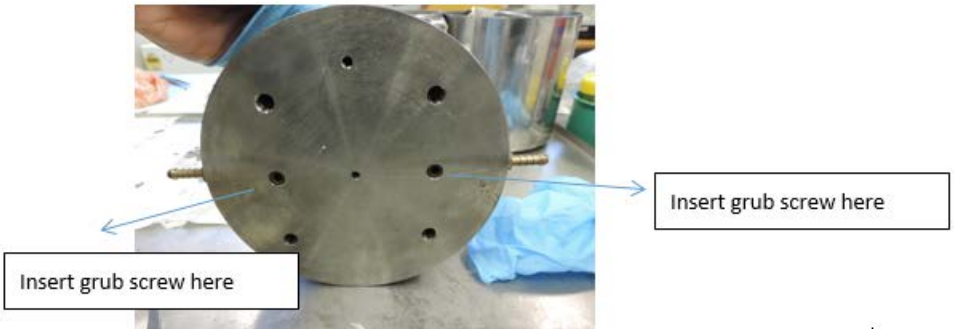

Figure 4: Bottom cup

10. Tape off the bottom part of the Counterbore holes where the thru hole starts on the **Top Cup.**

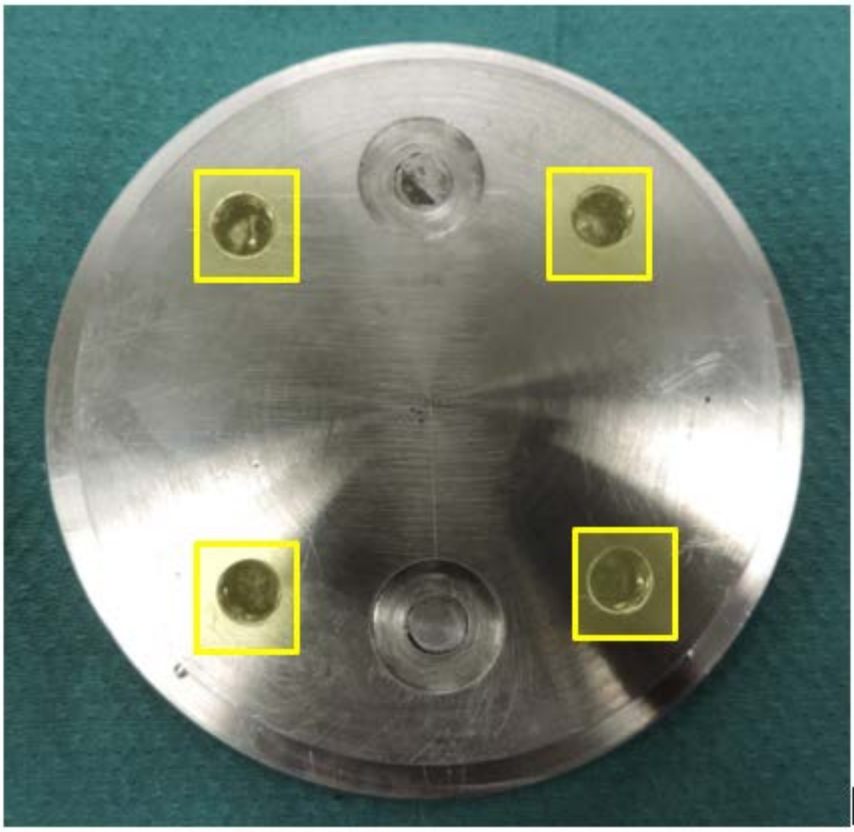

11. Tape around the top cup using Kapton tape to hold PMMA. Taping height is t +3mm (check step 6 under preparation) [See figure below]

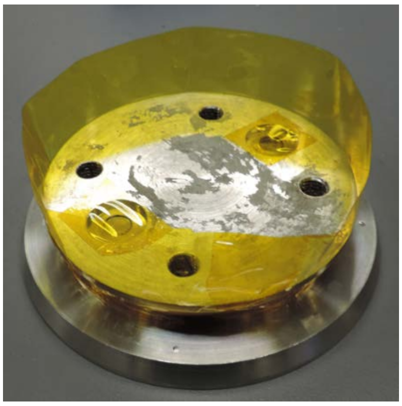

12. Move to the Fume hood and lay down the bench coat. Make sure specimen, cups, and alignment rig are in the fume hood for potting in PMMA.

13. Attach bottom cup with the plate to rig base. Make sure it is aligned correctly. [Figure 2] [Figure 3]. There is the only way to fix the bottom cup to the alignment plate so there is no chance of wrong orientation.

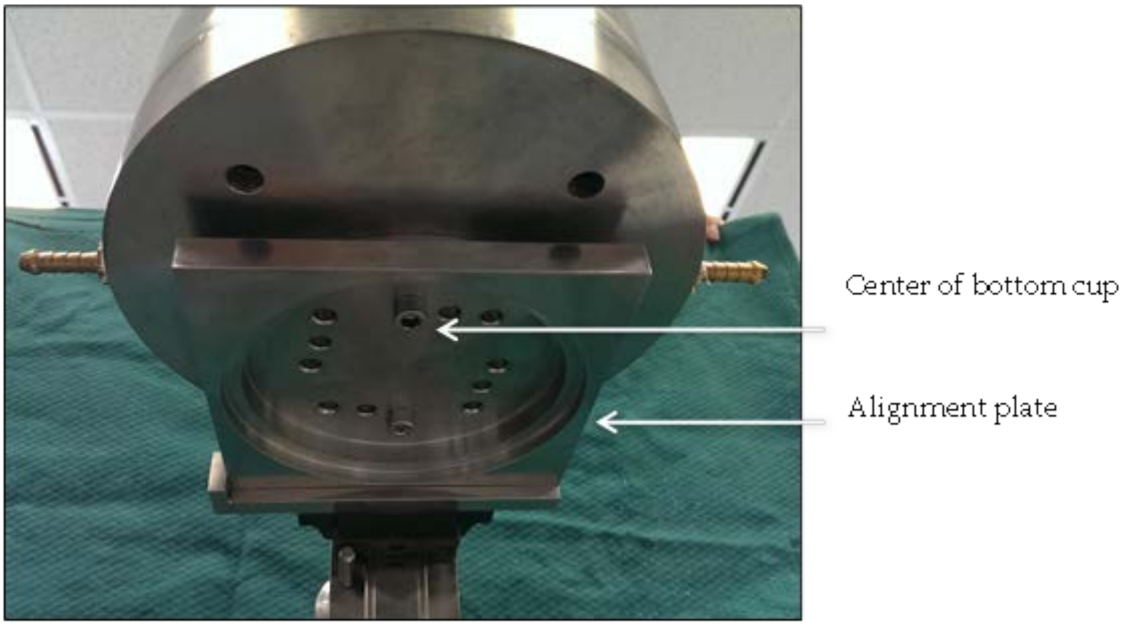

Figure 2

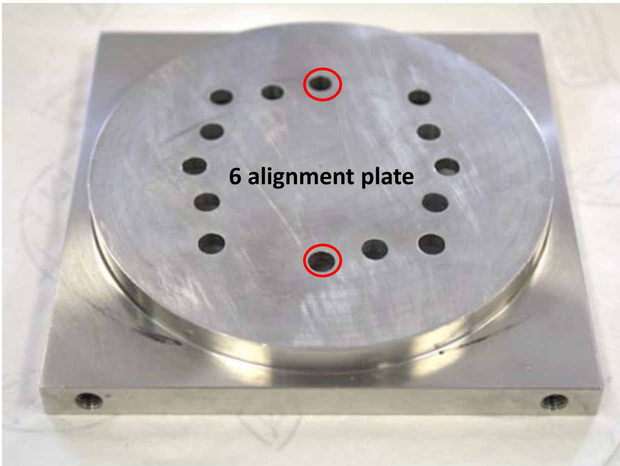

Figure 3

14. Dry specimen.

15. Place the Specimen into the bottom cup. Make sure the specimen is not rotated. Check specimen orientation for proper placement of FSU in potting medium. Is the superior vertebra on top? Is the inferior vertebra the one at the base of the bottom cup? Do the spineous processes line up with the permanent marker lines on the bottom cup?

16. Mix PMMA at a ratio of: 1.7 mL Powder to 1 mL liquid. Make sure it is liquidy in nature. To accomplish the liquidy feel of PMMA adds about 5 mL more of liquid to the mixture.

    a. Bottom Cup: Volume→ ~140 mL, Ratio→ 88 mL Powder, 52 mL Liquid

17. Pour PMMA into the bottom cup. **Make sure PMMA is not higher than the bottom lip. Continuously pour PMMA or the PMMA will not harden as a whole unit.**

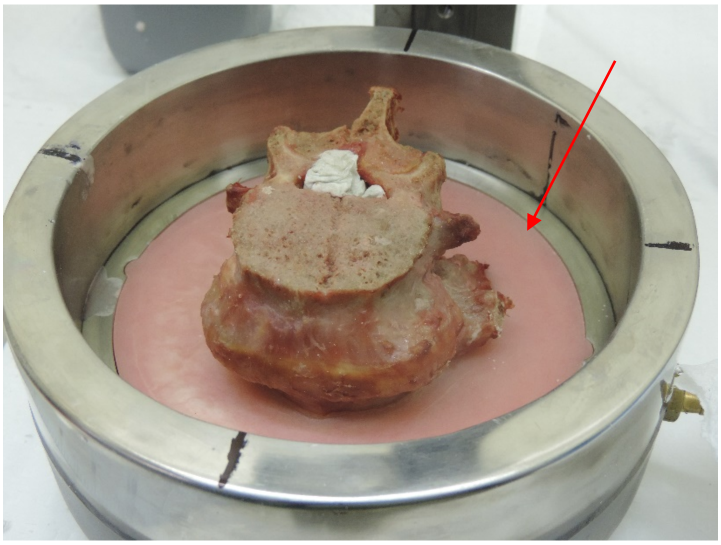

18. Allow PMMA to harden for about 15-20 minutes. Record start and end time of PMMA hardening process on Datasheet.

19. When the bottom cup is potted, measure 2 distances for IAR calculation [Figure 5] and record them in the datasheet.

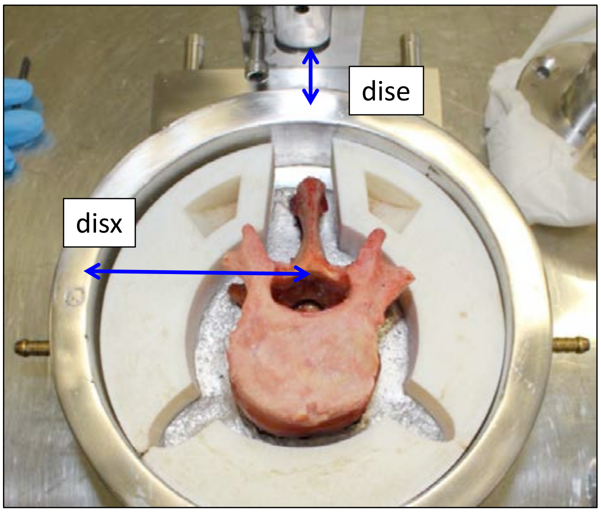

Figure the 5

20. When the bottom cup is potted, using a caliper measure 2 distances for IAR calculation (Y and X from disc centre to inner edge of the cup), and record them on the datasheet.

21. Use the inner diameter end of the caliper to measure the dise measurement [See Figure Below].

22. Use the depth end of the caliper to measure disx. First place a ruler flush against the alignment rig to find the middle of the vertebra (in line with the permanent

marker on the edge of the bottom cup [Figure 6]. Then place the one-end depth end of the caliper on the outer edge of the bottom cup and pull it out until it hits the ruler and makes a square corner/edge. Take the caliper measurement and subtract 14 mm (thickness dimension of the bottom cup) to obtain disx measurement. [PICTURE of the caliper and the process]

23. Detach bottom cup from rig base

24. Attach top cup with alignment plate to rig base

25. Attach the bottom cup to slide mount so it is upside down and let it rest on the pin.

26. Place Jacking Screw (Stopper for height) in the correct position. (Tirad: used when total FSU height is less than 60 mm to set interior cup separation to 60 mm when potting top cup)

27. Lower the specimen into the top ca up. Use jacking the screw for the right potting height! [Figure 7] Place it at the marked position to keep the mount slide at distance from the alignment rig base. The specimen and hexapod are now aligned. Potting height is now kept at 60 mm inside the cups [Figure 4] **Watch when lowering the bottom cup if posterior elements of the specimen fit into the diameter of the top cup!**

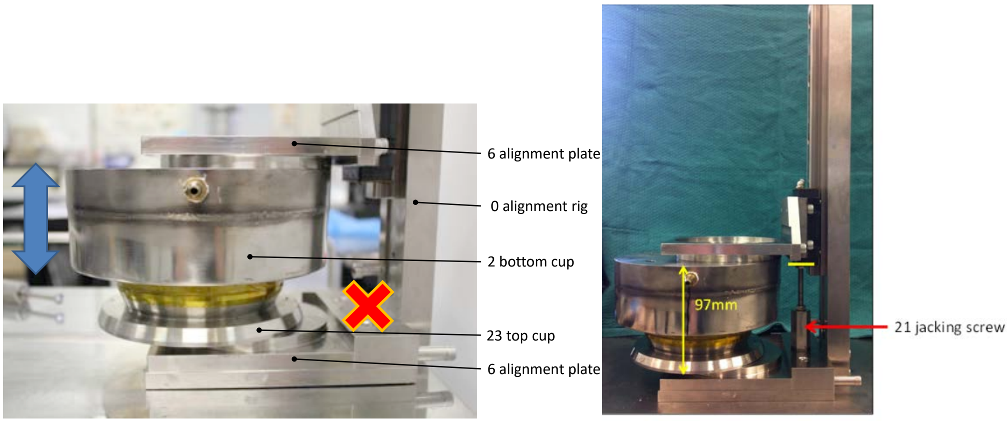

Figure 7

28. Mix PMMA at a ratio of: 1.7 mL Powder to 1 mL liquid. The volume and ratio amounts are located on Data Sheet. Make sure it is liquidy in nature.

    a. Top Cup: Volume→ Varies, should calculate each time by finding the new potting height (Figure 4, Preparation)

        i. Example: FSU height: 60 mm, t=12 mm, Volume→~140 mL, Ratio→88 mL Powder, 52 mL Liquid

29. Pour PMMA into the top cup. Make sure PMMA is 3 mm below tape edge and the right potting height, t.

30. Allow Specimen to cool for 15 minutes.

Appendix B: Geometric Centre Measurement

Prepping for overnight preload
1. Remove specimen from freezer
2. Thaw on bench for 2hrs
3. Take geometric centre measurements to calculate offsets

1. Measure the total height of the FSU

1. FSU height	1	2	3	Average
Height (mm)				0.00

2. Measure the height of the superior (top) vertebra

Superior	1	2	3	Average
Height (mm)				0.00

3. Measure the height of the inferior (bottom) vertebra

Inferior	1	2	3	Average
Height (mm)				0.00

4. Measure the height of the idisc
Take three measuments at left lateral, right lateral and the center of the disc

Disc	1	2	3	Average
Height (mm)				0.00

4. Calculate Z offset from the sum of specimen coupling plate, height of the top cup, superior vertebra and half the disc

Height of specimen Coupling plate (mm)	24
Height of Top Cup (mm)	
Z-Offset (mm)	24.00

4. Measure endplate dimensions using caliper

Superior	1	2	3	Average
AP_S (mm)				#DIV/0!
LAT_S (mm)				#DIV/0!

Inferior	1	2	3	Average
AP_I (mm)				#DIV/0!
LAT _I (mm)				#DIV/0!

Combined Superior/Inferior Avge Dimensions	
	Avgerage (mm)
Avge_AP =	#DIV/0!
Avge_LAT =	#DIV/0!

Disc Area	mm^2
0.84 x Avge_AP x Avge_LAT	#DIV/0!

After Potting Base Cup

5. Measure the X offset
take this measurment once the specime has been potted in the bottom cup
measure from the center of the disc to the inside left edge of the cup
or the outside of the cup and subtract the width of the cup wall

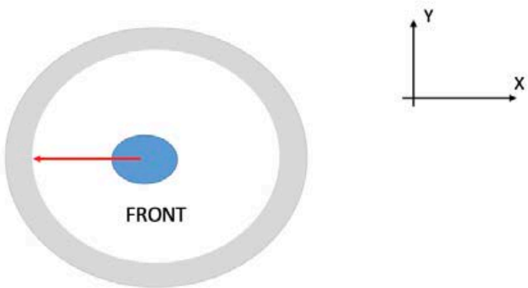

X-Offset	1	2	3	Average
Length (mm)				0.00

Inner Radius of Cup (mm)	45
X-Offset	-45.00

6. Measure the Y offset

take this measurment once the specime has been potted in the bottom cup

measure from the center of the disc to the inside front edge of the cup or the outside of the cup and subtract the width of the cup wall

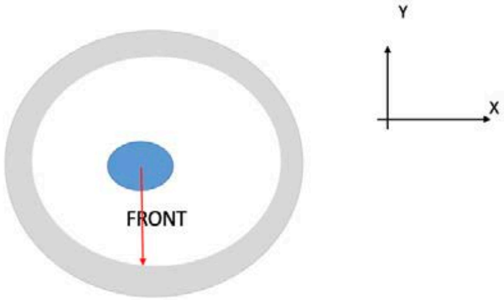

Y-Offset	1	2	3	Average
Length (mm)				0.00

Inner Radius of Cup (mm)	45

Y-Offset (mm)	-45.00

7. Once potted, measure the height of the potted assembly

take one measurment and then rotate the assembly 90 degress, repeat anouther three times

	1	2	3	4
height (mm)				

5. Calculate testing parameters:

	Preload (N)	Follower (N)	Reference (N)
	0.1MPa (Area*0.1)/1.5	0.5MPa (Area*-0.5)/1.5	0.6MPa (Area*-0.6)/1.6
Compressive Loads	#DIV/0!	#DIV/0!	#DIV/0!

6. Take specimen photos
7. Preload outside of hexapod using weights

Preload weights	Start height	Start Time	End Height	End Time

8. Leave specimens in rig outside hexapod overnight
9. Set up LVDT for measuring displacements during preloading x5

Appendix C: MATLAB Codes

Appendix C.1 6DOF plot and load-displacement curves for position, load, and hybrid control

- The code needs to be run in a separate folder for each position, load, and hybrid control.

Content removed for privacy reasons

Content removed for privacy reasons

Content removed for privacy reasons

Content removed for privacy reasons

Content removed for privacy reasons

Content removed for privacy reasons

Content removed for privacy reasons

Content removed for privacy reasons

Content removed for privacy reasons

Content removed for privacy reasons

Content removed for privacy reasons

Content removed for privacy reasons

Content removed for privacy reasons

Content removed for privacy reasons

Content removed for privacy reasons

Content removed for privacy reasons

Content removed for privacy reasons

Appendix C.2 Phase angle

Content removed for privacy reasons

Appendix C.3 Overnight hydration

Content removed for privacy reasons

Content removed for privacy reasons

Content removed for privacy reasons

Appendix C.4 Recovery between control modes

Content removed for privacy reasons

Content removed for privacy reasons

Appendix C.5 Comparison between the last cycles from each control mode

- Variables from each control mode have to be extracted as '.mat' files and numbers in the bracket (i.e., Tx_pos.Tx_lastc(7)) need to be changed according to the order in each file.

Content removed for privacy reasons

Content removed for privacy reasons

Content removed for privacy reasons

Content removed for privacy reasons

Content removed for privacy reasons

Content removed for privacy reasons

Content removed for privacy reasons

Content removed for privacy reasons

Content removed for privacy reasons

Content removed for privacy reasons

Content removed for privacy reasons

Content removed for privacy reasons

Content removed for privacy reasons

Appendix D: Pilot Test Result

Appendix D.1 CM01 (5 cycles at 0.1Hz)

PILOT TEST

Multiaxial Spine Segment Testing: Position vs Load Control and Physiological Relevance

Flinders University

Masters Thesis

Daniel Kim

kim0872@flinders.edu.au

SPECIMEN SPECIFICATION

Specimen Prep Date	21/06/2021	Specimen ID	CM01
Testing Date	22/06/2021	Disc Level	L4 – L5

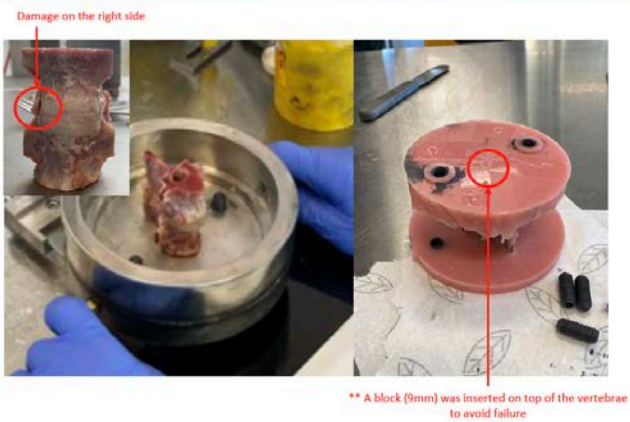

OFFSET	(mm)
X-offset	0.47
Y-offset	-12.30
Z-offset	73.62

COMPRESSIVE LOAD	(N)
Preload	-7.66
Follower	-138.31
Reference	-170.97

RECOVERY

BEFRE POSITION CONTRL	AFTER POSITION CONTROL	AFTER LOAD CONTROL	AFTER HYBRID CONTROL
-147.555	-147.475 (+0.08)	-147.525 (+0.03)	-147.549 (+0.006)

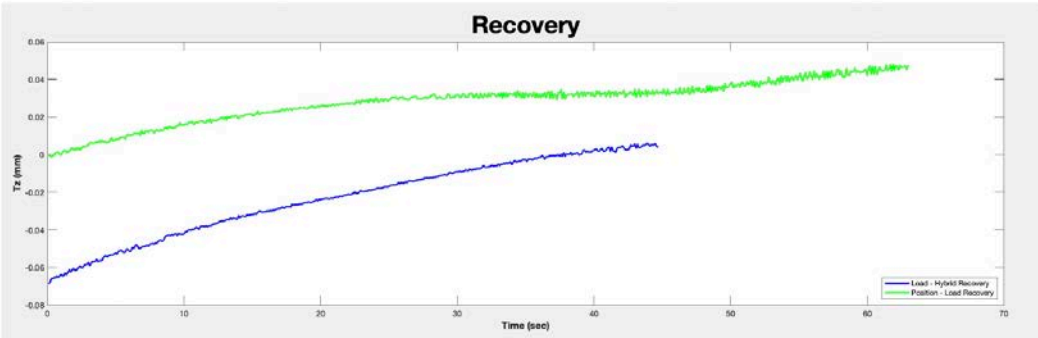

LEFT LATERAL SHEAR (Tx -0.6mm)

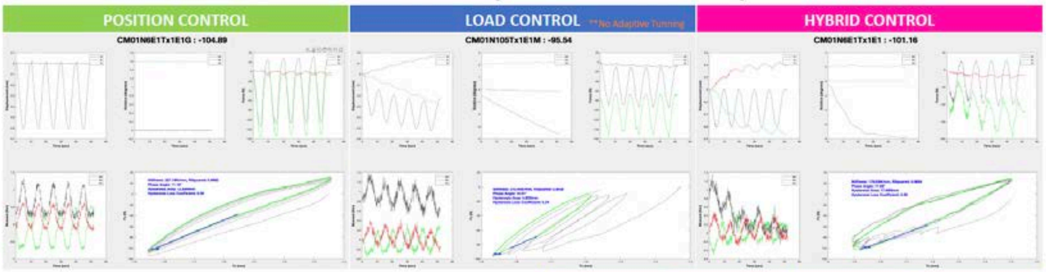

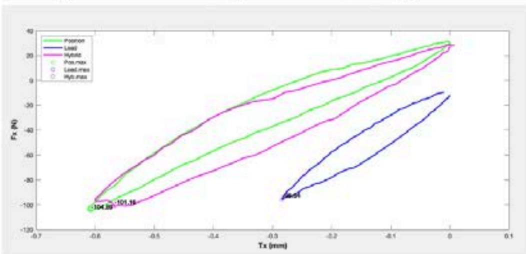

	POSITION CONTROL	LOAD CONTROL	HYBRID CONTROL
Stiffness (N/mm) (RSqaured)	227.19 (0.9982)	210.46 (0.9938)	176.03 (0.9804)
Phase Angle (°)	11.16	14.91	17.68
Hysteresis Area (Nmm)	12.85	4.90	17.65
Hysteresis Loss Coefficient	0.30	0.34	0.38
Maximum Reaction Force (N)	-104.89	-95.54	-101.16

RIGHT LATERAL SHEAR (Tx +0.6mm)

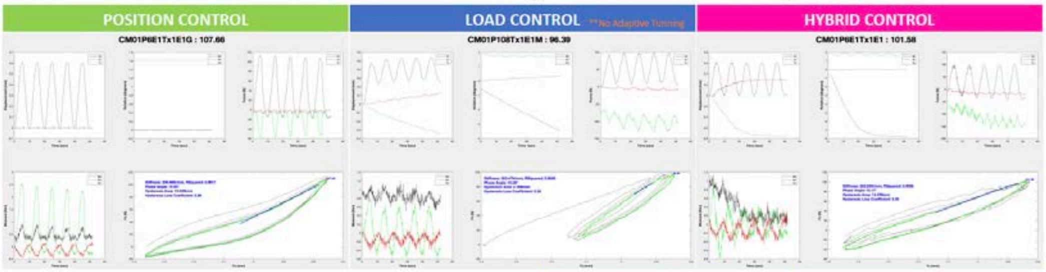

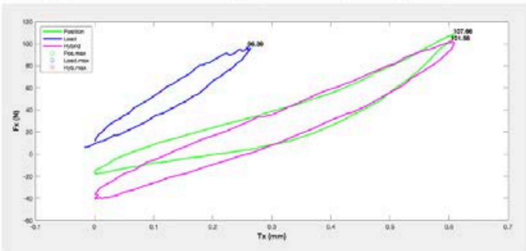

	POSITION CONTROL	LOAD CONTROL	HYBRID CONTROL
Stiffness (N/mm) (RSqaured)	236.96 (0.9917)	302.47 (0.9690)	222.29 (0.9988)
Phase Angle (°)	12.83	15.05	13.17
Hysteresis Area (Nmm)	13.33	4.39	14.23
Hysteresis Loss Coefficient	0.36	0.30	0.30
Maximum Reaction Force (N)	107.66	96.39	101.58

RECOVERY BEFORE POSTERIOR SHEAR

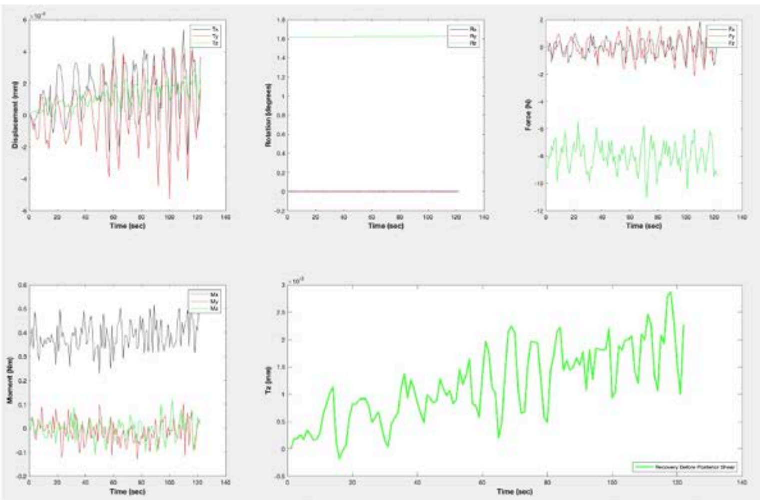

POSTERIOR SHEAR (Ty -0.6mm)

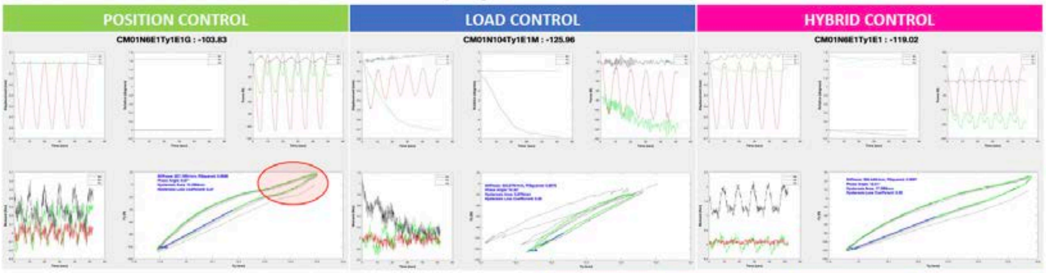

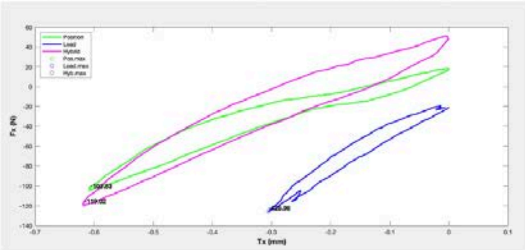

	POSITION CONTROL	LOAD CONTROL	HYBRID CONTROL
Stiffness (N/mm) (RSqaured)	227.19 (0.9996)	333.97 (0.8879)	266.44 (0.9997)
Phase Angle (°)	9.87	10.30	12.51
Hysteresis Area (Nmm)	10.09	3.97	17.39
Hysteresis Loss Coefficient	0.27	0.25	0.30
Maximum Reaction Force (N)	-103.83	-125.96	-119.02

RECOVERY AFTER POSTERIOR SHEAR

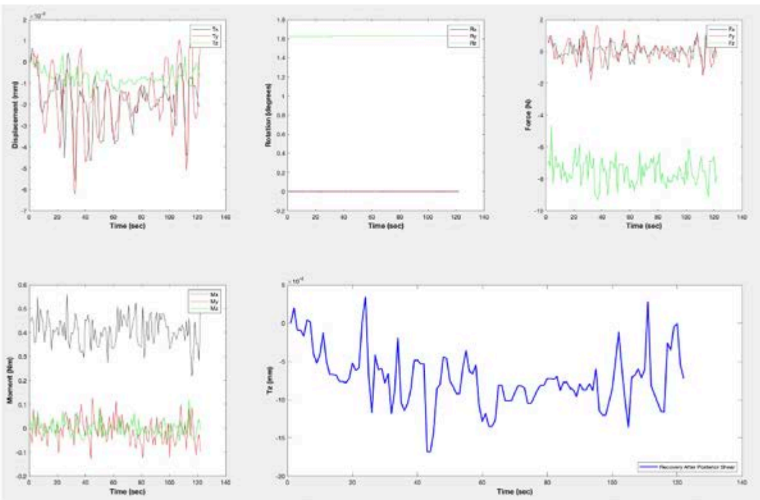

ANTERIOR SHEAR (Ty +0.6mm)

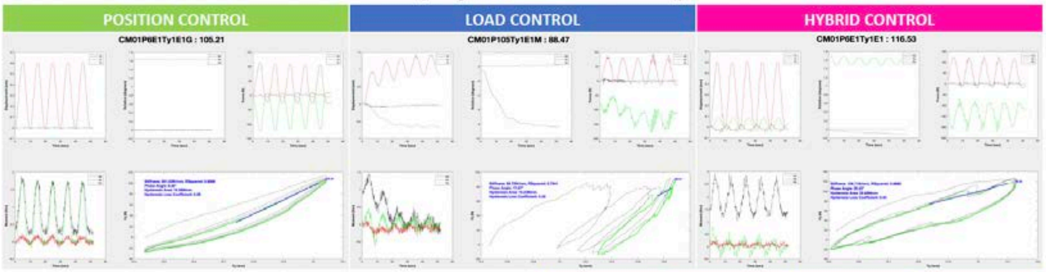

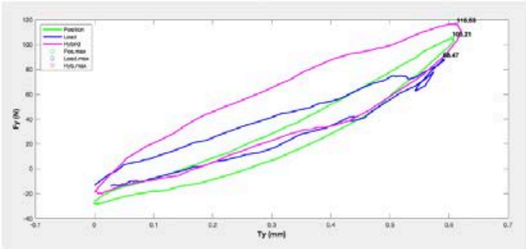

	POSITION CONTROL	LOAD CONTROL	HYBRID CONTROL
Stiffness (N/mm) (RSqaured)	**261.23 (0.9989)**	**95.72 (0.7541)**	**156.71 (0.9885)**
Phase Angle (°)	**9.35**	**17.37**	**20.53**
Hysteresis Area (Nmm)	**10.06**	**10.23**	**22.85**
Hysteresis Loss Coefficient	**0.26**	**0.32**	**0.44**
Maximum Reaction Force (N)	**105.21**	**88.47**	**116.53**

RECOVERY AFTER ANTERIOR SHEAR

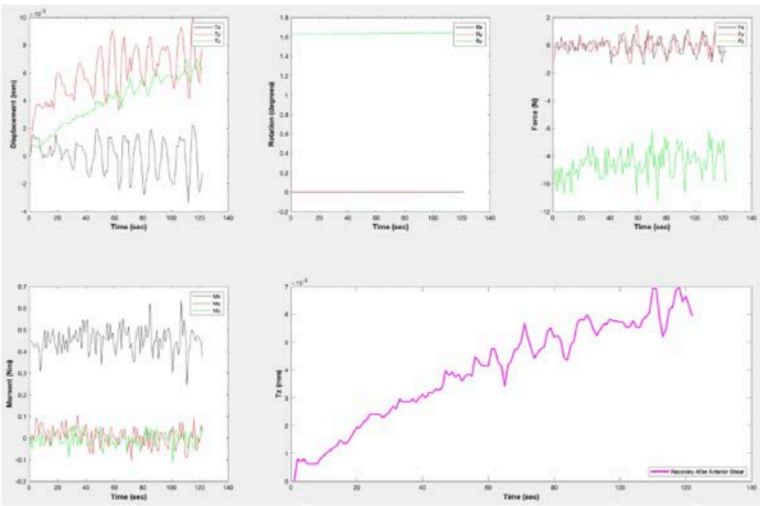

LEFT AXIAL ROTATION (Rz +2°)

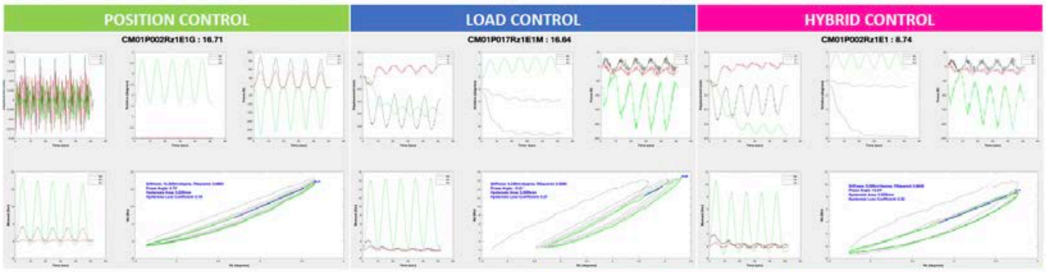

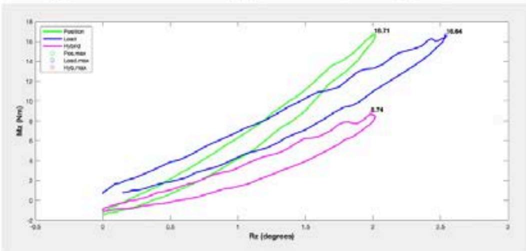

	POSITION CONTROL	LOAD CONTROL	HYBRID CONTROL
Stiffness (Nm/°) (RSqaured)	10.35 (0.9983)	6.33 (0.9580)	5.39 (0.9849)
Phase Angle (°)	6.79	10.91	13.04
Hysteresis Area (Nm°)	3.22	5.52	3.03
Hysteresis Loss Coefficient	0.19	0.27	0.32
Maximum Reaction Moment (Nm)	16.71	16.64	8.74

RIGHT AXIAL ROTATION (Rz -2°)

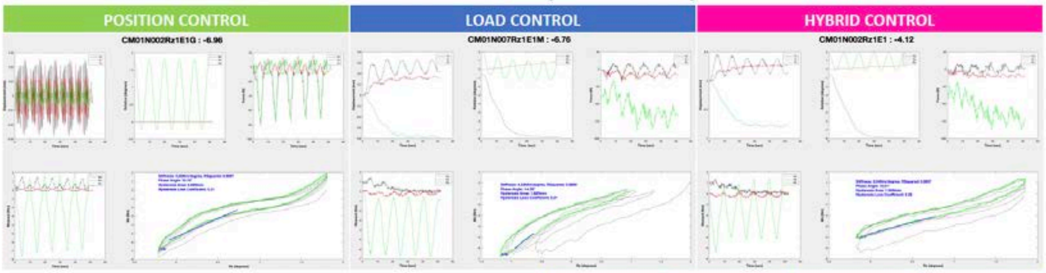

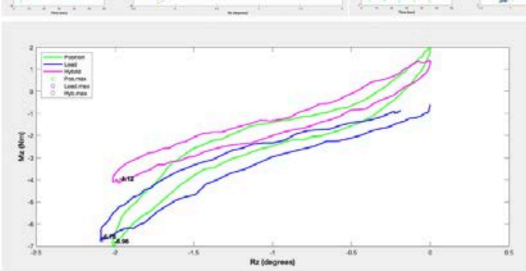

	POSITION CONTROL	LOAD CONTROL	HYBRID CONTROL
Stiffness (Nm/°) (RSqaured)	4.25 (0.9697)	4.52 (0.9859)	2.04 (0.9807)
Phase Angle (°)	10.10	14.28	13.01
Hysteresis Area (Nm°)	2.02	1.82	1.54
Hysteresis Loss Coefficient	0.21	0.31	0.23
Maximum Reaction Moment (Nm)	-6.96	-6.76	-4.12

LEFT LATERAL BENDING (Ry -3°)

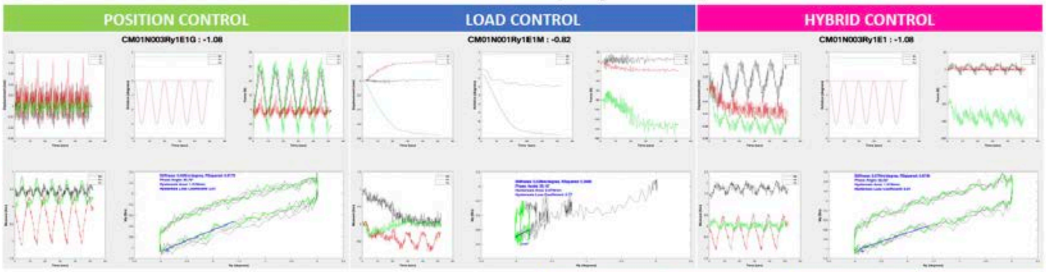

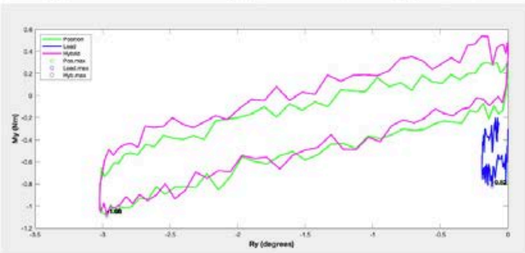

	POSITION CONTROL	LOAD CONTROL	HYBRID CONTROL
Stiffness (Nm/°) (RSqaured)	0.40 (0.9179)	0.53 (0.2490)	0.37 (0.8740)
Phase Angle (°)	30.70	55.18	32.02
Hysteresis Area (Nm°)	1.31	0.07	1.61
Hysteresis Loss Coefficient	0.51	0.77	0.51
Maximum Reaction Moment (Nm)	-1.08	-0.82	-1.08

RIGHT LATERAL BENDING (Ry +3°)

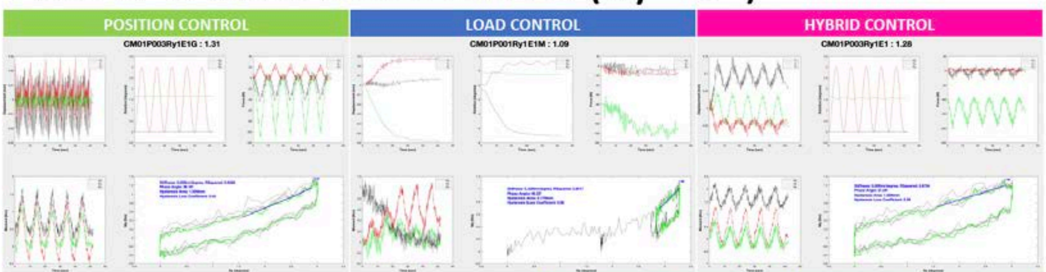

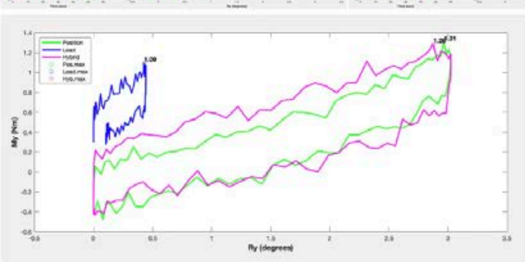

	POSITION CONTROL	LOAD CONTROL	HYBRID CONTROL
Stiffness (Nm/°) (RSqaured)	0.50 (0.9455)	0.83 (0.8017)	0.36 (0.8704)
Phase Angle (°)	26.16	46.55	37.06
Hysteresis Area (Nm°)	1.33	0.17	1.93
Hysteresis Loss Coefficient	0.43	0.69	0.56
Maximum Reaction Moment (Nm)	1.31	1.09	1.28

FLEXION (Rx -5°)

POSITION CONTROL	LOAD CONTROL	HYBRID CONTROL

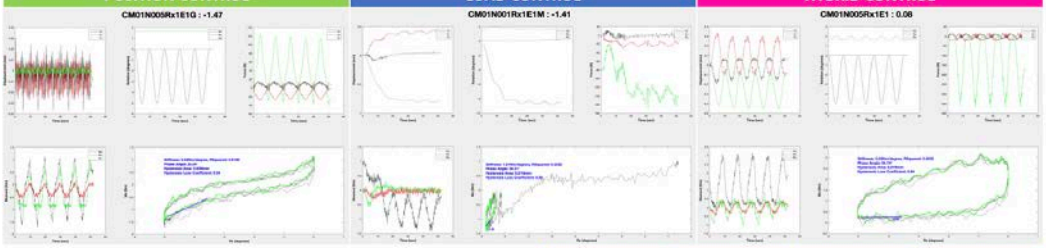

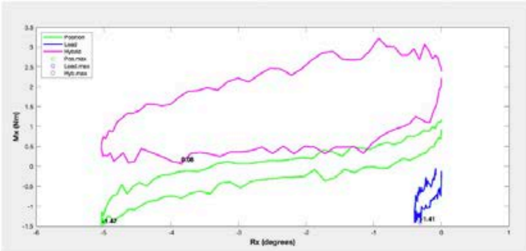

	POSITION CONTROL	LOAD CONTROL	HYBRID CONTROL
Stiffness (Nm/°) (RSqaured)	0.55 (0.9106)	1.01 (0.3332)	0.02 (0.0035)
Phase Angle (°)	20.04	34.51	54.74
Hysteresis Area (Nm°)	2.63	0.21	8.81
Hysteresis Loss Coefficient	0.34	0.59	0.64
Maximum Reaction Moment (Nm)	-1.47	-1.41	0.08

EXTENSION (Rx +2°)

POSITION CONTROL	LOAD CONTROL	HYBRID CONTROL

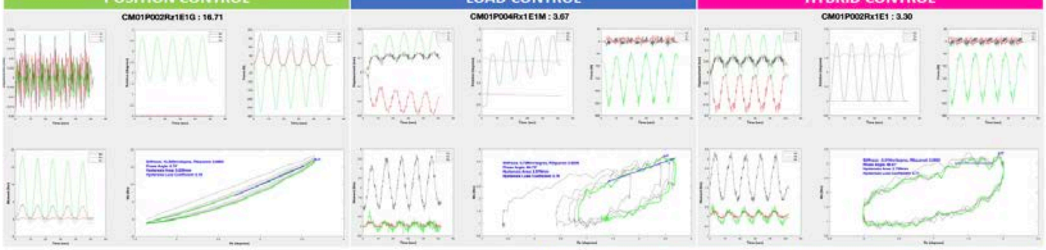

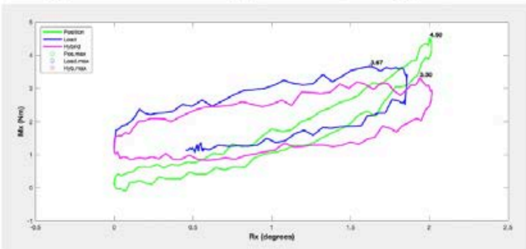

	POSITION CONTROL	LOAD CONTROL	HYBRID CONTROL
Stiffness (Nm/°) (RSqaured)	10.35 (0.9983)	0.73 (0.8206)	-0.01 (0.0002)
Phase Angle (°)	6.79	44.70	49.41
Hysteresis Area (Nm°)	3.22	2.57	2.73
Hysteresis Loss Coefficient	0.19	0.76	0.77
Maximum Reaction Moment (Nm)	16.71	3.67	3.30

AXIAL COMPRESSION (Tz -0.3mm)

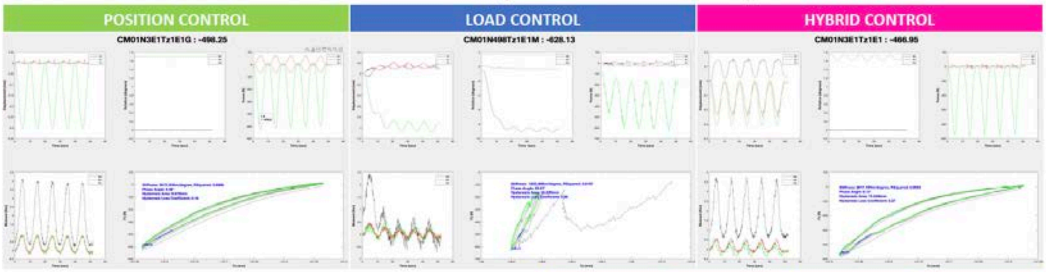

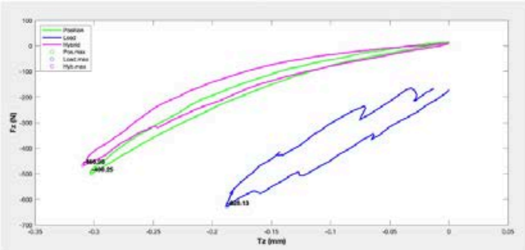

	POSITION CONTROL	LOAD CONTROL	HYBRID CONTROL
Stiffness (N/mm) (RSqaured)	**2672.35 (0.9996)**	**1823.36 (0.9197)**	**2647.19 (0.9930)**
Phase Angle (°)	**4.46**	**20.25**	**8.13**
Hysteresis Area (Nmm)	**9.67**	**18.22**	**15.54**
Hysteresis Loss Coefficient	**0.16**	**0.38**	**0.27**
Maximum Reaction Force (N)	**-498.25**	**-628.13**	**-466.95**

Appendix D.2 CM02 (5 cycles at 0.1Hz)

PILOT TEST 2

Multiaxial Spine Segment Testing: Position vs Load Control and Physiological Relevance

Flinders University
Masters Thesis
Daniel Kim
kim0872@flinders.edu.au

SPECIMEN SPECIFICATION

Specimen Prep Date	17/08/2021	Specimen ID	CM02
Testing Date	18/08/2021	Disc Level	L2 – L3

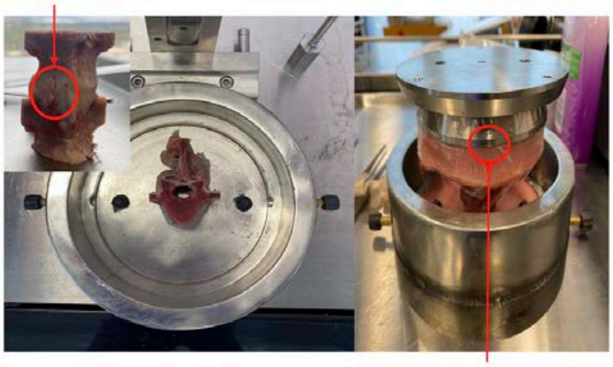

OFFSET	(mm)
X-offset	-0.2
Y-offset	-7.93
Z-offset	73.78

COMPRESSIVE LOAD	(N)
Preload	-6.94
Follower	-134.69
Reference	-166.63

OVERNIGHT HYDRATION

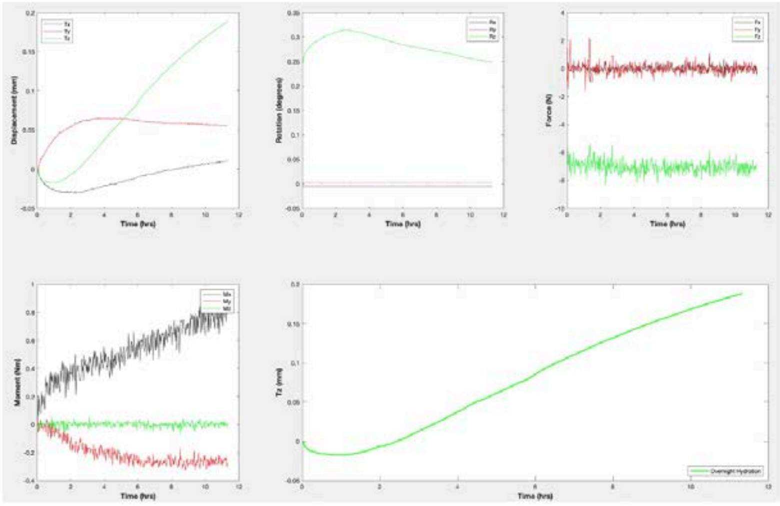

RECOVERY

BEFORE OVERNIGHT HYDRATION	BEEFORE LOAD CONTROL	BEFORE HYBRID CONTROL	AFTER HYBRID CONTROL
-147.498	-147.219 (+0.28)	-147.223 (+0.28)	-147.278 (+0.22)

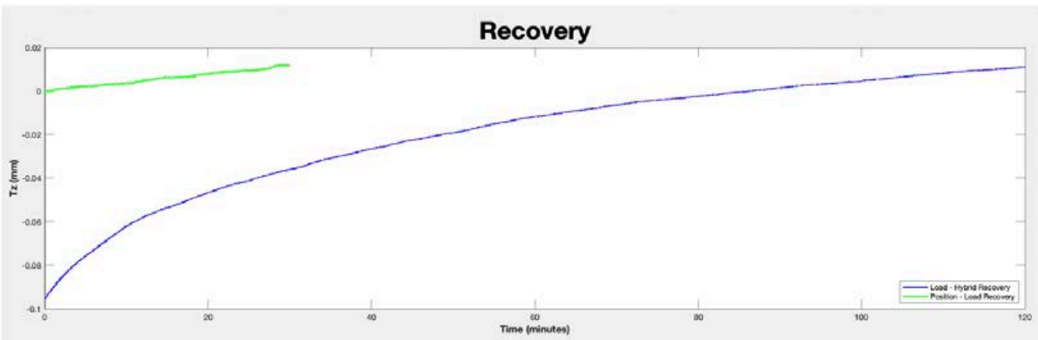

LEFT LATERAL SHEAR (Tx -0.6mm)

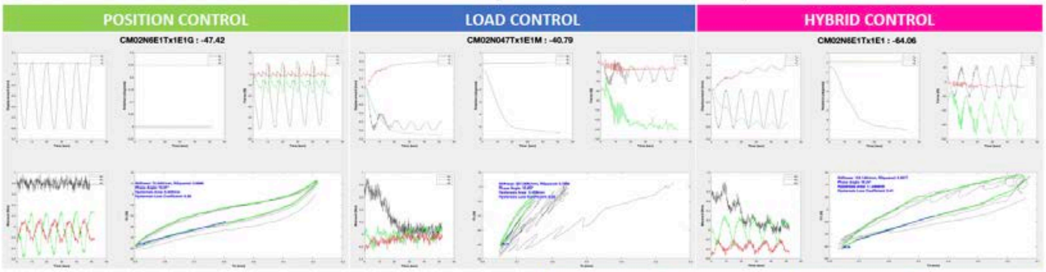

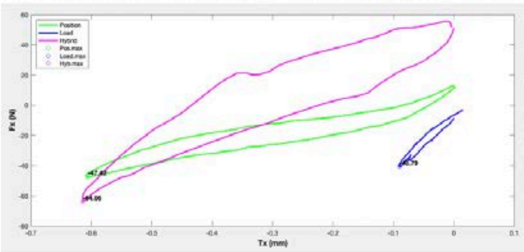

	POSITION CONTROL	LOAD CONTROL	HYBRID CONTROL
Stiffness (N/mm) (RSqaured)	70.54 (0.9896)	297.08 (0.7366)	153.14 (0.9977)
Phase Angle (°)	13.91	10.65	19.24
Hysteresis Area (Nmm)	6.45	0.45	17.09
Hysteresis Loss Coefficient	0.28	0.22	0.41
Maximum Reaction Force (N)	-47.42	-40.79	-64.06

RIGHT LATERAL SHEAR (Tx +0.6mm)

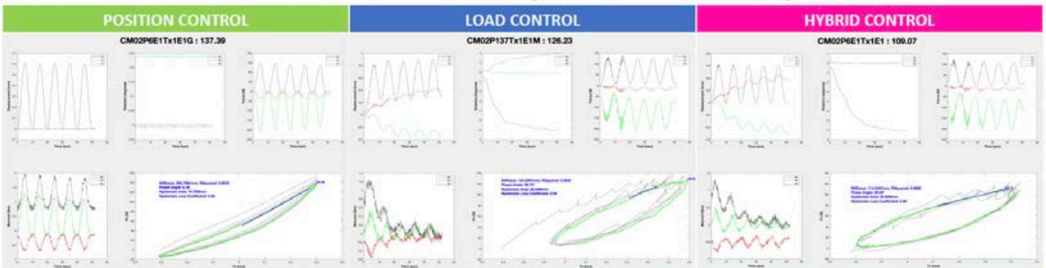

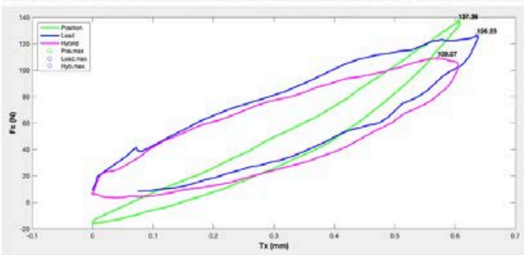

	POSITION CONTROL	LOAD CONTROL	HYBRID CONTROL
Stiffness (N/mm) (RSqaured)	295.79 (0.9975)	154.20 (0.9587)	114.24 (0.9882)
Phase Angle (°)	8.39	26.72	29.09
Hysteresis Area (Nmm)	10.76	25.55	24.80
Hysteresis Loss Coefficient	0.25	0.54	0.59
Maximum Reaction Force (N)	137.39	126.23	109.07

RECOVERY BEFORE POSTERIOR SHEAR

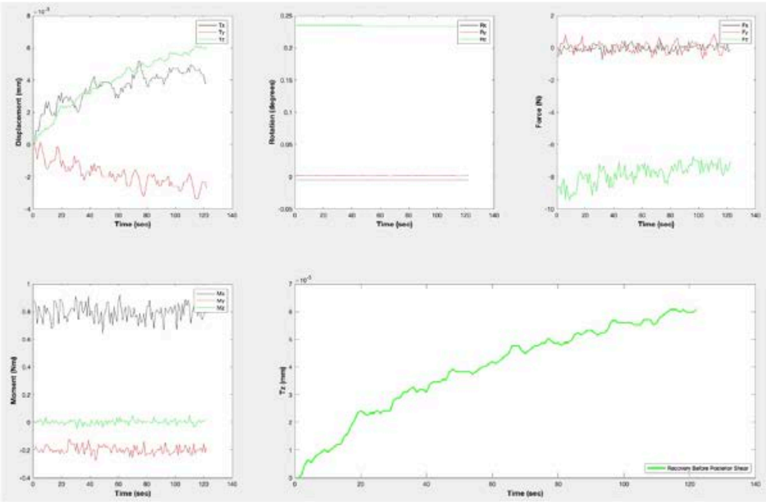

POSTERIOR SHEAR (Ty -0.6mm)

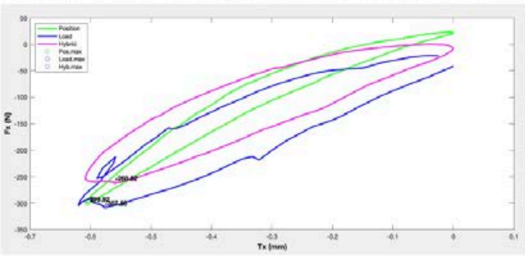

	POSITION CONTROL	LOAD CONTROL	HYBRID CONTROL
Stiffness (N/mm) (RSqaured)	654.04 (0.9996)	419.52 (0.9753)	390.70 (0.9859)
Phase Angle (°)	8.03	23.98	23.01
Hysteresis Area (Nmm)	21.92	52.09	50.45
Hysteresis Loss Coefficient	0.25	0.49	0.54
Maximum Reaction Force (N)	-299.92	-307.58	-260.82

RECOVERY AFTER POSTERIOR SHEAR

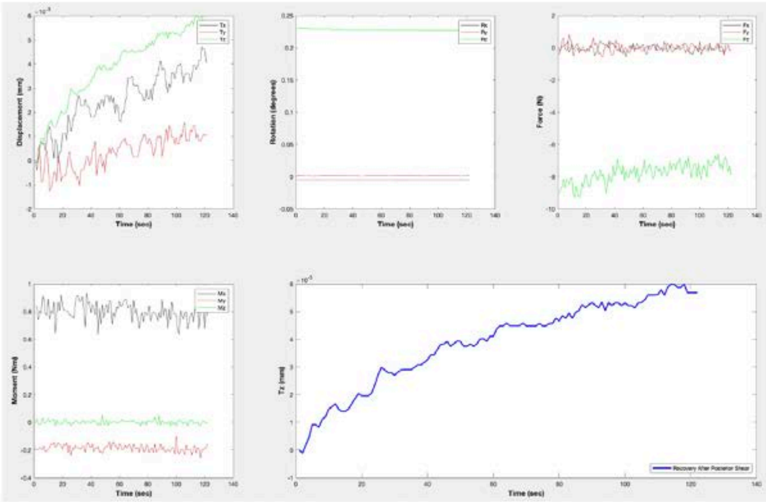

ANTERIOR SHEAR (Ty +0.6mm)

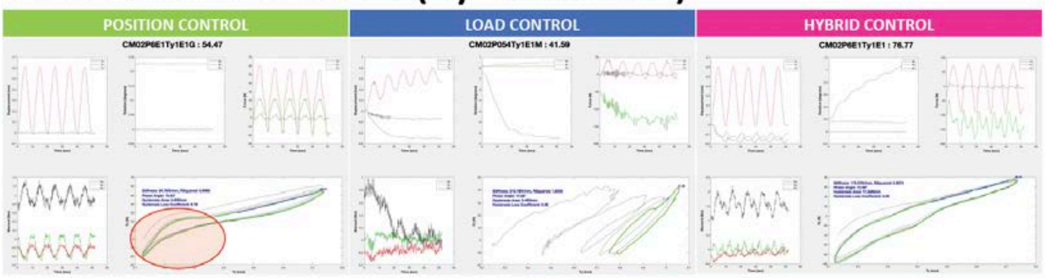

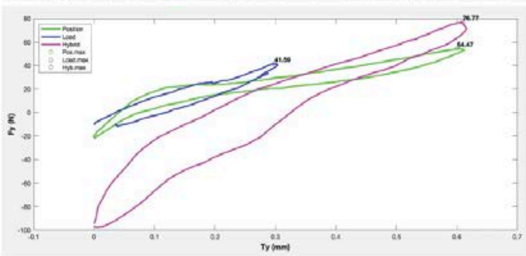

	POSITION CONTROL	LOAD CONTROL	HYBRID CONTROL
Stiffness (N/mm) (RSqaured)	84.78 (0.9980)	210.16 (1.0000)	170.37 (0.9974)
Phase Angle (°)	10.63	14.98	12.58
Hysteresis Area (Nmm)	5.93	3.46	17.55
Hysteresis Loss Coefficient	0.19	0.38	0.25
Maximum Reaction Force (N)	54.47	41.59	76.77

RECOVERY AFTER ANTERIOR SHEAR

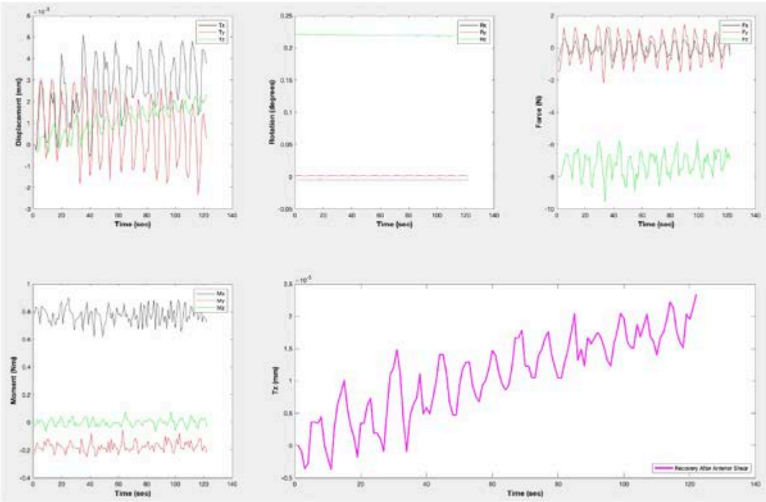

LEFT AXIAL ROTATION (Rz +2°)

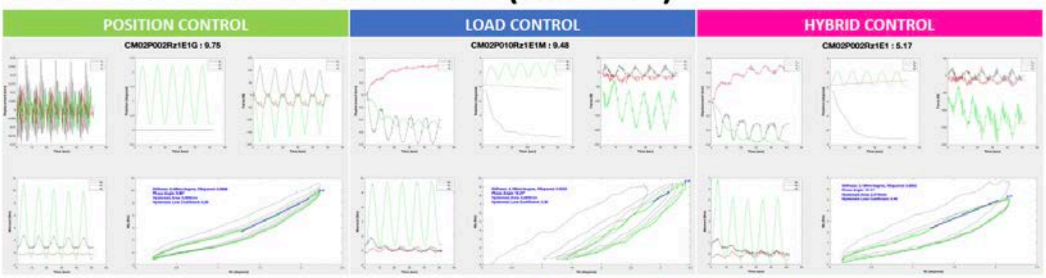

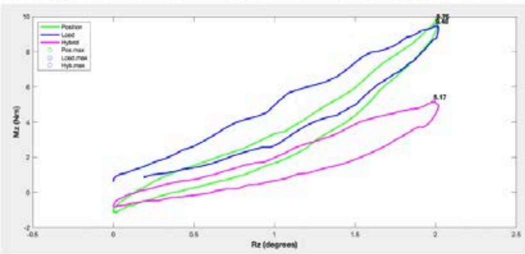

	POSITION CONTROL	LOAD CONTROL	HYBRID CONTROL
Stiffness (Nm/°) (RSqaured)	6.48 (0.9968)	4.18 (0.9252)	3.18 (0.9853)
Phase Angle (°)	9.85	15.27	18.31
Hysteresis Area (Nm°)	2.60	3.22	2.51
Hysteresis Loss Coefficient	0.26	0.36	0.40
Maximum Reaction Moment (Nm)	9.75	9.48	5.17

LEFT LATERAL BENDING (Ry -3°)

POSITION CONTROL	LOAD CONTROL	HYBRID CONTROL

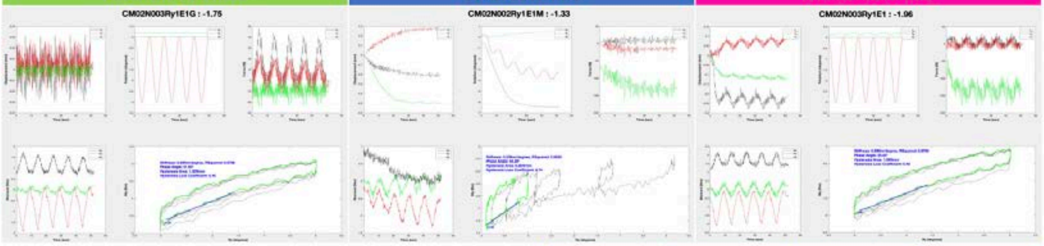

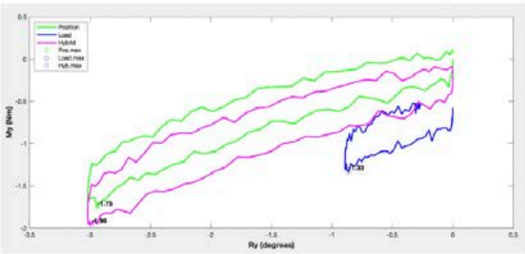

	POSITION CONTROL	LOAD CONTROL	HYBRID CONTROL
Stiffness (Nm/°) (RSqaured)	0.60 (0.9798)	0.53 (0.9200)	0.58 (0.9784)
Phase Angle (°)	21.83	44.20	23.42
Hysteresis Area (Nm°)	1.32	0.35	1.54
Hysteresis Loss Coefficient	0.45	0.74	0.49
Maximum Reaction Moment (Nm)	-1.75	-1.33	-1.96

RIGHT LATERAL BENDING (Ry +3°)

POSITION CONTROL	LOAD CONTROL	HYBRID CONTROL

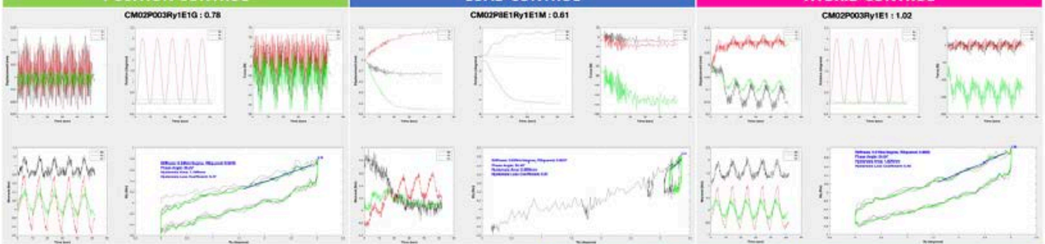

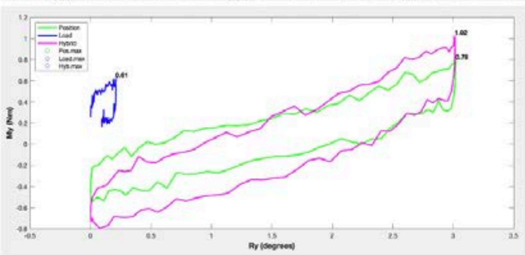

	POSITION CONTROL	LOAD CONTROL	HYBRID CONTROL
Stiffness (Nm/°) (RSqaured)	0.34 (0.9418)	0.60 (0.6037)	0.51 (0.9683)
Phase Angle (°)	28.23	50.49	24.84
Hysteresis Area (Nm°)	1.16	0.06	1.50
Hysteresis Loss Coefficient	0.47	0.87	0.48
Maximum Reaction Moment (Nm)	0.78	0.61	1.02

FLEXION (Rx -5°)

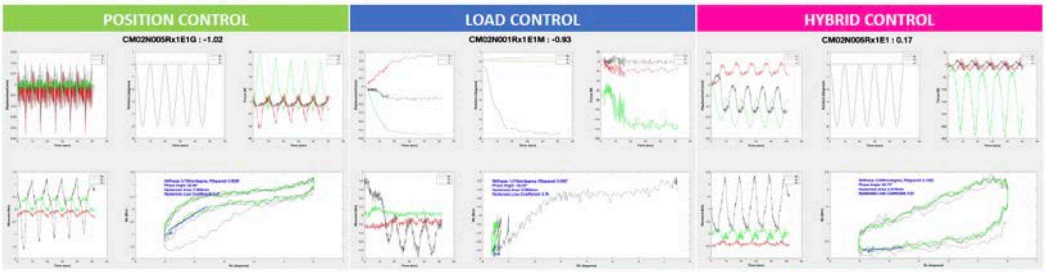

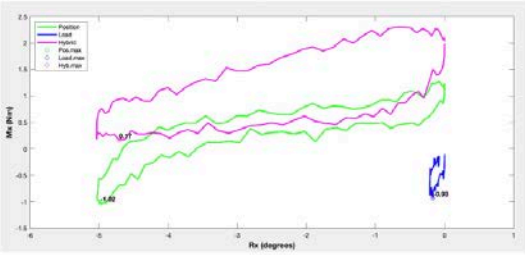

	POSITION CONTROL	LOAD CONTROL	HYBRID CONTROL
Stiffness (Nm/°) (RSqaured)	0.75 (0.9029)	1.21 (0.3357)	0.05 (0.1353)
Phase Angle (°)	22.88	-63.03	45.75
Hysteresis Area (Nm°)	2.36	0.09	5.47
Hysteresis Loss Coefficient	0.41	0.76	0.61
Maximum Reaction Moment (Nm)	-1.02	-0.93	0.17

EXTENSION (Rx +2°)

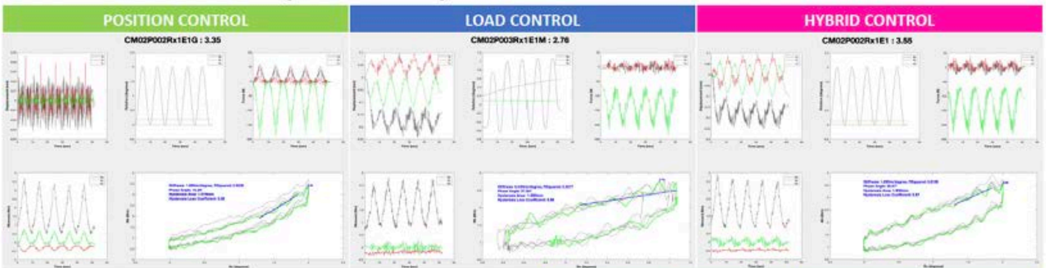

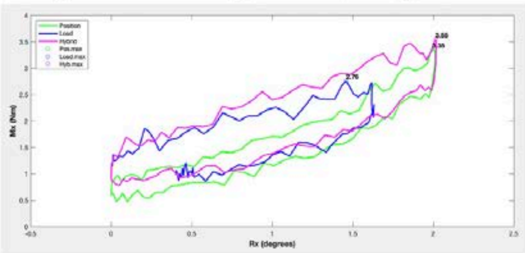

	POSITION CONTROL	LOAD CONTROL	HYBRID CONTROL
Stiffness (Nm/°) (RSqaured)	1.96 (0.9228)	0.44 (0.3577)	1.26 (0.8186)
Phase Angle (°)	15.39	37.54	30.67
Hysteresis Area (Nm°)	1.01	1.29	1.90
Hysteresis Loss Coefficient	0.38	0.68	0.57
Maximum Reaction Moment (Nm)	3.35	2.76	3.55

AXIAL COMPRESSION (Tz -0.3mm)

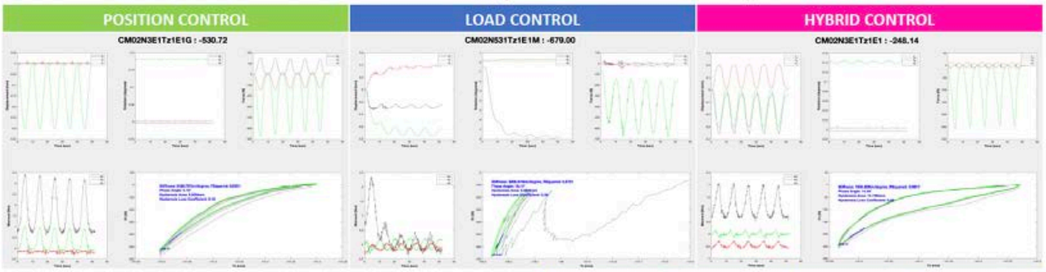

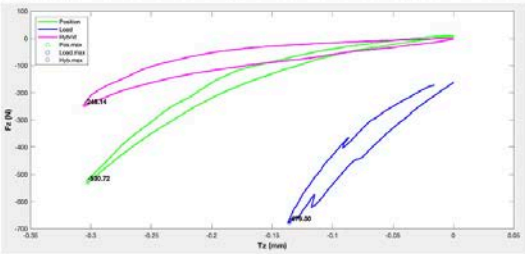

	POSITION CONTROL	LOAD CONTROL	HYBRID CONTROL
Stiffness (N/mm) (RSqaured)	**3429.79 (0.9994)**	**3909.81 (0.8731)**	**1534.82 (0.9917)**
Phase Angle (°)	**4.79**	**15.14**	**14.46**
Hysteresis Area (Nmm)	**9.83**	**9.98**	**13.79**
Hysteresis Loss Coefficient	**0.18**	**0.29**	**0.45**
Maximum Reaction Force (N)	**-530.72**	**-679.00**	**-248.14**

Appendix D.3 CM02-1 (10 cycles at 0.1Hz, Flexion magnitude: -7°)

PILOT TEST 3

Multiaxial Spine Segment Testing: Position vs Load Control and Physiological Relevance

Flinders University

Masters Thesis

Daniel Kim

kim0872@flinders.edu.au

Supervisor: A.Professor John Costi, Co-Supervisor: Mr Michael Russo

SPECIMEN SPECIFICATION

Specimen Prep Date	17/08/2021	Specimen ID	CM02 (Reused)
Testing Date	02/09/2021	Disc Level	L2 – L3

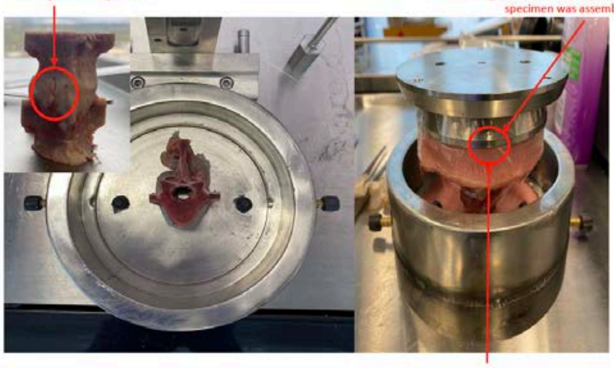

OFFSET	(mm)
X-offset	-0.2
Y-offset	-7.93
Z-offset	73.78

COMPRESSIVE LOAD	(N)
Preload	-6.94
Follower	-134.69
Reference	-166.63

TIMETABLE

Date	Time	Status		Duration	Notes
01.09.21	16:15	Start	Overnight Hydration	15:30	On the hexapod
02.09.21	07:45	End			
	08:20	Start	Position Control	00:30	"Constrained except for Fz" didn't work Terminated testing after 3 tests
	08:50	End			
	08:57	Start	Recovery	00:30	Because of the termination, give 30 mins of recovery
	09:27	End			
	09:33	Start	Position Control - 2	00:50	Redo the position control with "Fully unconstrained"
	10:23	End			
	10:30	Start	Pos-Load Recovery	02:00	** Data missing **
	12:30	End			
	12:35	Start	Load Control	00:50	
	13:25	End			
	13:55	Start	Load-Hyb Recovery	02:00	
	15:55	End			
	16:11	Start	Hybrid Control	00:50	
	17:05	End			

OVERNIGHT HYDRATION

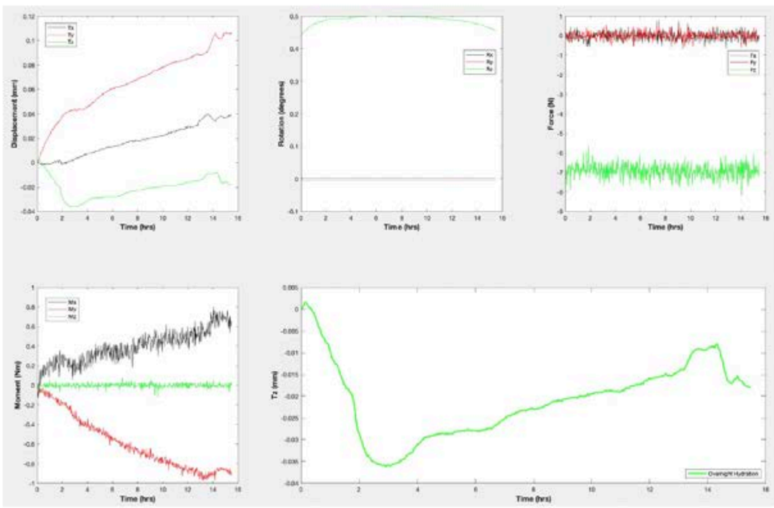

RECOVERY

BEFORE OVERNIGHT HYDRATION	BEEFORE POSITION CONTROL	BEFORE LOAD CONTROL	BEFORE HYBRID CONTROL
-146.791	-147.056 (-0.27)	-147.036 (-0.25)	-147.202 (-0.41)

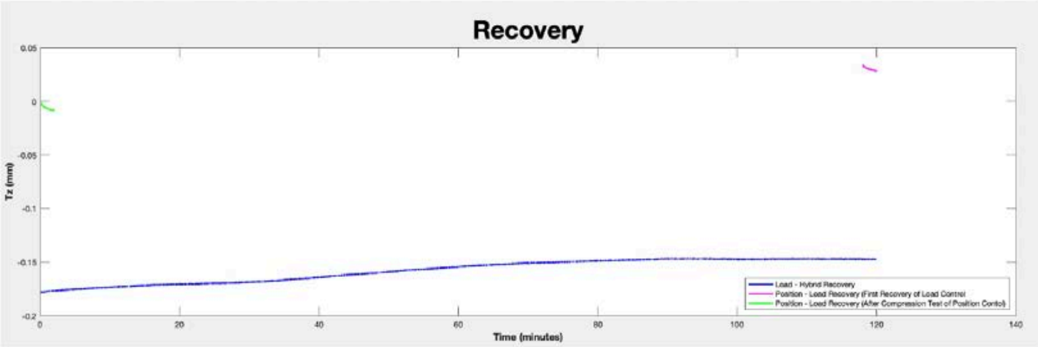

LEFT LATERAL SHEAR (Tx -0.6mm)

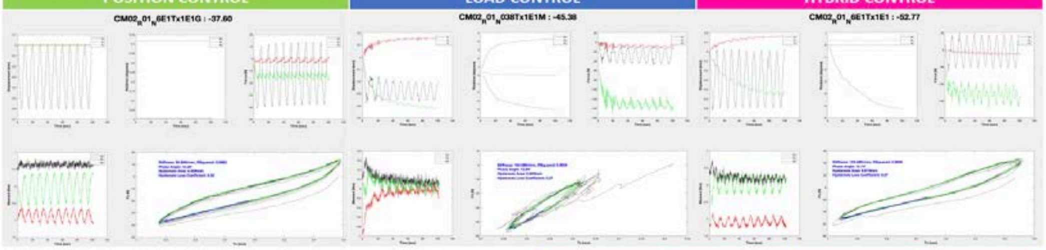

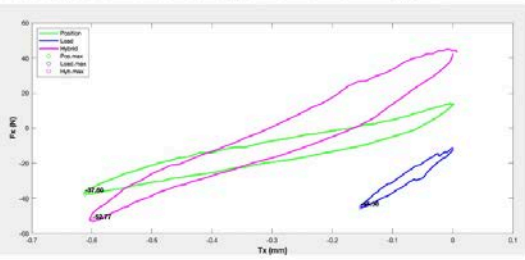

	POSITION CONTROL	LOAD CONTROL	HYBRID CONTROL
Stiffness (N/mm) (RSqaured)	59.60 (0.9982)	194.58 (0.9934)	122.48 (0.9906)
Phase Angle (°)	14.39	13.94	12.74
Hysteresis Area (Nmm)	6.05	0.82	9.61
Hysteresis Loss Coefficient	0.30	0.27	0.27
Maximum Reaction Force (N)	-37.60	-45.38	-52.77

RIGHT LATERAL SHEAR (Tx +0.6mm)

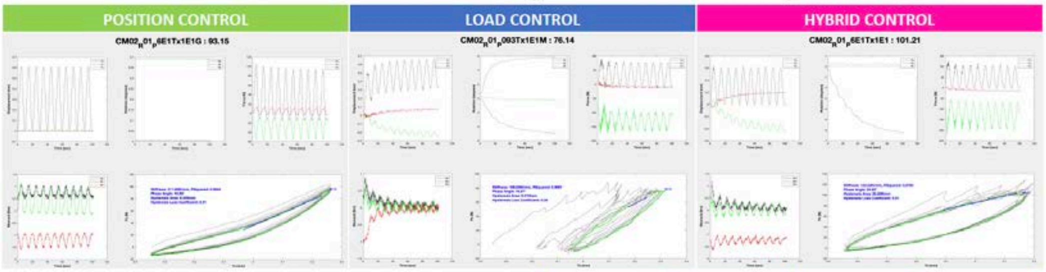

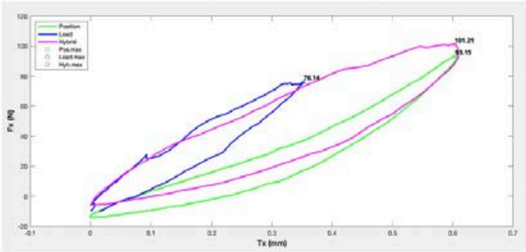

	POSITION CONTROL	LOAD CONTROL	HYBRID CONTROL
Stiffness (N/mm) (RSqaured)	211.66 (0.9944)	188.50 (0.9967)	123.22 (0.9794)
Phase Angle (°)	10.55	16.87	24.82
Hysteresis Area (Nmm)	9.24	6.21	20.82
Hysteresis Loss Coefficient	0.31	0.34	0.51
Maximum Reaction Force (N)	93.15	76.14	101.21

RECOVERY BEFORE POSTERIOR SHEAR

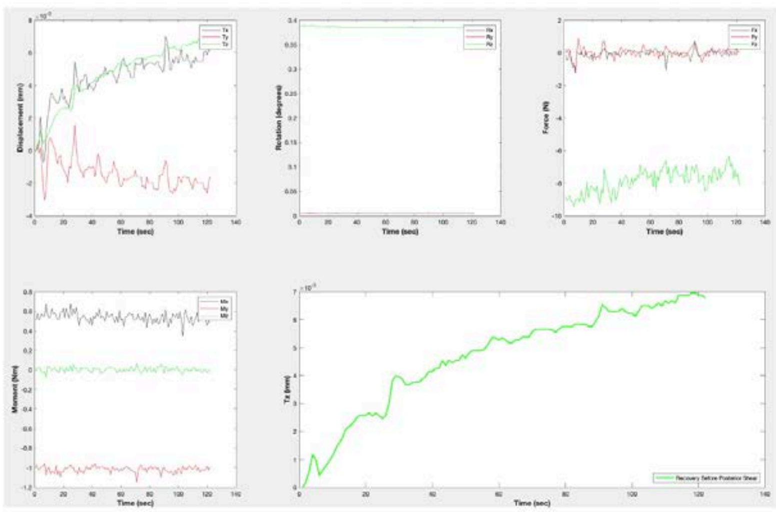

POSTERIOR SHEAR (Ty -0.6mm)

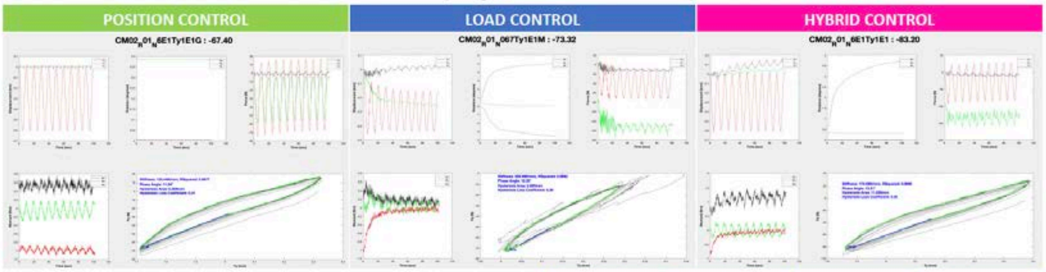

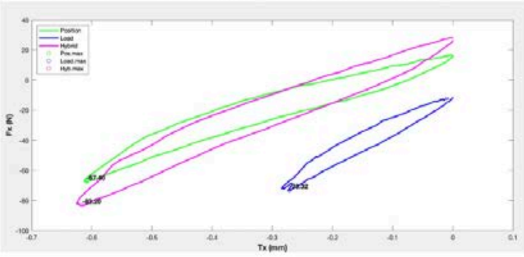

	POSITION CONTROL	LOAD CONTROL	HYBRID CONTROL
Stiffness (N/mm) (RSqaured)	135.44 (0.9977)	209.46 (0.9982)	174.06 (0.9990)
Phase Angle (°)	11.94	12.33	12.51
Hysteresis Area (Nmm)	8.50	2.86	11.25
Hysteresis Loss Coefficient	0.31	0.30	0.30
Maximum Reaction Force (N)	-67.40	-73.32	-83.20

RECOVERY AFTER POSTERIOR SHEAR

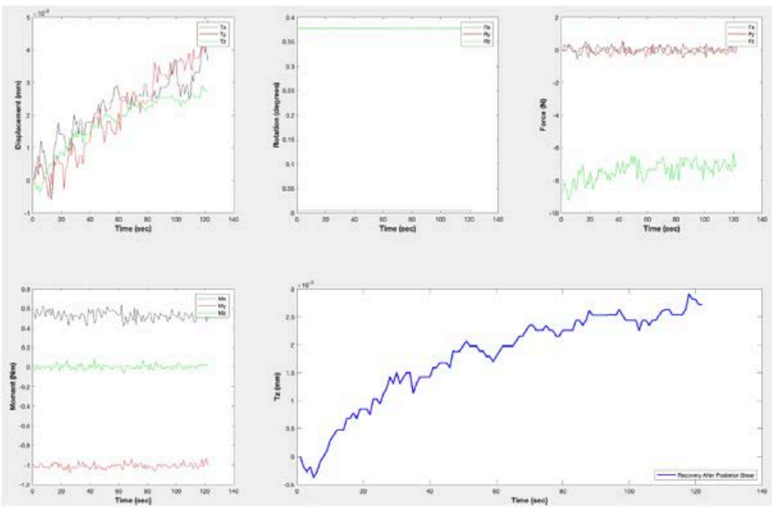

ANTERIOR SHEAR (Ty +0.6mm)

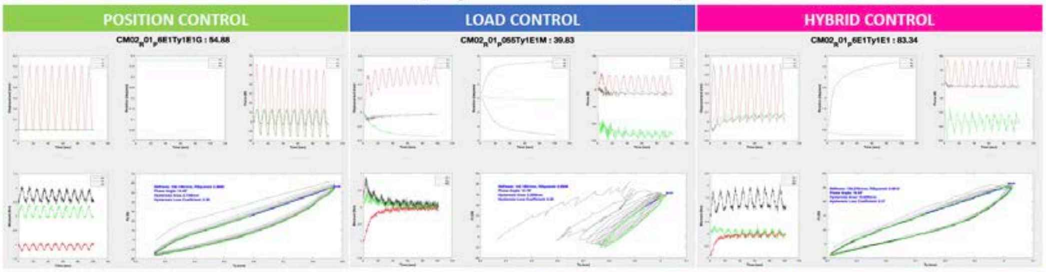

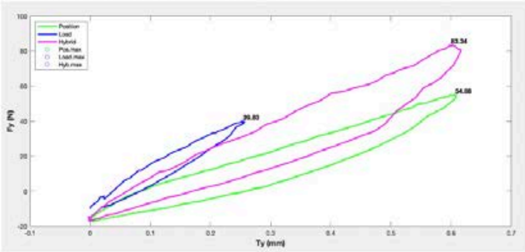

	POSITION CONTROL	LOAD CONTROL	HYBRID CONTROL
Stiffness (N/mm) (RSqaured)	108.14 (0.9990)	142.16 (0.9906)	139.27 (0.9915)
Phase Angle (°)	14.46	14.78	16.50
Hysteresis Area (Nmm)	8.73	2.20	12.62
Hysteresis Loss Coefficient	0.36	0.30	0.37
Maximum Reaction Force (N)	54.88	39.83	83.34

RECOVERY AFTER ANTERIOR SHEAR

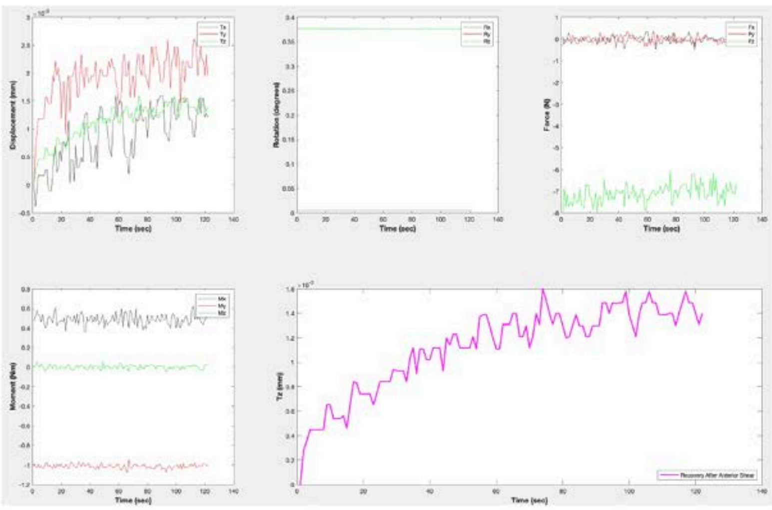

LEFT AXIAL ROTATION (Rz +2°)

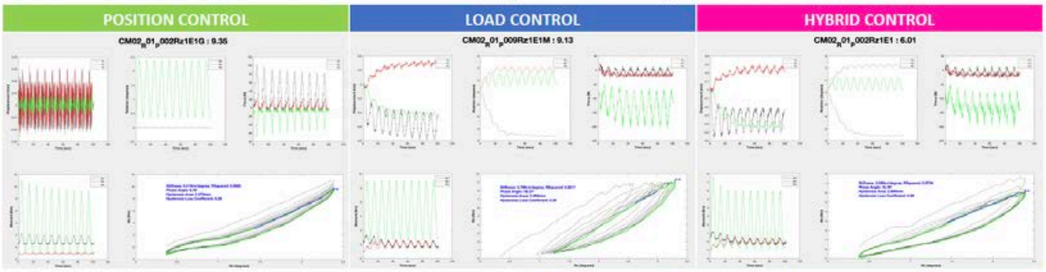

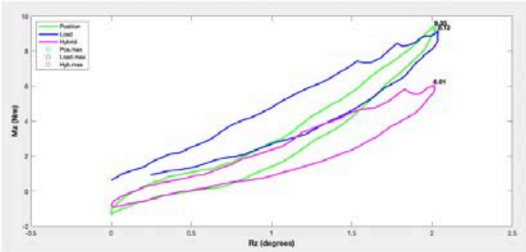

	POSITION CONTROL	LOAD CONTROL	HYBRID CONTROL
Stiffness (Nm/°) (RSqaured)	6.41 (0.9985)	3.79 (0.9217)	3.56 (0.9754)
Phase Angle (°)	8.78	16.37	15.76
Hysteresis Area (Nm°)	2.27	3.36	2.59
Hysteresis Loss Coefficient	0.23	0.39	0.36
Maximum Reaction Moment (Nm)	9.35	9.13	6.01

RIGHT AXIAL ROTATION (Rz -2°)

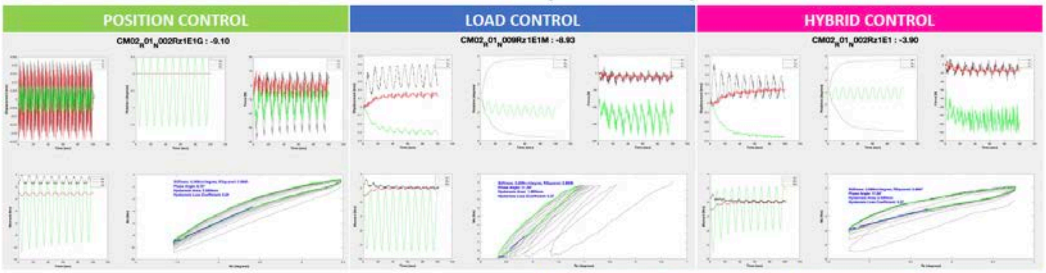

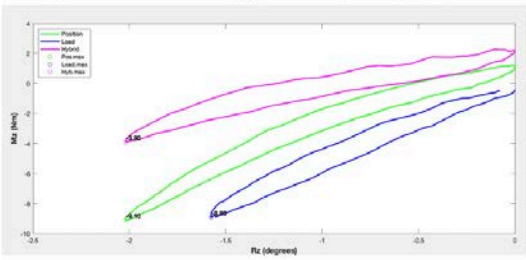

	POSITION CONTROL	LOAD CONTROL	HYBRID CONTROL
Stiffness (Nm/°) (RSqaured)	6.06 (0.9980)	5.30 (0.9958)	2.98 (0.9967)
Phase Angle (°)	8.70	11.36	17.28
Hysteresis Area (Nm°)	2.32	1.86	2.43
Hysteresis Loss Coefficient	0.24	0.27	0.37
Maximum Reaction Moment (Nm)	-9.10	-8.93	-3.90

LEFT LATERAL BENDING (Ry -3°)

POSITION CONTROL	LOAD CONTROL	HYBRID CONTROL

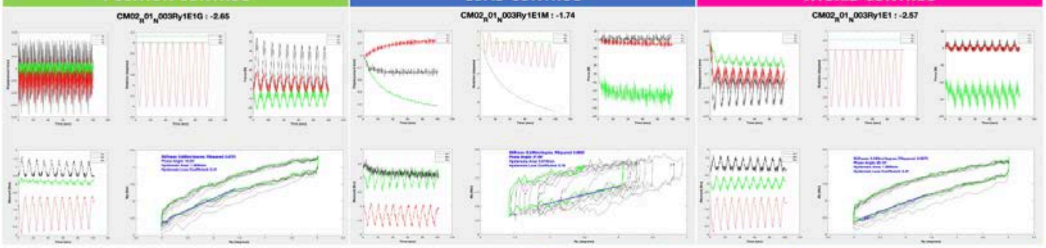

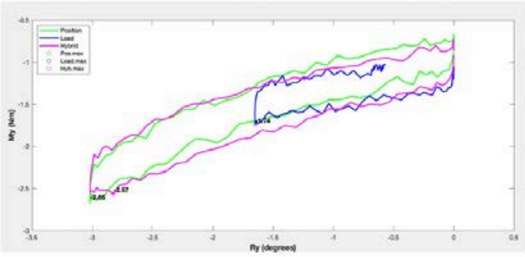

	POSITION CONTROL	LOAD CONTROL	HYBRID CONTROL
Stiffness (Nm/°) (RSqaured)	0.68 (0.9721)	0.24 (0.8502)	0.56 (0.9879)
Phase Angle (°)	19.55	47.69	25.10
Hysteresis Area (Nm°)	1.30	0.61	1.58
Hysteresis Loss Coefficient	0.41	0.78	0.47
Maximum Reaction Moment (Nm)	-2.65	-1.74	-2.57

RIGHT LATERAL BENDING (Ry +3°)

POSITION CONTROL	LOAD CONTROL	HYBRID CONTROL

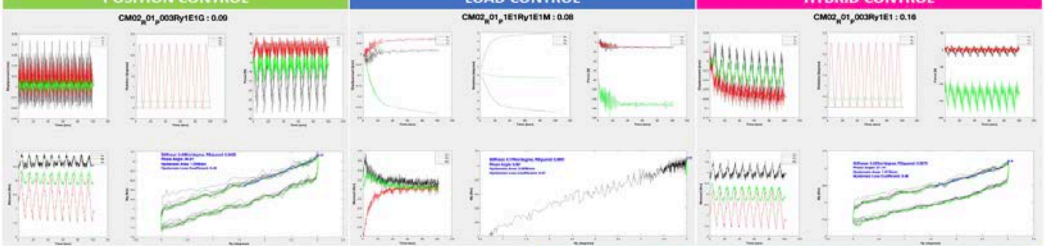

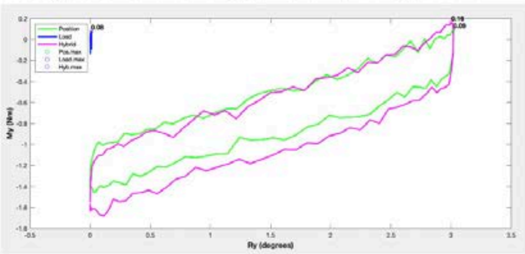

	POSITION CONTROL	LOAD CONTROL	HYBRID CONTROL
Stiffness (Nm/°) (RSqaured)	0.40 (0.9429)	- (-)	0.42 (0.9679)
Phase Angle (°)	24.81	-	27.14
Hysteresis Area (Nm°)	1.23	-	1.61
Hysteresis Loss Coefficient	0.43	-	0.46
Maximum Reaction Moment (Nm)	0.09	-	0.16

FLEXION (Rx -7°)

(Stiffness range : -4.9 ~ -6.9)

POSITION CONTROL	LOAD CONTROL	HYBRID CONTROL

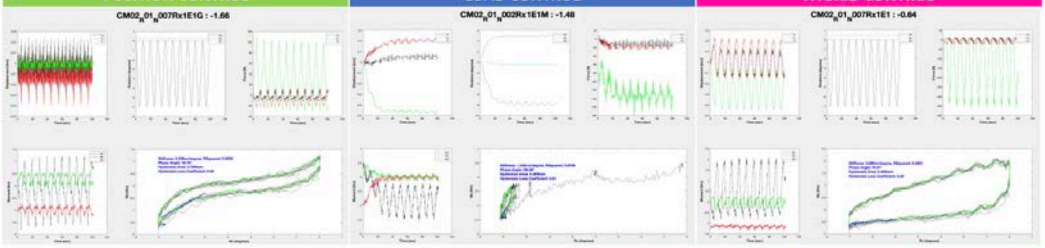

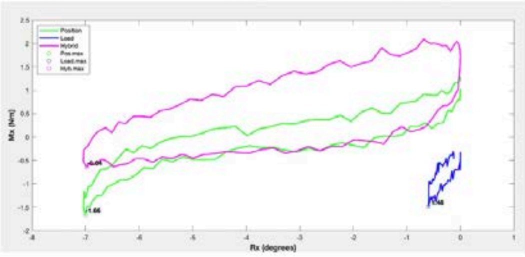

	POSITION CONTROL	LOAD CONTROL	HYBRID CONTROL
Stiffness (Nm/°) (RSqaured)	0.53 (0.9230)	1.24 (0.6709)	0.08 (0.4901)
Phase Angle (°)	18.74	34.58	44.91
Hysteresis Area (Nm°)	3.70	0.26	9.48
Hysteresis Loss Coefficient	0.33	0.61	0.59
Maximum Reaction Moment (Nm)	-1.66	-1.48	-0.64

EXTENSION (Rx +2°)

POSITION CONTROL	LOAD CONTROL	HYBRID CONTROL

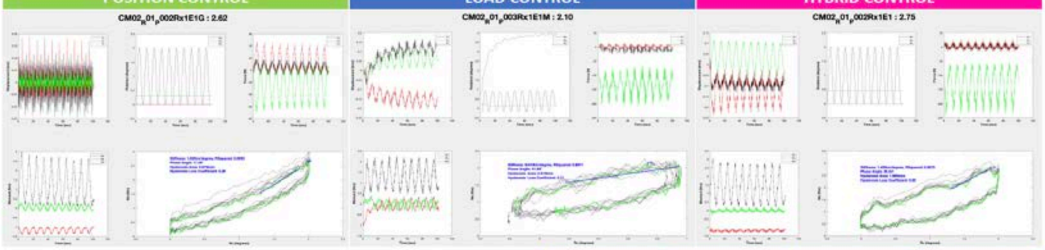

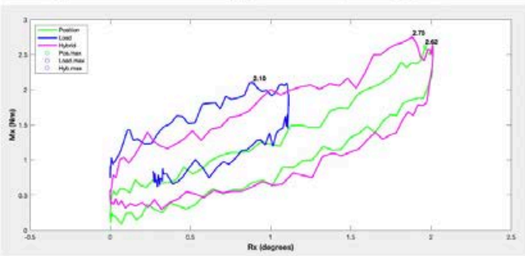

	POSITION CONTROL	LOAD CONTROL	HYBRID CONTROL
Stiffness (Nm/°) (RSqaured)	1.55 (0.9693)	0.61 (0.6971)	1.45 (0.8973)
Phase Angle (°)	17.48	41.86	35.54
Hysteresis Area (Nm°)	0.97	0.81	1.98
Hysteresis Loss Coefficient	0.38	0.71	0.65
Maximum Reaction Moment (Nm)	2.62	2.10	2.75

AXIAL COMPRESSION (Tz -0.3mm)

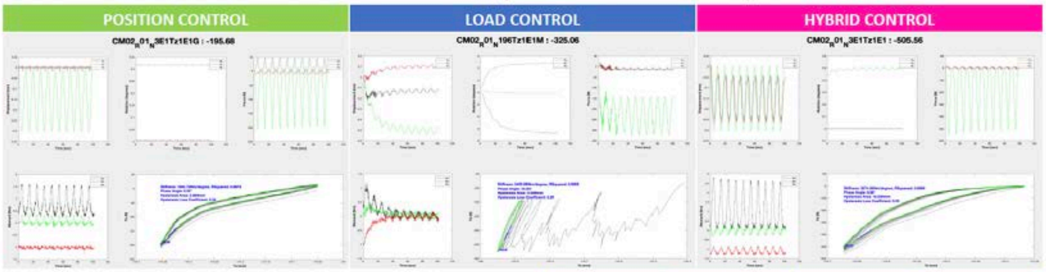

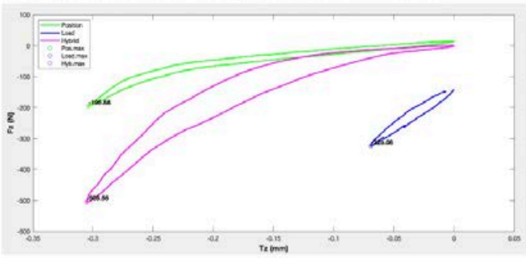

	POSITION CONTROL	LOAD CONTROL	HYBRID CONTROL
Stiffness (N/mm) (RSqaured)	1943.72 (0.9979)	2452.69 (0.9905)	3274.26 (0.9989)
Phase Angle (°)	6.92	18.83	8.88
Hysteresis Area (Nmm)	5.39	2.04	18.02
Hysteresis Loss Coefficient	0.24	0.29	0.33
Maximum Reaction Force (N)	-195.68	-325.06	-505.56

LEFT LATERAL SHEAR (Tx -0.6mm) - FAILED

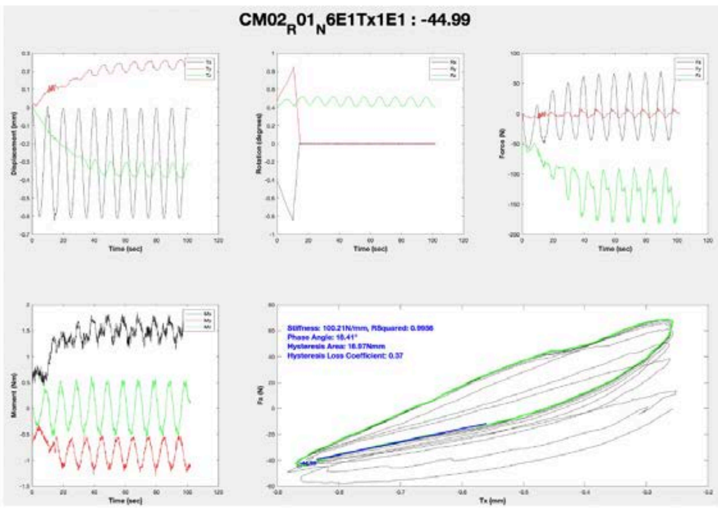

RIGHT LATERAL SHEAR (Tx +0.6mm) - FAILED

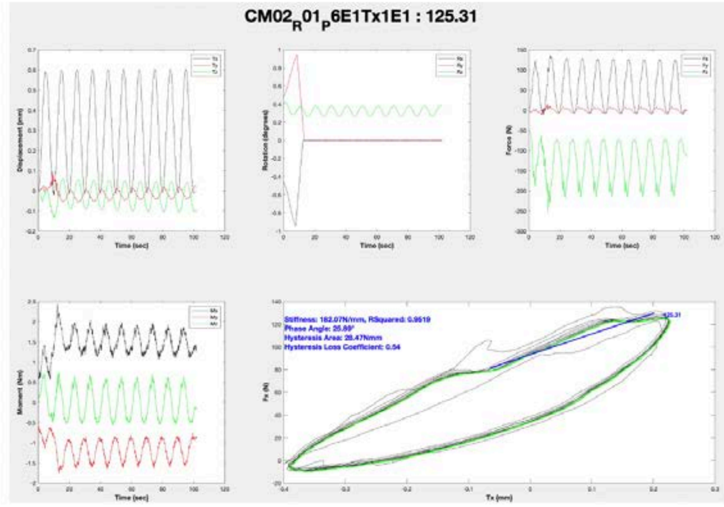

POSTERIOR SHEAR (Ty -0.6mm) - FAILED

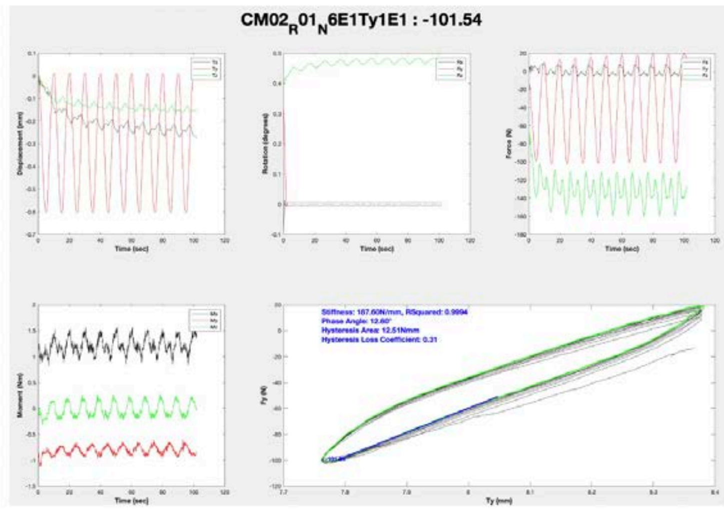

Appendix E: Test Result

Appendix E.1 CM03 (10 cycles at 0.1Hz, additional flexion test for 5 cycles at 0.01Hz)

CM03

Multiaxial Spine Segment Testing: Position vs Load Control and Physiological Relevance

Flinders University
Masters Thesis
Daniel Kim
kim0872@flinders.edu.au
Supervisor: A.Professor John Costi, Co-Supervisor: Mr Michael Russo

SPECIMEN SPECIFICATION

Specimen Prep Date	08/09/2021	Specimen ID	CM03
Testing Date	09/09/2021	Disc Level	L4 – L5

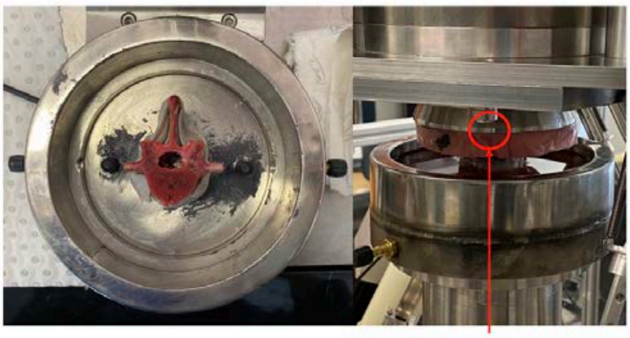

** A block (8.1mm) was inserted on top of the vertebrae to avoid failure

OFFSET	(mm)
X-offset	-1.4
Y-offset	-10.37
Z-offset	77.62

COMPRESSIVE LOAD	(N)
Preload	-12.81
Follower	-164.04
Reference	-201.85

TIMETABLE

Date	Time		Status	Duration	Notes
08.09.21	14:30	Start	Measurement & Potting	03:30	On the hexapod
	17:45	End			
	17:45	Start	Specimen Setup & Overnight Hydration	00:45	Fx, Fy, and Fz oscillates -5N ~ 5N Tried turning on/off adaptive tuning -> still oscillates Changed value of "preload" -> still oscillates, peak changes Stopped batch -> Data wasn't saved -> Video taken by Michael
	18:30	End			
	18:30	Start	Overnight Hydration	13:30	Wasn't able to remove oscillations Fix the value of adaptive tuning as 3000/3000/9000/15/15/15 preload : -20N
09.09.21	08:00	End			
	08:47	Start	Recovery	00:30	Unbolt and re-bolt the cup -> apply 30 mins recovery Still oscillates
	09:17	End			
	09:17	Start	Load Control	01:00	10cycles of 11 directional tests + additional Flexion test (0.01Hz, 5 cycles) Shear Tests : 200N -> Grap the range of Translation Rotational Tests : 5Nm -> Grap the range of Rotation Compression : 1.1Mpa (N) -> -201.86N
	10:21	End			
	10:27	Start	Load-Pos Recovery	02:00	
	12:30	End			

Date	Time		Status	Duration	Notes
09.09.21	12:51	Start	Position Control	00:03	Hit the limit -> Tried to make Tx and Ty 0 Batch Stopped
	12:54	End			
	13:06	Start	Contrain Test	00:07	Angle of Contrain "Current angle" -> Worked!
	13:11	End			
	13:15	Start	Position Control	01:00	Edited batch for Angle of Contrain "Current angle" Adaptive tunning working -> hit the minimum value of Tz stiffness fast (6000 -> 1500) about a half of the cycle Adaptive tuning is "ON" till the end
	14:22	End			
	14:32	Start	Pos-Hyb Recovery	02:00	
	16:37	End			
	16:40	Start	Hybrid Control	01:00	
	17:45	End			

OVERNIGHT HYDRATION

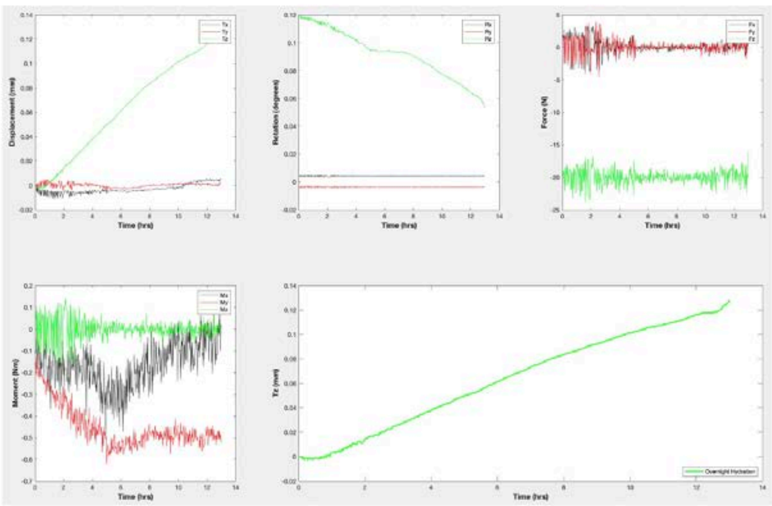

RECOVERY

BEFORE OVERNIGHT HYDRATION	BEEFORE LOAD CONTROL	BEFORE POSITION CONTROL	BEFORE HYBRID CONTROL
-152.977	-152.913 (+0.064)	-152.87 (+0.107)	-152.914 (+0.063)

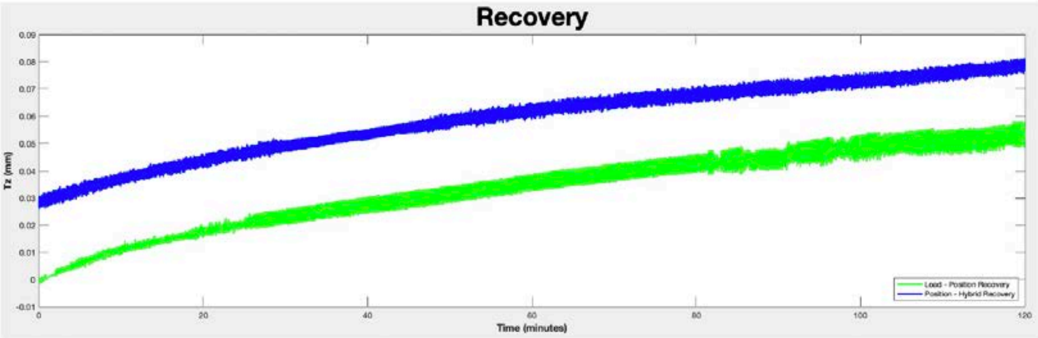

LEFT LATERAL SHEAR (Fx -200N) (Tx -0.42mm)

LOAD CONTROL	POSITION CONTROL	HYBRID CONTROL
CM03N200Tx1E1M : -198.35 (0.87 ~ 0.45 / -0.42)	CM03N4E1Tx1E1 : -200.38 (1.06 ~ 0.63 / -0.43)	CM03N4E1Tx1E1 : -165.49 (1.09 ~ 0.66 / -0.43)

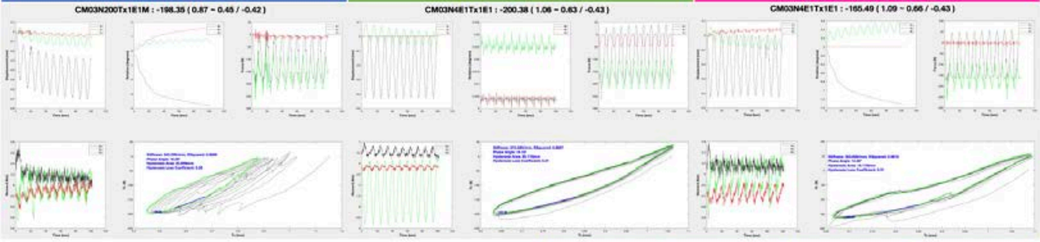

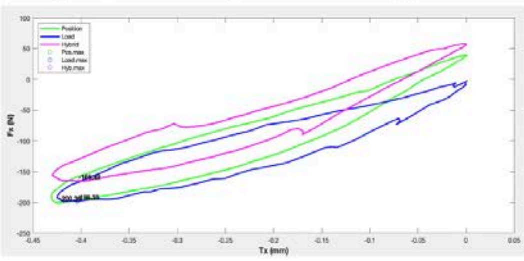

	LOAD CONTROL	POSITION CONTROL	HYBRID CONTROL
Stiffness (N/mm) (RSqaured)	345.29 (0.9866)	372.35 (0.9967)	353.90 (0.9915)
Phase Angle (°)	19.59	14.10	14.60
Hysteresis Area (Nmm)	20.86	20.11	19.11
Hysteresis Loss Coefficient	0.38	0.31	0.31
Maximum Reaction Force (N)	-198.35	-200.38	-165.49

RIGHT LATERAL SHEAR (Fx +200N) (Tx +0.53mm)

LOAD CONTROL	POSITION CONTROL	HYBRID CONTROL

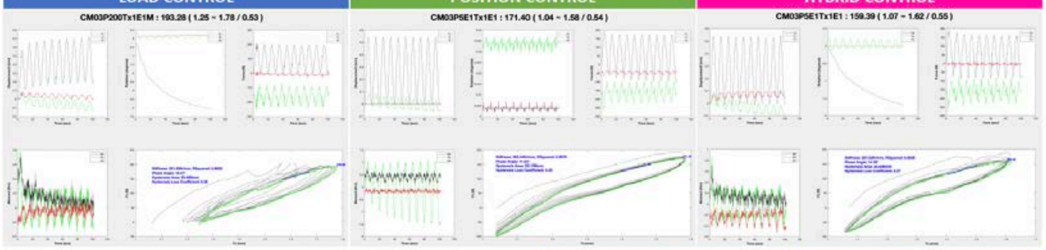

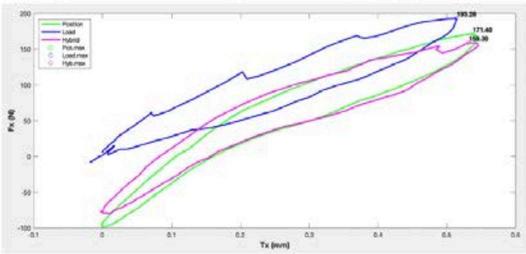

	LOAD CONTROL	POSITION CONTROL	HYBRID CONTROL
Stiffness (N/mm) (RSqaured)	251.50 (0.8652)	302.44 (0.9976)	297.52 (0.9636)
Phase Angle (°)	18.47	11.01	14.39
Hysteresis Area (Nmm)	23.40	22.10	23.93
Hysteresis Loss Coefficient	0.35	0.23	0.27
Maximum Reaction Force (N)	193.28	171.40	159.39

POSTERIOR SHEAR (Fy -200N) (Ty -0.31mm)

LOAD CONTROL	POSITION CONTROL	HYBRID CONTROL

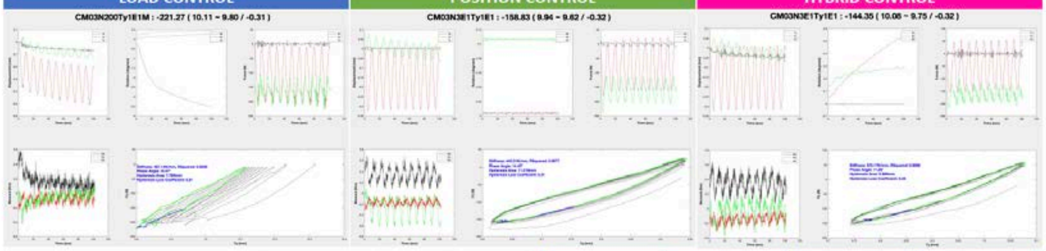

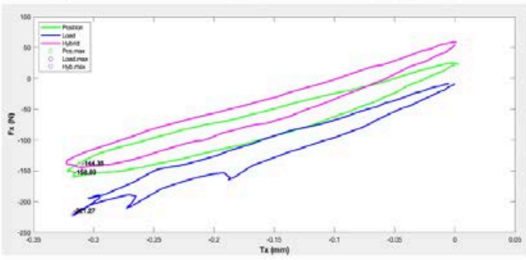

	LOAD CONTROL	POSITION CONTROL	HYBRID CONTROL
Stiffness (N/mm) (RSqaured)	487.14 (0.8599)	442.31 (0.9977)	575.17 (0.9969)
Phase Angle (°)	10.47	14.45	11.58
Hysteresis Area (Nmm)	7.78	11.21	9.98
Hysteresis Loss Coefficient	0.21	0.31	0.25
Maximum Reaction Force (N)	-221.27	-158.83	-144.35

ANTERIOR SHEAR (Fy +200N) (Ty +0.68mm)

LOAD CONTROL	POSITION CONTROL	HYBRID CONTROL
CM03P200Ty1E1M : 181.95 (10.42 ~ 11.10 / 0.68)	CM03P7E1Ty1E1 : 172.73 (9.89 ~ 10.58 / 0.70)	CM03P7E1Ty1E1 : 195.18 (9.97 ~ 10.67 / 0.70)

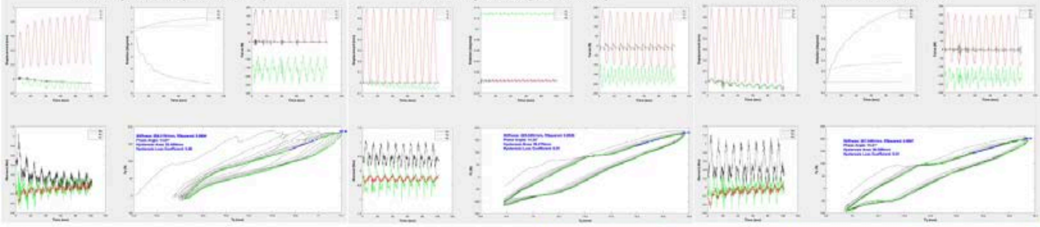

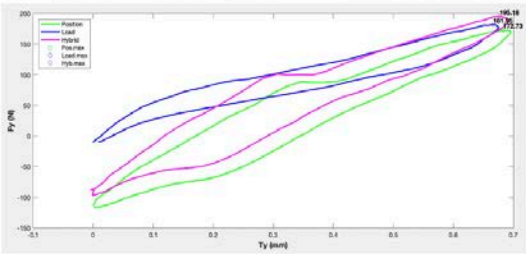

	LOAD CONTROL	POSITION CONTROL	HYBRID CONTROL
Stiffness (N/mm) (RSqaured)	256.31 (0.9994)	325.50 (0.9926)	307.04 (0.9997)
Phase Angle (°)	14.31	14.32	14.31
Hysteresis Area (Nmm)	22.45	39.27	39.28
Hysteresis Loss Coefficient	0.28	0.31	0.31
Maximum Reaction Force (N)	181.95	172.73	195.18

LEFT AXIAL ROTATION (Mz +5Nm) (Rz +0.88°)

LOAD CONTROL	POSITION CONTROL	HYBRID CONTROL
CM03P005Rz1E1M : 4.87 (1.22 ~ 2.10 / 0.88)	CM03P9E1Rz1E1 : 4.97 (0.15 ~ 1.04 / 0.89)	CM03P9E1Rz1E1 : 2.77 (0.21 ~ 1.11 / 0.89)

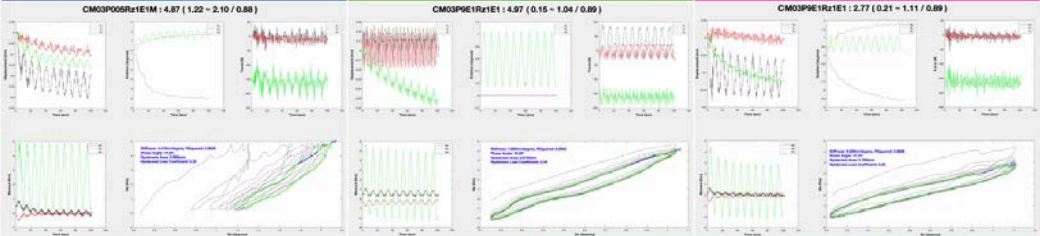

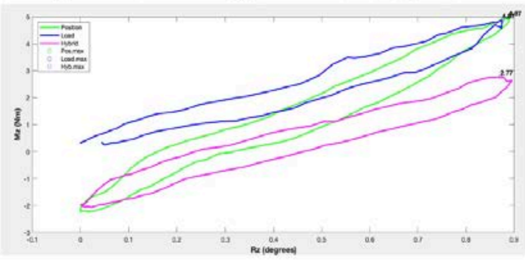

	LOAD CONTROL	POSITION CONTROL	HYBRID CONTROL
Stiffness (Nm/°) (RSqaured)	4.41 (0.9629)	7.86 (0.9903)	6.56 (0.9998)
Phase Angle (°)	14.04	10.88	15.20
Hysteresis Area (Nm°)	0.68	0.87	0.76
Hysteresis Loss Coefficient	0.32	0.24	0.30
Maximum Reaction Moment (Nm)	4.87	4.97	2.77

RIGHT AXIAL ROTATION (Mz -5Nm) (Rz -0.77°)

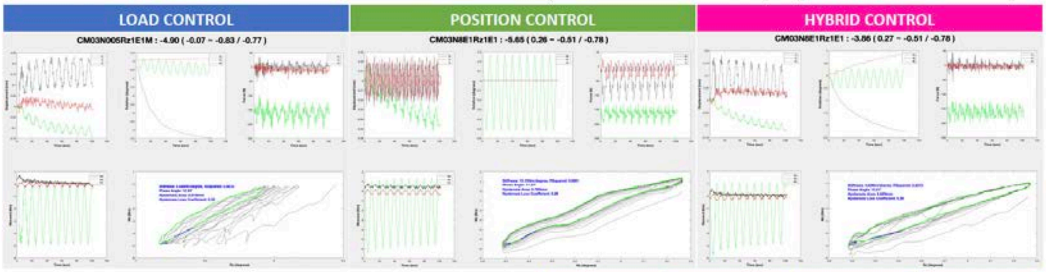

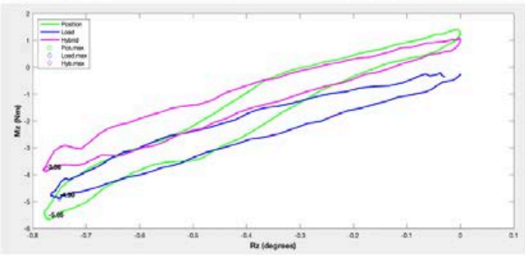

	LOAD CONTROL	POSITION CONTROL	HYBRID CONTROL
Stiffness (Nm/°) (RSqaured)	5.48 (0.9970)	13.15 (0.9861)	4.63 (0.9373)
Phase Angle (°)	12.95	11.47	13.51
Hysteresis Area (Nm°)	0.61	0.78	0.62
Hysteresis Loss Coefficient	0.32	0.28	0.29
Maximum Reaction Moment (Nm)	-4.90	-5.65	-3.86

LEFT LATERAL BENDING (My -5Nm) (Ry -1.81°)

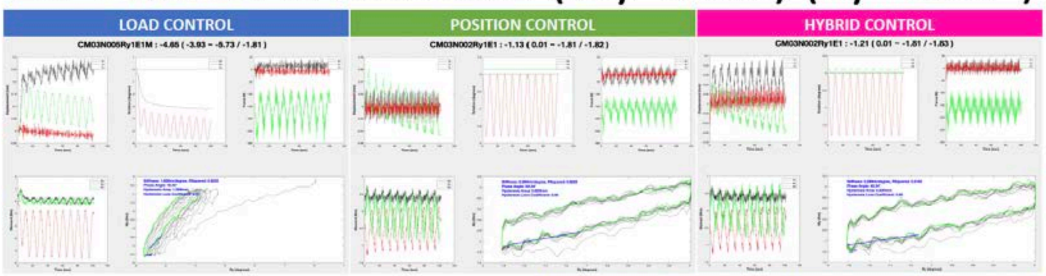

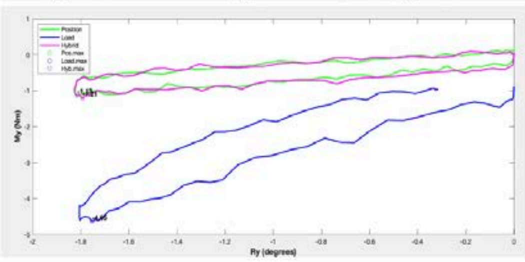

	LOAD CONTROL	POSITION CONTROL	HYBRID 28NTROL
Stiffness (Nm/°) (RSqaured)	1.85 (0.9252)	0.35 (0.6223)	0.56 (0.5163)
Phase Angle (°)	18.45	33.24	40.34
Hysteresis Area (Nm°)	1.59	0.82	0.93
Hysteresis Loss Coefficient	0.47	0.55	0.60
Maximum Reaction Moment (Nm)	-4.65	-1.13	-1.21

RIGHT LATERAL BENDING (My +5Nm) (Ry +1.89°)

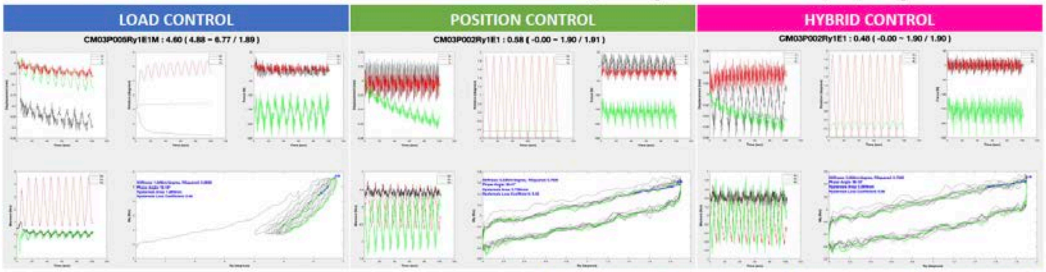

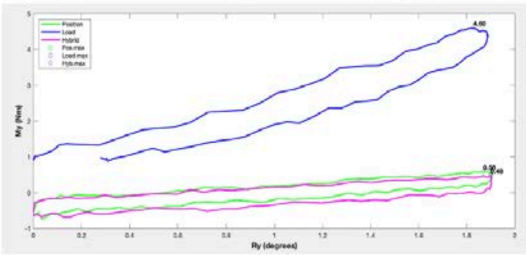

	LOAD CONTROL	POSITION CONTROL	HYBRID CONTROL
Stiffness (Nm/°) (RSqaured)	1.84 (0.8906)	0.33 (0.7695)	0.26 (0.7305)
Phase Angle (°)	15.15	28.47	39.12
Hysteresis Area (Nm°)	1.38	0.73	0.89
Hysteresis Loss Coefficient	0.40	0.42	0.58
Maximum Reaction Moment (Nm)	4.60	0.58	0.48

FLEXION (@0.01Hz) (Mx -5Nm) (Rx -2.58°)

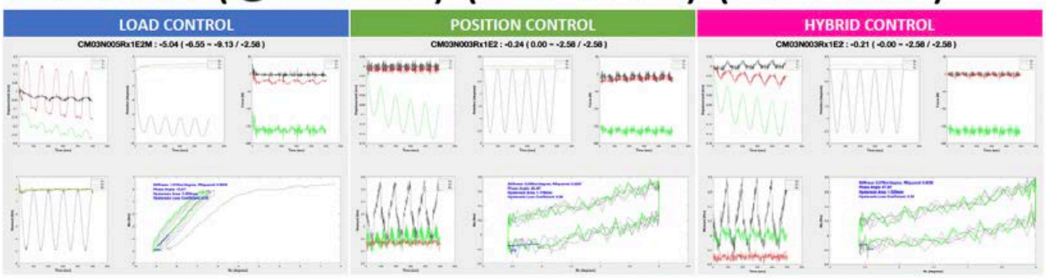

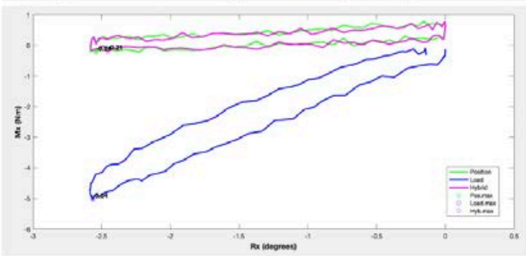

	LOAD CONTROL	POSITION CONTROL	HYBRID CONTROL
Stiffness (Nm/°) (RSqaured)	1.81 (0.9503)	0.05 (0.0267)	0.07 (0.0035)
Phase Angle (°)	12.67	48.46	47.20
Hysteresis Area (Nm°)	2.25	1.11	1.02
Hysteresis Loss Coefficient	0.34	0.56	0.52
Maximum Reaction Moment (Nm)	-5.04	-0.24	-0.21

FLEXION (Mx -5Nm) (Rx -1.66°)

LOAD CONTROL	POSITION CONTROL	HYBRID CONTROL
CM03N005Rx1E1M : -4.72 (-7.10 ~ -8.76 / -1.66)	CM03N002Rx1E1 : -0.17 (0.01 ~ -1.66 / -1.67)	CM03N002Rx1E1 : -0.25 (0.00 ~ -1.67 / -1.67)

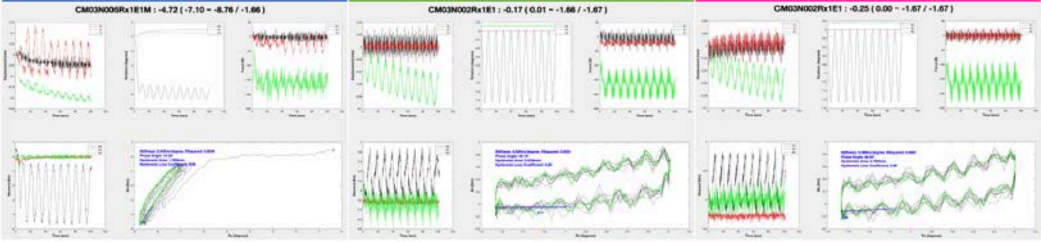

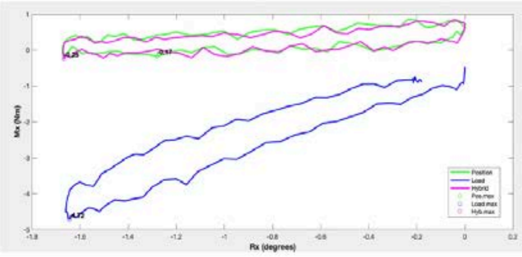

	LOAD CONTROL	POSITION CONTROL	HYBRID CONTROL
Stiffness (Nm/°) (RSqaured)	2.34 (0.8549)	0.02 (0.0031)	0.09 (0.0481)
Phase Angle (°)	14.32	49.16	48.63
Hysteresis Area (Nm°)	1.39	0.83	0.76
Hysteresis Loss Coefficient	0.38	0.60	0.56
Maximum Reaction Moment (Nm)	-4.72	-0.17	-0.25

EXTENSION (Mx +5Nm) (Rx +2°)

LOAD CONTROL	POSITION CONTROL	HYBRID CONTROL
CM03P005Rx1E1M : 4.61 (1.98 ~ 3.98 / 2.00)	CM03P002Rx1E1 : 1.94 (-0.01 ~ 2.01 / 2.02)	CM03P002Rx1E1 : 2.01 (-0.01 ~ 2.00 / 2.02)

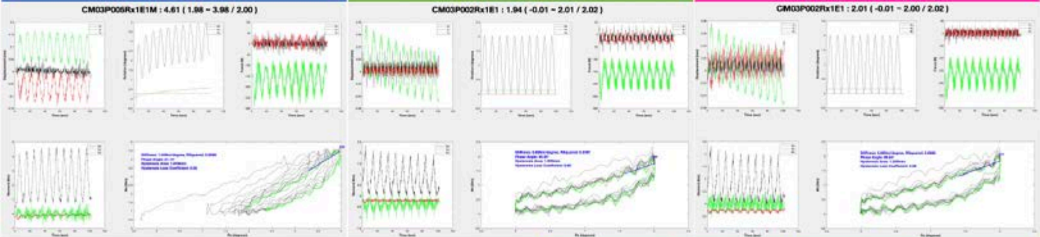

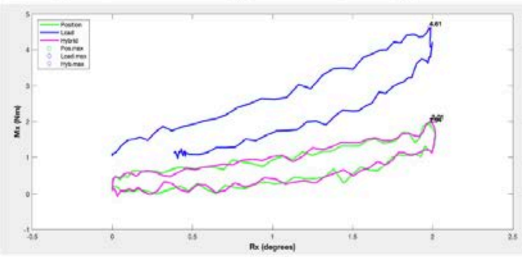

	LOAD CONTROL	POSITION CONTROL	HYBRID CONTROL
Stiffness (Nm/°) (RSqaured)	1.64 (0.8268)	0.80 (0.3787)	0.86 (0.6968)
Phase Angle (°)	21.14	30.35	29.64
Hysteresis Area (Nm°)	1.91	1.22	1.24
Hysteresis Loss Coefficient	0.53	0.60	0.56
Maximum Reaction Moment (Nm)	4.61	1.94	2.01

AXIAL COMPRESSION (Fz -201.85N) (Tz -0.04mm)

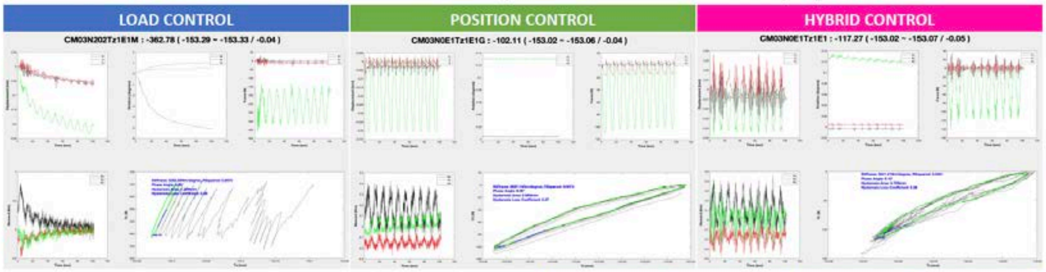

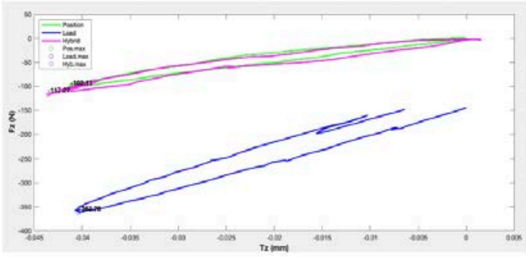

	LOAD CONTROL	POSITION CONTROL	HYBRID CONTROL
Stiffness (N/mm) (RSqaured)	5362.68 (0.9970)	2867.14 (0.9974)	2041.21 (0.5351)
Phase Angle (°)	9.69	8.29	9.10
Hysteresis Area (Nmm)	1.29	0.58	0.70
Hysteresis Loss Coefficient	0.28	0.27	0.28
Maximum Reaction Force (N)	-362.78	-102.11	-117.27

Appendix E.2 CM04 (10 cycles at 0.1Hz, additional flexion test for 5 cycles at 0.01Hz)

CM04

Multiaxial Spine Segment Testing: Position vs Load Control and Physiological Relevance

Flinders University
Masters Thesis
Daniel Kim
kim0872@flinders.edu.au
Supervisor: A.Professor John Costi, Co-Supervisor: Mr Michael Russo

SPECIMEN SPECIFICATION

Specimen Prep Date	15/09/2021	Specimen ID	CM04
Testing Date	16/09/2021	Disc Level	L4 – L5

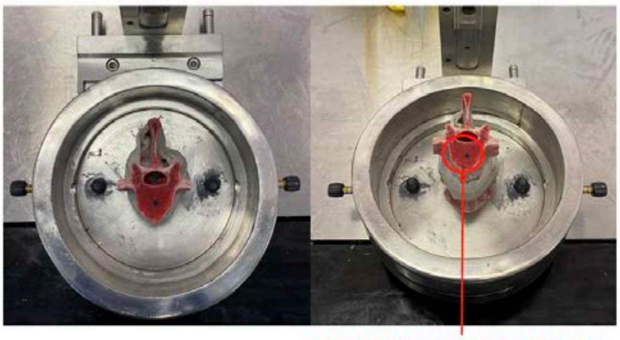

** A block (8.1mm) was inserted on top of the vertebrae to avoid failure

OFFSET	(mm)
X-offset	-0.33
Y-offset	-9.33
Z-offset	78.17

COMPRESSIVE LOAD	(N)
Preload	-16.05
Follower	-180.23
Reference	-221.27

TIMETABLE

Date	Time		Status	Duration	Notes
15.09.21	10:48	Start	Measurement & Defrosting	00:30	
	16:15	End			
	17:15	Start	Specimen potting/setup, Hexapod setup	00:45	
	18:30	End			
	18:51	Start	Overnight Hydration	12:43	didn't zero out moments of x and y 0 out preload and Turned the load control off and record initial offsets
16.09.21	-	End			
	-	Start	Load Control	01:00	Shear Tests : 200N Rotational Tests : 5Nm Compression : 0.6MPa -> -221.27N
	08:39	End			
	08:45	Start	Load-Pos Recovery	02:00	1Hz 7200s
	10:45	End			
	10:52	Start	Position Control	01:30	Updated batch for Angle of Contrain "Current angle" stopped during PRy - door touched saved files in separate folder run 2 mins of recovery - data collected and saved re-started test from Pry stopped at the beginning of compression test run 2 mins of recovery - data collected and saved re-started test from NTz Changed range (-0.5 -> -0.07)
	11:32	Stop			
	11:42	Start			
	12:08	Stop			
	12:18	Start			
	12:25	End			
	12:25	Start	Pos-Hyb Recovery	02:00	1Hz 7200s
	14:25	End			
	14:28	Start	Hybrid Control	01:00	
	15:35	End			

The bottom piller bolts were not tightened
two in the back (?)

OVERNIGHT HYDRATION

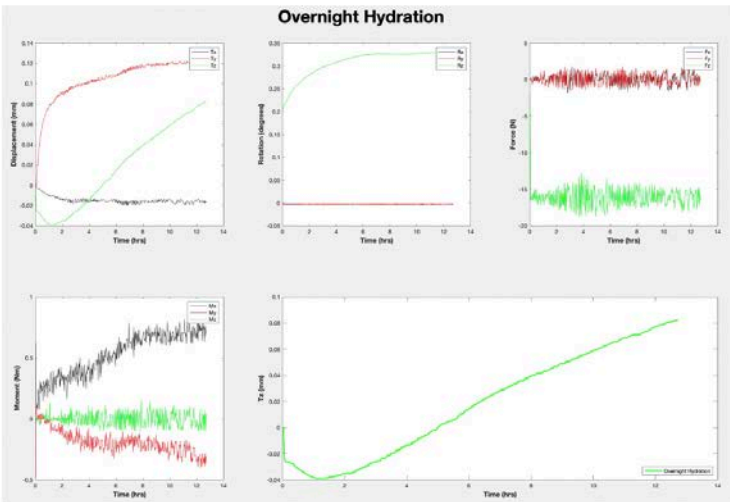

RECOVERY

BEFORE OVERNIGHT HYDRATION	BEEFORE LOAD CONTROL	BEFORE POSITION CONTROL	BEFORE HYBRID CONTROL
-144.46	-	-144.394 (+0.066)	-144.4 (+0.06)

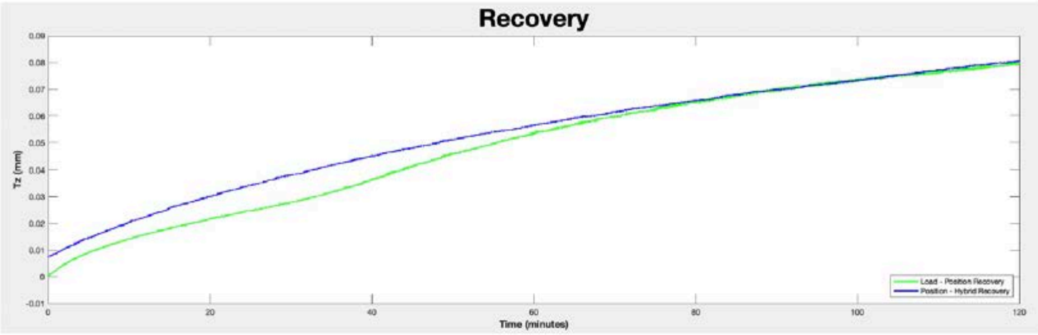

LEFT LATERAL SHEAR (Fx -200N) (Tx -0.63mm)

LOAD CONTROL	POSITION CONTROL	HYBRID CONTROL
CM04N200Tx1E1M : -193.66 (-0.35 ~ -0.98 / -0.63)	CM04N6E1Tx1E1 : -208.12 (-0.23 ~ -0.87 / -0.65)	CM04N6E1Tx1E1 : -144.85 (-0.16 ~ -0.80 / -0.64)

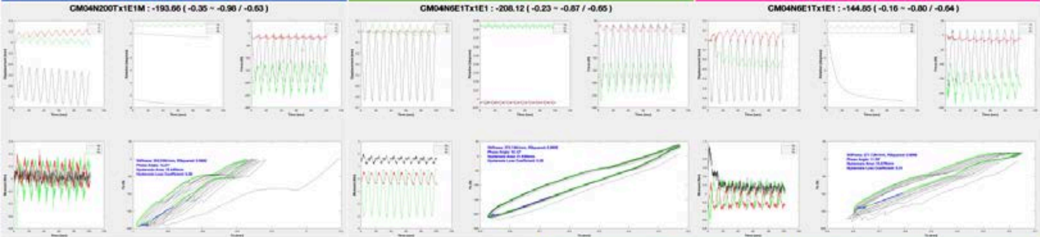

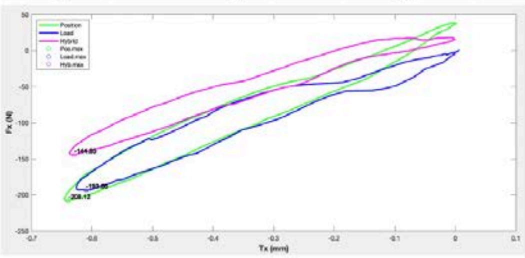

	LOAD CONTROL	POSITION CONTROL	HYBRID CONTROL
Stiffness (N/mm) (RSqaured)	302.53 (0.9982)	373.74 (0.9992)	277.72 (0.9966)
Phase Angle (°)	12.91	10.12	11.39
Hysteresis Area (Nmm)	19.44	21.63	15.67
Hysteresis Loss Coefficient	0.30	0.25	0.31
Maximum Reaction Force (N)	-193.66	-208.12	-144.85

RIGHT LATERAL SHEAR (Fx +200N) (Tx +0.75mm)

LOAD CONTROL	POSITION CONTROL	HYBRID CONTROL

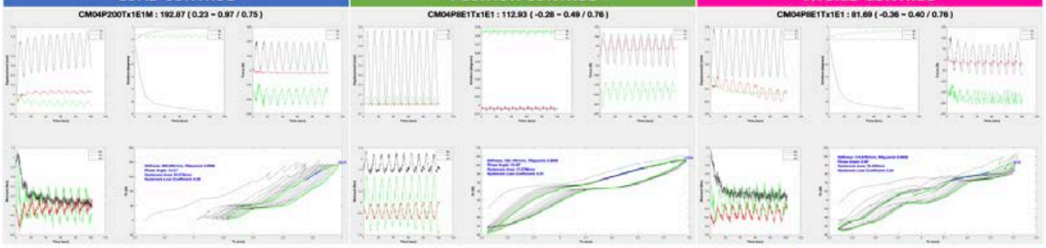

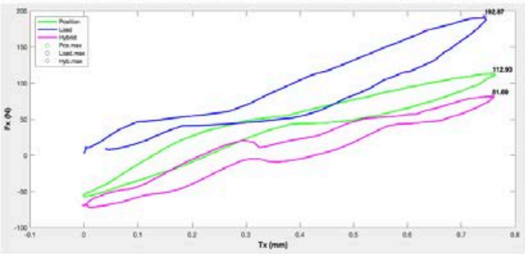

	LOAD CONTROL	POSITION CONTROL	HYBRID CONTROL
Stiffness (N/mm) (RSqaured)	299.36 (0.9995)	168.14 (0.9990)	110.87 (0.9402)
Phase Angle (°)	14.01	10.46	8.90
Hysteresis Area (Nmm)	23.91	17.57	16.44
Hysteresis Loss Coefficient	0.33	0.21	0.24
Maximum Reaction Force (N)	192.87	112.93	81.69

POSTERIOR SHEAR (Fy -200N) (Ty -0.50mm)

LOAD CONTROL	POSITION CONTROL	HYBRID CONTROL

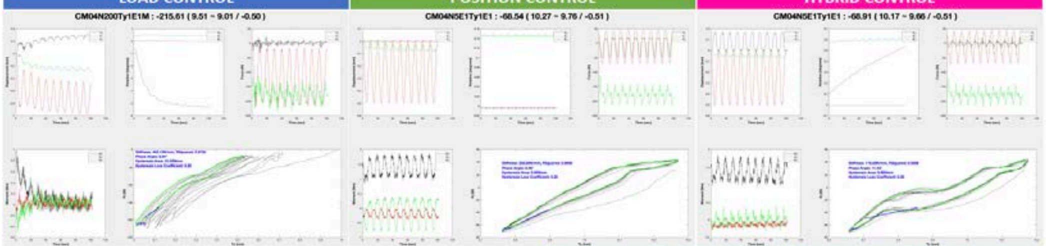

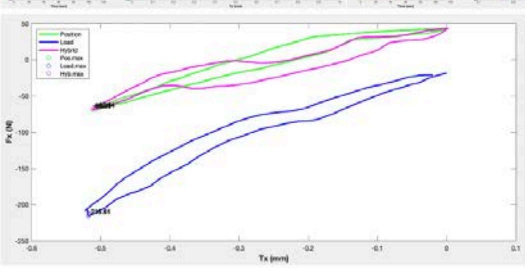

	LOAD CONTROL	POSITION CONTROL	HYBRID CONTROL
Stiffness (N/mm) (RSqaured)	442.15 (0.9730)	258.99 (0.9998)	116.08 (0.5898)
Phase Angle (°)	8.64	8.48	11.45
Hysteresis Area (Nmm)	10.02	6.69	9.68
Hysteresis Loss Coefficient	0.22	0.25	0.30
Maximum Reaction Force (N)	-215.61	-68.54	-68.91

ANTERIOR SHEAR (Fy +200N) (Ty +0.91mm)

LOAD CONTROL	POSITION CONTROL	HYBRID CONTROL

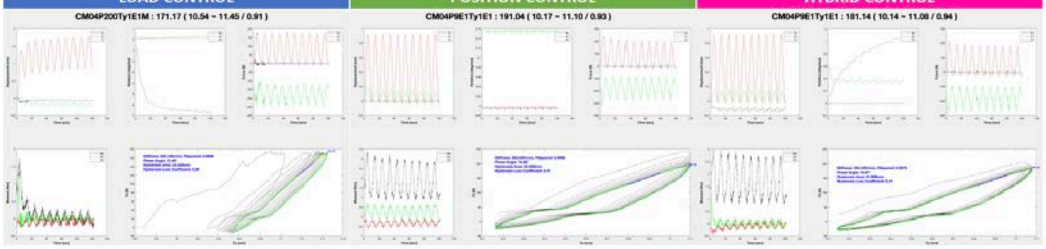

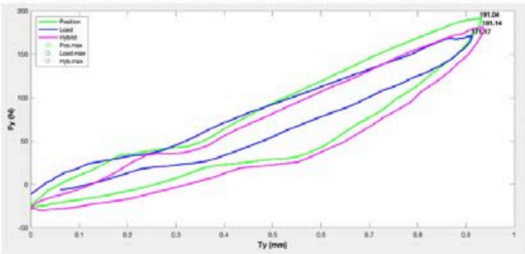

	LOAD CONTROL	POSITION CONTROL	HYBRID CONTROL
Stiffness (N/mm) (RSqaured)	200.13 (0.9999)	250.55 (0.9988)	250.33 (0.9976)
Phase Angle (°)	12.46	16.28	15.97
Hysteresis Area (Nmm)	25.00	43.59	41.86
Hysteresis Loss Coefficient	0.29	0.41	0.41
Maximum Reaction Force (N)	171.17	191.04	181.14

LEFT AXIAL ROTATION (Mz +5Nm) (Rz +0.62°)

LOAD CONTROL	POSITION CONTROL	HYBRID CONTROL

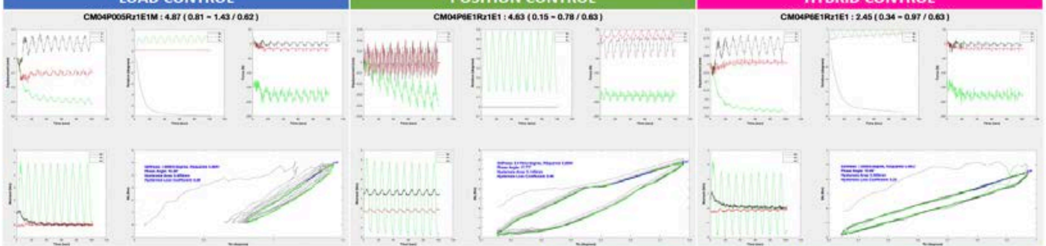

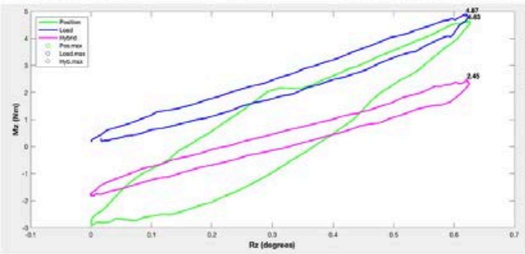

	LOAD CONTROL	POSITION CONTROL	HYBRID CONTROL
Stiffness (Nm/°) (RSqaured)	7.69 (0.9947)	9.41 (0.9994)	7.55 (0.9937)
Phase Angle (°)	10.38	17.77	10.48
Hysteresis Area (Nm°)	0.40	1.14	0.34
Hysteresis Loss Coefficient	0.26	0.40	0.23
Maximum Reaction Moment (Nm)	4.87	4.63	2.45

RIGHT AXIAL ROTATION (Mz -5Nm) (Rz -0.63°)

LOAD CONTROL	POSITION CONTROL	HYBRID CONTROL

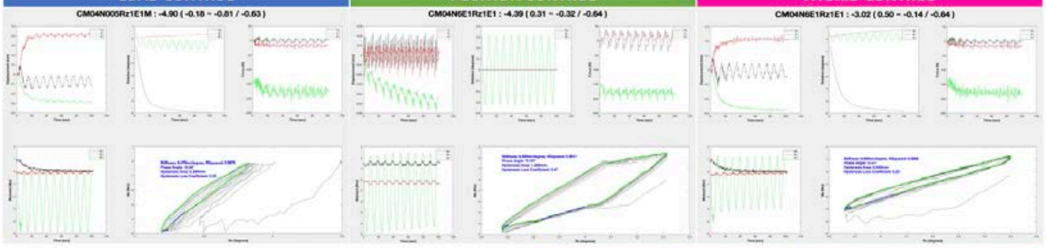

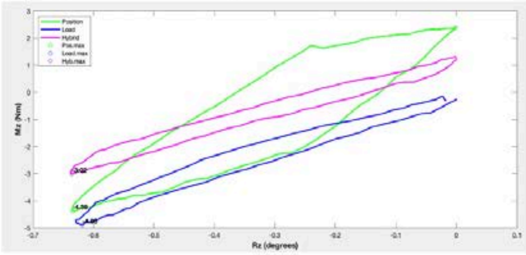

	LOAD CONTROL	POSITION CONTROL	HYBRID CONTROL
Stiffness (Nm/°) (RSqaured)	8.47 (0.9875)	6.90 (0.9917)	6.85 (0.9985)
Phase Angle (°)	10.40	20.60	10.41
Hysteresis Area (Nm°)	0.39	1.30	0.34
Hysteresis Loss Coefficient	0.25	0.47	0.23
Maximum Reaction Moment (Nm)	-4.90	-4.39	-3.02

LEFT LATERAL BENDING (My -5Nm) (Ry -2.37°)

LOAD CONTROL	POSITION CONTROL	HYBRID CONTROL

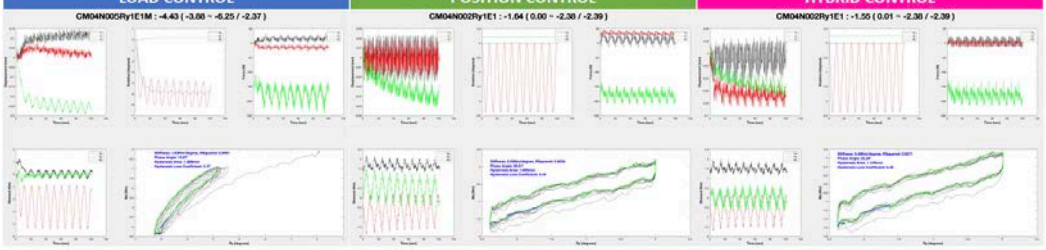

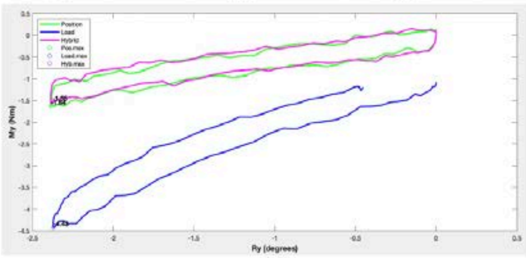

	LOAD CONTROL	POSITION CONTROL	HYBRID 28NTROL
Stiffness (Nm/°) (RSqaured)	1.63 (0.9461)	0.53 (0.8234)	0. 46 (0.6371)
Phase Angle (°)	13.67	22.51	25.29
Hysteresis Area (Nm°)	1.39	1.09	1.14
Hysteresis Loss Coefficient	0.37	0.44	0.46
Maximum Reaction Moment (Nm)	-4.43	-1.64	-1.55

** Test stopped and restarted

RIGHT LATERAL BENDING (My +5Nm) (Ry +2.12°)

LOAD CONTROL	POSITION CONTROL	HYBRID CONTROL
CM04P005Ry1E1M : 4.43 (4.94 ~ 7.06 / 2.12)	CM04P002Ry1E1 : 0.72 (-0.00 ~ 2.13 / 2.13)	CM04P002Ry1E1 : 0.77 (-0.00 ~ 2.13 / 2.13)

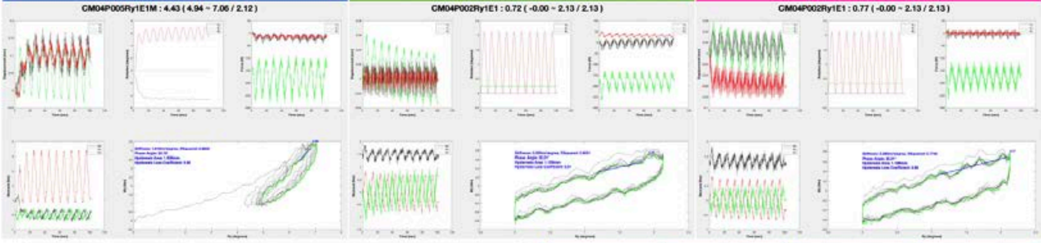

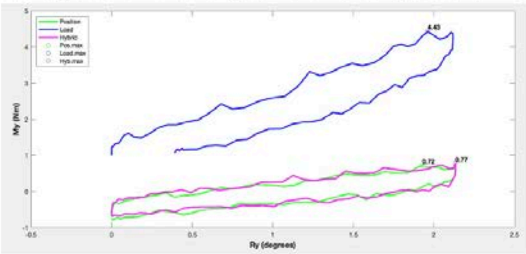

	LOAD CONTROL	POSITION CONTROL	HYBRID CONTROL
Stiffness (Nm/°) (RSqaured)	1.61 (0.8850)	0.35 (0.8021)	0.36 (0.7740)
Phase Angle (°)	20.76	32.51	35.91
Hysteresis Area (Nm°)	1.93	1.10	1.19
Hysteresis Loss Coefficient	0.50	0.51	0.58
Maximum Reaction Moment (Nm)	4.43	0.72	0.77

FLEXION (@0.01Hz) (Mx -5Nm) (Rx -2.15°)

LOAD CONTROL	POSITION CONTROL	HYBRID CONTROL
CM04N005Rx1E2M : -5.08 (-7.48 ~ -9.63 / -2.15)	CM04N002Rx1E2 : 0.64 (-0.00 ~ -2.15 / -2.15)	CM04N002Rx1E2 : 0.51 (-0.00 ~ -2.15 / -2.15)

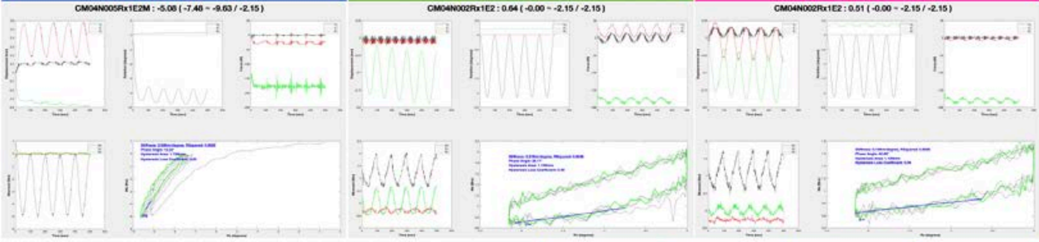

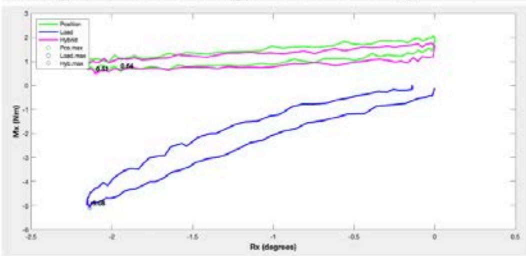

	LOAD CONTROL	POSITION CONTROL	HYBRID CONTROL
Stiffness (Nm/°) (RSqaured)	2.58 (0.9695)	0.21 (0.6346)	0.15 (0.6006)
Phase Angle (°)	12.22	38.17	42.88
Hysteresis Area (Nm°)	1.73	1.15	1.10
Hysteresis Loss Coefficient	0.33	0.48	0.54
Maximum Reaction Moment (Nm)	-5.08	0.64	0.51

FLEXION (Mx -5Nm) (Rx -1.44°)

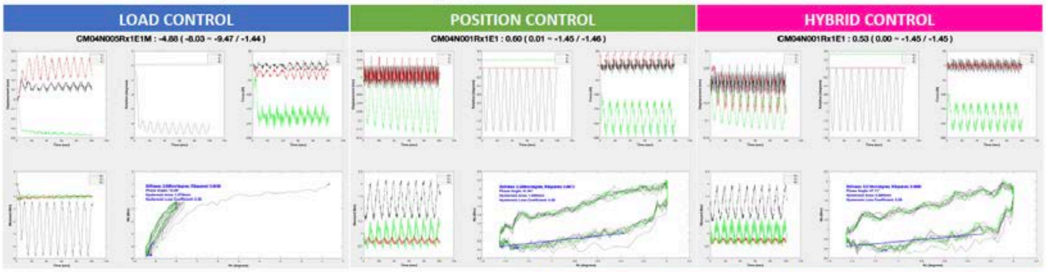

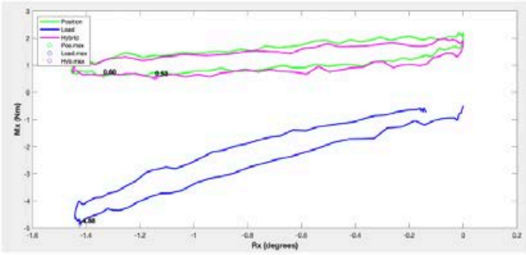

	LOAD CONTROL	POSITION CONTROL	HYBRID CONTROL
Stiffness (Nm/°) (RSqaured)	2.99 (0.9436)	0.28 (0.6473)	0.21 (0.3866)
Phase Angle (°)	13.06	41.94	47.11
Hysteresis Area (Nm°)	1.07	1.02	0.98
Hysteresis Loss Coefficient	0.35	0.55	0.58
Maximum Reaction Moment (Nm)	-4.88	0.60	0.53

EXTENSION (Mx +5Nm) (Rx +2.25°)

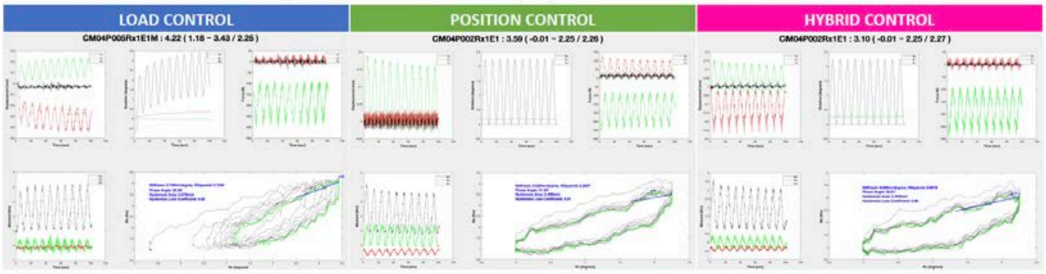

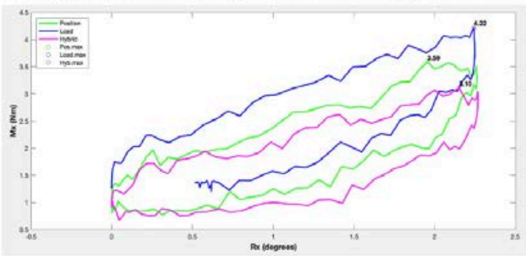

	LOAD CONTROL	POSITION CONTROL	HYBRID CONTROL
Stiffness (Nm/°) (RSqaured)	0.74 (0.7349)	0.52 (0.3597)	0.62 (0.6919)
Phase Angle (°)	32.39	31.29	36.81
Hysteresis Area (Nm°)	2.67	2.40	2.32
Hysteresis Loss Coefficient	0.65	0.61	0.66
Maximum Reaction Moment (Nm)	4.22	3.59	3.10

** Test stopped and restarted

AXIAL COMPRESSION (Fz -221.27N) (Tz -0.07mm)

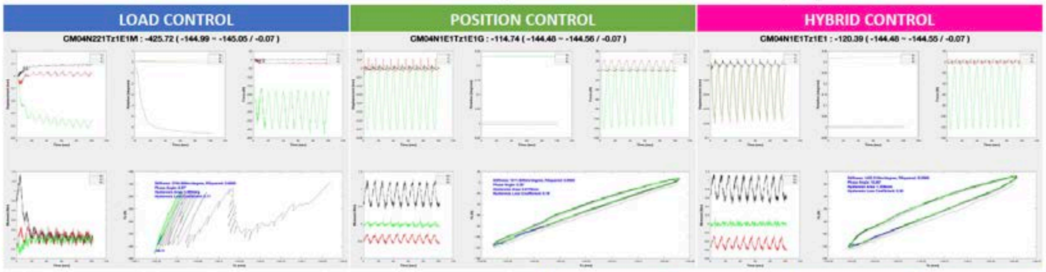

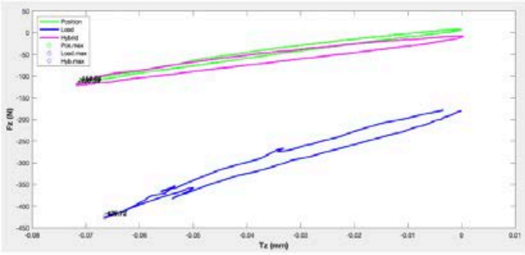

	LOAD CONTROL	POSITION CONTROL	HYBRID CONTROL
Stiffness (N/mm) (RSqaured)	3704.92 (0.8829)	1811.90 (0.9930)	1452.51 (0.9986)
Phase Angle (°)	8.97	5.35	10.80
Hysteresis Area (Nmm)	1.42	0.67	1.32
Hysteresis Loss Coefficient	0.17	0.16	0.30
Maximum Reaction Force (N)	-425.72	-114.74	-120.39

% DIFFERENCES

	CM04											
	Maximum Reaction Force(N) / Moment(Nm)		Under/Overshoot	% Difference	Maximum Reaction Force(N) / Moment(Nm)		Under/Overshoot	% Difference	Maximum Reaction Force(N) / Moment(Nm)		Under/Overshoot	% Difference
	Load	Position			Load	Hybrid			Position	Hybrid		
Left Lateral Shear (-Fx / -Tx)	-193.66	-208.12	Overshoot	7.47%	-193.66	-144.85	Undershoot	25.20%	-208.12	-144.85	Undershoot	30.40%
Right Lateral Shear (+Fx / + Tx)	192.87	112.93	Undershoot	41.45%	192.87	81.69	Undershoot	57.65%	112.93	81.69	Undershoot	27.67%
Posterior Shear (Fy -200N / Ty -0.31mm)	-215.61	-68.54	Undershoot	68.21%	-215.61	-68.91	Undershoot	68.04%	-68.54	-68.91	Overshoot	0.53%
Anterior Shear (Fy +200N / Ty +0.68mm)	171.17	191.04	Overshoot	11.60%	171.17	181.14	Overshoot	5.82%	191.04	181.14	Undershoot	5.18%
Left Axial Rotation (Mz +5Nm / Rz +0.88°)	4.87	4.63	Undershoot	4.84%	4.87	2.45	Undershoot	49.67%	4.63	2.45	Undershoot	47.10%
Right Axial Rotation (Mz -5Nm / Rz -0.77°)	-4.90	-4.39	Undershoot	10.45%	-4.90	-3.02	Undershoot	38.28%	-4.39	-3.02	Undershoot	31.08%
Left Lateral Bending (My -5Nm / Ry -1.81°)	-4.43	-1.64	Undershoot	62.99%	-4.43	-1.55	Undershoot	65.09%	-1.64	-1.55	Undershoot	5.69%
Right Lateral Bending (My +5Nm / Ry +1.89°)	4.43	0.72	Undershoot	83.79%	4.43	0.77	Undershoot	82.63%	0.72	0.77	Overshoot	7.16%
Flexion (0.01Hz) (Mx -5Nm / Rx -2.58°)	-5.08	0.64	Undershoot	112.62%	-5.08	0.51	Undershoot	110.07%	0.64	0.51	Undershoot	20.20%
Flexion (Mx -5Nm / Rx -1.66°)	-4.88	0.60	Undershoot	112.32%	-4.88	0.53	Undershoot	110.86%	0.60	0.53	Undershoot	11.86%
Extension (Mx +5Nm / Rx +2°)	4.22	3.59	Undershoot	14.98%	4.22	3.10	Undershoot	26.43%	3.59	3.10	Undershoot	13.46%
Axial Compression (Fz -201.85N / Tz -0.04mm)	-425.72	-114.74	Undershoot	73.05%	-425.72	-120.39	Undershoot	71.72%	-114.74	-120.39	Overshoot	4.92%

Appendix E.3 CM05 (10 cycles at 0.1Hz, additional flexion test for 5 cycles at 0.01Hz)

CM05

Multiaxial Spine Segment Testing: Position vs Load Control and Physiological Relevance

Flinders University

Masters Thesis

Daniel Kim

kim0872@flinders.edu.au

Supervisor: A.Professor John Costi, Co-Supervisor: Mr Michael Russo

SPECIMEN SPECIFICATION

Specimen Prep Date	16/09/2021	Specimen ID	CM05
Testing Date	17/09/2021	Disc Level	L4 – L5

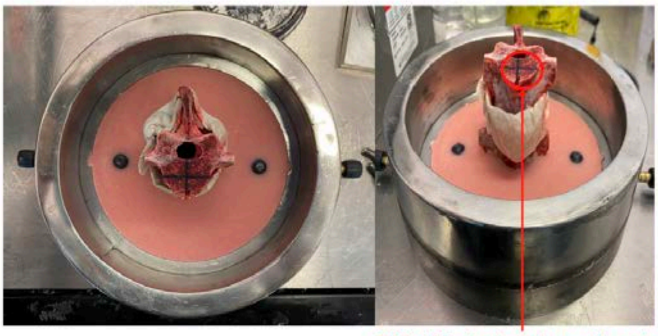

** A block (8.1mm) was inserted on top of the vertebrae to avoid failure

OFFSET	(mm)
X-offset	-1.87
Y-offset	-6.63
Z-offset	76.10

COMPRESSIVE LOAD	(N)
Preload	-13.15
Follower	-165.77
Reference	-203.92

TIMETABLE

Date	Time		Status	Duration	Notes
16.09.21	14:40	Start	Measurement & Defrosting	00:30	
	15:10	End			
	16:35	Start	Specimen potting/setup, Hexapod setup	01:25	
	18:00	End			
	18:03	Start	Overnight Hydration	13:00	
17.09.21	(07:00)	End			
	(07:00)	Start	Load Control	01:01	Shear Tests : 200N Rotational Tests : 5Nm Compression : 0.6MPa -> -221.27N
	(08:00)	End			
	(08:00)	Start	Load-Pos Recovery	02:00	
	09:47	End			
	09:55	Start	Position Control	01:01	
	11:00	End			
	11:00	Start	Pos-Hyb Recovery	02:00	
	13:00	End			
	13:05	Start	Hybrid Control	01:01	
	14:10	End			

OVERNIGHT HYDRATION

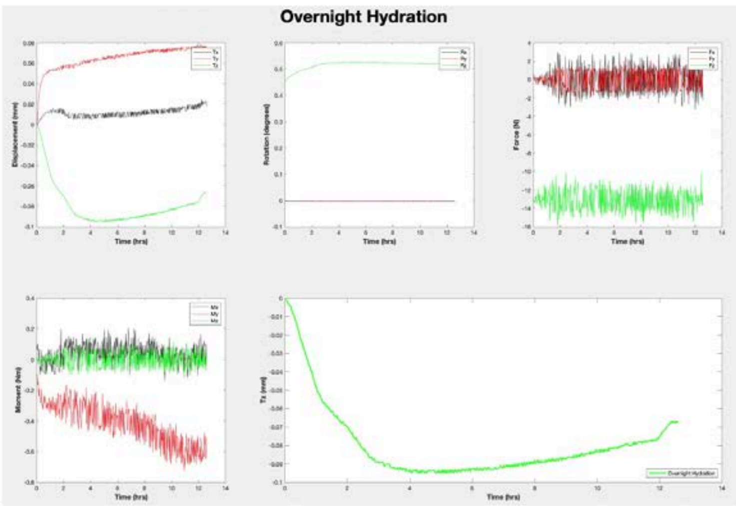

RECOVERY

BEFORE OVERNIGHT HYDRATION	BEEFORE LOAD CONTROL	BEFORE POSITION CONTROL	BEFORE HYBRID CONTROL
-148.608	-	-148.802 (-0.194)	-148.809 (-0.201)

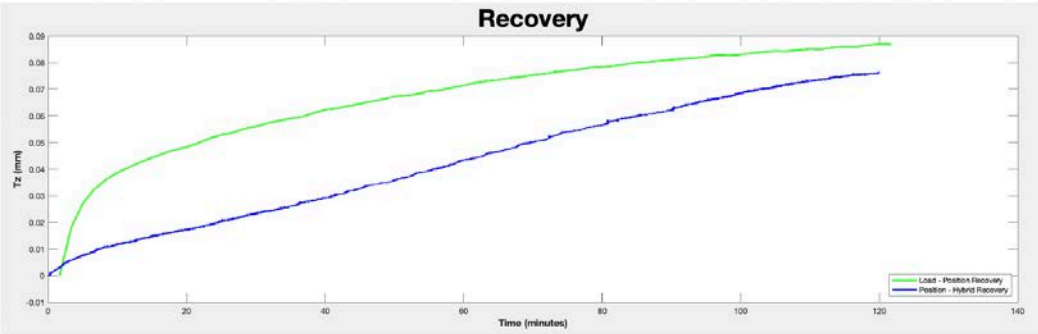

LEFT LATERAL SHEAR (Fx -200N) (Tx -0.49mm)

LOAD CONTROL	POSITION CONTROL	HYBRID CONTROL

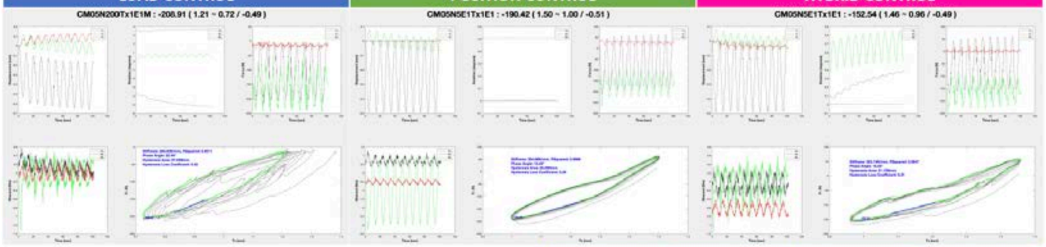

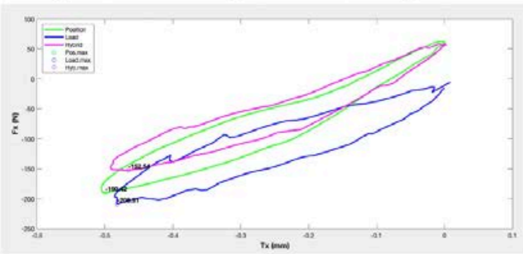

	LOAD CONTROL	POSITION CONTROL	HYBRID CONTROL
Stiffness (N/mm) (RSqaured)	350.92 (0.9511)	354.98 (0.9966)	303.74 (0.9947)
Phase Angle (°)	22.49	13.42	15.55
Hysteresis Area (Nmm)	27.02	23.08	21.15
Hysteresis Loss Coefficient	0.42	0.29	0.31
Maximum Reaction Force (N)	-208.91	-190.42	-152.54

RIGHT LATERAL SHEAR (Fx +200N) (Tx +0.66mm)

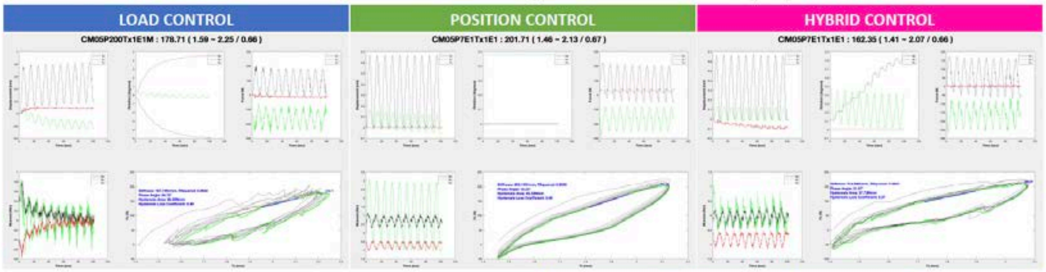

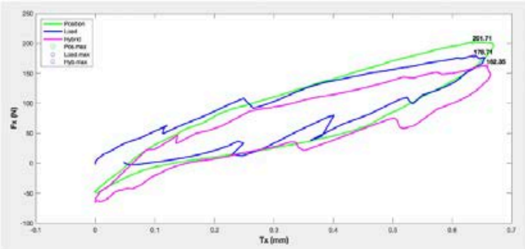

	LOAD CONTROL	POSITION CONTROL	HYBRID CONTROL
Stiffness (N/mm) (RSqaured)	197.74 (0.9922)	295.16 (0.9995)	214.68 (0.9957)
Phase Angle (°)	24.72	19.23	21.07
Hysteresis Area (Nmm)	36.30	43.33	37.73
Hysteresis Loss Coefficient	0.49	0.40	0.37
Maximum Reaction Force (N)	178.71	201.71	162.35

POSTERIOR SHEAR (Fy -200N) (Ty -0.41mm)

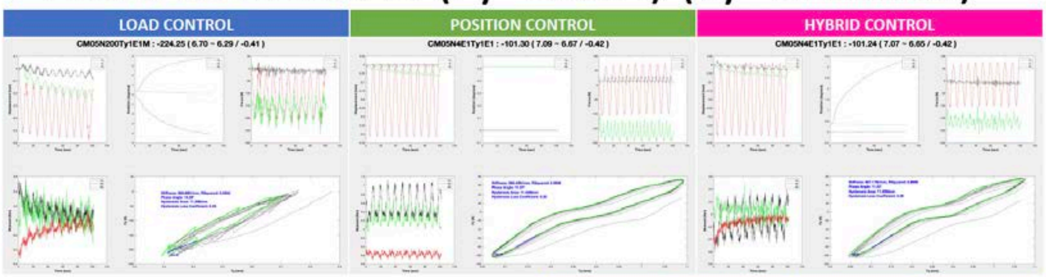

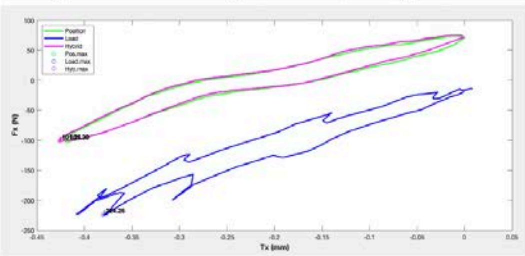

	LOAD CONTROL	POSITION CONTROL	HYBRID CONTROL
Stiffness (N/mm) (RSqaured)	388.68 (0.5554)	590.42 (0.9998)	607.17 (0.9989)
Phase Angle (°)	13.39	11.37	11.23
Hysteresis Area (Nmm)	11.29	11.44	11.40
Hysteresis Loss Coefficient	0.25	0.30	0.29
Maximum Reaction Force (N)	-224.25	-101.30	-101.24

ANTERIOR SHEAR (Fy +200N) (Ty +0.63mm)

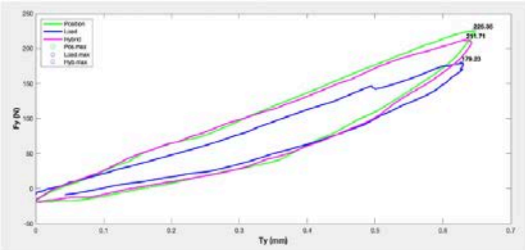

	LOAD CONTROL	POSITION CONTROL	HYBRID CONTROL
Stiffness (N/mm) (RSqaured)	260.79 (0.9306)	383.93 (0.9996)	399.26 (0.9973)
Phase Angle (°)	15.48	15.98	16.98
Hysteresis Area (Nmm)	21.23	34.40	33.66
Hysteresis Loss Coefficient	0.36	0.42	0.42
Maximum Reaction Force (N)	179.23	225.35	211.71

LEFT AXIAL ROTATION (Mz +5Nm) (Rz +0.88°)

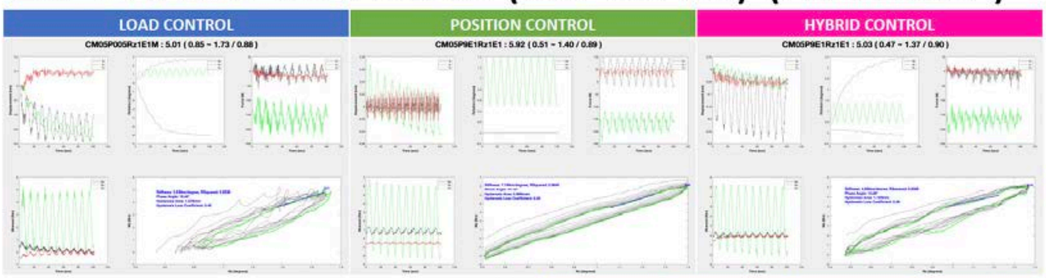

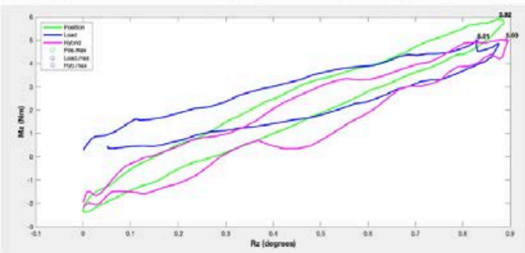

	LOAD CONTROL	POSITION CONTROL	HYBRID CONTROL
Stiffness (Nm/°) (RSqaured)	3.63 (0.9339)	7.74 (0.9840)	4.56 (0.9395)
Phase Angle (°)	19.48	10.14	13.26
Hysteresis Area (Nm°)	1.07	0.99	1.12
Hysteresis Loss Coefficient	0.45	0.23	0.29
Maximum Reaction Moment (Nm)	5.01	5.92	5.03

RIGHT AXIAL ROTATION (Mz -5Nm) (Rz -0.79°)

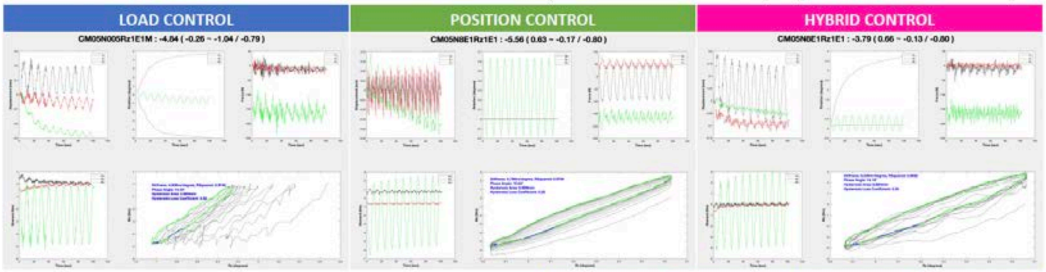

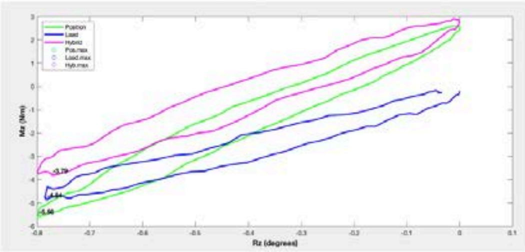

	LOAD CONTROL	POSITION CONTROL	HYBRID CONTROL
Stiffness (Nm/°) (RSqaured)	4.90 (0.9745)	9.79 (0.9794)	6.33 (0.9682)
Phase Angle (°)	14.45	10.64	14.18
Hysteresis Area (Nm°)	0.66	0.93	0.96
Hysteresis Loss Coefficient	0.30	0.25	0.30
Maximum Reaction Moment (Nm)	-4.84	-5.56	-3.79

LEFT LATERAL BENDING (My -5Nm) (Ry -2.36°)

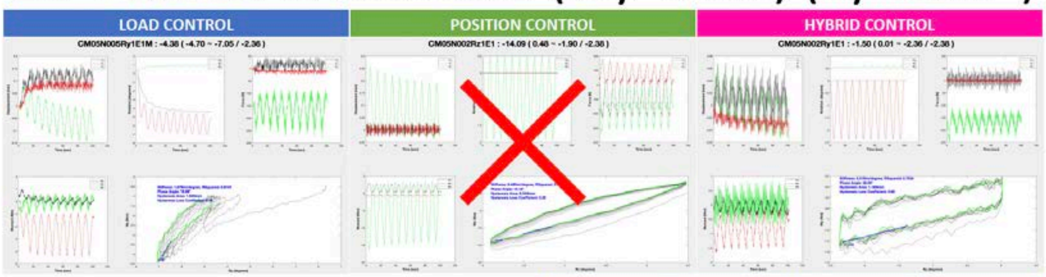

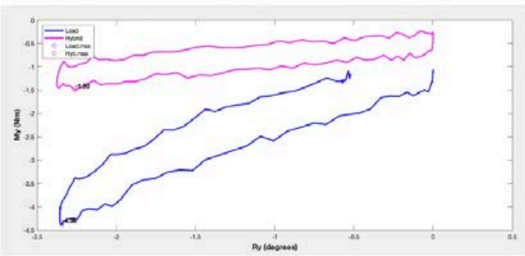

	LOAD CONTROL	POSITION CONTROL	HYBRID 28NTROL
Stiffness (Nm/°) (RSqaured)	1.87 (0.9147)	- (-)	0.31 (0.7534)
Phase Angle (°)	19.88	-	38.90
Hysteresis Area (Nm°)	1.94	-	1.18
Hysteresis Loss Coefficient	0.48	-	0.60
Maximum Reaction Moment (Nm)	-4.38	-	-1.50

RIGHT LATERAL BENDING (My +5Nm) (Ry +1.68°)

LOAD CONTROL	POSITION CONTROL	HYBRID CONTROL

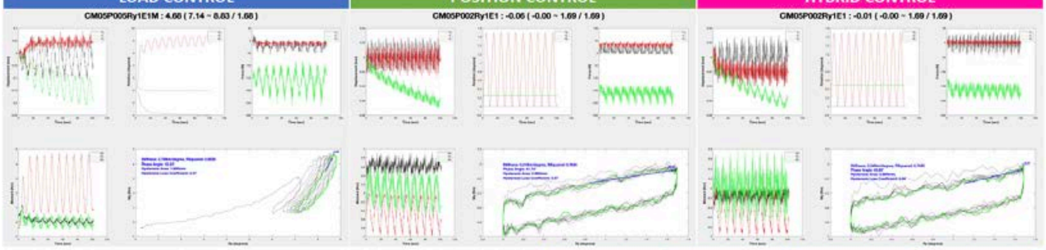

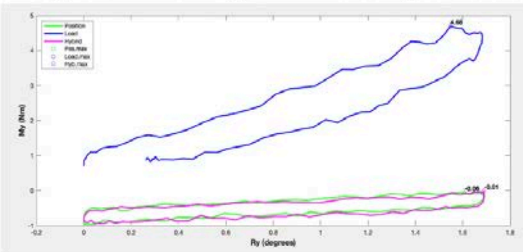

	LOAD CONTROL	POSITION CONTROL	HYBRID CONTROL
Stiffness (Nm/°) (RSqaured)	2.76 (0.8529)	0.21 (0.7534)	0.34 (0.7400)
Phase Angle (°)	19.03	41.75	43.88
Hysteresis Area (Nm°)	1.66	0.66	0.66
Hysteresis Loss Coefficient	0.47	0.57	0.64
Maximum Reaction Moment (Nm)	4.68	-0.06	-0.01

FLEXION (@0.01Hz) (Mx -5Nm) (Rx -2.79°)

LOAD CONTROL	POSITION CONTROL	HYBRID CONTROL

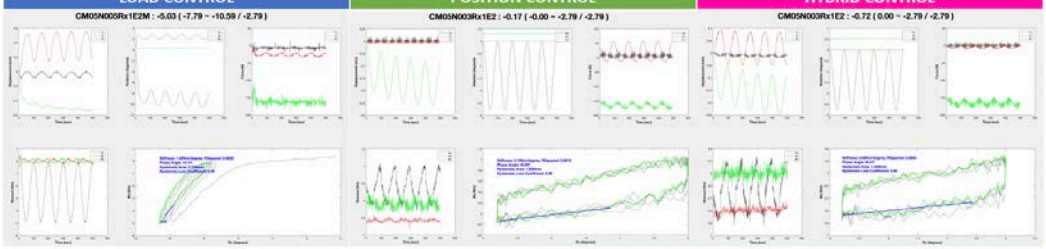

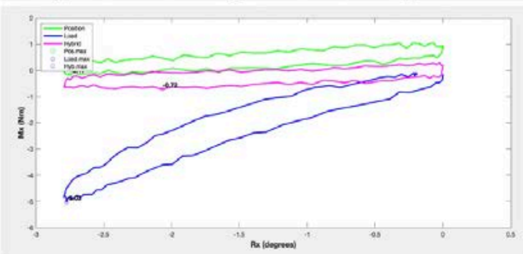

	LOAD CONTROL	POSITION CONTROL	HYBRID CONTROL
Stiffness (Nm/°) (RSqaured)	1.80 (0.9828)	0.15 (0.6915)	0.09 (0.5993)
Phase Angle (°)	14.74	43.93	54.07
Hysteresis Area (Nm°)	2.74	1.50	1.43
Hysteresis Loss Coefficient	0.40	0.58	0.62
Maximum Reaction Moment (Nm)	-5.03	-0.17	-0.72

FLEXION (Mx -5Nm) (Rx -1.76°)

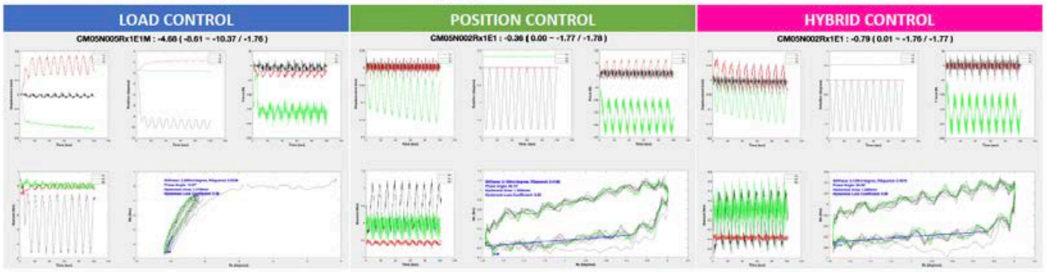

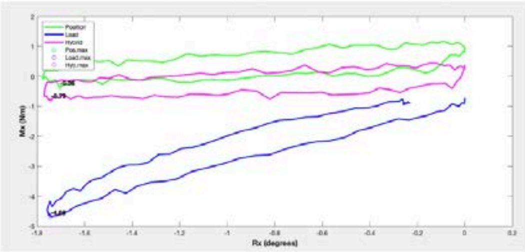

	LOAD CONTROL	POSITION CONTROL	HYBRID CONTROL
Stiffness (Nm/°) (RSqaured)	2.28 (0.9336)	0.16 (0.4188)	0.13 (0.4876)
Phase Angle (°)	14.97	48.70	54.06
Hysteresis Area (Nm°)	1.31	1.30	1.22
Hysteresis Loss Coefficient	0.38	0.63	0.69
Maximum Reaction Moment (Nm)	-4.68	-0.36	-0.79

EXTENSION (Mx +5Nm) (Rx +1.93°)

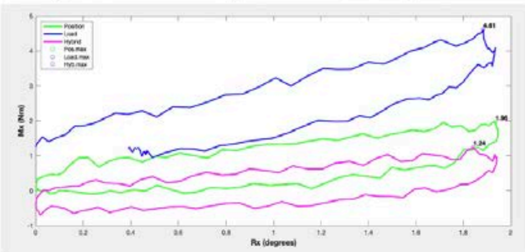

	LOAD CONTROL	POSITION CONTROL	HYBRID CONTROL
Stiffness (Nm/°) (RSqaured)	0.90 (0.3354)	0.53 (0.6950)	0.26 (0.2325)
Phase Angle (°)	28.17	41.21	45.83
Hysteresis Area (Nm°)	2.37	1.89	1.70
Hysteresis Loss Coefficient	0.60	0.72	0.69
Maximum Reaction Moment (Nm)	4.61	1.96	1.24

AXIAL COMPRESSION (Fz -221.27N) (Tz -0.05mm)

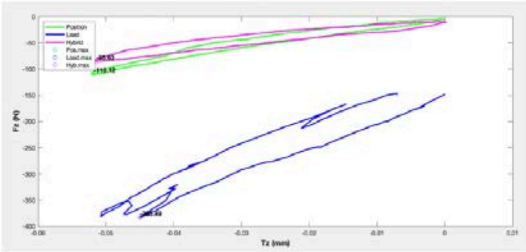

	LOAD CONTROL	POSITION CONTROL	HYBRID CONTROL
Stiffness (N/mm) (RSqaured)	4287.88 (0.6509)	2234.96 (0.9966)	1671.31 (0.9912)
Phase Angle (°)	18.11	7.42	13.42
Hysteresis Area (Nmm)	2.09	0.61	0.81
Hysteresis Loss Coefficient	0.32	0.23	0.39
Maximum Reaction Force (N)	-383.49	-110.12	-85.63

% DIFFERENCES

	CM05											
	Maximum Reaction Force(N) / Moment(Nm)		Under/Overshoot	% Difference	Maximum Reaction Force(N) / Moment(Nm)		Under/Overshoot	% Difference	Maximum Reaction Force(N) / Moment(Nm)		Under/Overshoot	% Difference
	Load	Position			Load	Hybrid			Position	Hybrid		
Left Lateral Shear (-Fx / -Tx)	-208.91	-190.42	Undershoot	8.85%	-208.91	-152.54	Undershoot	26.99%	-190.42	-152.54	Undershoot	19.89%
Right Lateral Shear (+Fx / + Tx)	178.71	201.71	Overshoot	12.87%	178.71	162.35	Undershoot	9.15%	201.71	162.35	Undershoot	19.51%
Posterior Shear (Fy -200N / Ty -0.31mm)	-224.25	-101.30	Undershoot	54.83%	-224.25	-101.24	Undershoot	54.85%	-101.30	-101.24	Undershoot	0.06%
Anterior Shear (Fy +200N / Ty +0.68mm)	179.23	225.35	Overshoot	25.73%	179.23	211.71	Overshoot	18.12%	225.35	211.71	Undershoot	6.05%
Left Axial Rotation (Mz +5Nm / Rz +0.88°)	5.01	5.92	Overshoot	18.35%	5.01	5.03	Overshoot	0.51%	5.92	5.03	Undershoot	15.07%
Right Axial Rotation (Mz -5Nm / Rz -0.77°)	-4.84	-5.56	Overshoot	14.77%	-4.84	-3.79	Undershoot	21.68%	-5.56	-3.79	Undershoot	31.76%
Left Lateral Bending (My -5Nm / Ry -1.81°)	-4.38		-	-	-4.38	-1.50	Undershoot	65.73%		-1.50	-	-
Right Lateral Bending (My +5Nm / Ry +1.89°)	4.68	-0.06	Undershoot	101.25%	4.68	-0.01	Undershoot	100.25%	-0.06	-0.01	Undershoot	80.21%
Flexion (0.01Hz) (Mx -5Nm / Rx -2.58°)	-5.03	-0.17	Undershoot	96.70%	-5.03	-0.72	Undershoot	85.61%	-0.17	-0.72	Overshoot	335.62%
Flexion (Mx -5Nm / Rx -1.66°)	-4.68	-0.36	Undershoot	92.35%	-4.68	-0.79	Undershoot	83.11%	-0.36	-0.79	Overshoot	120.87%
Extension (Mx +5Nm / Rx +2°)	4.61	1.96	Undershoot	57.41%	4.61	1.24	Undershoot	73.18%	1.96	1.24	Undershoot	37.04%
Axial Compression (Fz -201.85N / Tz -0.04mm)	-383.49	-110.12	Undershoot	71.28%	-383.49	-85.63	Undershoot	77.67%	-110.12	-85.63	Undershoot	22.24%

Appendix E.4 CM06 (10 cycles at 0.1Hz, additional flexion test for 5 cycles at 0.01Hz)

CM06

Multiaxial Spine Segment Testing: Position vs Load Control and Physiological Relevance

Flinders University
Masters Thesis
Daniel Kim
kim0872@flinders.edu.au
Supervisor: A.Professor John Costi, Co-Supervisor: Mr Michael Russo

SPECIMEN SPECIFICATION

Specimen Prep Date	20/09/2021	Specimen ID	CM06
Testing Date	21/09/2021	Disc Level	L4 – L5

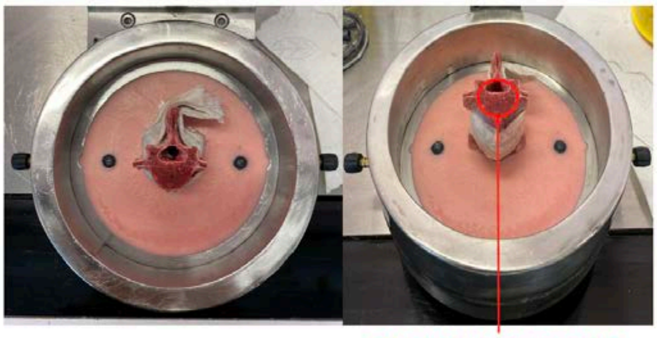

** A block (12.9mm) was inserted on top of the vertebrae to avoid failure

OFFSET	(mm)
X-offset	-1.50
Y-offset	-6.70
Z-offset	76.48

COMPRESSIVE LOAD	(N)
Preload	-3.57 (-8)
Follower	-117.86
Reference	-146.44

** -8N of preload was applied for all testings due to the oscillations

TIMETABLE

Date	Time		Status	Duration	Notes
20.09.21	13:58	Start	Measurement & Defrosting		
	15:22	End			
	15:22	Start	Specimen potting/setup, Hexapod setup		
	17:40	End			
	(17:45)	Start	Overnight Hydration		preload: -3.57N -> -8N (due to the oscillations) (For all test) Adoptive Tuning On
21.09.21	(06:45)	End			
	(06:45)	Start	Load Control	01:01	Shear Tests : 200N Rotational Tests : 5Nm Compression : 0.6MPa -> -146.44N
	(07:45)	End			
	(07:45)	Start	Load-Pos Recovery	02:00	
	(09:45)	End			
	09:57	Start	Position Control	01:01	
	10:58	End			
	11:05	Start	Pos-Hyb Recovery	02:00	
	13:05	End			
	13:15	Start	Hybrid Control	01:01	
	14:20	End			

OVERNIGHT HYDRATION

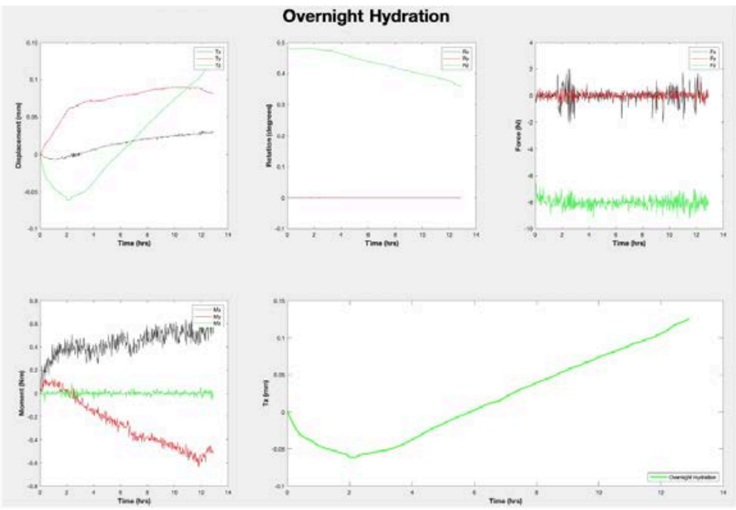

RECOVERY

BEFORE OVERNIGHT HYDRATION	BEEFORE LOAD CONTROL	BEFORE POSITION CONTROL	BEFORE HYBRID CONTROL
-153.941	-	-153.915 (+0.026)	-153.877 (+0.064)

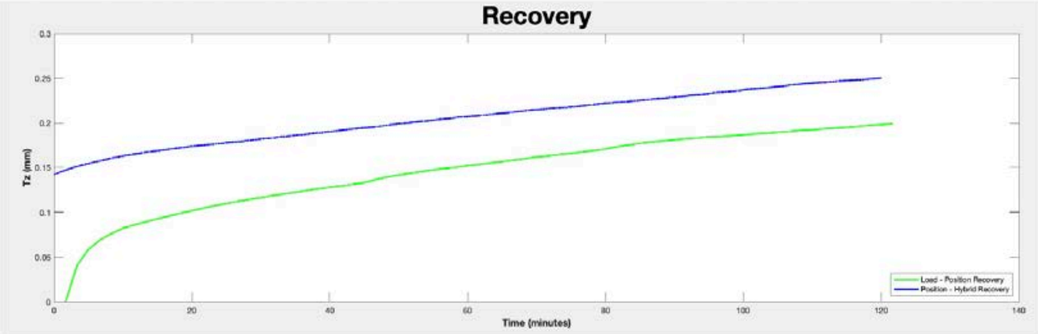

LEFT LATERAL SHEAR (Fx -200N) (Tx -0.41mm)

LOAD CONTROL	POSITION CONTROL	HYBRID CONTROL
CM06N200Tx1E1M : -197.11 (0.66 ~ 0.25 / -0.41)	CM06N4E1Tx1E1 : -128.82 (1.13 ~ 0.71 / -0.42)	CM06N4E1Tx1E1 : -116.98 (1.14 ~ 0.73 / -0.42)

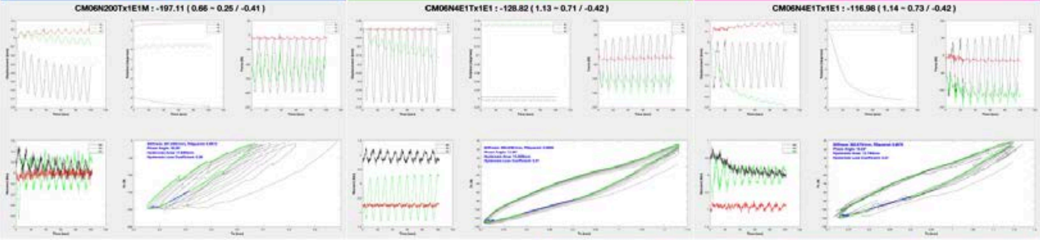

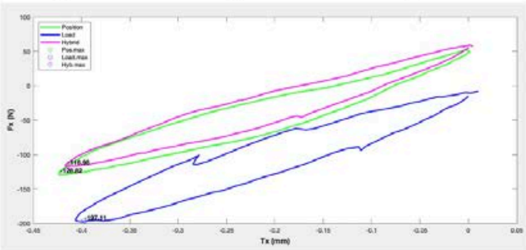

	LOAD CONTROL	POSITION CONTROL	HYBRID CONTROL
Stiffness (N/mm) (RSqaured)	397.05 (0.9973)	285.83 (0.9994)	282.87 (0.9976)
Phase Angle (°)	18.28	13.96	15.03
Hysteresis Area (Nmm)	17.09	14.56	13.74
Hysteresis Loss Coefficient	0.36	0.31	0.31
Maximum Reaction Force (N)	-197.11	-128.82	-116.98

RIGHT LATERAL SHEAR (Fx +200N) (Tx +0.46mm)

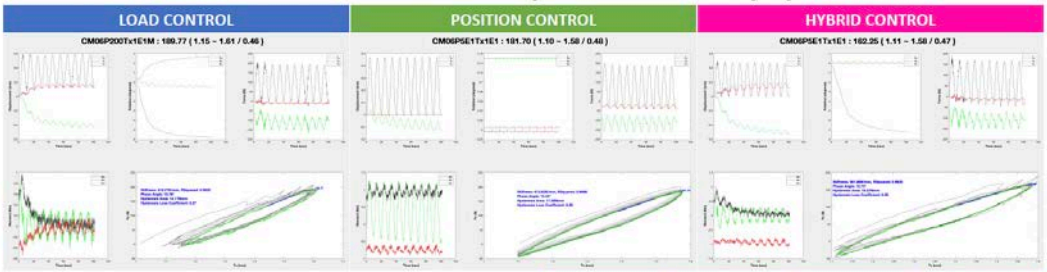

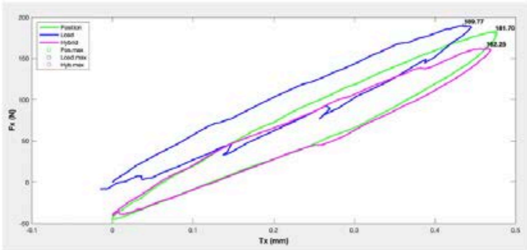

	LOAD CONTROL	POSITION CONTROL	HYBRID CONTROL
Stiffness (N/mm) (RSqaured)	416.27 (0.9920)	413.62 (0.9988)	361.86 (0.9820)
Phase Angle (°)	13.76	12.23	12.70
Hysteresis Area (Nmm)	14.17	17.59	15.27
Hysteresis Loss Coefficient	0.27	0.28	0.28
Maximum Reaction Force (N)	189.77	181.70	162.25

POSTERIOR SHEAR (Fy -200N) (Ty -0.53mm)

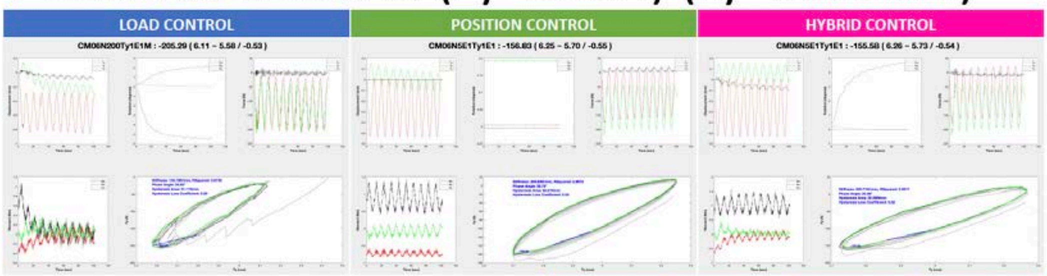

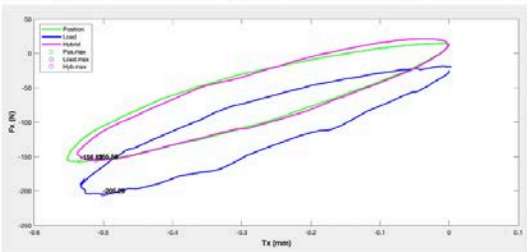

	LOAD CONTROL	POSITION CONTROL	HYBRID CONTROL
Stiffness (N/mm) (RSqaured)	146.18 (0.6745)	246.60 (0.9973)	230.71 (0.9917)
Phase Angle (°)	24.82	25.70	24.98
Hysteresis Area (Nmm)	31.11	32.01	32.26
Hysteresis Loss Coefficient	0.50	0.53	0.52
Maximum Reaction Force (N)	-205.29	-156.83	-155.58

ANTERIOR SHEAR (Fy +200N) (Ty +0.63mm)

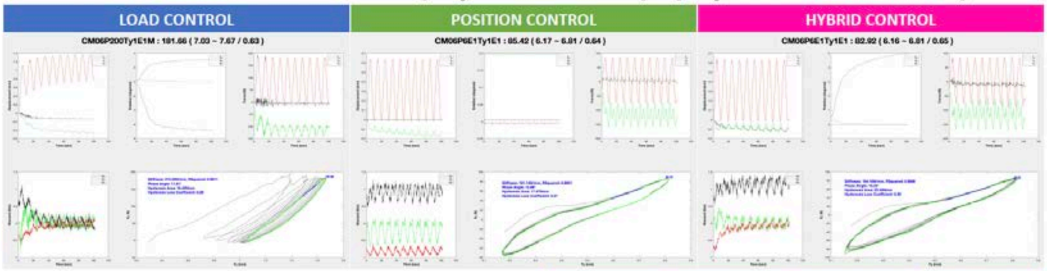

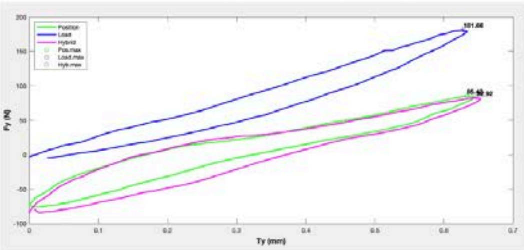

	LOAD CONTROL	POSITION CONTROL	HYBRID CONTROL
Stiffness (N/mm) (RSqaured)	315.20 (0.9911)	191.14 (0.9951)	184.16 (0.9986)
Phase Angle (°)	11.81	12.98	16.02
Hysteresis Area (Nmm)	16.42	17.67	23.49
Hysteresis Loss Coefficient	0.28	0.27	0.33
Maximum Reaction Force (N)	181.66	85.42	82.92

LEFT AXIAL ROTATION (Mz +5Nm) (Rz +1.19°)

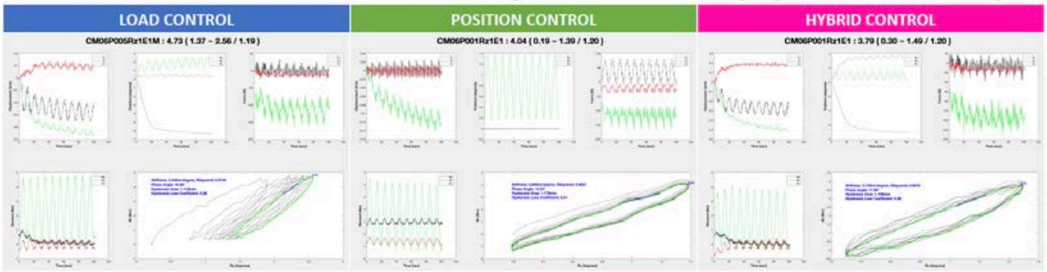

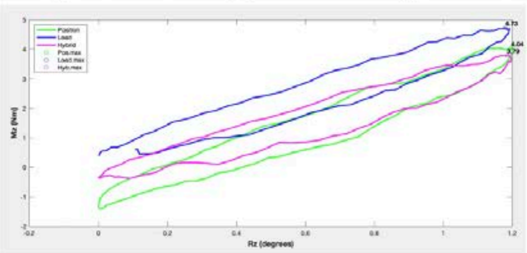

	LOAD CONTROL	POSITION CONTROL	HYBRID CONTROL
Stiffness (Nm/°) (RSqaured)	3.44 (0.9745)	3.00 (0.9657)	3.14 (0.9579)
Phase Angle (°)	16.28	14.34	17.58
Hysteresis Area (Nm°)	1.11	1.17	1.10
Hysteresis Loss Coefficient	0.38	0.31	0.39
Maximum Reaction Moment (Nm)	4.73	4.04	3.79

RIGHT AXIAL ROTATION (Mz -5Nm) (Rz -1.03°)

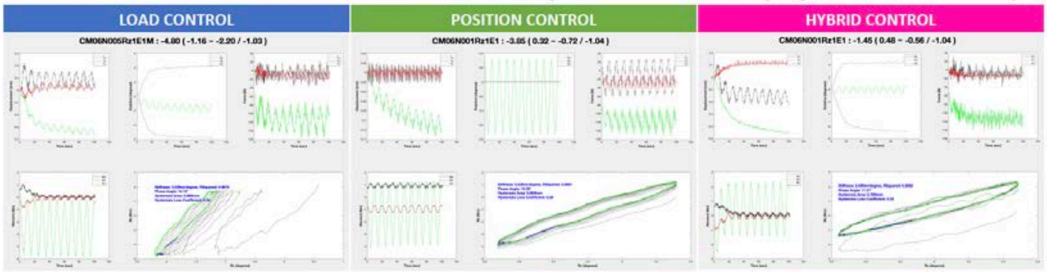

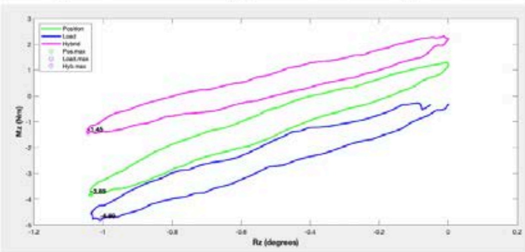

	LOAD CONTROL	POSITION CONTROL	HYBRID CONTROL
Stiffness (Nm/°) (RSqaured)	3.22 (0.9870)	5.52 (0.9961)	2.42 (0.9562)
Phase Angle (°)	14.12	12.28	17.27
Hysteresis Area (Nm°)	0.89	0.86	0.79
Hysteresis Loss Coefficient	0.34	0.29	0.33
Maximum Reaction Moment (Nm)	-4.80	-3.85	-1.45

LEFT LATERAL BENDING (My -5Nm) (Ry -2.36°)

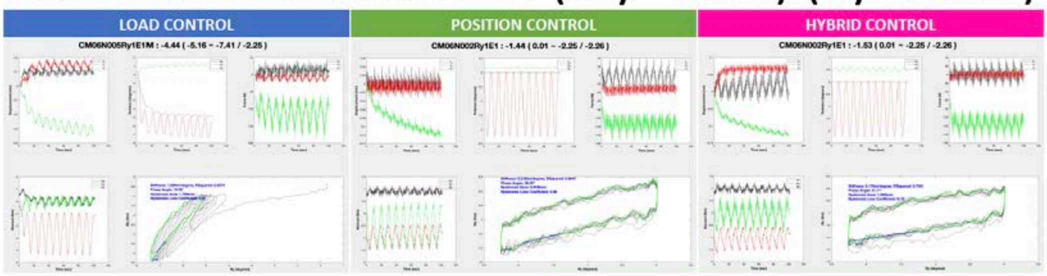

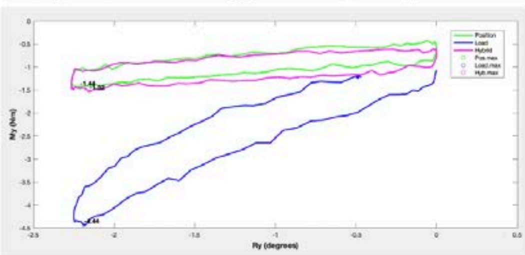

	LOAD CONTROL	POSITION CONTROL	HYBRID 28NTROL
Stiffness (Nm/°) (RSqaured)	1.50 (0.9374)	0.23 (0.8047)	0.17 (0.7031)
Phase Angle (°)	19.30	38.92	47.71
Hysteresis Area (Nm°)	1.79	0.91	1.08
Hysteresis Loss Coefficient	0.47	0.56	0.73
Maximum Reaction Moment (Nm)	-4.44	-1.44	-1.53

RIGHT LATERAL BENDING (My +5Nm) (Ry +1.97°)

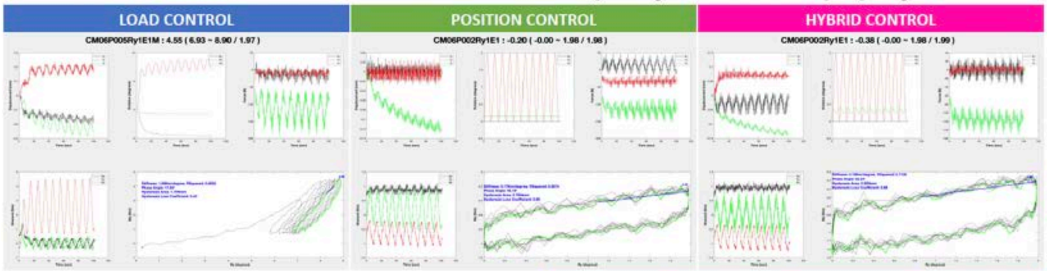

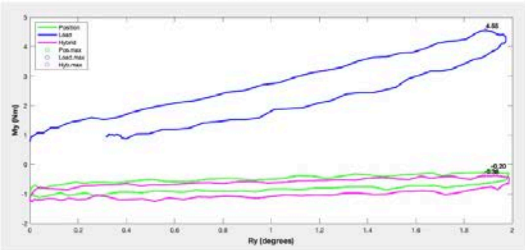

	LOAD CONTROL	POSITION CONTROL	HYBRID CONTROL
Stiffness (Nm/°) (RSqaured)	1.69 (0.9502)	0.17 (0.5874)	0.16 (0.7105)
Phase Angle (°)	17.84	45.19	52.24
Hysteresis Area (Nm°)	1.70	0.76	0.92
Hysteresis Loss Coefficient	0.43	0.60	0.68
Maximum Reaction Moment (Nm)	4.55	-0.20	-0.38

FLEXION (@0.01Hz) (Mx -5Nm) (Rx -2.95°)

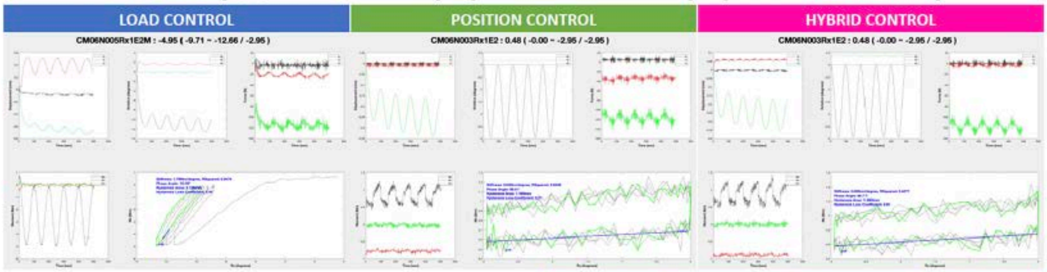

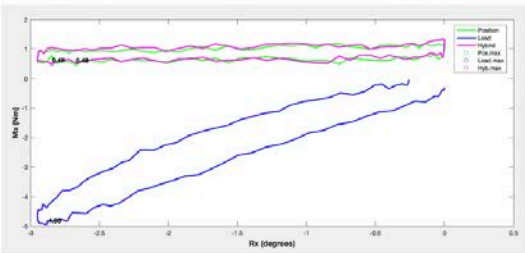

	LOAD CONTROL	POSITION CONTROL	HYBRID CONTROL
Stiffness (Nm/°) (RSqaured)	1.76 (0.9474)	0.04 (0.2459)	0.06 (0.4277)
Phase Angle (°)	15.59	68.01	66.77
Hysteresis Area (Nm°)	3.12	1.15	1.26
Hysteresis Loss Coefficient	0.40	0.71	0.61
Maximum Reaction Moment (Nm)	-4.95	0.48	0.48

FLEXION (Mx -5Nm) (Rx -1.88°)

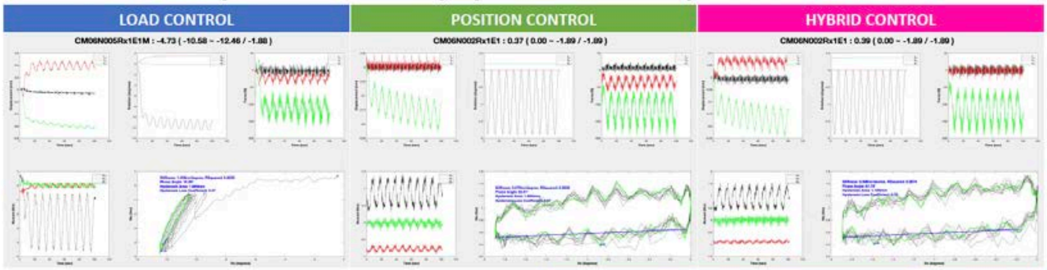

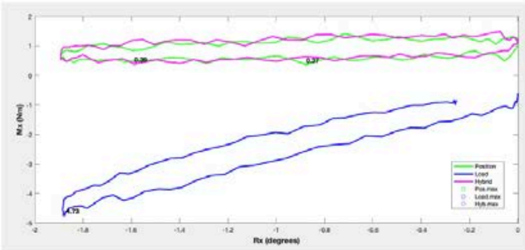

	LOAD CONTROL	POSITION CONTROL	HYBRID CONTROL
Stiffness (Nm/°) (RSqaured)	1.45 (0.8225)	0.07 (0.2559)	0.08 (0.2674)
Phase Angle (°)	15.25	62.91	61.78
Hysteresis Area (Nm°)	1.48	1.06	1.19
Hysteresis Loss Coefficient	0.37	0.67	0.70
Maximum Reaction Moment (Nm)	-4.73	0.37	0.39

EXTENSION (Mx +5Nm) (Rx +2.23°)

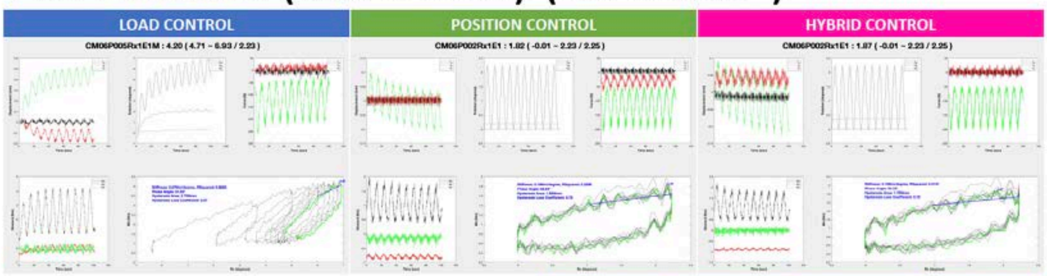

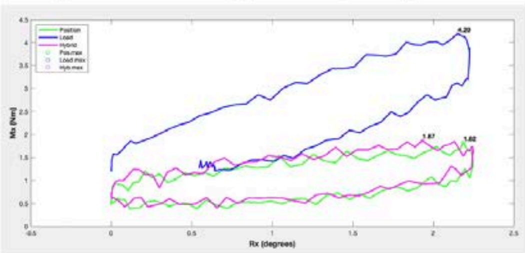

	LOAD CONTROL	POSITION CONTROL	HYBRID CONTROL
Stiffness (Nm/°) (RSqaured)	0.67 (0.6983)	0.18 (0.3296)	0.16 (0.3131)
Phase Angle (°)	31.63	50.09	50.05
Hysteresis Area (Nm°)	2.70	1.59	1.72
Hysteresis Loss Coefficient	0.67	0.73	0.72
Maximum Reaction Moment (Nm)	4.20	1.82	1.87

AXIAL COMPRESSION (Fz -146.44N) (Tz -0.06mm)

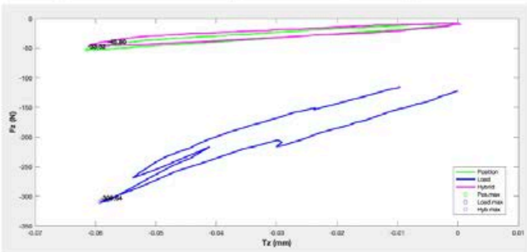

	LOAD CONTROL	POSITION CONTROL	HYBRID CONTROL
Stiffness (N/mm) (RSqaured)	4399.15 (1.0000)	656.52 (0.9913)	497.03 (0.9915)
Phase Angle (°)	16.17	11.66	18.76
Hysteresis Area (Nmm)	1.79	0.50	0.68
Hysteresis Loss Coefficient	0.32	0.33	0.47
Maximum Reaction Force (N)	-309.64	-53.52	-45.80

% DIFFERENCES

	CM06											
	Maximum Reaction Force(N) / Moment(Nm)		Under/Overshoot	% Difference	Maximum Reaction Force(N) / Moment(Nm)		Under/Overshoot	% Difference	Maximum Reaction Force(N) / Moment(Nm)		Under/Overshoot	% Difference
	Load	Position			Load	Hybrid			Position	Hybrid		
Left Lateral Shear (-Fx / -Tx)	-197.11	-128.82	Undershoot	34.64%	-197.11	-116.98	Undershoot	40.65%	-128.82	-116.98	Undershoot	9.19%
Right Lateral Shear (+Fx / + Tx)	189.77	181.70	Undershoot	4.25%	189.77	162.25	Undershoot	14.50%	181.70	162.25	Undershoot	10.71%
Posterior Shear (Fy -200N / Ty -0.31mm)	-205.29	-156.83	Undershoot	23.61%	-205.29	-155.58	Undershoot	24.22%	-156.83	-155.58	Undershoot	0.80%
Anterior Shear (Fy +200N / Ty +0.68mm)	181.66	85.42	Undershoot	52.98%	181.66	82.92	Undershoot	54.35%	85.42	82.92	Undershoot	2.92%
Left Axial Rotation (Mz +5Nm / Rz +0.88°)	4.73	4.04	Undershoot	14.57%	4.73	3.79	Undershoot	19.85%	4.04	3.79	Undershoot	6.18%
Right Axial Rotation (Mz -5Nm / Rz -0.77°)	-4.80	-3.85	Undershoot	19.78%	-4.80	-1.45	Undershoot	69.83%	-3.85	-1.45	Undershoot	62.39%
Left Lateral Bending (My -5Nm / Ry -1.81°)	-4.44	-1.44	Undershoot	67.49%	-4.44	-1.53	Undershoot	65.48%	-1.44	-1.53	Overshoot	6.18%
Right Lateral Bending (My +5Nm / Ry +1.89°)	4.55	-0.20	Undershoot	104.37%	4.55	-0.38	Undershoot	108.40%	-0.20	-0.38	Overshoot	92.25%
Flexion (0.01Hz) (Mx -5Nm / Rx -2.58°)	-4.95	0.48	Undershoot	109.60%	-4.95	0.48	Undershoot	109.75%	0.48	0.48	Overshoot	1.52%
Flexion (Mx -5Nm / Rx -1.66°)	-4.73	0.37	Undershoot	107.89%	-4.73	0.39	Undershoot	108.32%	0.37	0.39	Overshoot	5.55%
Extension (Mx +5Nm / Rx +2°)	4.20	1.82	Undershoot	56.59%	4.20	1.87	Undershoot	55.45%	1.82	1.87	Overshoot	2.62%
Axial Compression (Fz -201.85N / Tz -0.04mm)	-309.64	-53.52	Undershoot	82.71%	-309.64	-45.80	Undershoot	85.21%	-53.52	-45.80	Undershoot	14.43%

Appendix E.5 CM07 (10 cycles at 0.1Hz, additional flexion test for 5 cycles at 0.01Hz)

CM07

Multiaxial Spine Segment Testing: Position vs Load Control and Physiological Relevance

Flinders University
Masters Thesis
Daniel Kim
kim0872@flinders.edu.au
Supervisor: A.Professor John Costi, Co-Supervisor: Mr Michael Russo

SPECIMEN SPECIFICATION

Specimen Prep Date	23/09/2021	Specimen ID	CM07
Testing Date	24/09/2021	Disc Level	L4 – L5

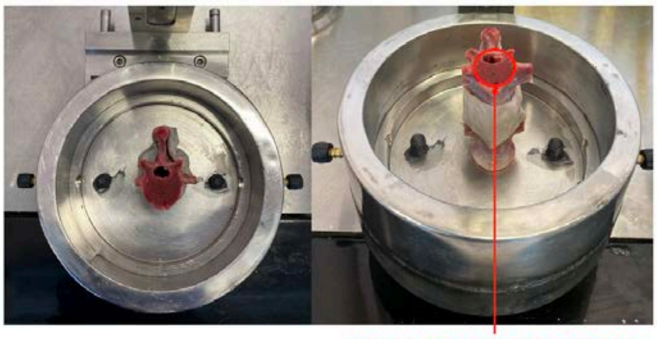

** A block (8.1mm) was inserted on top of the vertebrae to avoid failure

OFFSET	(mm)
X-offset	0.6
Y-offset	-7.63
Z-offset	75.52

COMPRESSIVE LOAD	(N)
Preload	-3.65
Follower	-118.25
Reference	-146.90

TIMETABLE

Date	Time	Status		Duration	Notes
23.09.21	14:00	Start	Measurement & Defrosting	01:30	
	15:30	End			
	15:30	Start	Specimen potting/setup, Hexapod setup	01:10	
	16:40	End			
	16:50	Start	Overnight Hydration	13:40	
24.09.21	(06:30)	End			
	(06:30)	Start	Load Control	01:01	
	(07:30)	End			
	(07:30)	Start	Load-Pos Recovery	02:00	
	09:33	End			
	09:38	Start	Position Control	01:01	
	10:43	End			
	10:43	Start	Pos-Hyb Recovery	02:00	
	12:44	End			
	12:45	Start	Hybrid Control	01:01	
	13:50	End			

OVERNIGHT HYDRATION

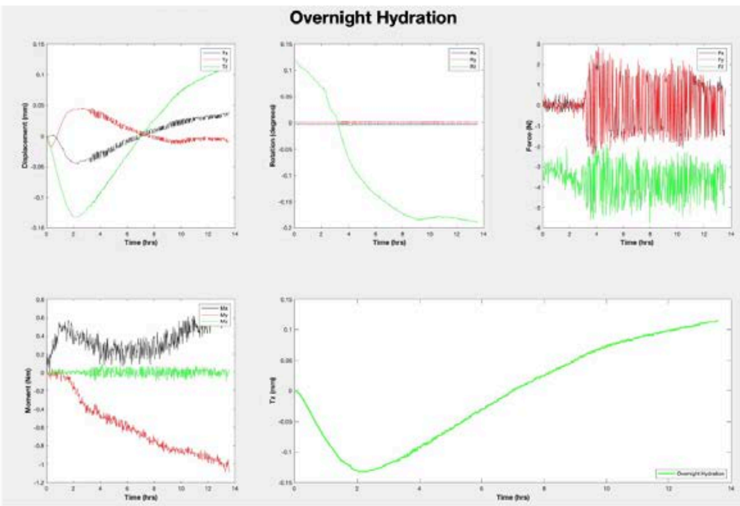

RECOVERY

BEFORE OVERNIGHT HYDRATION	BEEFORE LOAD CONTROL	BEFORE POSITION CONTROL	BEFORE HYBRID CONTROL
-148.481	-	-148.468 (+0.013)	-148.356 (+0.125)

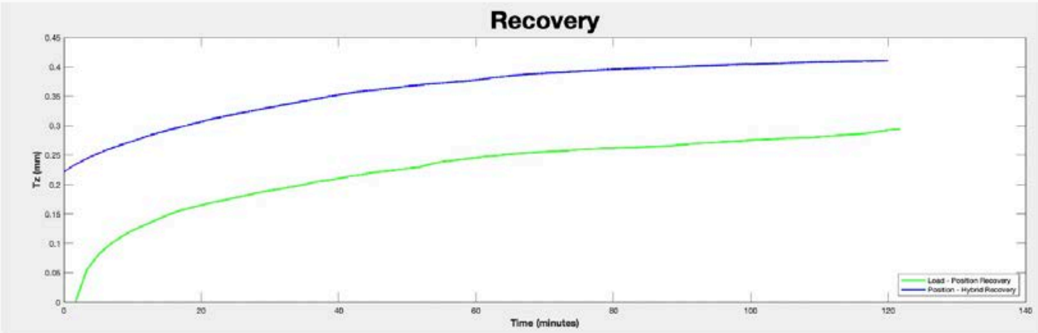

LEFT LATERAL SHEAR (Fx -200N) (Tx -0.73mm)

LOAD CONTROL	POSITION CONTROL	HYBRID CONTROL
CM07N200Tx1E1M : -213.17 (-1.21 ~ -1.94 / -0.73)	CM07N7E1Tx1E1 : -123.58 (-0.58 ~ -1.33 / -0.75)	CM07N7E1Tx1E1 : -97.40 (-0.58 ~ -1.33 / -0.75)

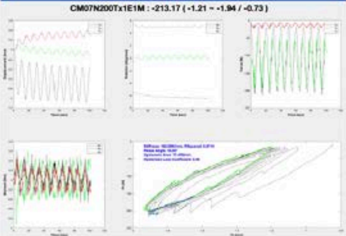

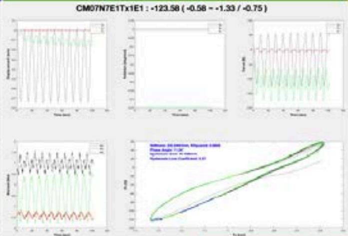

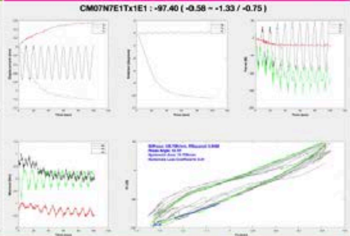

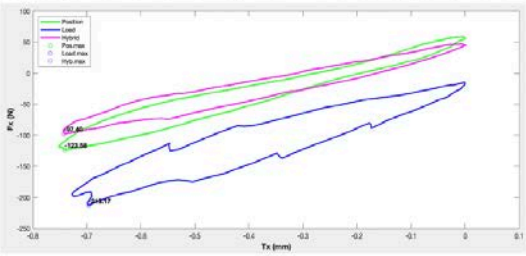

	LOAD CONTROL	POSITION CONTROL	HYBRID CONTROL
Stiffness (N/mm) (RSqaured)	162.59 (0.8714)	232.84 (0.9955)	126.79 (0.9488)
Phase Angle (°)	19.93	11.34	13.70
Hysteresis Area (Nmm)	33.46	20.59	19.35
Hysteresis Loss Coefficient	0.40	0.27	0.31
Maximum Reaction Force (N)	-213.17	-123.58	-97.40

RIGHT LATERAL SHEAR (Fx +200N) (Tx +0.61mm)

LOAD CONTROL	POSITION CONTROL	HYBRID CONTROL
CM07P200Tx1E1M : 180.60 (-0.37 ~ 0.24 / 0.61)	CM07P6E1Tx1E1 : 153.82 (-0.66 ~ -0.04 / 0.63)	CM07P6E1Tx1E1 : 119.36 (-0.64 ~ -0.02 / 0.62)

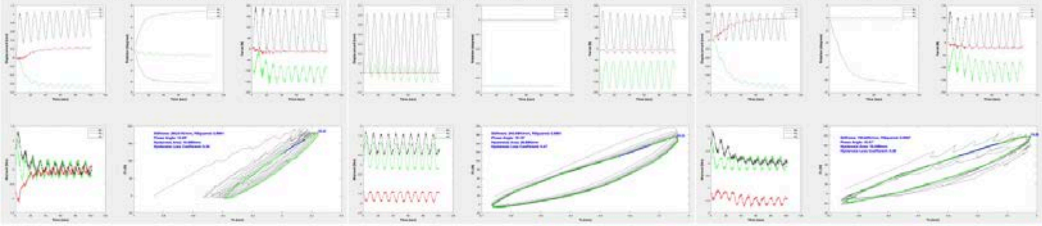

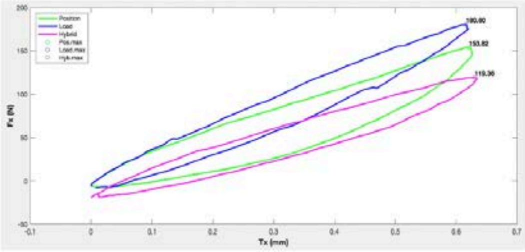

	LOAD CONTROL	POSITION CONTROL	HYBRID CONTROL
Stiffness (N/mm) (RSqaured)	260.61 (0.9961)	240.98 (0.9981)	190.62 (0.9987)
Phase Angle (°)	13.00	19.19	18.07
Hysteresis Area (Nmm)	19.66	26.86	18.49
Hysteresis Loss Coefficient	0.30	0.47	0.36
Maximum Reaction Force (N)	180.60	153.82	119.36

POSTERIOR SHEAR (Fy -200N) (Ty -0.57mm)

LOAD CONTROL	POSITION CONTROL	HYBRID CONTROL
CM07N200Ty1E1M : -206.55 (7.36 ~ 6.78 / -0.57)	CM07N6E1Ty1E1 : -139.60 (7.50 ~ 6.90 / -0.60)	CM07N6E1Ty1E1 : -104.12 (7.56 ~ 6.96 / -0.60)

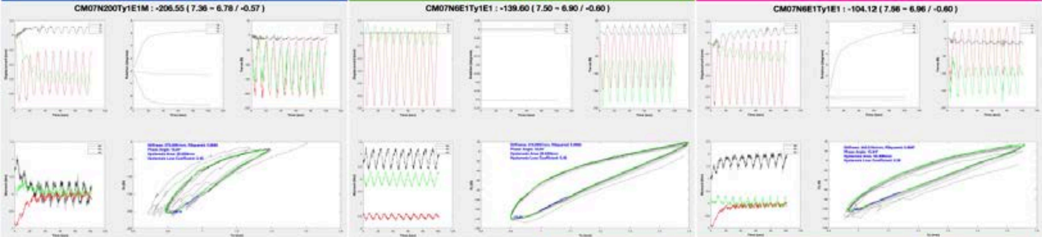

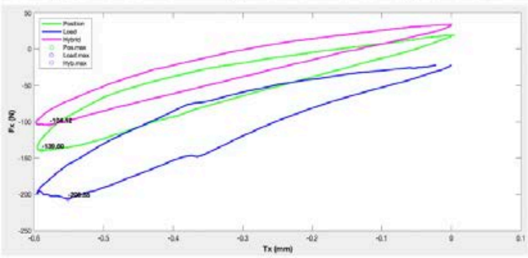

	LOAD CONTROL	POSITION CONTROL	HYBRID CONTROL
Stiffness (N/mm) (RSqaured)	379.26 (0.9995)	316.99 (0.9983)	242.51 (0.9987)
Phase Angle (°)	19.84	18.84	15.94
Hysteresis Area (Nmm)	26.65	22.52	16.99
Hysteresis Loss Coefficient	0.46	0.45	0.39
Maximum Reaction Force (N)	-206.55	-139.60	-104.12

ANTERIOR SHEAR (Fy +200N) (Ty +0.77mm)

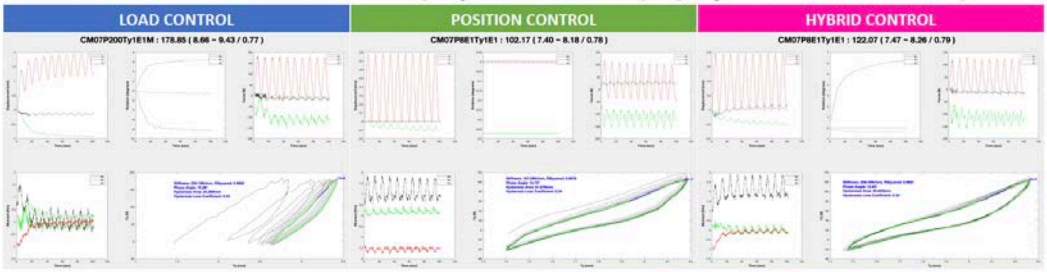

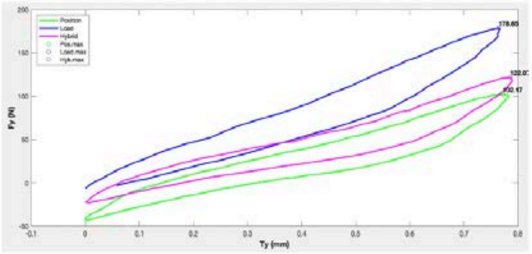

	LOAD CONTROL	POSITION CONTROL	HYBRID CONTROL
Stiffness (N/mm) (RSqaured)	259.19 (0.9992)	197.08 (0.9978)	208.40 (0.9951)
Phase Angle (°)	15.28	14.73	14.63
Hysteresis Area (Nmm)	24.36	21.87	20.62
Hysteresis Loss Coefficient	0.33	0.34	0.34
Maximum Reaction Force (N)	178.85	102.17	122.07

LEFT AXIAL ROTATION (Mz +5Nm) (Rz +1.40°)

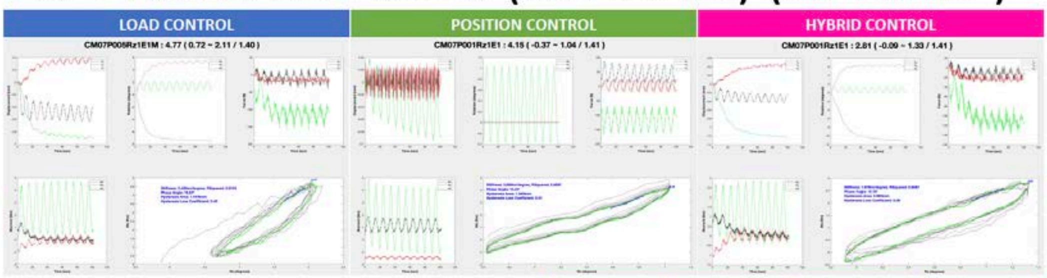

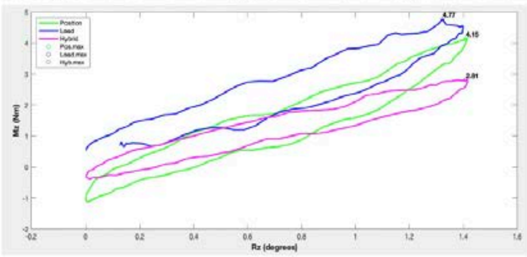

	LOAD CONTROL	POSITION CONTROL	HYBRID CONTROL
Stiffness (Nm/°) (RSqaured)	2.42 (0.9103)	3.80 (0.9597)	1.97 (0.8487)
Phase Angle (°)	19.67	14.34	19.35
Hysteresis Area (Nm°)	1.41	1.34	0.96
Hysteresis Loss Coefficient	0.43	0.31	0.35
Maximum Reaction Moment (Nm)	4.77	4.15	2.81

RIGHT AXIAL ROTATION (Mz -5Nm) (Rz -1.07°)

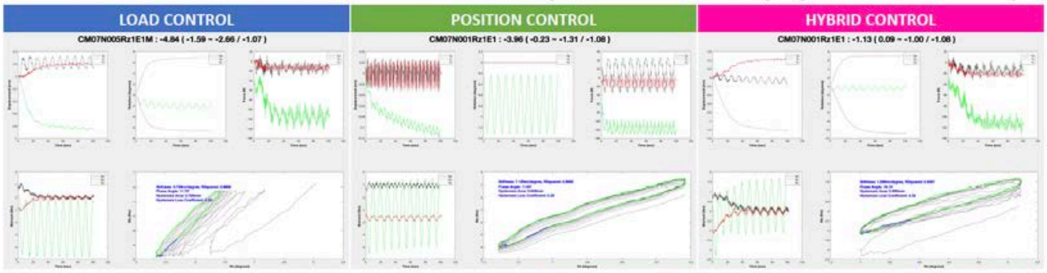

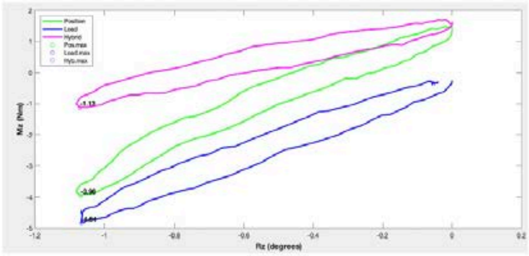

	LOAD CONTROL	POSITION CONTROL	HYBRID CONTROL
Stiffness (Nm/°) (RSqaured)	3.73 (0.9886)	7.12 (0.9992)	1.59 (0.9367)
Phase Angle (°)	11.78	11.05	19.19
Hysteresis Area (Nm°)	0.79	0.84	0.69
Hysteresis Loss Coefficient	0.30	0.28	0.39
Maximum Reaction Moment (Nm)	-4.84	-3.96	-1.13

LEFT LATERAL BENDING (My -5Nm) (Ry -2.73°)

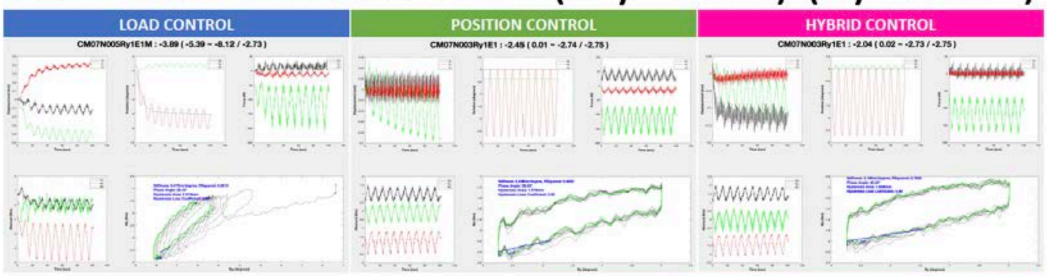

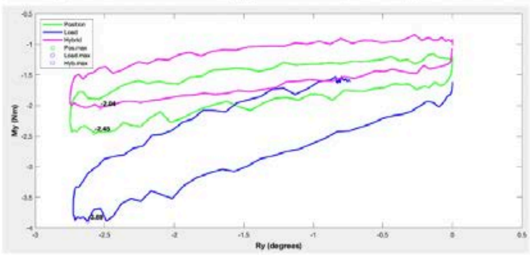

	LOAD CONTROL	POSITION CONTROL	HYBRID 28NTROL
Stiffness (Nm/°) (RSqaured)	0.47 (0.5615)	0.24 (0.4693)	0.18 (0.7923)
Phase Angle (°)	29.43	39.60	45.32
Hysteresis Area (Nm°)	2.31	1.47	1.63
Hysteresis Loss Coefficient	0.63	0.65	0.69
Maximum Reaction Moment (Nm)	-3.89	-2.45	-2.04

RIGHT LATERAL BENDING (My +5Nm) (Ry +2.14°)

LOAD CONTROL	POSITION CONTROL	HYBRID CONTROL

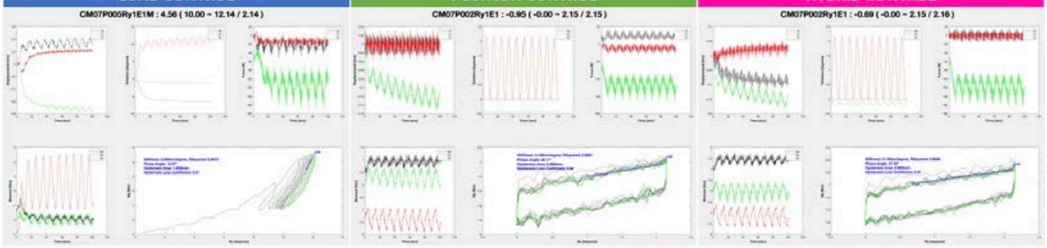

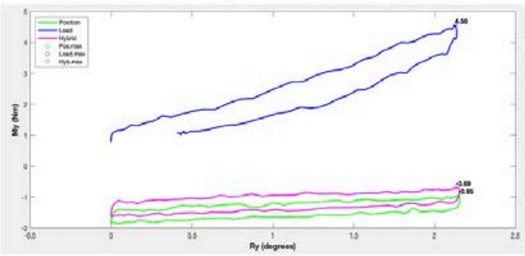

	LOAD CONTROL	POSITION CONTROL	HYBRID CONTROL
Stiffness (Nm/°) (RSqaured)	2.00 (0.9672)	0.16 (0.8087)	0.15 (0.8008)
Phase Angle (°)	14.97	46.17	47.92
Hysteresis Area (Nm°)	1.65	0.88	0.98
Hysteresis Loss Coefficient	0.41	0.64	0.67
Maximum Reaction Moment (Nm)	4.56	-0.95	-0.69

FLEXION (@0.01Hz) (Mx -5Nm) (Rx -3.95°)

LOAD CONTROL	POSITION CONTROL	HYBRID CONTROL

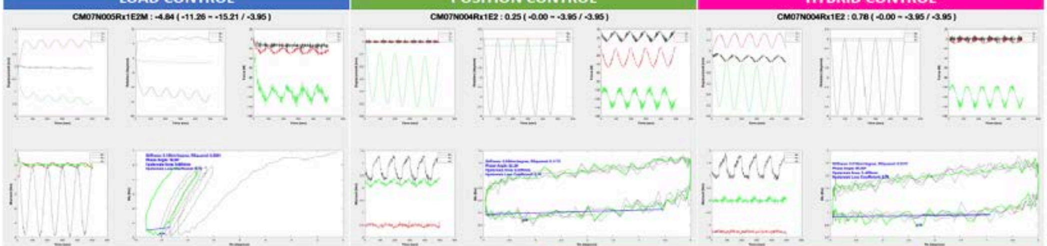

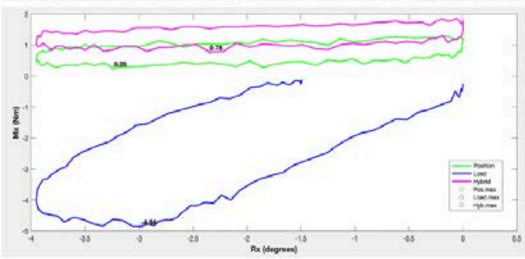

	LOAD CONTROL	POSITION CONTROL	HYBRID CONTROL
Stiffness (Nm/°) (RSqaured)	0.12 (0.0581)	0.03 (0.1173)	0.01 (0.0157)
Phase Angle (°)	18.94	62.26	65.50
Hysteresis Area (Nm°)	9.05	2.54	2.40
Hysteresis Loss Coefficient	0.74	0.75	0.70
Maximum Reaction Moment (Nm)	-4.84	0.25	0.78

FLEXION (Mx -5Nm) (Rx -1.89°)

LOAD CONTROL	POSITION CONTROL	HYBRID CONTROL

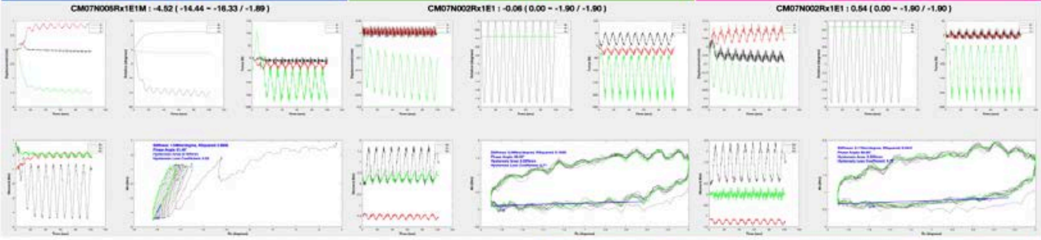

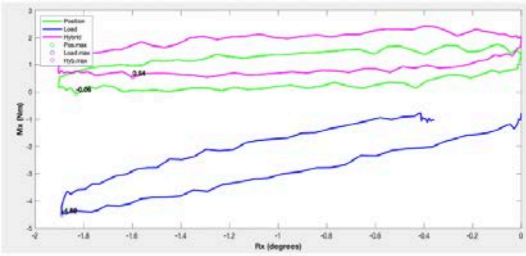

	LOAD CONTROL	POSITION CONTROL	HYBRID CONTROL
Stiffness (Nm/°) (RSqaured)	1.54 (0.8992)	0.09 (0.1835)	0.11 (0.3441)
Phase Angle (°)	21.49	56.62	60.60
Hysteresis Area (Nm°)	2.15	2.02	2.25
Hysteresis Loss Coefficient	0.52	0.71	0.72
Maximum Reaction Moment (Nm)	-4.52	-0.06	0.54

EXTENSION (Mx +5Nm) (Rx +0.78°)

LOAD CONTROL	POSITION CONTROL	HYBRID CONTROL

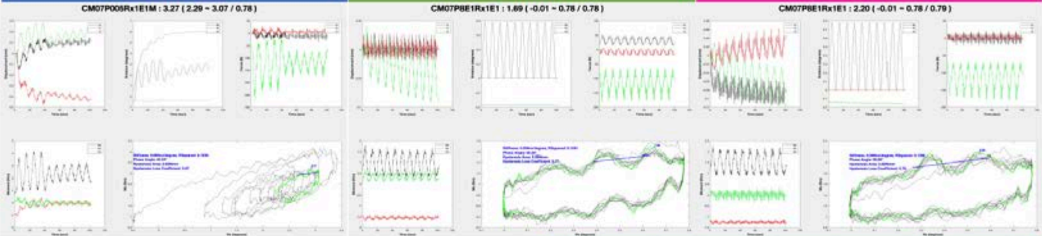

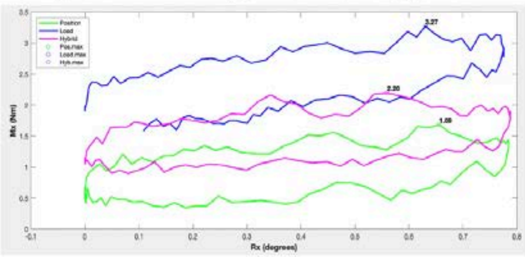

	LOAD CONTROL	POSITION CONTROL	HYBRID CONTROL
Stiffness (Nm/°) (RSqaured)	0.30 (0.1256)	0.50 (0.1091)	0.54 (0.1592)
Phase Angle (°)	42.53	55.30	59.68
Hysteresis Area (Nm°)	0.63	0.59	0.60
Hysteresis Loss Coefficient	0.67	0.77	0.78
Maximum Reaction Moment (Nm)	3.27	1.69	2.20

AXIAL COMPRESSION (Fz -146.90N) (Tz -0.06mm)

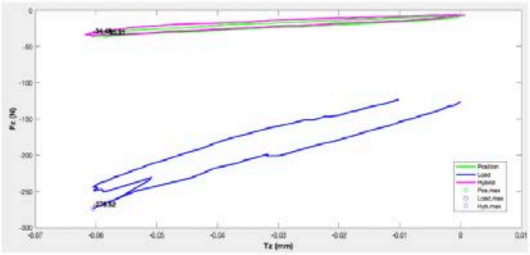

	LOAD CONTROL	POSITION CONTROL	HYBRID CONTROL
Stiffness (N/mm) (RSqaured)	2022.02 (1.0000)	353.53 (0.9635)	418.56 (0.9692)
Phase Angle (°)	21.96	11.94	16.66
Hysteresis Area (Nmm)	1.80	0.33	0.44
Hysteresis Loss Coefficient	0.39	0.34	0.42
Maximum Reaction Force (N)	-273.52	-35.81	-34.49

% DIFFERENCES

	CM06											
	Maximum Reaction Force(N) / Moment(Nm)		Under/Overshoot	% Difference	Maximum Reaction Force(N) / Moment(Nm)		Under/Overshoot	% Difference	Maximum Reaction Force(N) / Moment(Nm)		Under/Overshoot	% Difference
	Load	Position			Load	Hybrid			Position	Hybrid		
Left Lateral Shear (-Fx / -Tx)	-213.17	-123.58	Undershoot	42.03%	-213.17	-97.40	Undershoot	54.31%	-123.58	-97.40	Undershoot	21.19%
Right Lateral Shear (+Fx / + Tx)	180.60	153.82	Undershoot	14.83%	180.60	119.36	Undershoot	33.91%	153.82	119.36	Undershoot	22.41%
Posterior Shear (Fy -200N / Ty -0.31mm)	-206.55	-139.60	Undershoot	32.42%	-206.55	-104.12	Undershoot	49.59%	-139.60	-104.12	Undershoot	25.41%
Anterior Shear (Fy +200N / Ty +0.68mm)	178.85	102.17	Undershoot	42.87%	178.85	122.07	Undershoot	31.75%	102.17	122.07	Overshoot	19.47%
Left Axial Rotation (Mz +5Nm / Rz +0.88°)	4.77	4.15	Undershoot	13.13%	4.77	2.81	Undershoot	41.14%	4.15	2.81	Undershoot	32.24%
Right Axial Rotation (Mz -5Nm / Rz -0.77°)	-4.84	-3.96	Undershoot	18.24%	-4.84	-1.13	Undershoot	76.61%	-3.96	-1.13	Undershoot	71.39%
Left Lateral Bending (My -5Nm / Ry -1.81°)	-3.89	-2.45	Undershoot	37.11%	-3.89	-2.04	Undershoot	47.69%	-2.45	-2.04	Undershoot	16.83%
Right Lateral Bending (My +5Nm / Ry +1.89°)	4.56	-0.95	Undershoot	120.77%	4.56	-0.69	Undershoot	115.15%	-0.95	-0.69	Undershoot	27.05%
Flexion (0.01Hz) (Mx -5Nm / Rx -2.58°)	-4.84	0.25	Undershoot	105.25%	-4.84	0.78	Undershoot	116.07%	0.25	0.78	Overshoot	206.07%
Flexion (Mx -5Nm / Rx -1.66°)	-4.52	-0.06	Undershoot	98.62%	-4.52	0.54	Undershoot	111.98%	-0.06	0.54	Overshoot	970.45%
Extension (Mx +5Nm / Rx +2°)	3.27	1.69	Undershoot	48.50%	3.27	2.20	Undershoot	32.89%	1.69	2.20	Overshoot	30.32%
Axial Compression (Fz -201.85N / Tz -0.04mm)	-273.52	-35.81	Undershoot	86.91%	-273.52	-34.49	Undershoot	87.39%	-35.81	-34.49	Undershoot	3.67%

Appendix F: Statistical Analysis

Appendix F.1 Overall main effects and interaction effects (n=4, CM03, CM04, CM06, CM07)

[Tests of Within-Subjects Effects]

Univariate Tests

Source	Measure		Type III Sum of Squares	df	Mean Square	F	Sig.	Partial Eta Squared
Control_Mode	Stiffness	Sphericity Assumed	1871990.14	2	935995.071	33.900	<.001	.919
		Greenhouse-Geisser	1871990.14	1.150	1628089.63	33.900	.006	.919
		Huynh-Feldt	1871990.14	1.405	1332525.41	33.900	.003	.919
		Lower-bound	1871990.14	1.000	1871990.14	33.900	.010	.919
	Phase_Angle	Sphericity Assumed	1818.054	2	909.027	42.366	<.001	.934
		Greenhouse-Geisser	1818.054	1.122	1620.867	42.366	.005	.934
		Huynh-Feldt	1818.054	1.324	1373.323	42.366	.003	.934
		Lower-bound	1818.054	1.000	1818.054	42.366	.007	.934
	Hysteresis_Area	Sphericity Assumed	4.570	2	2.285	.224	.805	.070
		Greenhouse-Geisser	4.570	1.140	4.008	.224	.694	.070
		Huynh-Feldt	4.570	1.377	3.319	.224	.732	.070
		Lower-bound	4.570	1.000	4.570	.224	.668	.070
	Hysteresis_Loss_Coefficient	Sphericity Assumed	.081	2	.041	16.563	.004	.847
		Greenhouse-Geisser	.081	1.448	.056	16.563	.011	.847
		Huynh-Feldt	.081	2.000	.041	16.563	.004	.847
		Lower-bound	.081	1.000	.081	16.563	.027	.847
	Maximum_Reaction_Forces_Moments	Sphericity Assumed	25503.303	2	12751.651	133.577	<.001	.978
		Greenhouse-Geisser	25503.303	1.310	19471.395	133.577	<.001	.978
		Huynh-Feldt	25503.303	1.916	13307.921	133.577	<.001	.978
		Lower-bound	25503.303	1.000	25503.303	133.577	.001	.978
Error(Control_Mode)	Stiffness	Sphericity Assumed	165664.799	6	27610.800			
		Greenhouse-Geisser	165664.799	3.449	48026.810			
		Huynh-Feldt	165664.799	4.215	39307.998			
		Lower-bound	165664.799	3.000	55221.600			
	Phase_Angle	Sphericity Assumed	128.738	6	21.456			
		Greenhouse-Geisser	128.738	3.365	38.258			
		Huynh-Feldt	128.738	3.972	32.416			
		Lower-bound	128.738	3.000	42.913			
	Hysteresis_Area	Sphericity Assumed	61.095	6	10.182			
		Greenhouse-Geisser	61.095	3.421	17.860			
		Huynh-Feldt	61.095	4.131	14.789			
		Lower-bound	61.095	3.000	20.365			
	Hysteresis_Loss_Coefficient	Sphericity Assumed	.015	6	.002			
		Greenhouse-Geisser	.015	4.344	.003			
		Huynh-Feldt	.015	6.000	.002			
		Lower-bound	.015	3.000	.005			
	Maximum_Reaction_Forces_Moments	Sphericity Assumed	572.778	6	95.463			
		Greenhouse-Geisser	572.778	3.929	145.769			
		Huynh-Feldt	572.778	5.749	99.627			
		Lower-bound	572.778	3.000	190.926			
DOF	Stiffness	Sphericity Assumed	46718055.2	10	4671805.52	16.096	<.001	.843
		Greenhouse-Geisser	46718055.2	1.036	45083929.4	16.096	.026	.843
		Huynh-Feldt	46718055.2	1.092	42770809.2	16.096	.023	.843
		Lower-bound	46718055.2	1.000	46718055.2	16.096	.028	.843
	Phase_Angle	Sphericity Assumed	15422.197	10	1542.220	31.511	<.001	.913
		Greenhouse-Geisser	15422.197	1.945	7930.334	31.511	<.001	.913
		Huynh-Feldt	15422.197	5.476	2816.292	31.511	<.001	.913
		Lower-bound	15422.197	1.000	15422.197	31.511	.011	.913
	Hysteresis_Area	Sphericity Assumed	13246.721	10	1324.672	20.165	<.001	.870
		Greenhouse-Geisser	13246.721	1.233	10747.497	20.165	.012	.870
		Huynh-Feldt	13246.721	1.658	7990.365	20.165	.005	.870
		Lower-bound	13246.721	1.000	13246.721	20.165	.021	.870
	Hysteresis_Loss_Coefficient	Sphericity Assumed	2.127	10	.213	27.471	<.001	.902
		Greenhouse-Geisser	2.127	1.978	1.075	27.471	.001	.902
		Huynh-Feldt	2.127	5.780	.368	27.471	<.001	.902
		Lower-bound	2.127	1.000	2.127	27.471	.014	.902
	Maximum_Reaction_Forces_Moments	Sphericity Assumed	1497626.52	10	149762.652	97.065	<.001	.970
		Greenhouse-Geisser	1497626.52	1.553	964578.067	97.065	<.001	.970
		Huynh-Feldt	1497626.52	2.909	514815.991	97.065	<.001	.970
		Lower-bound	1497626.52	1.000	1497626.52	97.065	.002	.970

Error(DOF)	Stiffness	Sphericity Assumed	8707210.47	30	290240.349			
		Greenhouse-Geisser	8707210.47	3.109	2800881.87			
		Huynh-Feldt	8707210.47	3.277	2657177.09			
		Lower-bound	8707210.47	3.000	2902403.49			
	Phase_Angle	Sphericity Assumed	1468.265	30	48.942			
		Greenhouse-Geisser	1468.265	5.834	251.668			
		Huynh-Feldt	1468.265	16.428	89.375			
		Lower-bound	1468.265	3.000	489.422			
	Hysteresis_Area	Sphericity Assumed	1970.728	30	65.691			
		Greenhouse-Geisser	1970.728	3.698	532.972			
		Huynh-Feldt	1970.728	4.974	396.245			
		Lower-bound	1970.728	3.000	656.909			
	Hysteresis_Loss_Coefficient	Sphericity Assumed	.232	30	.008			
		Greenhouse-Geisser	.232	5.933	.039			
		Huynh-Feldt	.232	17.341	.013			
		Lower-bound	.232	3.000	.077			
	Maximum_Reaction_Forces_Moments	Sphericity Assumed	46287.122	30	1542.904			
		Greenhouse-Geisser	46287.122	4.658	9937.400			
		Huynh-Feldt	46287.122	8.727	5303.804			
		Lower-bound	46287.122	3.000	15429.041			
Control_Mode * DOF	Stiffness	Sphericity Assumed	16524501.1	20	826225.054	24.466	<.001	.891
		Greenhouse-Geisser	16524501.1	1.263	13080805.0	24.466	.008	.891
		Huynh-Feldt	16524501.1	1.758	9400002.10	24.466	.002	.891
		Lower-bound	16524501.1	1.000	16524501.1	24.466	.016	.891
	Phase_Angle	Sphericity Assumed	4800.001	20	240.000	20.956	<.001	.875
		Greenhouse-Geisser	4800.001	1.922	2497.723	20.956	.002	.875
		Huynh-Feldt	4800.001	5.274	910.075	20.956	<.001	.875
		Lower-bound	4800.001	1.000	4800.001	20.956	.020	.875
	Hysteresis_Area	Sphericity Assumed	299.710	20	14.986	2.443	.004	.449
		Greenhouse-Geisser	299.710	1.461	205.179	2.443	.192	.449
		Huynh-Feldt	299.710	2.497	120.049	2.443	.148	.449
		Lower-bound	299.710	1.000	299.710	2.443	.216	.449
	Hysteresis_Loss_Coefficient	Sphericity Assumed	.224	20	.011	4.066	<.001	.575
		Greenhouse-Geisser	.224	1.911	.117	4.066	.081	.575
		Huynh-Feldt	.224	5.179	.043	4.066	.014	.575
		Lower-bound	.224	1.000	.224	4.066	.137	.575
	Maximum_Reaction_Forces_Moments	Sphericity Assumed	202846.496	20	10142.325	32.721	<.001	.916
		Greenhouse-Geisser	202846.496	1.715	118245.438	32.721	.001	.916
		Huynh-Feldt	202846.496	3.785	53592.938	32.721	<.001	.916
		Lower-bound	202846.496	1.000	202846.496	32.721	.011	.916
Error (Control_Mode*DOF)	Stiffness	Sphericity Assumed	2026249.62	60	33770.827			
		Greenhouse-Geisser	2026249.62	3.790	534660.139			
		Huynh-Feldt	2026249.62	5.274	384212.321			
		Lower-bound	2026249.62	3.000	675416.541			
	Phase_Angle	Sphericity Assumed	687.143	60	11.452			
		Greenhouse-Geisser	687.143	5.765	119.187			
		Huynh-Feldt	687.143	15.823	43.427			
		Lower-bound	687.143	3.000	229.048			
	Hysteresis_Area	Sphericity Assumed	368.075	60	6.135			
		Greenhouse-Geisser	368.075	4.382	83.994			
		Huynh-Feldt	368.075	7.490	49.144			
		Lower-bound	368.075	3.000	122.692			
	Hysteresis_Loss_Coefficient	Sphericity Assumed	.165	60	.003			
		Greenhouse-Geisser	.165	5.732	.029			
		Huynh-Feldt	.165	15.538	.011			
		Lower-bound	.165	3.000	.055			
	Maximum_Reaction_Forces_Moments	Sphericity Assumed	18597.930	60	309.965			
		Greenhouse-Geisser	18597.930	5.146	3613.768			
		Huynh-Feldt	18597.930	11.355	1637.885			
		Lower-bound	18597.930	3.000	6199.310			

[Profile Plots]

Control_Mode: 1-load control, 2-position control, 3-hybrid control

DOF: 1-LLS, 2-RLS, 3-PS, 4-AS, 5-LAR, 6-RAR, 7-LLB, 8-RLb, 9-Flex, 10-Ext, 11-Comp

Stiffness

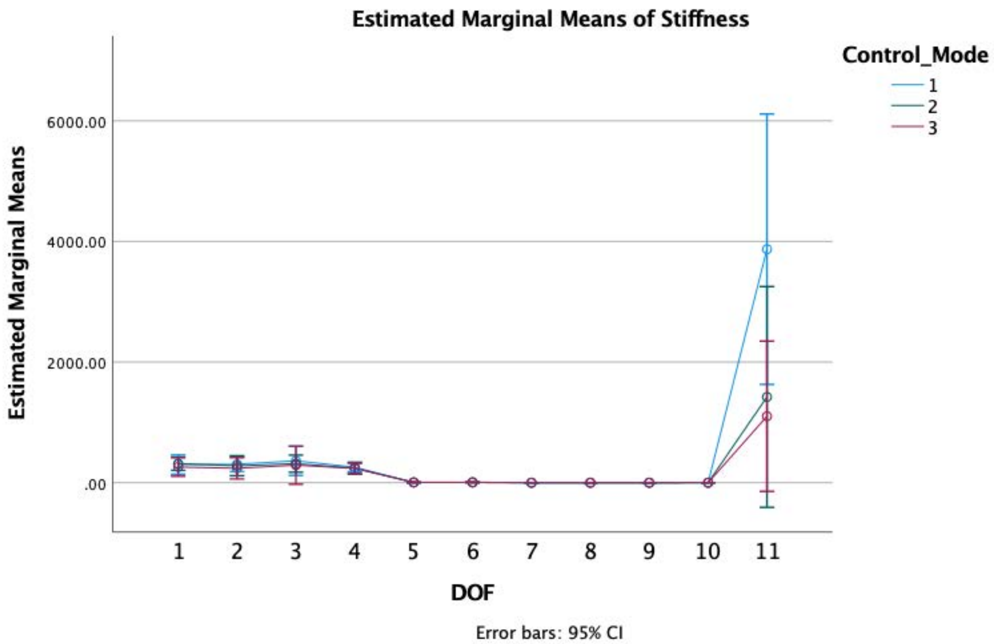

Phase_Angle

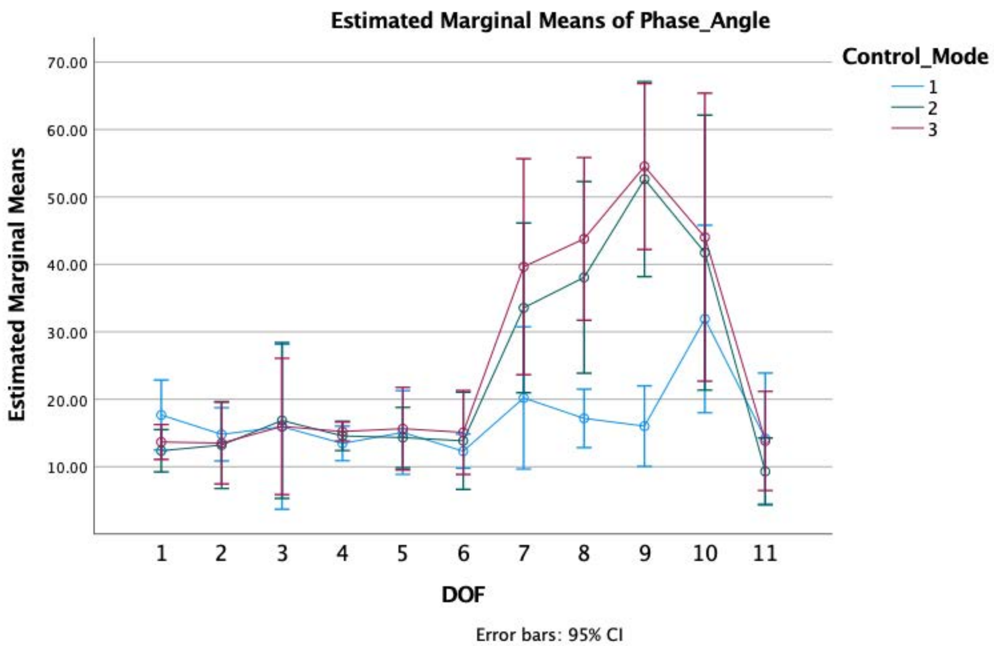

Hysteresis_Area

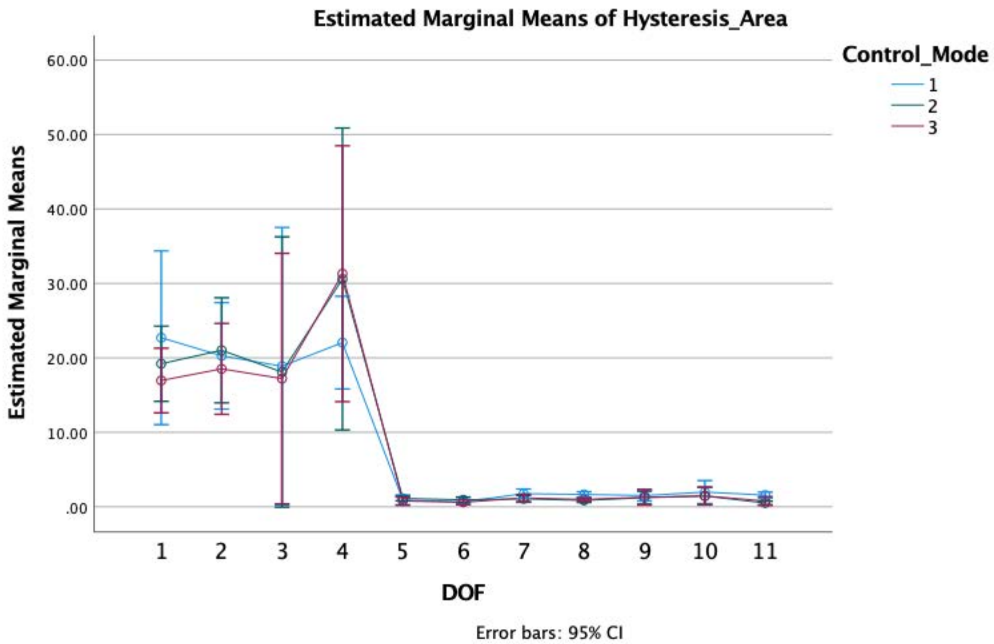

Hysteresis_Loss_Coefficient

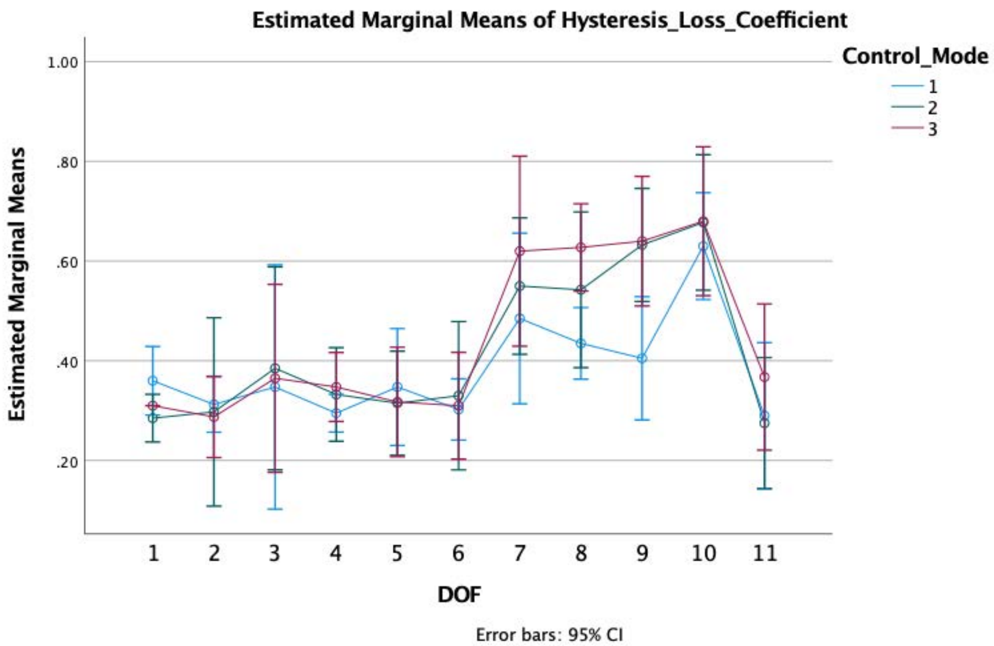

Maximum_Reaction_Forces_Moments

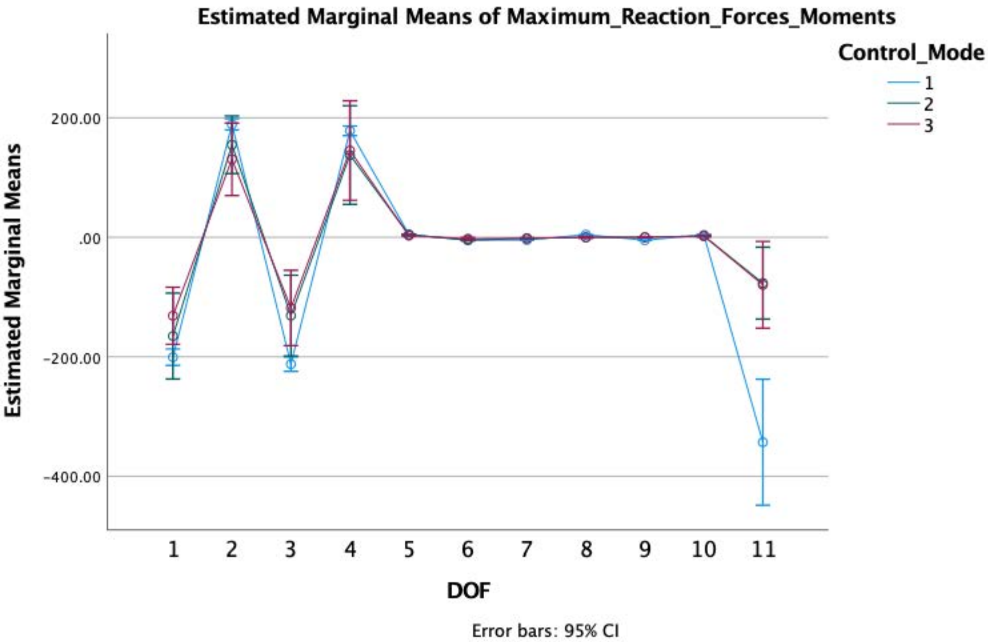

Appendix F.2 Pairwise Comparisons (n=4, CM03, CM04, CM06, CM07)

Control_Mode: 1-load control, 2-position control, 3-hybrid control

DOF: 1-LLS, 2-RLS, 3-PS, 4-AS, 5-LAR, 6-RAR, 7-LLB, 8-RLb, 9-Flex, 10-Ext, 11-Comp

Pairwise Comparisons

Measure	DOF	(I) Control_Mode	(J) Control_Mode	Mean Difference (I-J)	Std. Error	Sig.[b]	95% Confidence Interval for Difference[b]	
							Lower Bound	Upper Bound
Stiffness	1	1	2	-14.325	43.096	1.000	-223.628	194.978
			3	41.545	25.988	.625	-84.669	167.759
		2	1	14.325	43.096	1.000	-194.978	223.628
			3	55.870	26.347	.372	-72.087	183.827
		3	1	-41.545	25.988	.625	-167.759	84.669
			2	-55.870	26.347	.372	-183.827	72.087
	2	1	2	25.640	38.271	1.000	-160.231	211.511
			3	66.718	48.046	.777	-166.623	300.058
		2	1	-25.640	38.271	1.000	-211.511	160.231
			3	41.078	12.144	.129	-17.904	100.059
		3	1	-66.717	48.046	.777	-300.058	166.623
			2	-41.078	12.144	.129	-100.059	17.904
	3	1	2	47.460	58.101	1.000	-234.718	329.638
			3	72.565	99.521	1.000	-410.776	555.906
		2	1	-47.460	58.101	1.000	-329.638	234.718
			3	25.105	58.704	1.000	-260.000	310.210
		3	1	-72.565	99.521	1.000	-555.906	410.776
			2	-25.105	58.704	1.000	-310.210	260.000
	4	1	2	16.640	46.071	1.000	-207.111	240.391
			3	20.225	43.978	1.000	-193.360	233.810
		2	1	-16.640	46.071	1.000	-240.391	207.111
			3	3.585	6.233	1.000	-26.689	33.859
		3	1	-20.225	43.978	1.000	-233.810	193.360
			2	-3.585	6.233	1.000	-33.859	26.689
	5	1	2	-1.527	.797	.454	-5.399	2.344
			3	-.315	.615	1.000	-3.302	2.672
		2	1	1.527	.797	.454	-2.344	5.399
			3	1.213	.469	.244	-1.064	3.489
		3	1	.315	.615	1.000	-2.672	3.302
			2	-1.213	.469	.244	-3.489	1.064
	6	1	2	-2.947	1.900	.656	-12.176	6.281
			3	1.353	.323	.074	-.215	2.920
		2	1	2.947	1.900	.656	-6.281	12.176
			3	4.300	1.799	.290	-4.436	13.036
		3	1	-1.353	.323	.074	-2.920	.215
			2	-4.300	1.799	.290	-13.036	4.436
	7	1	2	1.025	.277	.103	-.322	2.372
			3	1.020	.246	.076	-.173	2.213
		2	1	-1.025	.277	.103	-2.372	.322
			3	-.005	.068	1.000	-.337	.327
		3	1	-1.020	.246	.076	-2.213	.173
			2	.005	.068	1.000	-.327	.337
	8	1	2	1.533*	.119	.003	.955	2.110
			3	1.553*	.123	.003	.956	2.149
		2	1	-1.533*	.119	.003	-2.110	-.955
			3	.020	.017	.996	-.064	.104
		3	1	-1.553*	.123	.003	-2.149	-.956
			2	-.020	.017	.996	-.104	.064
	9	1	2	1.965*	.328	.028	.374	3.556
			3	1.958*	.340	.031	.307	3.608
		2	1	-1.965*	.328	.028	-3.556	-.374
			3	-.007	.029	1.000	-.148	.133
		3	1	-1.957*	.340	.031	-3.608	-.307
			2	.007	.029	1.000	-.133	.148
	10	1	2	.337	.220	.666	-.729	1.404
			3	.293	.223	.844	-.792	1.377
		2	1	-.337	.220	.666	-1.404	.729
			3	-.045	.025	.509	-.166	.076
		3	1	-.292	.223	.844	-1.377	.792
			2	.045	.025	.509	-.076	.166
	11	1	2	2449.920*	464.933	.040	191.900	4707.940
			3	2769.865*	517.569	.038	256.211	5283.519
		2	1	-2449.920*	464.933	.040	-4707.940	-191.900
			3	319.945	189.633	.570	-601.038	1240.928
		3	1	-2769.865*	517.569	.038	-5283.519	-256.211
			2	-319.945	189.633	.570	-1240.928	601.038

Phase_Angle	1	1	2	5.298	1.229	.069	-.671	11.266
			3	3.998	1.027	.090	-.992	8.987
		2	1	-5.298	1.229	.069	-11.266	.671
			3	-1.300	.389	.133	-3.190	.590
		3	1	-3.998	1.027	.090	-8.987	.992
			2	1.300	.389	.133	-.590	3.190
	2	1	2	1.587	2.870	1.000	-12.350	15.525
			3	1.295	2.289	1.000	-9.822	12.412
		2	1	-1.587	2.870	1.000	-15.525	12.350
			3	-.292	1.118	1.000	-5.721	5.136
		3	1	-1.295	2.289	1.000	-12.412	9.822
			2	.292	1.118	1.000	-5.136	5.721
	3	1	2	-.925	1.088	1.000	-6.211	4.361
			3	-.045	1.425	1.000	-6.964	6.874
		2	1	.925	1.088	1.000	-4.361	6.211
			3	.880	1.381	1.000	-5.827	7.587
		3	1	.045	1.425	1.000	-6.874	6.964
			2	-.880	1.381	1.000	-7.587	5.827
	4	1	2	-1.112	.971	1.000	-5.828	3.603
			3	-1.767	1.224	.733	-7.711	4.176
		2	1	1.112	.971	1.000	-3.603	5.828
			3	-.655	.797	1.000	-4.528	3.218
		3	1	1.767	1.224	.733	-4.176	7.711
			2	.655	.797	1.000	-3.218	4.528
	5	1	2	.760	2.806	1.000	-12.866	14.386
			3	-.560	.397	.760	-2.489	1.369
		2	1	-.760	2.806	1.000	-14.386	12.866
			3	-1.320	2.893	1.000	-15.370	12.730
		3	1	.560	.397	.760	-1.369	2.489
			2	1.320	2.893	1.000	-12.730	15.370
	6	1	2	-1.538	2.897	1.000	-15.606	12.531
			3	-2.782	1.688	.593	-10.978	5.413
		2	1	1.538	2.897	1.000	-12.531	15.606
			3	-1.245	4.010	1.000	-20.720	18.230
		3	1	2.782	1.688	.593	-5.413	10.978
			2	1.245	4.010	1.000	-18.230	20.720
	7	1	2	-13.358*	2.447	.036	-25.243	-1.472
			3	-19.452*	3.654	.039	-37.199	-1.706
		2	1	13.358*	2.447	.036	1.472	25.243
			3	-6.095	1.271	.052	-12.267	.077
		3	1	19.453*	3.654	.039	1.706	37.199
			2	6.095	1.271	.052	-.077	12.267
	8	1	2	-20.905	4.906	.071	-44.734	2.924
			3	-26.617*	4.464	.028	-48.300	-4.935
		2	1	20.905	4.906	.071	-2.924	44.734
			3	-5.713	1.984	.191	-15.346	3.921
		3	1	26.618*	4.464	.028	4.935	48.300
			2	5.713	1.984	.191	-3.921	15.346
	9	1	2	-36.627*	3.949	.008	-55.809	-17.446
			3	-38.500*	2.918	.003	-52.674	-24.326
		2	1	36.628*	3.949	.008	17.446	55.809
			3	-1.873	1.584	.967	-9.565	5.820
		3	1	38.500*	2.918	.003	24.326	52.674
			2	1.873	1.584	.967	-5.820	9.565
	10	1	2	-9.835	4.113	.290	-29.809	10.139
			3	-12.123	3.384	.112	-28.556	4.311
		2	1	9.835	4.113	.290	-10.139	29.809
			3	-2.288	1.561	.717	-9.867	5.292
		3	1	12.123	3.384	.112	-4.311	28.556
			2	2.288	1.561	.717	-5.292	9.867
	11	1	2	4.888	1.832	.227	-4.008	13.783
			3	.368	1.778	1.000	-8.270	9.005
		2	1	-4.888	1.832	.227	-13.783	4.008
			3	-4.520	1.333	.128	-10.994	1.954
		3	1	-.368	1.778	1.000	-9.005	8.270
			2	4.520	1.333	.128	-1.954	10.994

Hysteresis_Area	1	1	2	3.490	3.275	1.000	-12.414	19.394
			3	5.745	2.822	.404	-7.961	19.451
		2	1	-3.490	3.275	1.000	-19.394	12.414
			3	2.255	1.238	.498	-3.758	8.268
		3	1	-5.745	2.822	.404	-19.451	7.961
			2	-2.255	1.238	.498	-8.268	3.758
	2	1	2	-.745	2.933	1.000	-14.988	13.498
			3	1.753	1.966	1.000	-7.795	11.300
		2	1	.745	2.933	1.000	-13.498	14.988
			3	2.498	2.143	.984	-7.911	12.906
		3	1	-1.753	1.966	1.000	-11.300	7.795
			2	-2.498	2.143	.984	-12.906	7.911
	3	1	2	.783	1.786	1.000	-7.891	9.456
			3	1.663	2.716	1.000	-11.530	14.855
		2	1	-.783	1.786	1.000	-9.456	7.891
			3	.880	1.779	1.000	-7.762	9.522
		3	1	-1.663	2.716	1.000	-14.855	11.530
			2	-.880	1.779	1.000	-9.522	7.762
	4	1	2	-8.543	5.357	.627	-34.559	17.474
			3	-9.255	4.906	.467	-33.083	14.573
		2	1	8.543	5.357	.627	-17.474	34.559
			3	-.712	1.742	1.000	-9.171	7.746
		3	1	9.255	4.906	.467	-14.573	33.083
			2	.712	1.742	1.000	-7.746	9.171
	5	1	2	-.230	.178	.861	-1.095	.635
			3	.110	.117	1.000	-.458	.678
		2	1	.230	.178	.861	-.635	1.095
			3	.340	.168	.409	-.476	1.156
		3	1	-.110	.117	1.000	-.678	.458
			2	-.340	.168	.409	-1.156	.476
	6	1	2	-.275	.216	.876	-1.322	.772
			3	.060	.026	.316	-.067	.187
		2	1	.275	.216	.876	-.772	1.322
			3	.335	.209	.623	-.682	1.352
		3	1	-.060	.026	.316	-.187	.067
			2	-.335	.209	.623	-1.352	.682
	7	1	2	.698*	.134	.042	.045	1.350
			3	.575*	.109	.040	.047	1.103
		2	1	-.697*	.134	.042	-1.350	-.045
			3	-.122	.027	.063	-.256	.011
		3	1	-.575*	.109	.040	-1.103	-.047
			2	.122	.027	.063	-.011	.256
	8	1	2	.798*	.060	.003	.504	1.091
			3	.670*	.064	.006	.358	.982
		2	1	-.798*	.060	.003	-1.091	-.504
			3	-.128*	.019	.020	-.219	-.036
		3	1	-.670*	.064	.006	-.982	-.358
			2	.128*	.019	.020	.036	.219
	9	1	2	.290	.120	.284	-.293	.873
			3	.228	.156	.723	-.530	.985
		2	1	-.290	.120	.284	-.873	.293
			3	-.062	.071	1.000	-.408	.283
		3	1	-.228	.156	.723	-.985	.530
			2	.063	.071	1.000	-.283	.408
	10	1	2	.528	.236	.335	-.620	1.675
			3	.508	.205	.268	-.486	1.501
		2	1	-.528	.236	.335	-1.675	.620
			3	-.020	.043	1.000	-.229	.189
		3	1	-.508	.205	.268	-1.501	.486
			2	.020	.043	1.000	-.189	.229
	11	1	2	1.055*	.191	.035	.126	1.984
			3	.790	.280	.201	-.572	2.152
		2	1	-1.055*	.191	.035	-1.984	-.126
			3	-.265	.129	.398	-.893	.363
		3	1	-.790	.280	.201	-2.152	.572
			2	.265	.129	.398	-.363	.893

Hysteresis_Loss_Coefficient	1	1	2	.075	.019	.086	-.017	.167
			3	.050	.022	.311	-.055	.155
		2	1	-.075	.019	.086	-.167	.017
			3	-.025	.015	.583	-.098	.048
		3	1	-.050	.022	.311	-.155	.055
			2	.025	.015	.583	-.048	.098
	2	1	2	.015	.069	1.000	-.319	.349
			3	.025	.036	1.000	-.151	.201
		2	1	-.015	.069	1.000	-.349	.319
			3	.010	.034	1.000	-.157	.177
		3	1	-.025	.036	1.000	-.201	.151
			2	-.010	.034	1.000	-.177	.157
	3	1	2	-.038	.023	.599	-.149	.074
			3	-.018	.032	1.000	-.172	.137
		2	1	.038	.023	.599	-.074	.149
			3	.020	.026	1.000	-.107	.147
		3	1	.018	.032	1.000	-.137	.172
			2	-.020	.026	1.000	-.147	.107
	4	1	2	-.037	.029	.847	-.177	.102
			3	-.052	.024	.348	-.169	.064
		2	1	.037	.029	.847	-.102	.177
			3	-.015	.015	1.000	-.088	.058
		3	1	.052	.024	.348	-.064	.169
			2	.015	.015	1.000	-.058	.088
	5	1	2	.033	.059	1.000	-.252	.317
			3	.030	.019	.621	-.061	.121
		2	1	-.033	.059	1.000	-.317	.252
			3	-.003	.058	1.000	-.285	.280
		3	1	-.030	.019	.621	-.121	.061
			2	.003	.058	1.000	-.280	.285
	6	1	2	-.027	.064	1.000	-.341	.286
			3	-.008	.028	1.000	-.143	.128
		2	1	.027	.064	1.000	-.286	.341
			3	.020	.076	1.000	-.350	.390
		3	1	.008	.028	1.000	-.128	.143
			2	-.020	.076	1.000	-.390	.350
	7	1	2	-.065	.016	.075	-.140	.010
			3	-.135	.044	.164	-.349	.079
		2	1	.065	.016	.075	-.010	.140
			3	-.070	.034	.393	-.235	.095
		3	1	.135	.044	.164	-.079	.349
			2	.070	.034	.393	-.095	.235
	8	1	2	-.107	.055	.434	-.374	.159
			3	-.192	.042	.057	-.394	.009
		2	1	.107	.055	.434	-.159	.374
			3	-.085	.027	.157	-.217	.047
		3	1	.192	.042	.057	-.009	.394
			2	.085	.027	.157	-.047	.217
	9	1	2	-.227*	.025	.008	-.349	-.106
			3	-.235*	.033	.018	-.397	-.073
		2	1	.227*	.025	.008	.106	.349
			3	-.008	.017	1.000	-.088	.073
		3	1	.235*	.033	.018	.073	.397
			2	.008	.017	1.000	-.073	.088
	10	1	2	-.047	.030	.648	-.195	.100
			3	-.050	.022	.311	-.155	.055
		2	1	.047	.030	.648	-.100	.195
			3	-.003	.019	1.000	-.094	.089
		3	1	.050	.022	.311	-.055	.155
			2	.003	.019	1.000	-.089	.094
	11	1	2	.015	.013	.957	-.046	.076
			3	-.077	.037	.378	-.256	.101
		2	1	-.015	.013	.957	-.076	.046
			3	-.092	.031	.174	-.243	.058
		3	1	.077	.037	.378	-.101	.256
			2	.092	.031	.174	-.058	.243

Maximum_Reaction_Forces_Moments	1	1	2	-35.347	25.667	.787	-160.002	89.307
			3	-69.392	18.313	.097	-158.333	19.548
		2	1	35.348	25.667	.787	-89.307	160.002
			3	-34.045	10.839	.155	-86.685	18.595
		3	1	69.392	18.313	.097	-19.548	158.333
			2	34.045	10.839	.155	-18.595	86.685
	2	1	2	34.167	15.763	.356	-42.389	110.724
			3	58.458	19.035	.164	-33.990	150.905
		2	1	-34.167	15.763	.356	-110.724	42.389
			3	24.290	5.212	.056	-1.022	49.602
		3	1	-58.458	19.035	.164	-150.905	33.990
			2	-24.290	5.212	.056	-49.602	1.022
	3	1	2	-81.230	22.297	.107	-189.518	27.058
			3	-93.940	20.619	.059	-194.079	6.199
		2	1	81.230	22.297	.107	-27.058	189.518
			3	-12.710	8.287	.668	-52.955	27.535
		3	1	93.940	20.619	.059	-6.199	194.079
			2	12.710	8.287	.668	-27.535	52.955
	4	1	2	40.567	27.445	.708	-92.725	173.860
			3	33.080	27.189	.932	-98.967	165.127
		2	1	-40.567	27.445	.708	-173.860	92.725
			3	-7.487	8.062	1.000	-46.644	31.669
		3	1	-33.080	27.189	.932	-165.127	98.967
			2	7.487	8.062	1.000	-31.669	46.644
	5	1	2	.363	.183	.426	-.527	1.252
			3	1.855*	.320	.031	.302	3.408
		2	1	-.363	.183	.426	-1.252	.527
			3	1.492	.460	.143	-.742	3.727
		3	1	-1.855*	.320	.031	-3.408	-.302
			2	-1.492	.460	.143	-3.727	.742
	6	1	2	-.398	.394	1.000	-2.313	1.518
			3	-2.495	.626	.085	-5.535	.545
		2	1	.398	.394	1.000	-1.518	2.313
			3	-2.097*	.323	.022	-3.666	-.529
		3	1	2.495	.626	.085	-.545	5.535
			2	2.097*	.323	.022	.529	3.666
	7	1	2	-2.687*	.443	.027	-4.840	-.535
			3	-2.770*	.333	.011	-4.385	-1.155
		2	1	2.688*	.443	.027	.535	4.840
			3	-.082	.117	1.000	-.649	.484
		3	1	2.770*	.333	.011	1.155	4.385
			2	.082	.117	1.000	-.484	.649
	8	1	2	4.498*	.402	.005	2.546	6.449
			3	4.490*	.365	.003	2.718	6.262
		2	1	-4.497*	.402	.005	-6.449	-2.546
			3	-.008	.097	1.000	-.477	.462
		3	1	-4.490*	.365	.003	-6.262	-2.718
			2	.008	.097	1.000	-.462	.477
	9	1	2	-4.897*	.240	<.001	-6.064	-3.731
			3	-5.015*	.197	<.001	-5.972	-4.058
		2	1	4.898*	.240	<.001	3.731	6.064
			3	-.117	.162	1.000	-.906	.671
		3	1	5.015*	.197	<.001	4.058	5.972
			2	.118	.162	1.000	-.671	.906
	10	1	2	1.815	.457	.086	-.406	4.036
			3	1.780	.399	.063	-.160	3.720
		2	1	-1.815	.457	.086	-4.036	.406
			3	-.035	.205	1.000	-1.029	.959
		3	1	-1.780	.399	.063	-3.720	.160
			2	.035	.205	1.000	-.959	1.029
	11	1	2	-266.370*	15.676	.001	-342.505	-190.235
			3	-263.427*	14.923	.001	-335.902	-190.953
		2	1	266.370*	15.676	.001	190.235	342.505
			3	2.942	4.903	1.000	-20.869	26.754
		3	1	263.427*	14.923	.001	190.953	335.902
			2	-2.942	4.903	1.000	-26.754	20.869

Based on estimated marginal means

*. The mean difference is significant at the .05 level.

b. Adjustment for multiple comparisons: Bonferroni.

- Pairwise comparison between control modes with Bonferroni adjustment. Red starts denote significant differences. Error bars indicates 95% confidence.

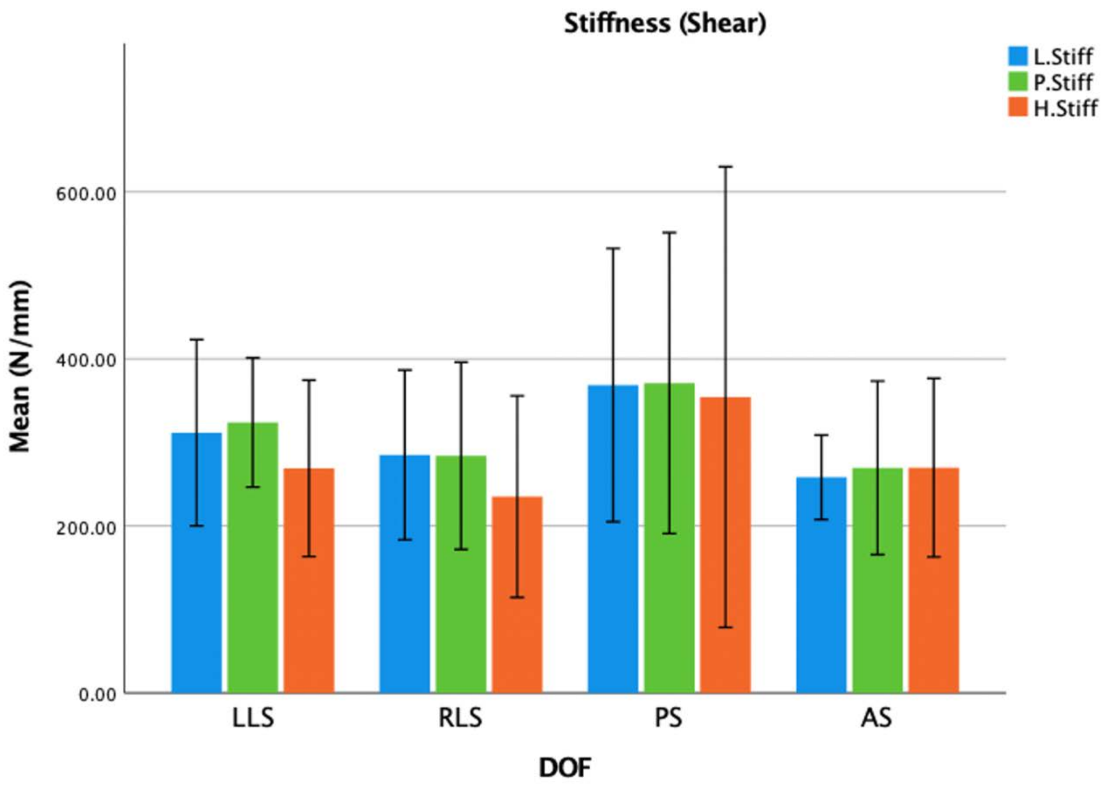

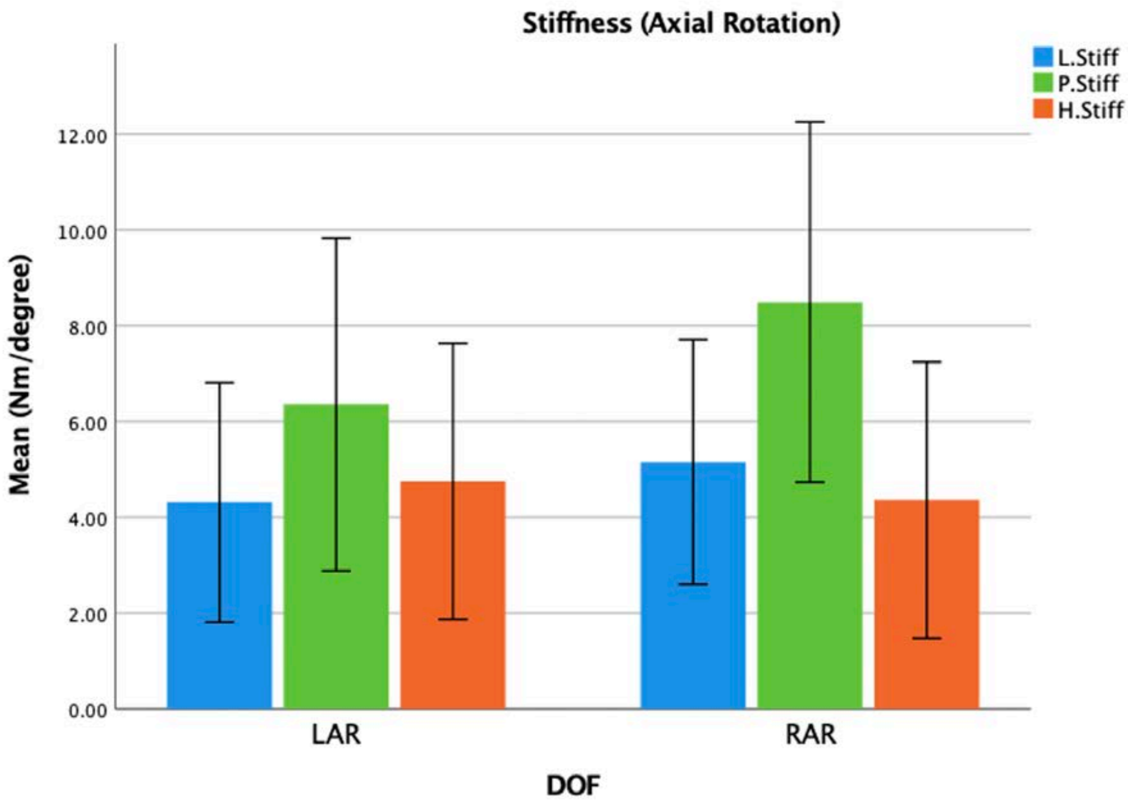

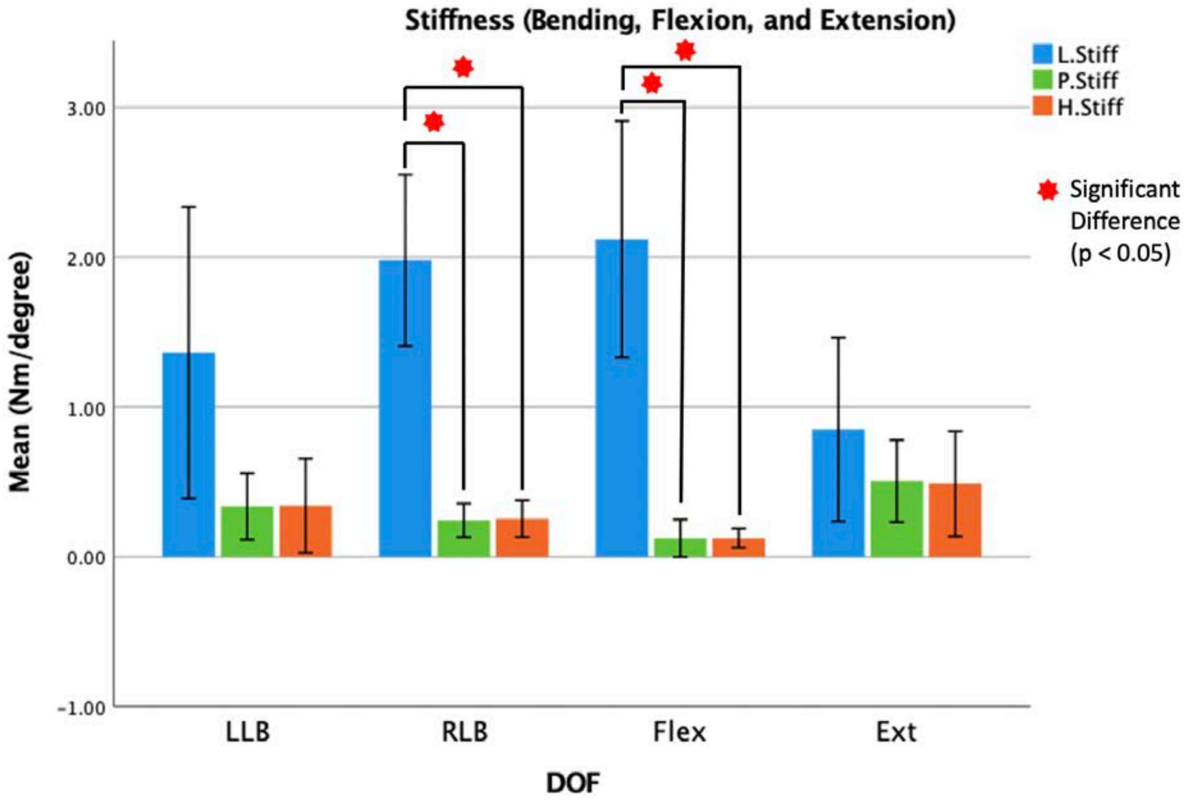
Stiffness (Bending, Flexion, and Extension)
L.Stiff
P.Stiff
H.Stiff
Significant Difference (p < 0.05)
Mean (Nm/degree)
3.00
2.00
1.00
0.00
-1.00
LLB
RLB
Flex
Ext
DOF

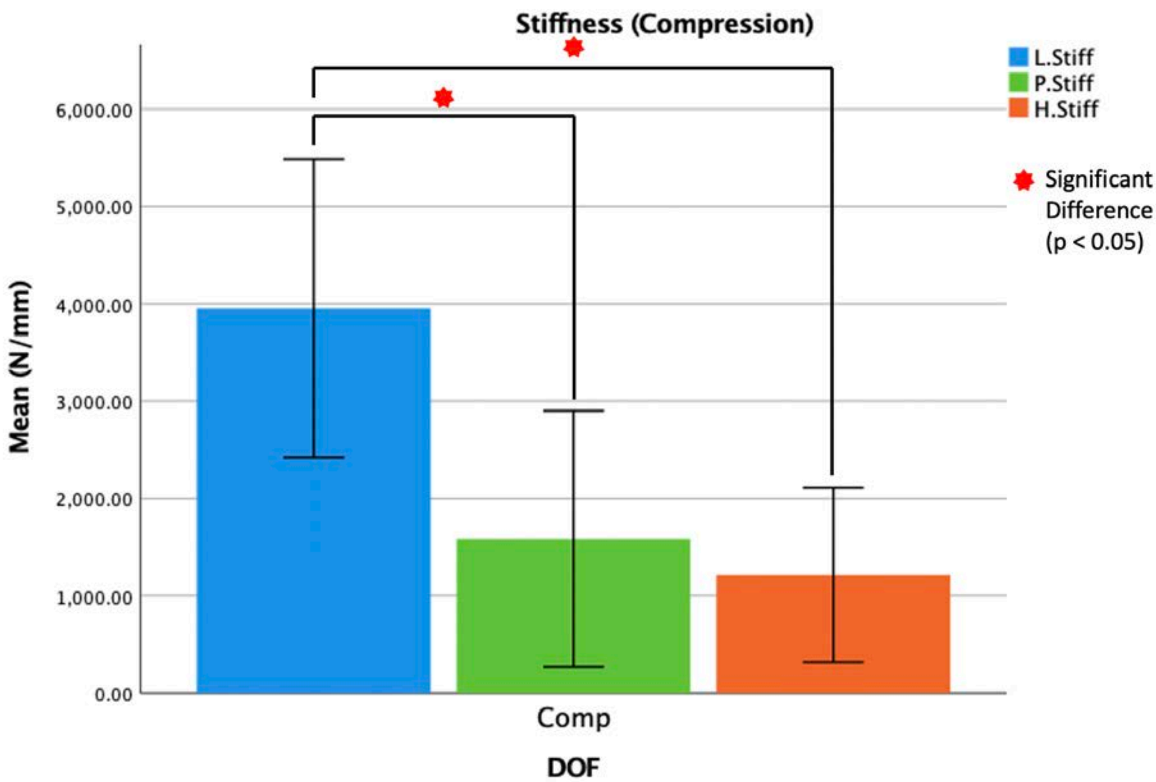
Stiffness (Compression)
L.Stiff
P.Stiff
H.Stiff
Significant Difference (p < 0.05)
Mean (N/mm)
6,000.00
5,000.00
4,000.00
3,000.00
2,000.00
1,000.00
0.00
Comp
DOF

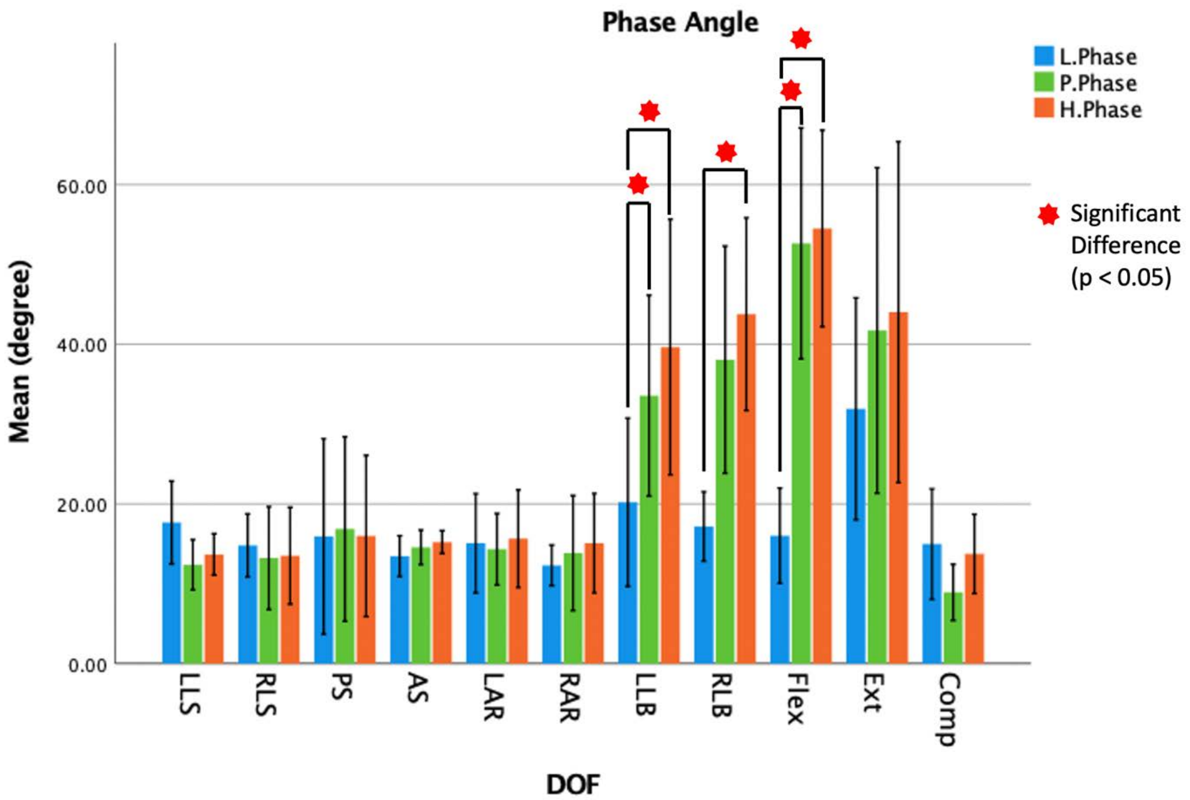
Phase Angle
L.Phase
P.Phase
H.Phase
Significant
Difference
(p < 0.05)
Mean (degree)
0.00
20.00
40.00
60.00
LLS
RLS
PS
AS
LAR
RAR
LLB
RLB
Flex
Ext
Comp
DOF

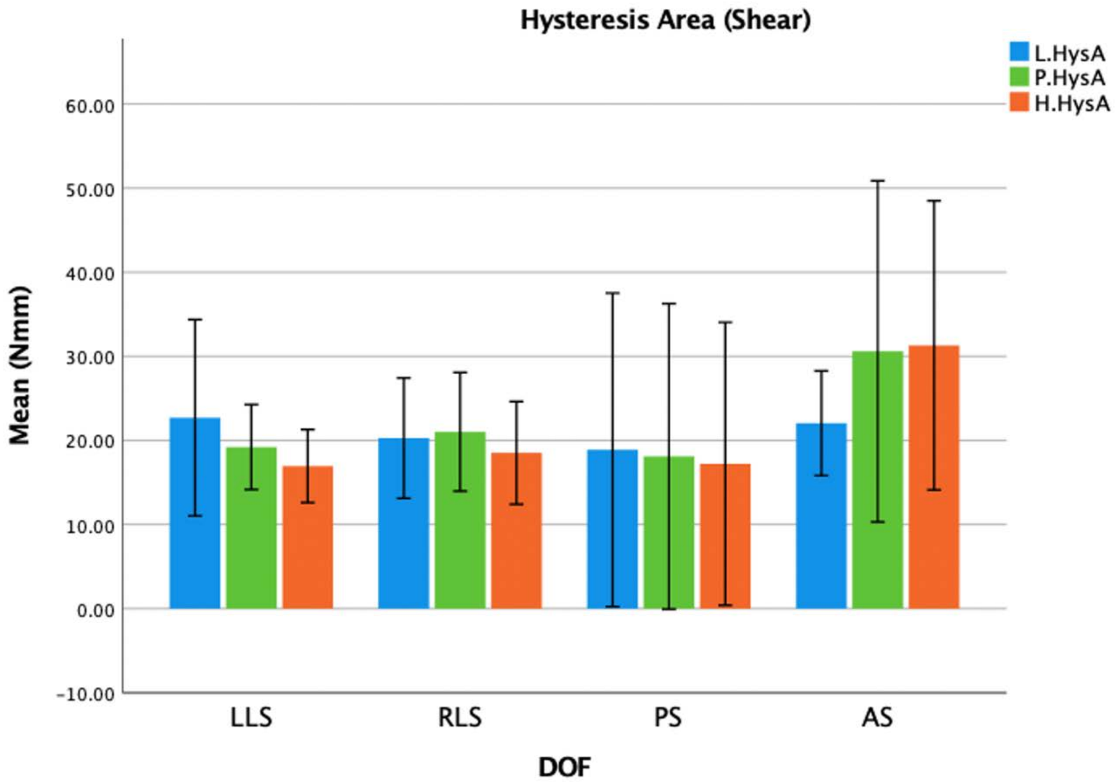
Hysteresis Area (Shear)
L.HysA
P.HysA
H.HysA
Mean (Nmm)
-10.00
0.00
10.00
20.00
30.00
40.00
50.00
60.00
LLS
RLS
PS
AS
DOF

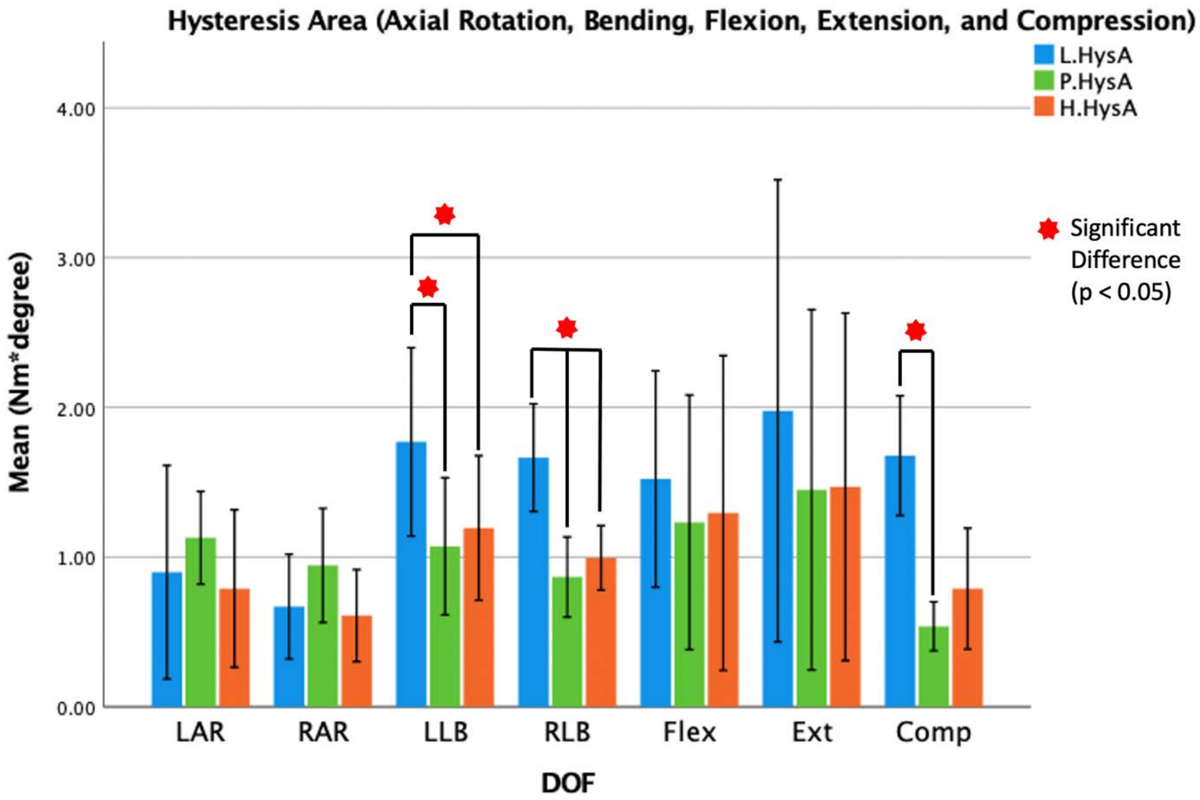
Hysteresis Area (Axial Rotation, Bending, Flexion, Extension, and Compression)
L.HysA
P.HysA
H.HysA
Significant Difference (p < 0.05)
Mean (Nm*degree)
4.00
3.00
2.00
1.00
0.00
LAR
RAR
LLB
RLB
Flex
Ext
Comp
DOF

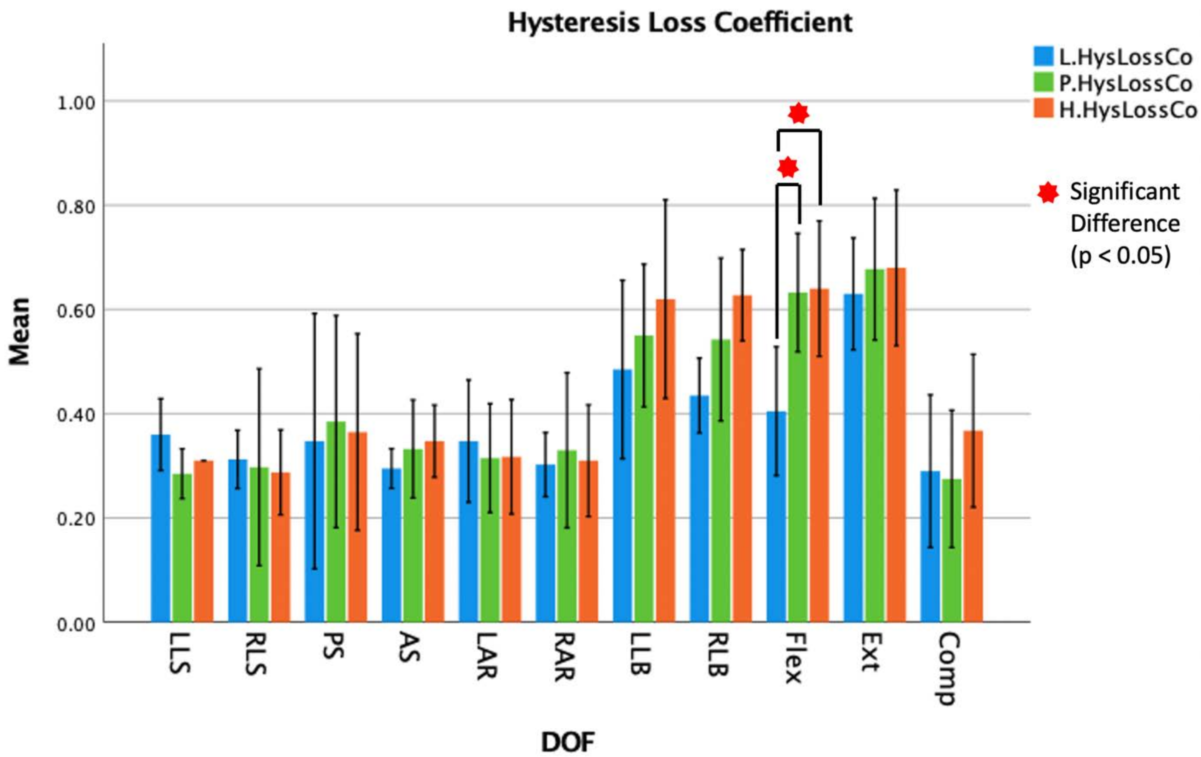
Hysteresis Loss Coefficient
L.HysLossCo
P.HysLossCo
H.HysLossCo
Significant Difference (p < 0.05)
Mean
1.00
0.80
0.60
0.40
0.20
0.00
LLS
RLS
PS
AS
LAR
RAR
LLB
RLB
Flex
Ext
Comp
DOF

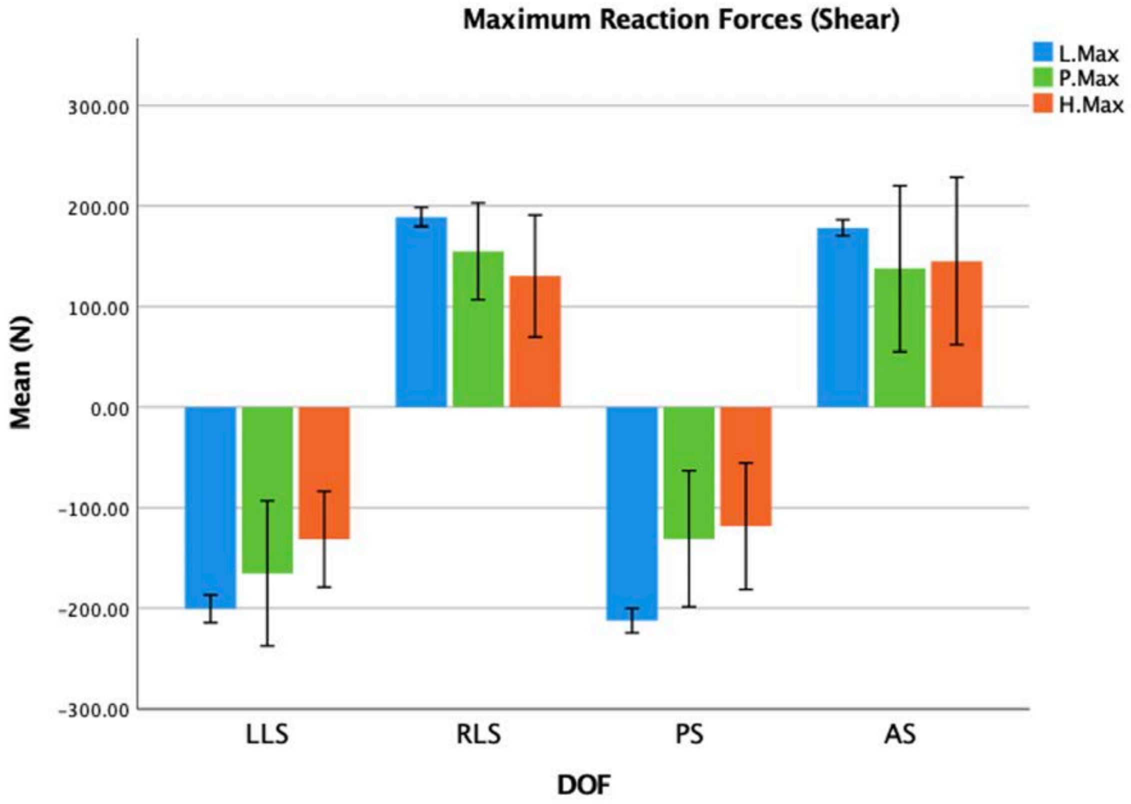
Maximum Reaction Forces (Shear)
L.Max
P.Max
H.Max
300.00
200.00
100.00
0.00
-100.00
-200.00
-300.00
Mean (N)
LLS
RLS
PS
AS
DOF

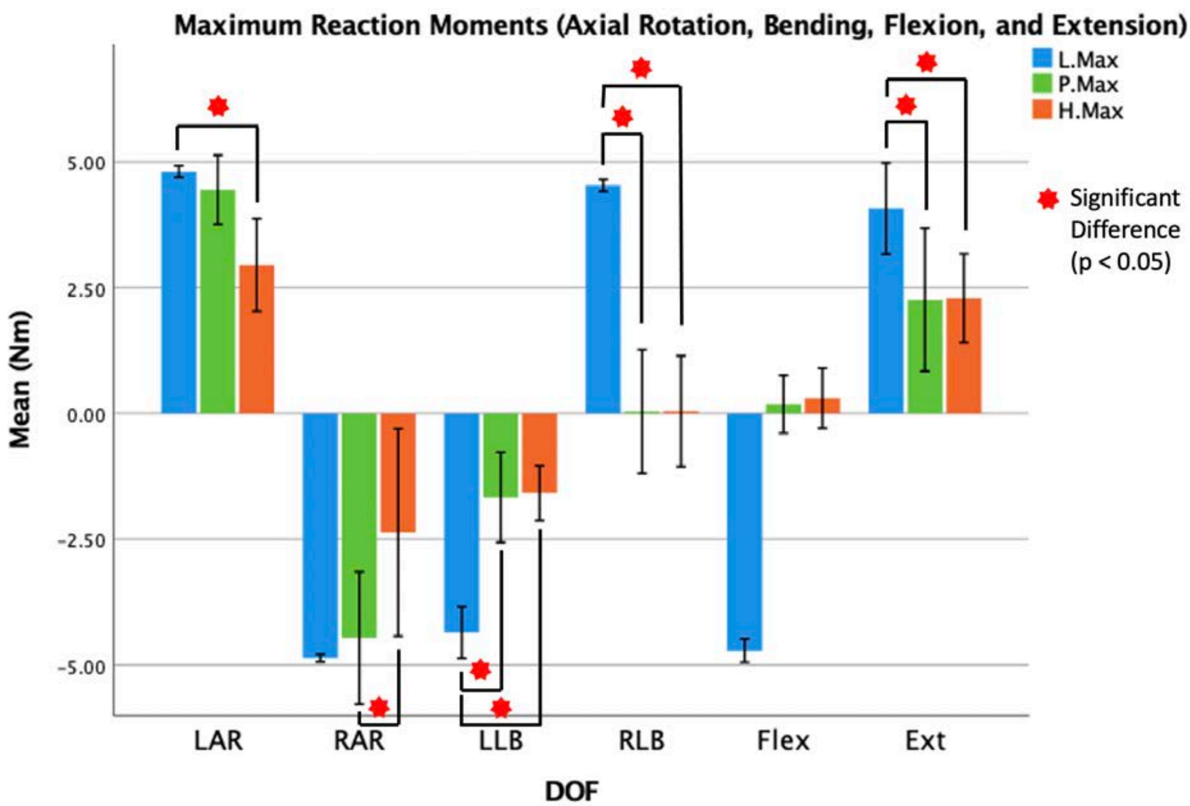
Maximum Reaction Moments (Axial Rotation, Bending, Flexion, and Extension)
L.Max
P.Max
H.Max
Significant Difference (p < 0.05)
5.00
2.50
0.00
-2.50
-5.00
Mean (Nm)
LAR
RAR
LLB
RLB
Flex
Ext
DOF

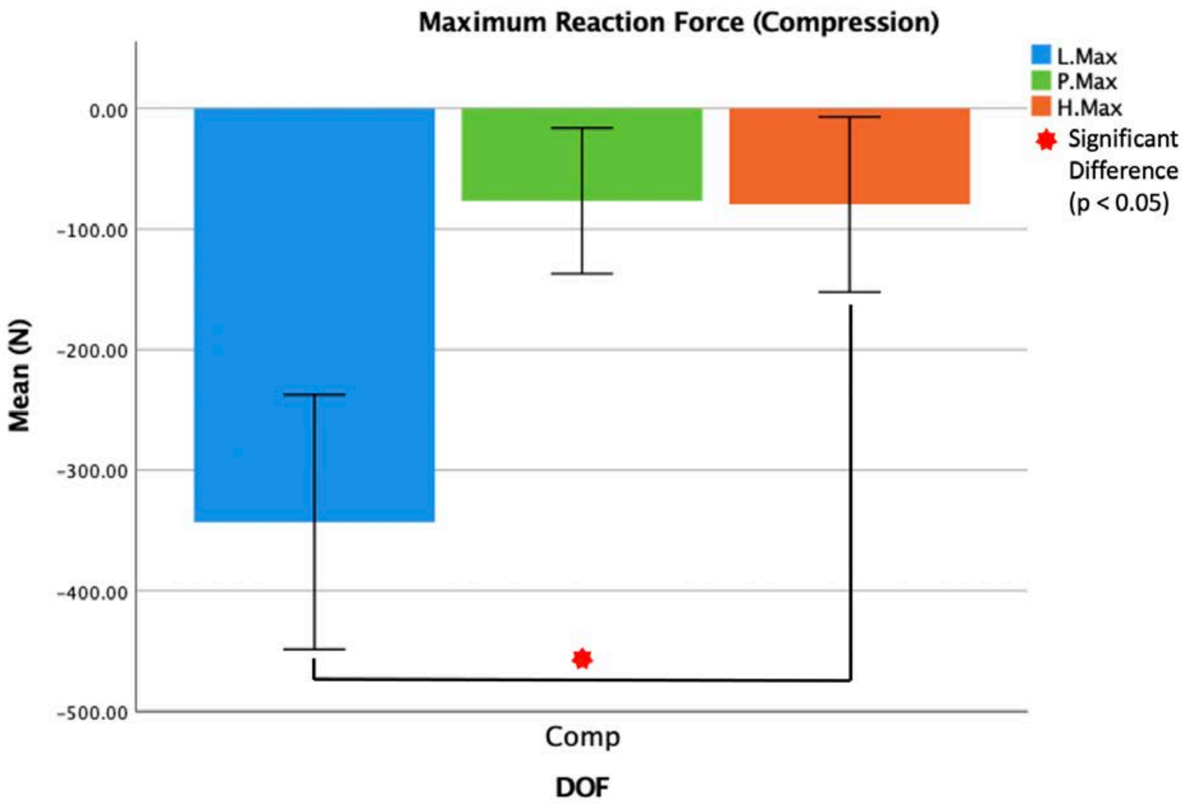
Maximum Reaction Force (Compression)
L.Max
P.Max
H.Max
Significant Difference (p < 0.05)
Mean (N)
0.00
-100.00
-200.00
-300.00
-400.00
-500.00
Comp
DOF

Appendix G: Mean (95% CI) Percentage Differences (load vs position, load vs hybrid)

- n=5 except for LLB under position control (n=4)
- LP: load vs position (blue line), LH: load vs hybrid (green line)
- Error bars indicate 95% confidence

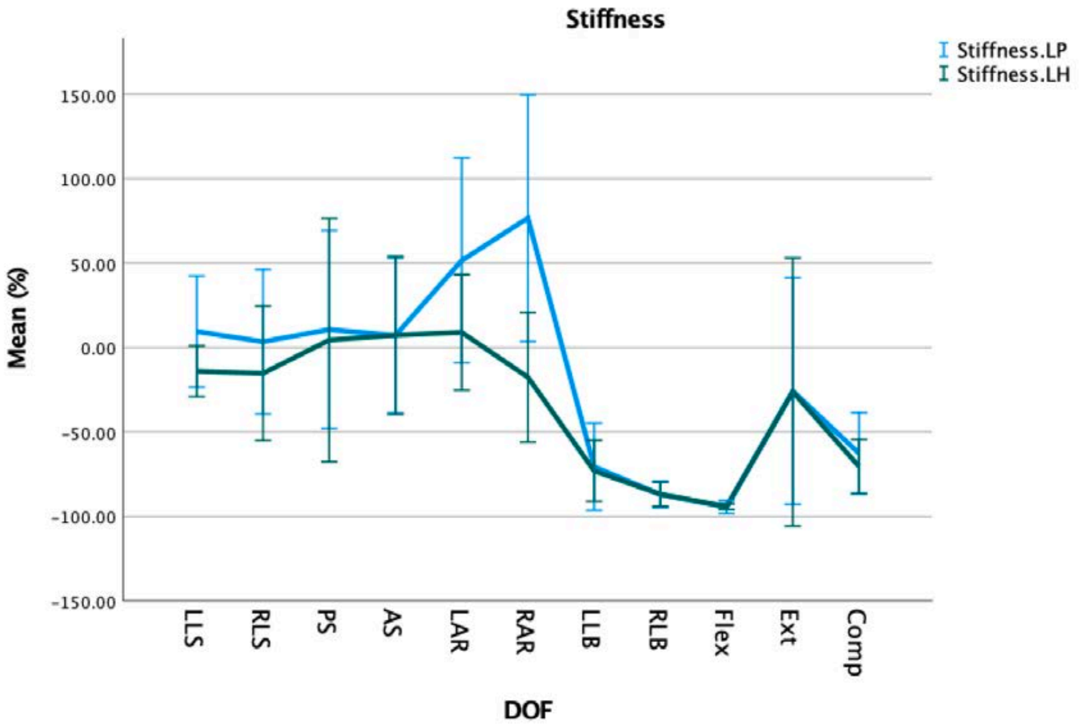

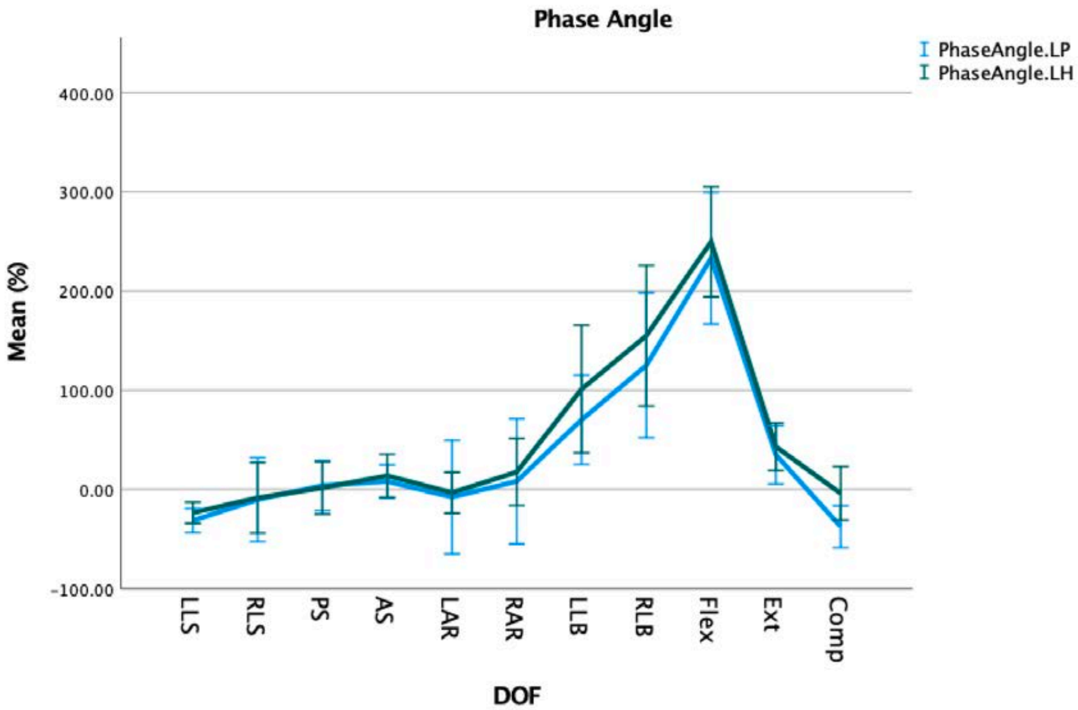

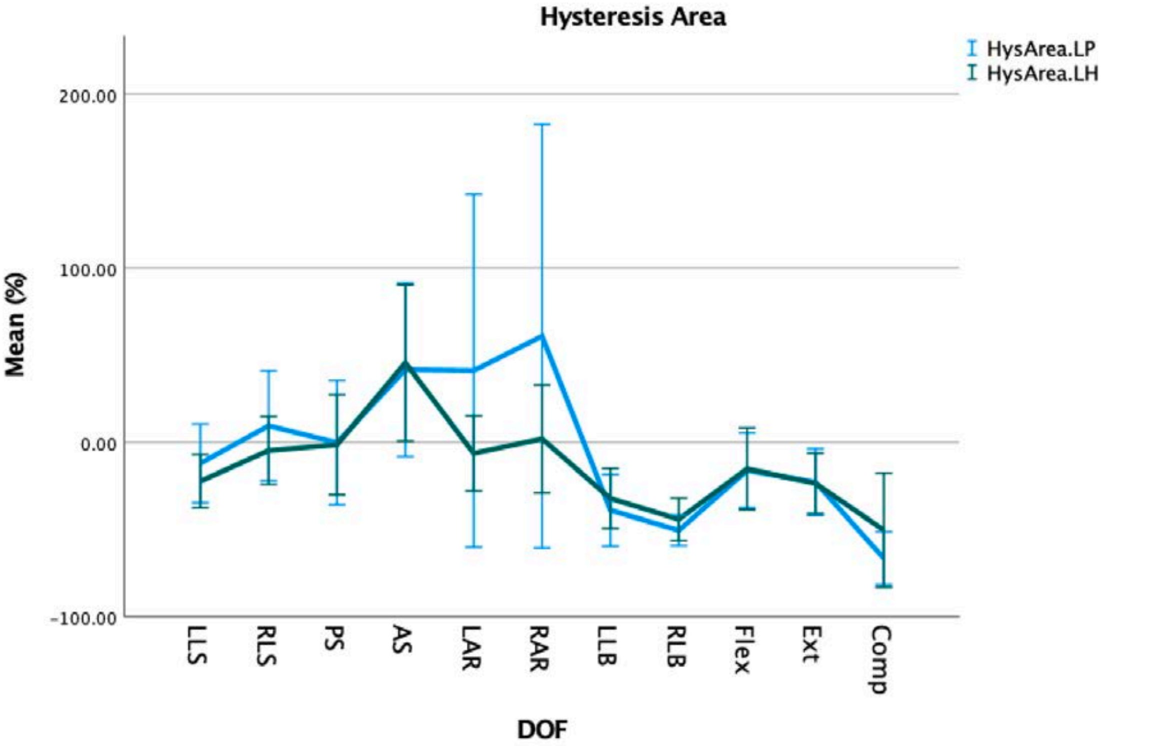

Hysteresis Area
HysArea.LP
HysArea.LH
200.00
100.00
0.00
-100.00
Mean (%)
LLS
RLS
PS
AS
LAR
RAR
LLB
RLB
Flex
Ext
Comp
DOF

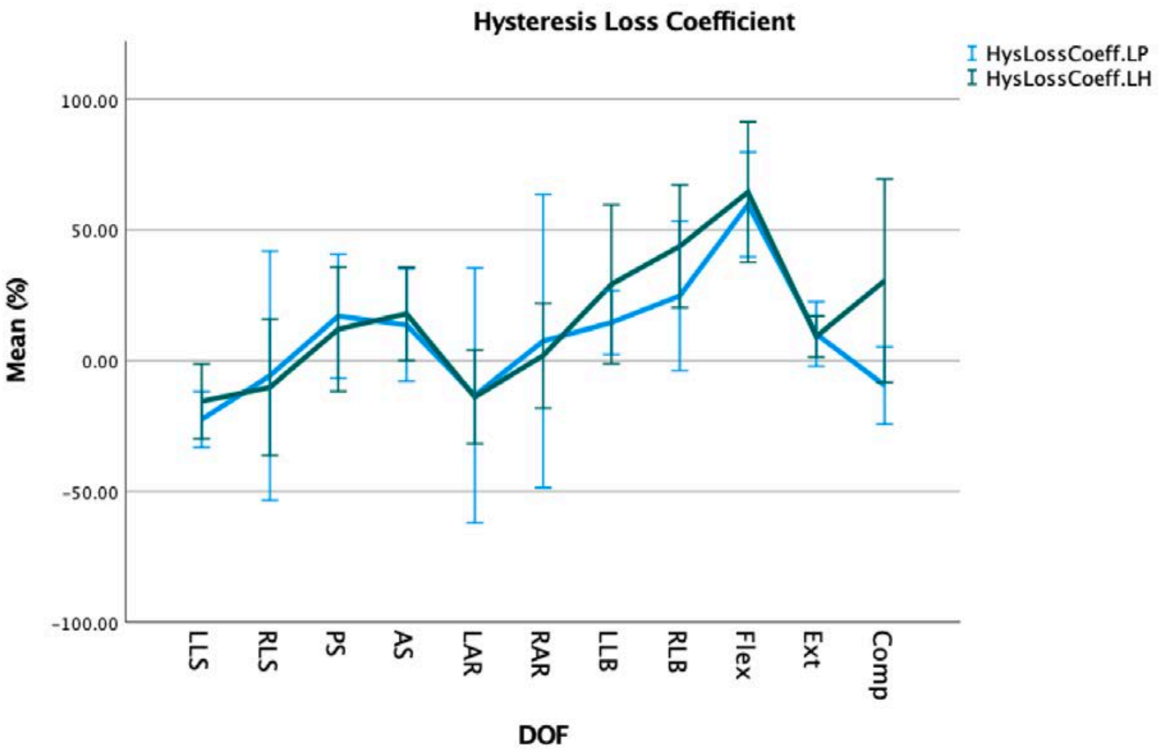

Hysteresis Loss Coefficient
HysLossCoeff.LP
HysLossCoeff.LH
100.00
50.00
0.00
-50.00
-100.00
Mean (%)
LLS
RLS
PS
AS
LAR
RAR
LLB
RLB
Flex
Ext
Comp
DOF

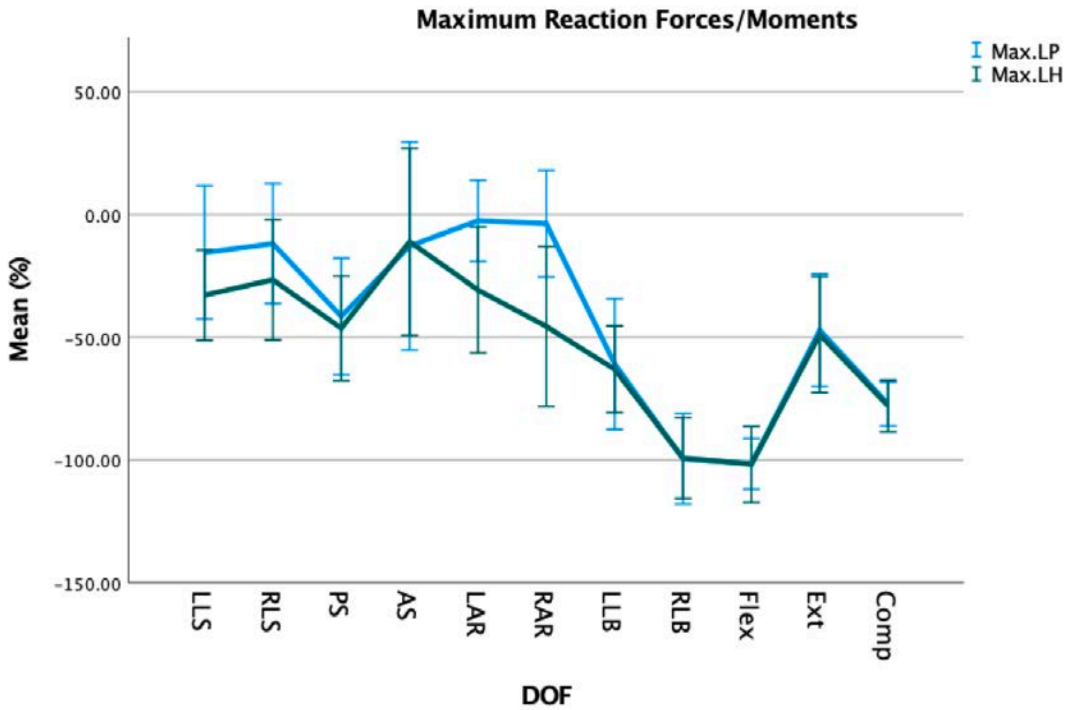
Maximum Reaction Forces/Moments
Max.LP
Max.LH
50.00
0.00
-50.00
-100.00
-150.00
Mean (%)
LLS
RLS
PS
AS
LAR
RAR
LLB
RLB
Flex
Ext
Comp
DOF

Appendix H: Mean (95% CI) percentage differences (hybrid vs load, hybrid vs position)

- n=5 except for LLB under position control (n=4)
- HL: hybrid vs load (blue line), HP: hybrid vs position (green line)
- Error bars indicate 95% confidence

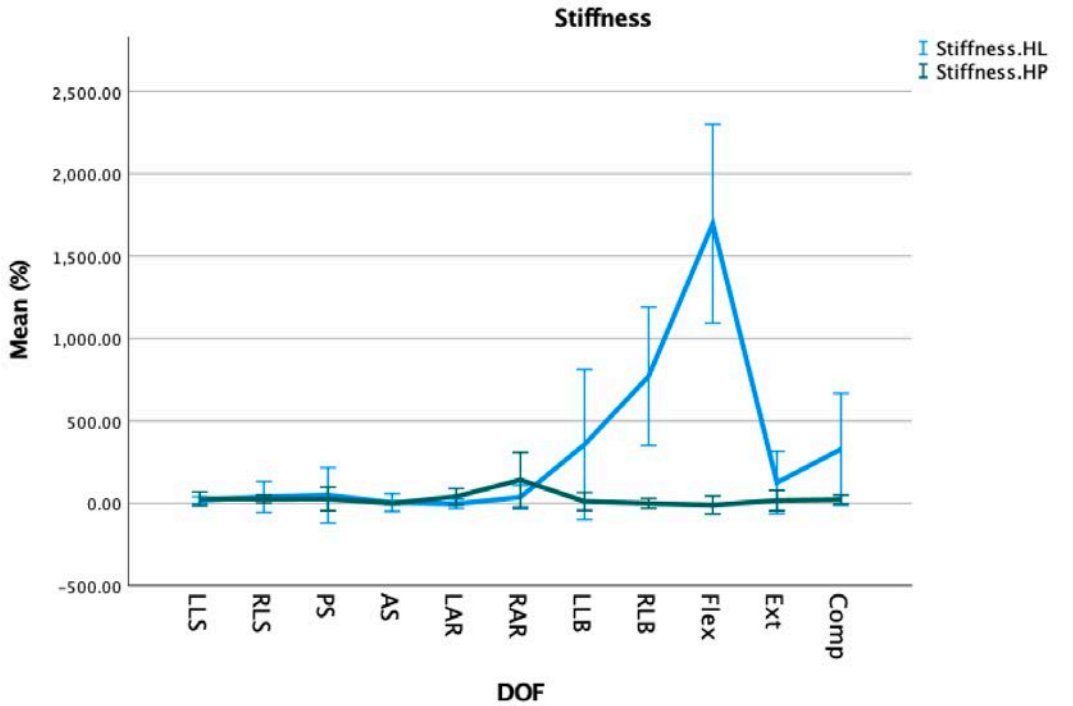

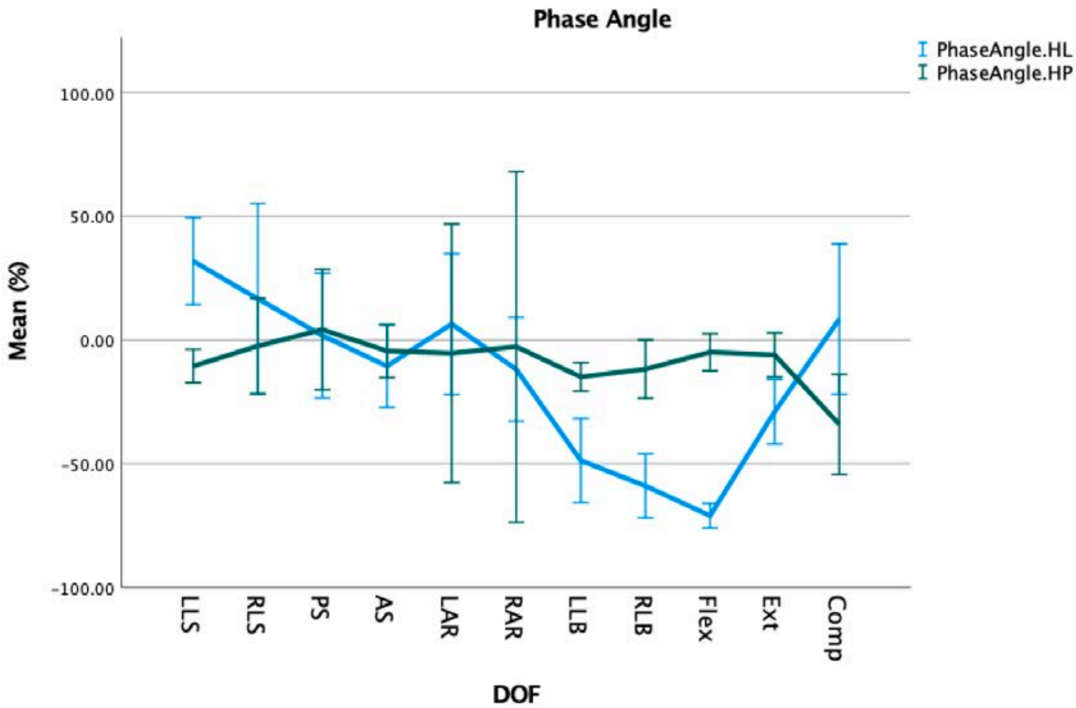

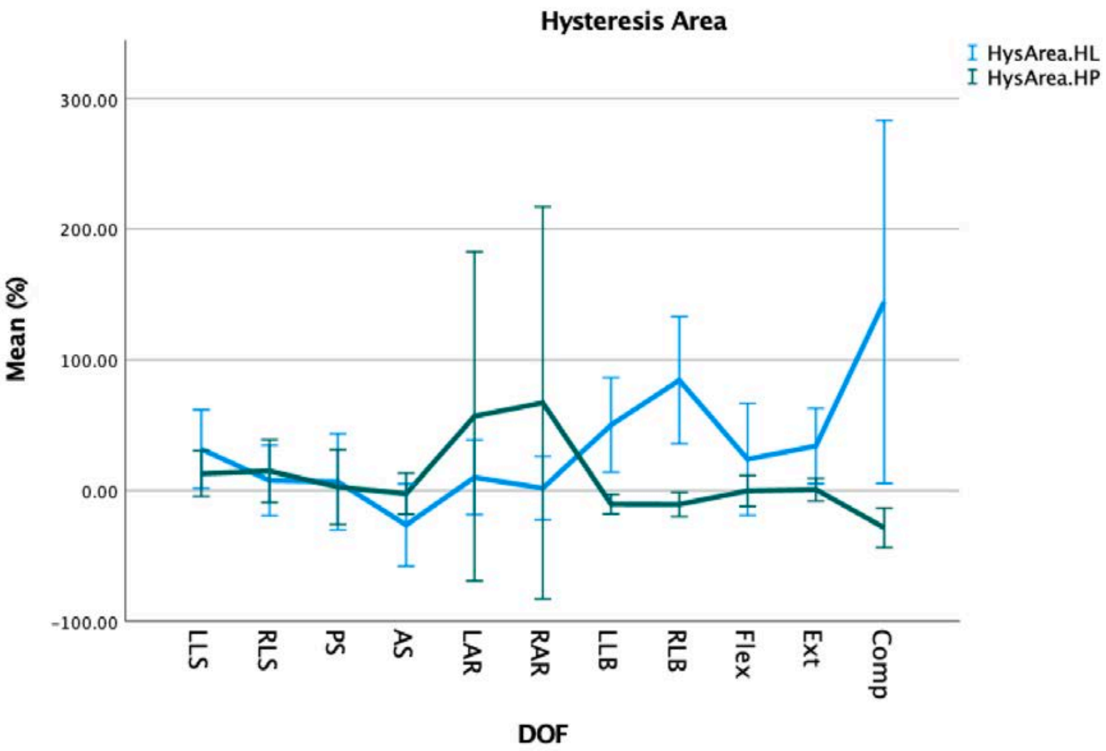
Hysteresis Area
HysArea.HL
HysArea.HP
300.00
200.00
100.00
0.00
-100.00
Mean (%)
LLS
RLS
PS
AS
LAR
RAR
LLB
RLB
Flex
Ext
Comp
DOF

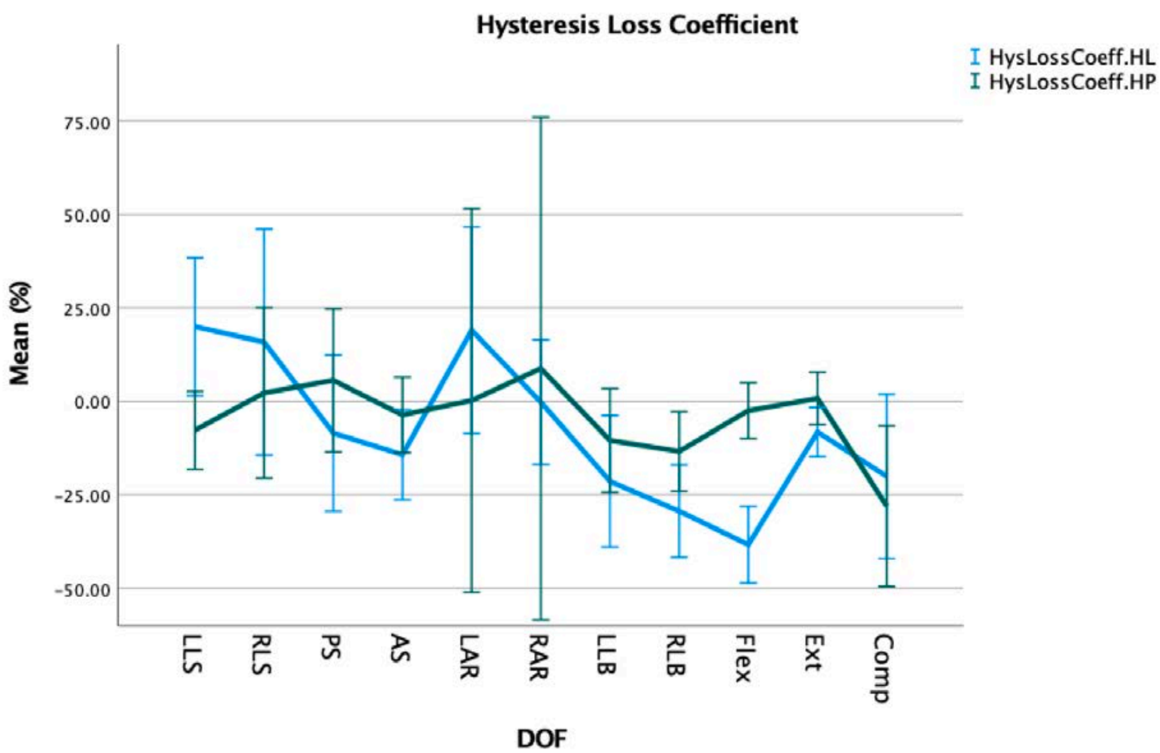
Hysteresis Loss Coefficient
HysLossCoeff.HL
HysLossCoeff.HP
75.00
50.00
25.00
0.00
-25.00
-50.00
Mean (%)
LLS
RLS
PS
AS
LAR
RAR
LLB
RLB
Flex
Ext
Comp
DOF

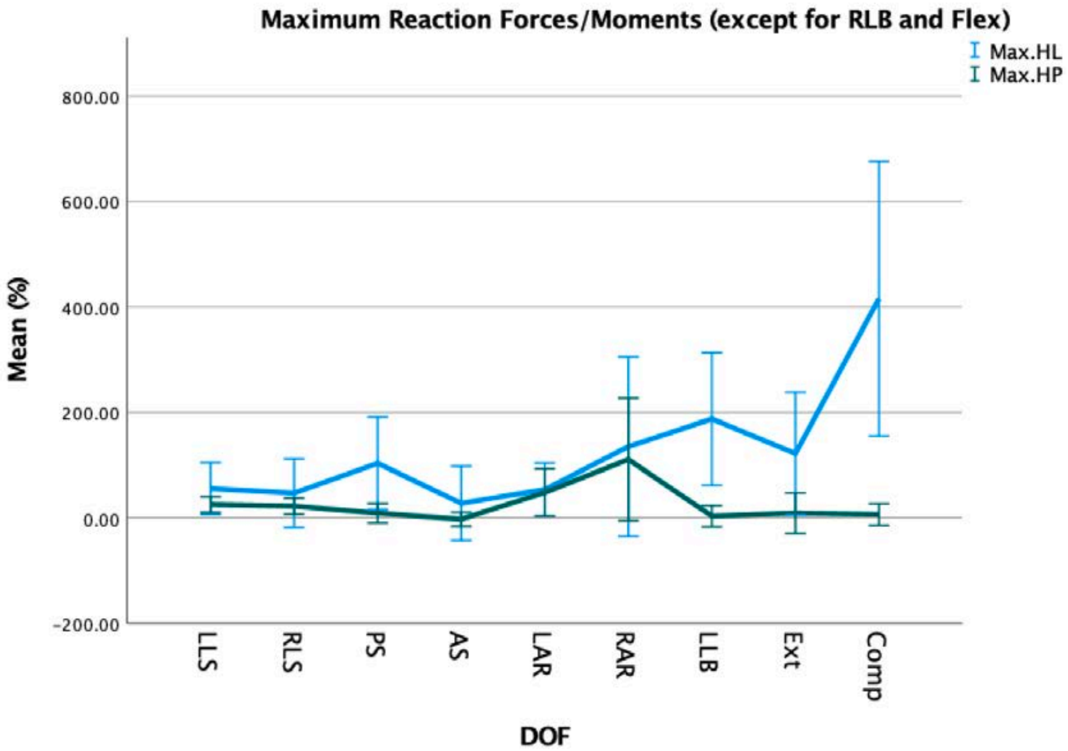

Maximum Reaction Forces/Moments (except for RLB and Flex)
Max.HL
Max.HP
800.00
600.00
400.00
200.00
0.00
-200.00
Mean (%)
LLS
RLS
PS
AS
LAR
RAR
LLB
Ext
Comp
DOF

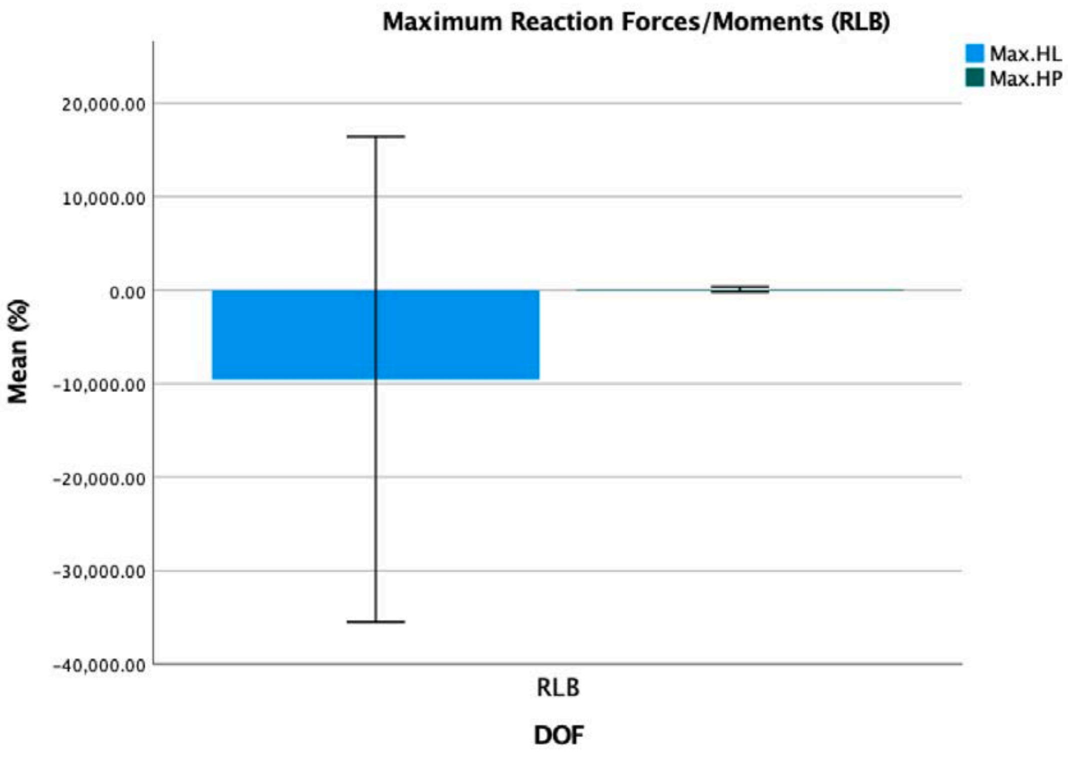

Maximum Reaction Forces/Moments (RLB)
Max.HL
Max.HP
20,000.00
10,000.00
0.00
-10,000.00
-20,000.00
-30,000.00
-40,000.00
Mean (%)
RLB
DOF

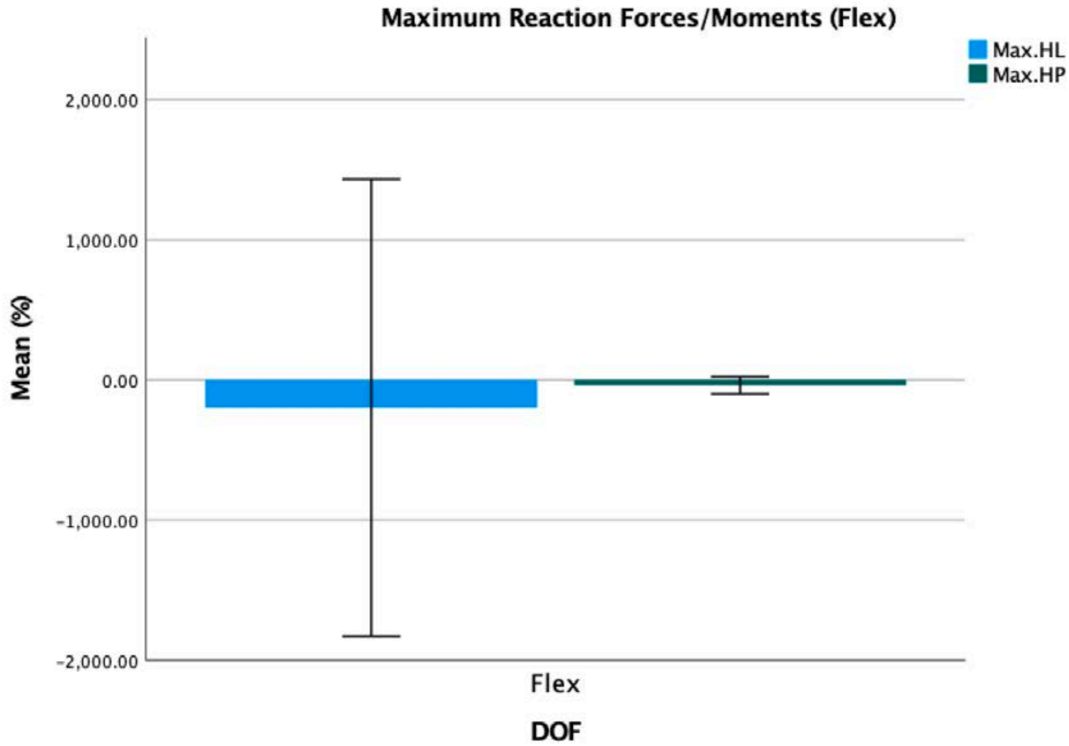

Maximum Reaction Forces/Moments (Flex)
Max.HL
Max.HP
2,000.00
1,000.00
0.00
-1,000.00
-2,000.00
Mean (%)
Flex
DOF